DOE/NASA/003780/2
NASA-CR-165130
DDA EDR 10086

ADVANCED GAS TURBINE (AGT) POWERTRAIN SYSTEM INITIAL DEVELOPMENT PROGRESS REPORT

Research Staff of Ford Motor Company and
AiResearch Manufacturing Company of Arizona
Division of the Garrett Corporation
August 1980

Prepared for
NATIONAL AERONAUTICS AND SPACE ADMINISTRATION
Lewis Research Center
Cleveland, Ohio 44135
Under Contract DEN 3-37
Amendment 2

For
U.S. DEPARTMENT OF ENERGY
Office of Transportation Programs
Division of Automotive Technology Development
Washington, D.C. 20585

FOREWORD

This report presents the results of an additional four-month study effort of an Advanced Gas Turbine Powertrain for automotive applications under partial sponsorship of DOE/NASA Contract Number DEN3-37. The work was performed by the Research Staff of the Ford Motor Company and AiResearch Manufacturing Company of Arizona, A Division of The Garrett Corporation, as a joint team effort.

The principal investigator for the program was Mr. B. T. Howes of the Ford Motor Company assisted by Mr. E. E. Strain, Mr. R. A. Rackley, and Mr. J. R. Kidwell of AiResearch. Report coordinator was Mr. D. L. Carriere of the Ford Motor Company and the NASA Program Manager was Mr. Richard P. Geye.

TABLE OF CONTENTS

TABLE OF CONTENTS (Cont'd)

LIST OF TABLES

SUMMARY

This report presents the results of an additional four-month in-depth study of an Advanced Gas Turbine (AGT) Powertrain for automotive application. This study was partially supported by the Research Staff of the Ford Motor Company in conjunction with AiResearch Manufacturing Company of Arizona, A Division of The Garrett Corporation, under modifications to DOE/NASA Contract DEN3-37. Results of a prior study conducted under this contract previously have been reported in "Conceptual Design Study of Improved Automotive Gas Turbine Powertrain — Final Report," DOE/NASA/0037-1, NASA CR-159580.

The principal objectives of the prior study were:

- Fuel economy a minimum of 20 percent better than 8.3 km/l (19.6 mpg) for a 1542 kg (3400 pounds) test weight baseline vehicle, when tested over the Combined Federal Driving Cycle at emissions objectives of 0.41 gm/mile HC, 3.4 gm/mile CO, and 0.4 gm/mile NO_X

- Acceleration capability of 15 seconds from 0 to 96.5 km/hr (0 to 60 mph)

- A design capable of reaching a level of development in 5 years (by the year 1983) such that a decision to start a production program could be considered

Additionally, Ford requirements for the engine were:

- A fuel economy objective of 30 to 50 percent better than the baseline vehicle

- A four-second vehicle start-up distance of 19.5 m (64 feet)

Prior to initiation of this additional four-month effort, a request for proposal — NASA RFP 3-823389Q — for the "Advanced Gas Turbine Powertrain System Development Project (Phase I and Phase II)" was received. Objectives, as stated in the RFP, are as follows:

- At least a 30 percent improvement in Combined Federal Driving Cycle (CFDC) economy (mpg) on the EPA test procedures over that presently predicted for a comparable 1984 production vehicle powered by a conventional spark-ignition powertrain system (baseline vehicle)

- Gaseous emissions and particulate levels less than the following: NO_X = 0.4, HC = 0.41, CO = 3.4 gm/mile and a total particulate level of 0.2 gm/mile using the same fuel as used for fuel economy measurements

- Ability to use a variety of alternate fuels

These objectives were adopted for this study conducted during the period of May 20 through September 24, 1979.

The major efforts conducted during the study reported herein were directed toward more detailed definition and analysis of the master design and performance of key components of the powertrain concept as derived during the prior study. A total "system design" philosophy was employed wherein distinct recognition was given to the passenger vehicle duty cycle over the CFDC, in particular, the amount of time expended at low power levels. Therefore, in the "system design" approach, component optimization was made primarily at intermediate power levels.

The reference powertrain design (RPD) resulting from these studies is defined as a continually updated, documented and characterized powertrain design that will serve as the finalized concept. It consists of a single shaft regenerated gas turbine engine utilizing ceramic hot section components, coupled to a split differential gearbox with an available variable stator torque converter (VSTC) and an available Ford Integral Overdrive (FIOD) four-speed automatic transmission. Predicted fuel economy using gasoline fuel over the CFDC is 15.3 km/l (36.0 mpg), which represents a 59 percent improvement over the spark-ignition-powered baseline vehicle. Using DF2 fuel, CFDC mileage estimates are 17.43 km/l (41.0 mpg). Zero to 96.6 km/hr (60 mph) acceleration time is 11.9 seconds with a four-second acceleration distance of 21.0 m (69 feet) which provides the AGT vehicle with driveability characteristics equal to or better than the baseline vehicle. All performance was estimated at 164.1 m (500 feet) elevation and 29.4°C (85°F).

During the Reference 1 Study, shaft speeds of 90,000, 100,000 and 118,000 rpm were evaluated with the 118,000 rpm speed point selected which resulted in the lowest rotor inertia and best rotor response time. Subsequent design studies on the compressor versus shaft speed indicate that at 118,000 rpm the high inducer Tip Mach number would result in low efficiency and increased technical risk associated with inducer leading edge blade thickness. In addition, studies indicate potential technical risks associated with the 118,000 rpm speed and the predicted third critical speed. For these reasons a 100,000 rpm design speed was selected.

Definition of the ceramic radial turbine rotor has evolved. The radial turbine, fabricated from near-net shape ceramic material using one of several different manufacturing approaches, is predicted to achieve good part-speed performance while sacrificing minimum performance potential at maximum power conditions. The study shows a stator vane count between 19 and 21 with a rotor blade count between 12 and 14. Stress analysis indicates a peak rotor stress near the rotor centerline of approximately 206.8 MPa (30 ksi) under maximum power steady state operating conditions.

The compressor is characterized as a 40- to 50-degree backward swept impeller having 12 full blades and 12 splitter blades. A radial diffuser system has been preliminarily evaluated to achieve the desired surge margin and efficiency characteristic over the range of AGT operating conditions.

Further definition of the variable geometry combustion system and fuel delivery concepts was conducted. Primary and dilution airflow optimization was evaluated for the wide range of operating characteristics to maintain the 1644°K (2500°F) turbine inlet temperature, low emission levels, and desired combustor pressure drop of three-percent.

Steady-state thermal and stress analyses have been conducted on the structural components of the RPD. Results indicate that with internal insulation, component stresses are acceptable over the operating range. Design iterations will continue with selected ceramic manufacturers to further address such problems as ceramic-to-ceramic and ceramic-to-metallic interfaces, manufacturability, part integrity and reliability, and the subtleties of near-net shape ceramic producibility.

Definition of the regenerator core, seals and drive system was accomplished. An extruded matrix core with a hydraulic diameter of 0.508 mm (0.020 inch) has been selected for the engine. Three inner seal configurations were examined and evaluated with respect to overall system efficiency. An equal flow area split design (balanced heat exchanger) design provides the best regenerator effectiveness and pressure drop combination throughout the engine operating range. A regenerator drive system, similar to the Ford 707 system, was analyzed and recommended for detailed design.

Two split path differential gearbox design configurations were evaluated. In one, the VSTC is required to operate briefly under a negative speed ratio up to a vehicle speed of 6.4 to 9.7 km/hr (4 to 6 mph). The second split path design configuration does not necessitate operation of the VSTC in the negative speed ratio. Determination of the recommended approach will be made following more detailed mapping of the variable stator torque converter characteristics.

The control system evaluated for the powertrain is a full authority electronic system. A microprocessor in the control package accepts the sensor signals, reacts, and drives the fuel control and variable geometry actuators to operate the powertrain in a responsive and fuel efficient manner. Automatic start sequencing and protective features have been defined to provide a safe basic philosophy and the same "feel" and drive input as a conventionally powered vehicle.

The ceramic radial rotor is the longest-lead, highest-risk ceramic component. Design studies indicate sintered Si_3N_4 and SiC, reaction sintered SiC (RSSiC) and hot isostatic pressed (HIP) Si_3N_4 have the potential for meeting the project requirements within the development timetable.

1.0 INTRODUCTION

This report, submitted by the Turbine Research Department of the Ford Motor Company in conjunction with the AiResearch Manufacturing Company of Arizona, a Division of The Garrett Corporation, presents the results of a recently completed four-month in-depth study as specified by modifications to DOE/NASA Contract DEN3-37, to continue definition and analysis of an advanced gas turbine (AGT) powertrain system for automotive application. The work reported herein covers the period of May 20, 1979 through September 24, 1979, and is considered an extension of the design study conducted under DOE/NASA Contract DEN3-37 previously reported as "Conceptual Design Study of Improved Automotive Gas Turbine Powertrain — Final Report," DOE/NASA/0037-79/1, NASA CR-159580, Reference (1).

The principal objectives of the reference study were:

- Fuel economy a minimum of 20 percent better than 8.3 km/l (19.6 mpg) for a 1542 kg (3400 pounds) test weight baseline vehicle, when tested over the CFDC at emissions objectives of 0.41 gm/mile HC, 3.4 gm/mile CO, and 0.4 gm/mile NO_x
- Acceleration capability of 15 seconds from 0 to 96.5 km/hr (0 to 60 mph)
- A design capable of reaching a level of development in 5 years (by the year 1983) such that a decision to start a production program could be considered

Additionally, Ford requirements for the engine were:

- A fuel economy objective of 30 to 50 percent better than the baseline vehicle
- A 4-second vehicle start-up distance of 19.5 m (64 feet)

Investigation during the initial study included some twenty-two different engine configurations and nineteen candidate transmission concepts (three for a two-shaft configuration). Selection criteria were established and used to evaluate the concepts. These criteria were weighed and appear as follows in order of rank; fuel economy, manufacturing cost, technical risk, installation considerations, and development and growth potential. As reported in Reference 1, AiResearch Document 31-3529, a single shaft regenerative engine with a centrifugal compressor with variable inlet guide vanes (VIGV), variable geometry combustor and single stage ceramic radial turbine rotor coupled to a differential gearbox containing an available VSTC and an available Ford FIOD four-speed automatic transmission, was recommended for further study.

Prior to initiation of the continued study, a Request For Proposal — NASA RFP 3-823389Q — for the "Advanced Gas Turbine Powertrain System Development Project (Phase I and Phase II)" was received. Objectives, as stated in the RFP, are as follows:

- At least a 30 percent improvement in CFDC economy (mpg) on EPA test procedures over that presently predicted for a compatible 1984-production vehicle powered by a conventional spark-ignition powertrain system (baseline vehicle)

- Gaseous emissions and particulate levels less than the following: NO_X = 0.4, HC = 0.41, CO = 3.4 gm/mile and a total particulate level of 0.2 gm/mile using the same fuel as used for fuel economy measurements

- Ability to use a variety of alternate fuels

Therefore, all performance comparisons and supporting analysis is in response to the goals stated in the RFP. In addition, the RFP identified the following nomenclature and interpretative definition for the powertrain program, which has been adopted as follows:

- Reference Powertrain Design (RPD) — Continually updated, documented and characterized powertrain design that will serve as the finalized concept

- Mod I Engine — A stepping stone engine incorporating the advancing technologies being derived from the component development activities

The definition and analysis efforts of this study were based on the recommended conceptual design layout as presented in Reference 1. The principal tasks included:

- Continued definition of the hot section of the engine and ceramic components including aerodynamic and stress analysis of the turbine exhaust diffuser and regenerator/turbine ducting; and analysis of potential regenerator configurations, including core and seal geometries and regenerator drive and housings

- Continue to analyze performance considering effects of the engine definition iterations, including determining the effects of differential and split-path variable stator torque converter/gearbox/transmission concepts on combined federal driving cycle performance; and effects of control system relative to powertrain/vehicle transient characteristics

- Continue aerodynamic and stress definition of the ceramic turbine wheel concepts and definition of metallic turbine wheel concept including preliminary specifications for a turbine test rig and a rotor dynamic simulator to permit suitable testing of the resulting designs

- Continued definition of the compressor concepts for aerodynamic stress, and material considerations including VIGVs and effects of impeller/VIGV interaction; and preliminary specifications for the compressor test rig and VIGV rig

- Continue definition of alternate combustor configurations and analysis of relative performance including preliminary definition of a baseline variable geometry combustor and preliminary specification of a combustor test rig

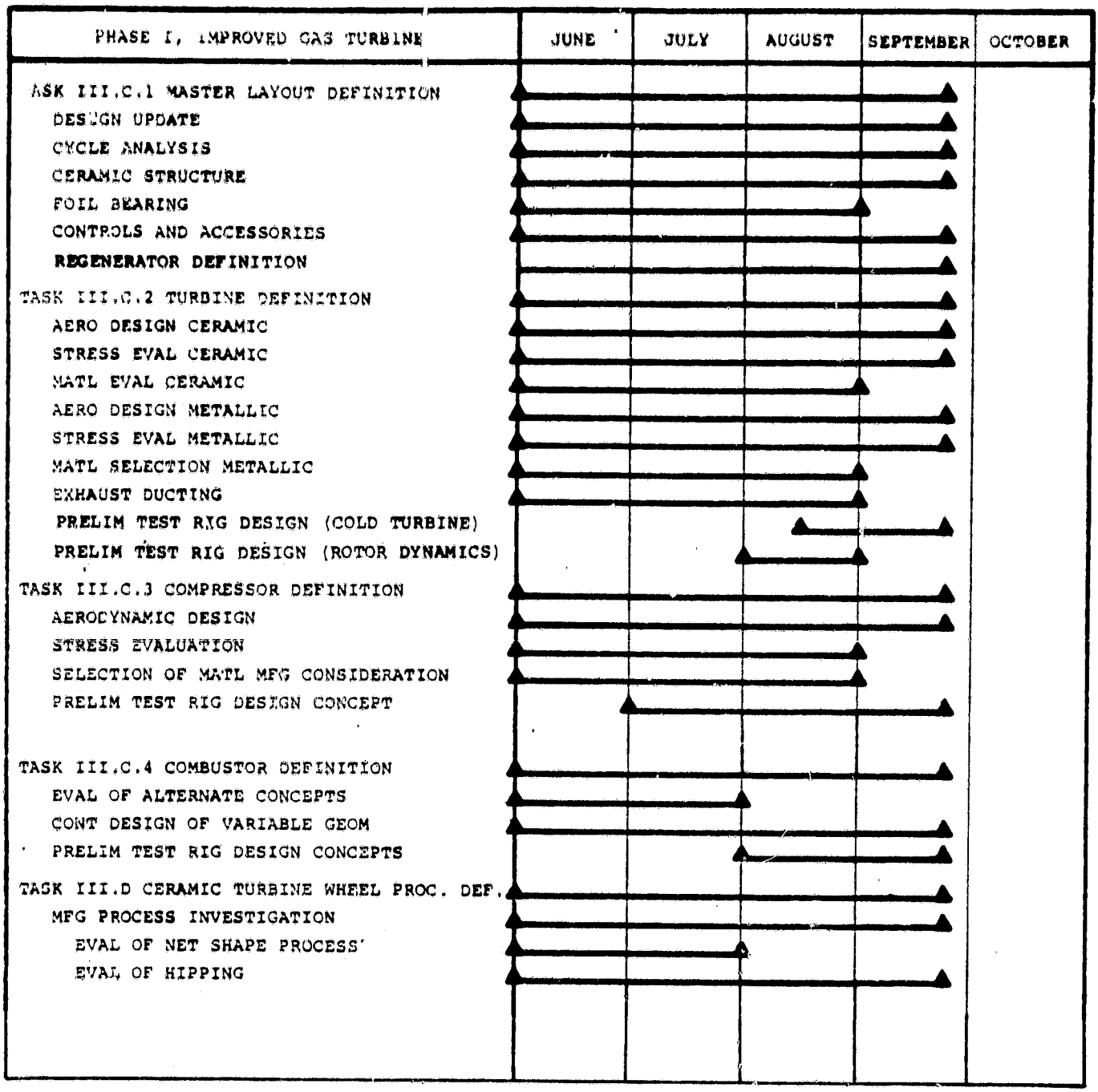

Figure 1. Program Master Schedule.

- Continued investigation of silicon nitride and silicon carbide ceramic radial turbine wheel net shape fabrication processes to attain higher strength including hot isostatic pressing alternatives

Figure 1 shows the program master schedule.

A total "system design" philosophy was employed during the definition and analysis efforts. Through an iterative design process a reference powertrain design is being established. The philosophy of "system design" incorporates a distinct recognition of a passenger vehicle duty cycle over the CDFC and, in particular, the amount of time expended at low power levels. Therefore, in the "system design" approach, component optimization is made at intermediate (off design) power levels and not at maximum power (design point) as is typical of normal gas turbine design techniques. Basic guidelines used in arriving at the reference powertrain design included:

- Performance — Enviromental Impact — Consumer Marketability

- Technology demonstration for a go/no-go production enginering decision as early as 1983

- Demonstration of all vehicle/performance aspects by 1984

- Probability of success and assessment of technical risk

This powertrain design is identical in concept to the powertrain concept of Reference 1 differing only in the details of key components and subsequent refinements to the performance predictions. It consists of a single shaft regenerated gas turbine engine utilizing ceramic hot section components, coupled to a split differential gearbox with an available VSTC and an available Ford FIOD four-speed automatic transmission. Controls feature accurate microprocessor full authority digital technology, integrating all powertrain control functions into one master control system, stressing driveability and integrated performance as related to consumer acceptance. The RPD package has the flexibility of providing either front- or rear-wheel drive.

The following sections discuss the continued definition of key components and subsystems.

2.0 TECHNICAL DISCUSSION

The following paragraphs describe the continuing definition of the Advanced Gas Turbine (AGT) and key components.

2.1 Master Layout Definition

Master layout definition and refinement has included:

- Powertrain
- Power Section
- Gearbox
- Transmission
- Controls Analysis
- Cycle Analysis
- Vehicle Performance
- Compressor Definition
- Regenerator Definition
- Combustor Definition
- Turbine Definition
- Ceramic Rotor Process Definition

2.1.1 Powertrain Layout

As shown in Figure 2 the reference powertrain design (RPD) addressed in this study incorporates a power section containing the single-shaft ceramic gas turbine and related ceramic hot section components, a variable speed differential variable stator torque converter (VSTC) gearbox, and a Ford integral overdrive (FIOD) automatic 4-speed transmission.

Due to inherent characteristics of the differential gearbox design selected, the VSTC is required to operate briefly under a negative speed during the first 6.4 to 9.7 km/h (4 to 6 mph) of vehicle speed. Specific VSTC characteristics under negative speed ratios could not be confirmed during the study. Consequently, a second powertrain configuration with a variable speed gearbox not requiring negative speed ratios in the VSTC is being investigated.

Preliminary analysis has indicated that either configuration meets the performance goals.

Both powertrain designs are approximately 1447.8 mm (57.0 inches) long and weigh 237.2 kg (523 pounds) exclusive of conventional automotive accessories, such as power steering pump, alternator, and starter. The power section is approximately 552.45 mm (21.75 inches) in diameter by 520.7 mm (20.5 inches) long. The variable speed gearbox and VSTC sections are approximately 698.5 mm (27.5 inches) wide by 609.6 mm (24.0 inches) high by 279.4 mm (11.0 inches) long including accessory mounts. The FIOD transmission is approximately 330.2 mm (13 inches) wide by 330.2 (13 inches) high by 647.7 mm (25.5 inches) long. It is anticipated that significant weight reduction can be obtained during detail design.

Figure 3 shows a powertrain utilizing a split path gearbox that does not require operation of the VSTC under negative speed ratio.

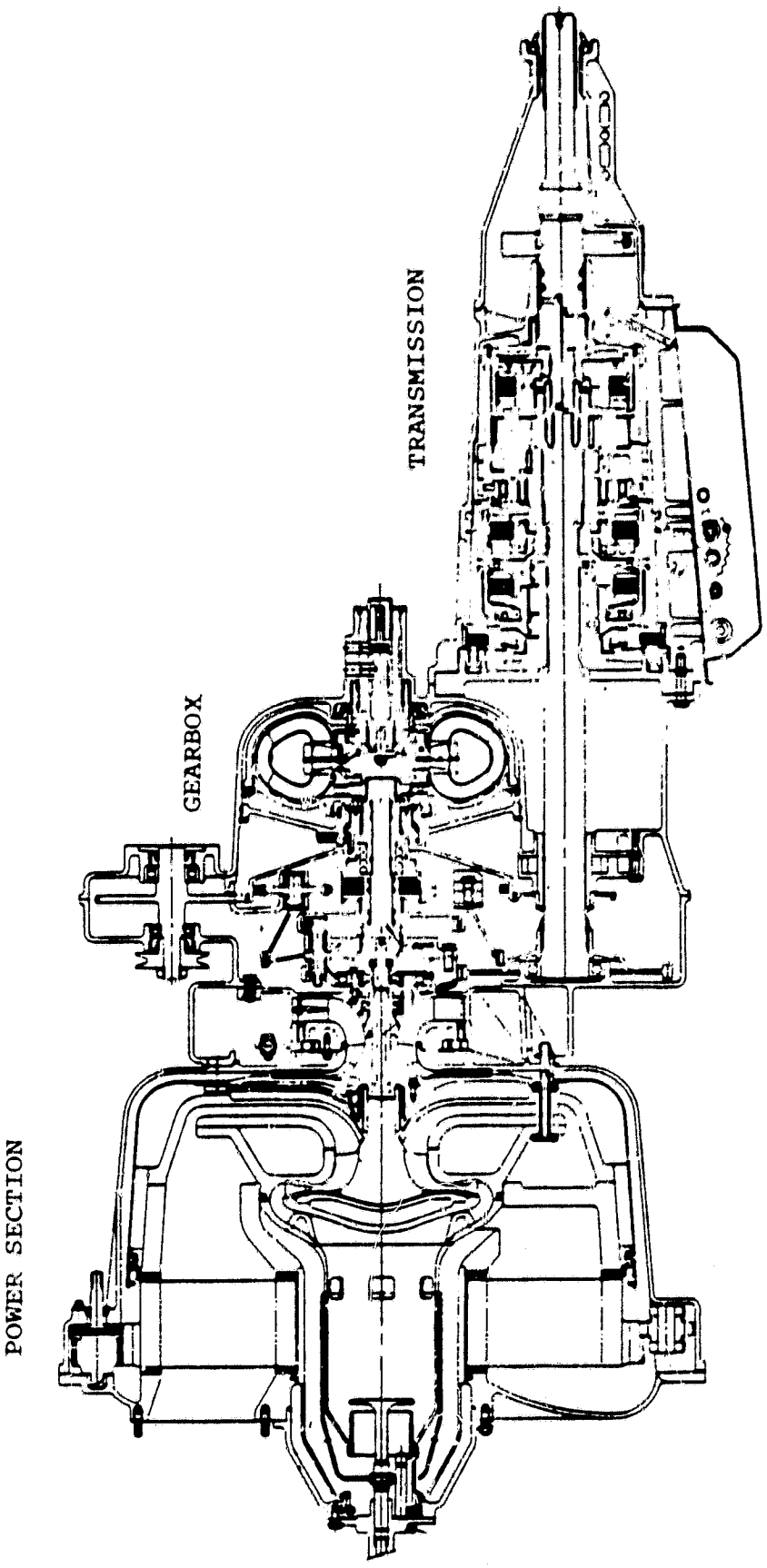

Figure 2. Powertrain Layout with a Differential Gearbox.

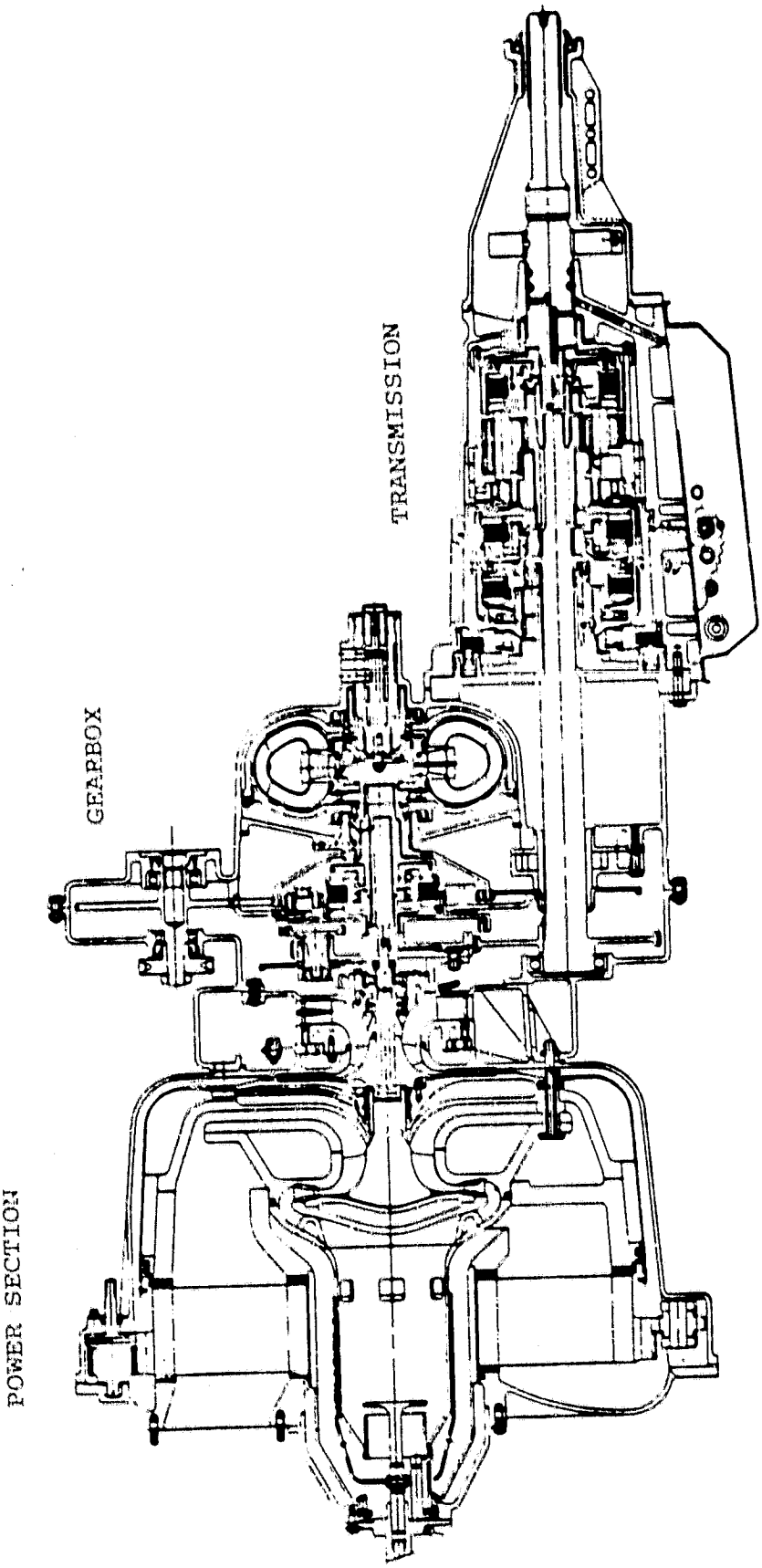

Figure 3. Powertrain Layout with a Split Path Gearbox.

2.1.2 Power Section

The AGT power section incorporates a larger ceramic regenerator, ceramic hot section components, improved aerodynamic flowpaths, improved structural load paths, and a bolted front regenerator cover in comparison to the Reference 1 configuration.

2.1.2.1 Aerodynamic Flowpath

The AGT engine aerodynamic flowpath is shown in Figure 4. Air enters the compressor inlet plenum at Station (1), flows through the inlet guide vanes (2) into the radial compressor (3), through the compressor diffuser (4), and into an annular space (5) surrounded by the AGT outer housing (6). Compressor discharge air flows from the annular space (5), around the regenerator drive gear and roller (7), into the high-pressure side of the regenerator (8), out of the regenerator and ducted through the flow separator housing (9) to the combustor (10) via the primary ports (11) and dilution ports (12). Fuel is supplied to the combustor through the fuel nozzle (13), and combustion products are directed around the combustor baffle (14), through the turbine nozzle (15), and into the radial turbine (16). Turbine discharge gases are directed radially to a plenum (17) and through the low-pressure side of the regenerator (18) to the turbine exhaust (19).

2.1.2.2 Structural Load Path

As shown in Figure 5, AGT pressure containment is provided by the AGT outer housing (1), and regenerator cover (2). The regenerator seal preloads (3), and aerodynamic forces (4) are reacted through the flow separator housing (5) to bosses (6), and through to the compressor inlet housing and engine mounts on the mating gearbox. Aerodynamic loads (7) on the flow separator housing (5) are reacted through the same path. Combustor preload (8) is transmitted through the combustor liner (9), to the turbine shroud/nozzle (10), and into the same bosses (6) as the pressure loads. Aerodynamic forces (11) are reacted through this same load path.

2.1.2.3 Rotor Dynamics

During the Reference 1 study, shaft speeds of 90,000, 100,000 and 118,000 rpm were evaluated with the 118,000 rpm speed point selected which resulted in the lowest rotor inertia and best rotor response time. Subsequent design studies on the compressor versus shaft speed have indicated that, at 118,000 rpm, the high inducer tip Mach Number would result in low efficiency and increased technical risk associated with inducer leading edge blade thickness. In addition, studies indicated potential technical risks associated with the 118,000 rpm speed and the predicted third critical speed. For these reasons a 100,000 rpm design speed was selected. Further analysis of the AGT engine configuration again indicated insufficient margin between engine rotor operating speed and pre-

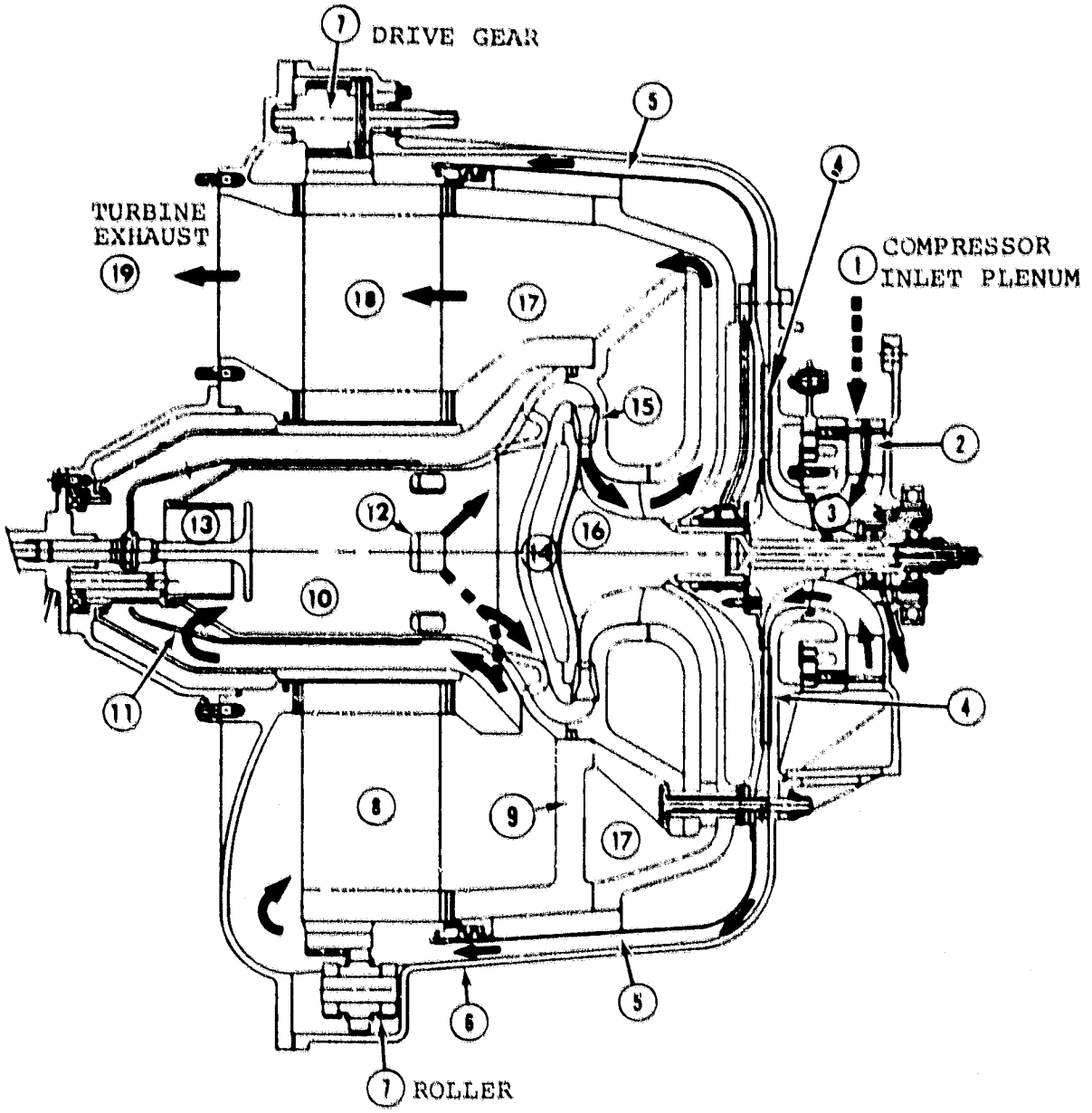

Figure 4. Power Section Aerodynamic Flowpath.

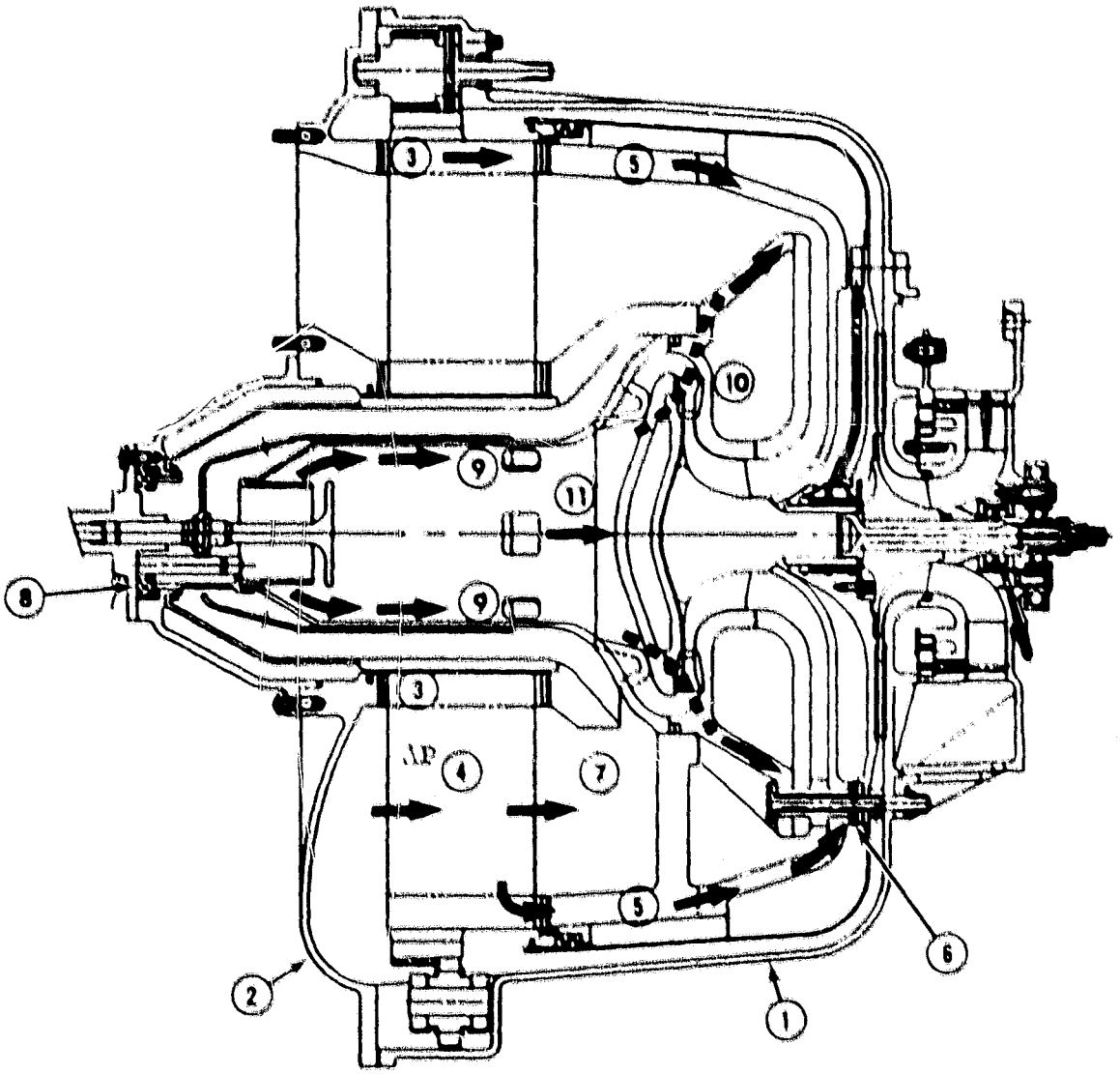

Figure 5. Power Section Structural Load Paths.

dicted third critical speed. To correct this potential problem, the rotor dynamic analysis was continued and changes were incorporated. The rotor shaft was shortened 9.5 mm (0.375 inch), the aluminum impeller forward face was piloted on the drive shaft instead of a curvic coupling, and the foil bearing diameter was increased 2.54 mm (0.1 inch). Combining all modifications and assuming that the gear end bearing had 4,387 N/mm (25,000 pound/inch) stiffness and the foil bearing 700 N/mm (4,000 pound/inch) stiffness, the critical speeds were calculated as follows:

Critical Speeds	rpm	Description
1	4,090	Metallic turbine
2	38,000	Metallic turbine
3	134,700	Metallic turbine
4	268,600	Metallic turbine
1	5,850	Ceramic turbine
2	38,260	Ceramic turbine
3	135,200	Ceramic turbine
4	267,100	Ceramic turbine

The third critical speed had a margin of 34.7 percent over 100 percent speed (100,000 rpm) for the metallic turbine and 35.2 percent for the ceramic turbine, which is consistent with Ford and AiResearch experience.

The following bearing loads were calculated for a normal CG eccentricity of 0.0127 mm (0.0005 inch).

Absolute Bearing Loads, N(Pounds)

rpm	Gear End Bearing	Foil Bearing	Description
100,000	182.4 (41)	13.3 (3)	Metallic turbine
100,000	160.1 (36)	8.9 (2)	Ceramic turbine

The effect of the planetary gearset on rotor dynamics could not be satisfactorily resolved analytically due to the wide divergence of data and experience. Gearset influence factors on the AGT rotor must be established by actual test in a rotor dynamics test rig.

2.1.2.4 Bearings and Seals

The high speed ball bearing and shaft seal arrangement currently under evaluation is depicted in Figure 6.

Bearing analysis was based on load and speed profiles expected over the 160,934 km (100,000 mile) vehicle operational life. On the basis of CFDC, the high speed bearing would be operated for 3890 hours at speeds between 55,000 and 84,000 rpm. The bear-

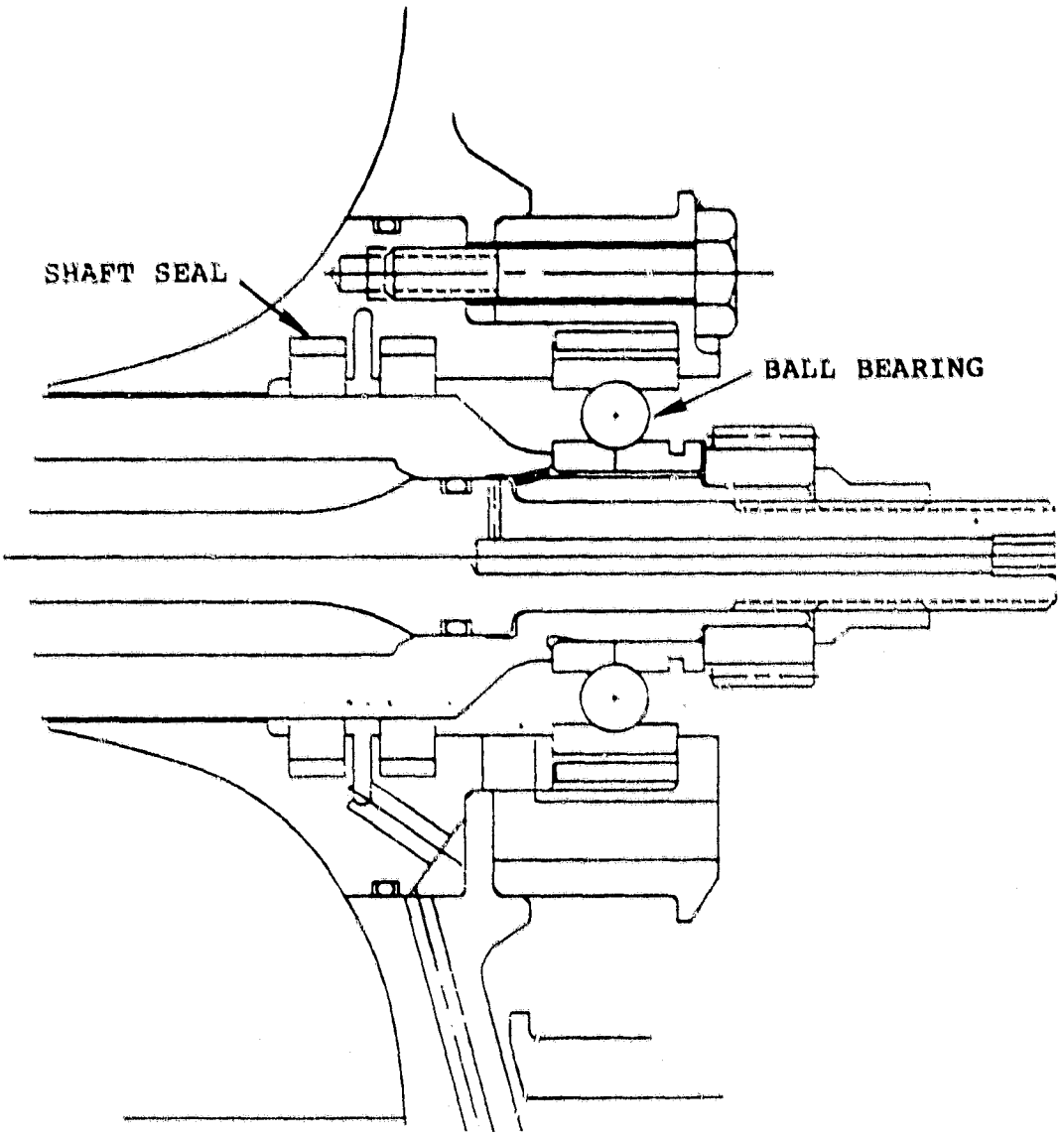

Figure 6. High Speed Ball Bearing and Shaft Seal.

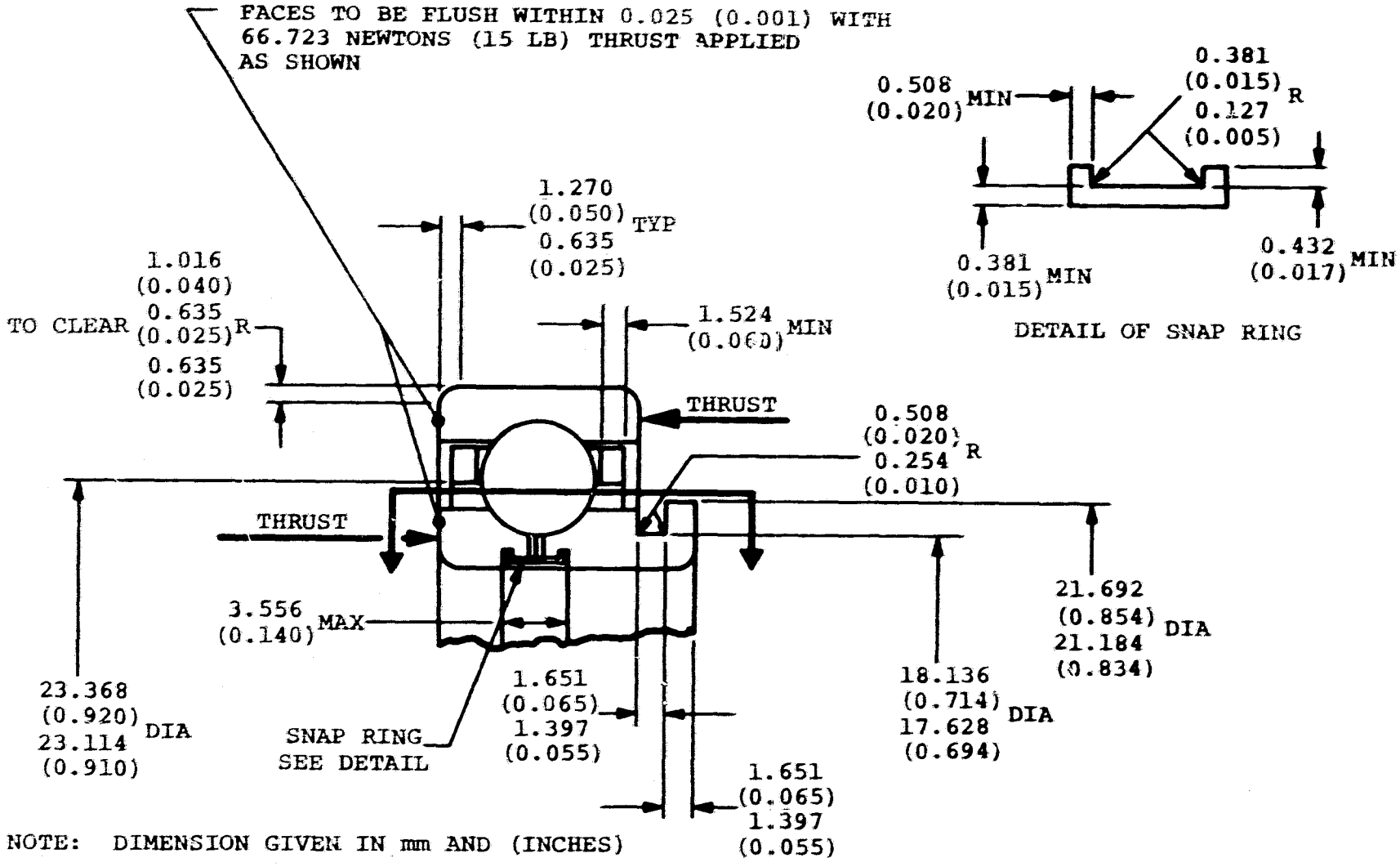

Figure 7. Bearing Design.

TABLE 1

BEARING DESCRIPTION — BALL, SPLIT-INNER-RING, 202 **GRADE ABEC 5**

Inner Ring	**Outer Ring**
Material — SAE 52100 STL — R_C 58-64	Material — SAE 52100 STL — R_C 58-64
Bore 15 mm (0.5904-0.5906	O D 1.3778-1.3780 (35 mm)
Width 13.335-13.589 mm (0.525-0.535)	Width 0.4281-0.4331 (11 mm)
Race Depth 24 Min. % Ball/Roller Dia.	Race Depth 16 Min. % Ball/Roller Dia.
Race Curvature — 51.6-52.4%	Race Curvature — 50.6 -51.4%
Ball/Roller Dia.	Ball/Roller Dia.
Separator Pilot Land	Separator Pilot Land
To Groove Runout TIR	To Groove Runout 0.0127 (0.0005) TIR
Separator	**Rolling Elements**
Material — SAE 4340 STL — R_C 34-38	Material — SAE 52100 STL — R_C 58-64
Silver Plated 0.0005-0.0015 Thick Per AMS 2410	
Construction Machined	Elements Per Row 10
Assembly One-Piece	Element Dia. 6.35 mm (0.25 Inch)
Piloting Surface — Outer Ring Lands	Element Length
Pilot Clearance 0.254-0.406 (0.010-0.016)	**Closures**
Total AXIAL Clearance of 0.198 (0.0078) Max Under 1 Lb Gauge Load	Number
	Material
	Construction

	Commercial Pack	Military Spares Pack	
Preservative — MIL-L-6085	See Note 3	See Notes 1 and 3	
AiResearch Part Number	3822082-1		-4

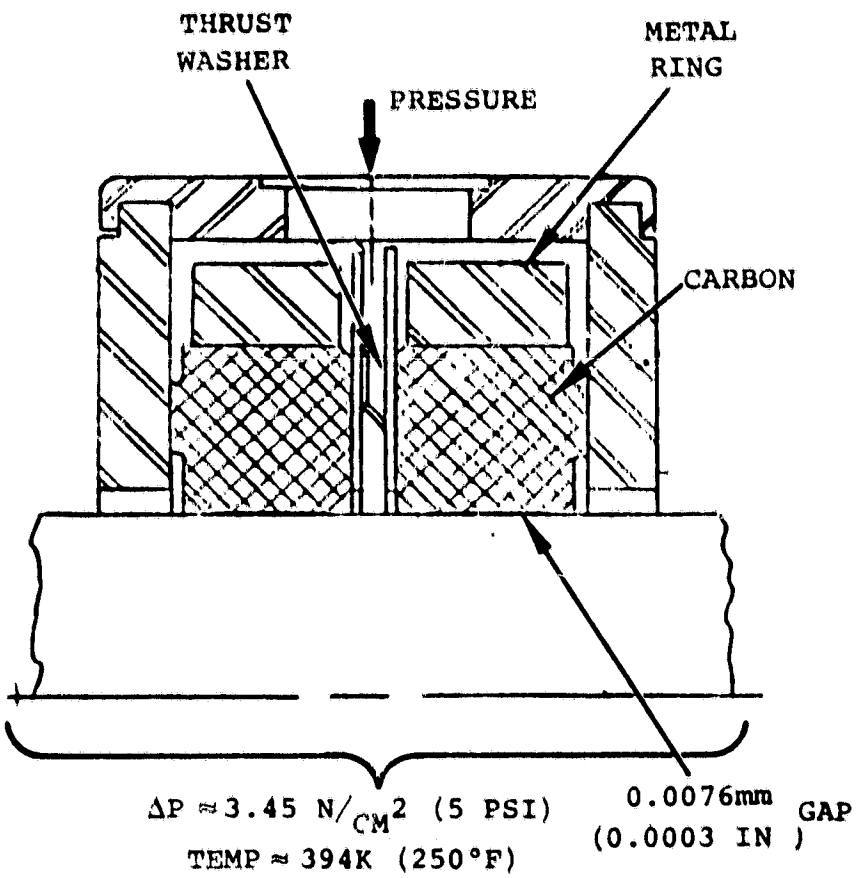

Figure 8. Floating Ring Seal.

ing would operate at 55,000 to 56,000 rpm for 58 percent of the projected 160,934 km (100,000 mile) vehicle life. Bearing lubrication and cooling would be provided by automotive transmission fluid (ATF) jetted into the shaft center and delivered centrifugally to the ball bearing split inner race.

Using a 15 mm (0.59 inch) 202 series bearing, the ball bearing concept provides 221 hours B_1 life operating at 100,000 rpm and an aerodynamic thrust load of 1134.3 N (255 pounds). This thrust load corresponds to design conditions of 302.7K (85°F) ambient temperature and 152.4 m (500 feet) altitude. The bearing would provide 135 hours B_1 life at the maximum thrust load of 1334.5 N (300 pounds), corresponding to low ambient temperature conditions. In either case, the bearing appears adequate for maximum load and speed conditions, since only 12 hours of predicted vehicle engine operation over 160,934 km (100,000 miles) will be at 100,000 rpm and maximum thrust.

The bearing design is shown in Figure 7. The bearing specifications are given in Table 1.

The high speed rotor shaft seal between the gearbox and compressor (Figure 8) is a double floating ring design. Each seal consists of a carbon ring that provides face and bore sealing surfaces. A metallic ring is shrunk on the carbon OD to provide mechanical strength. A spring is placed between the two carbon rings to preload face sealing surfaces. Additional sealing force is provided by a purge air supply between the seals. The air purge feature also prevents any possible oil leakage into the compressor inlet.

As a result of changes required to provide adequate margin between operating and third critical speeds, the foil journal bearing between the turbine and compressor has been increased in diameter 2.54 mm (0.1 inch) to 34.29 mm (1.350 inches). It has been determined that bearing axial length of 27.3 mm (1.075 inch) is adequate for AGT application. Seven overlapping foils of a nominal 0.127 mm (0.005 inch) thickness are recommended for the initial design pending final rotor analysis and design.

2.1.2.5 Ceramic Turbine Shaft Attachment

Two methods of attaching the AGT ceramic turbine wheel to a metallic shaft have been selected for consideration. The shrink-fit concept shown in Figure 9 involves a metallic sleeve shrunk over a ceramic turbine stub shaft. The second concept, shown in Figure 10, incorporates a curvic coupling joint between the ceramic turbine and metallic compressor. The curvic coupling concept has been demonstrated on the Ford 820 turbine attachment, but involves difficult ceramic machining and high local stresses.

The shrink-fit concept appears to offer the most reliable, and ultimately, the lowest cost attachment for the AGT ceramic turbine. Analysis of the concept considered sintered silicon nitride and sintered silicon carbide turbine wheels with thermal expansion characteristics as shown in Figure 11. The IN903 metallic sleeve material was se-

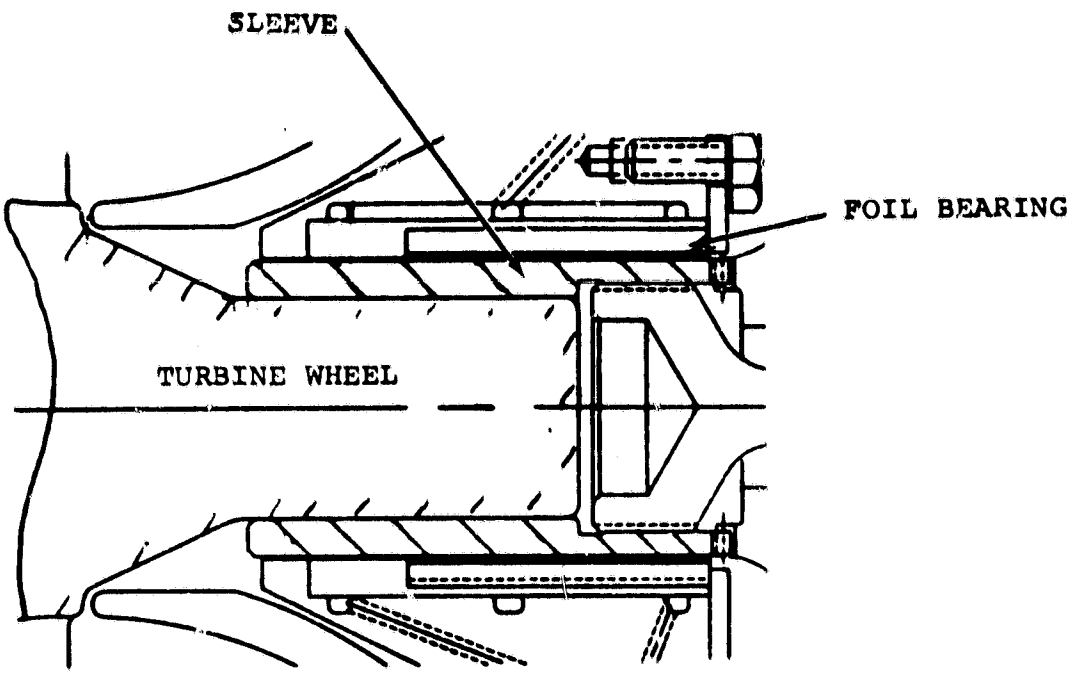

Figure 9. Ceramic Turbine Wheel Sleeve Attachment.

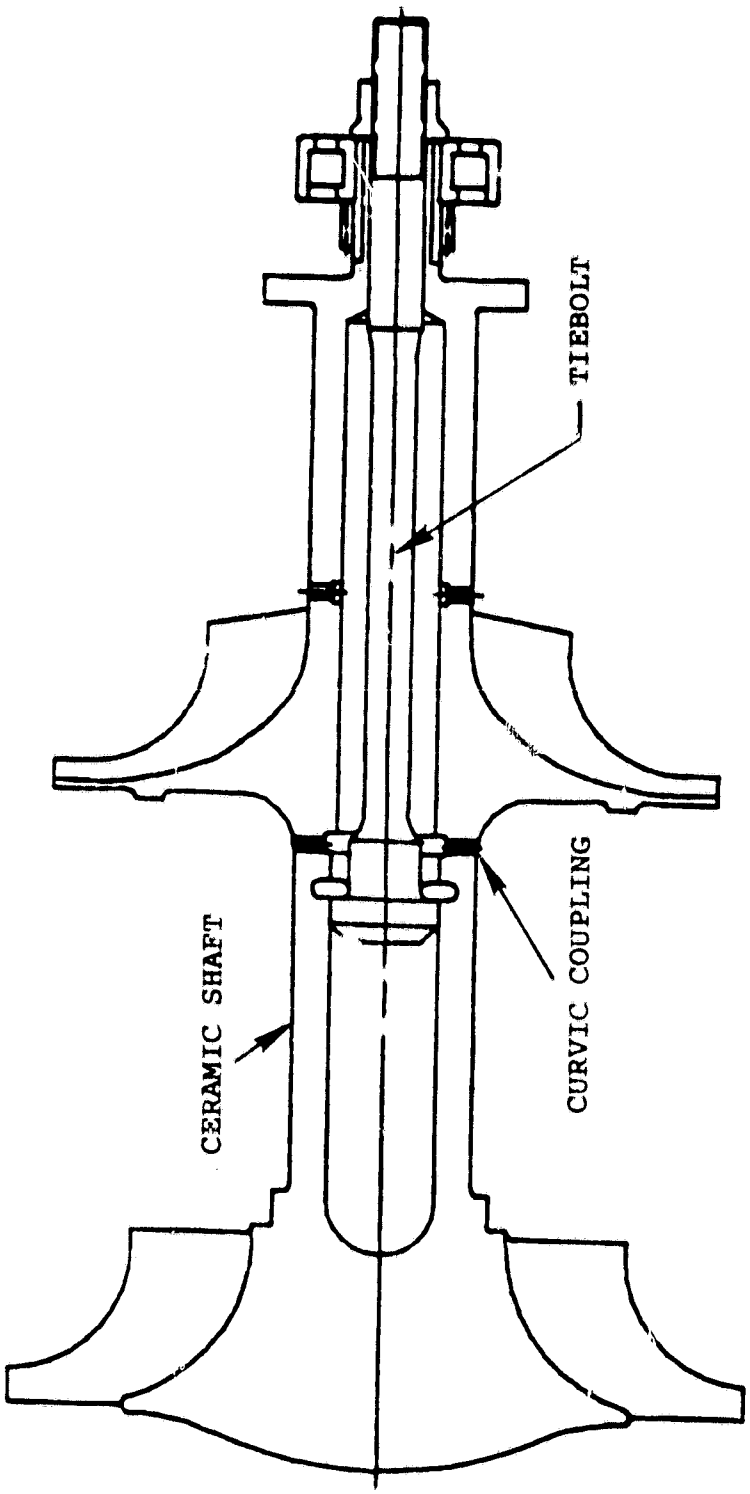

Figure 10. Ceramic Turbine Curvic Attachment.

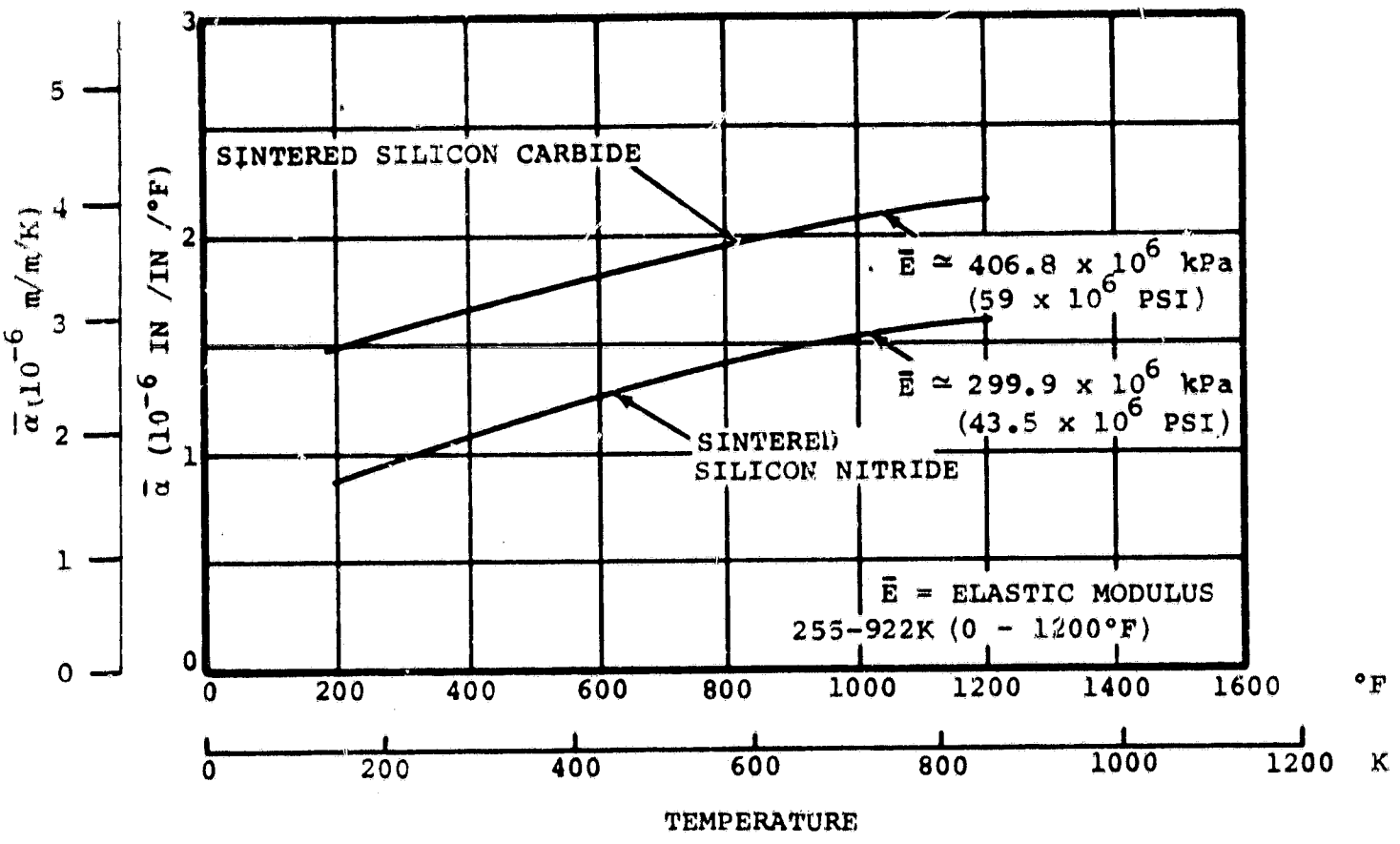

Figure 11. Mean Thermal Expansion Coefficient Turbine Candidate Ceramics.

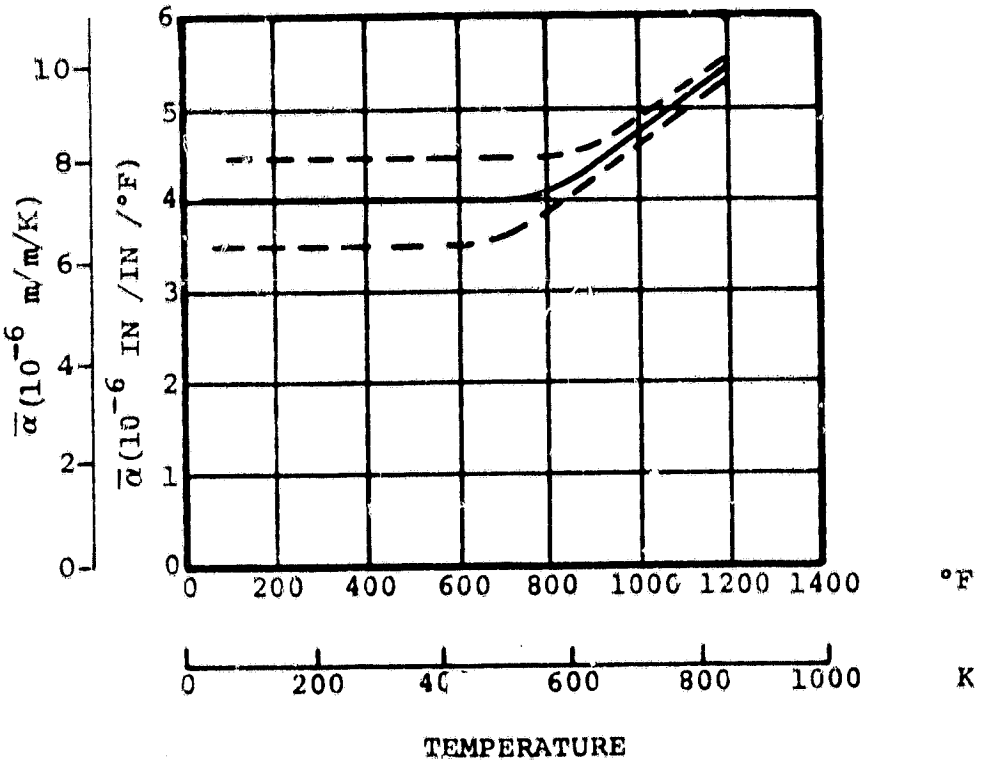

Figure 12. Mean Thermal Expansion Coefficient, IN903.

lected for low thermal expansion characteristics and the physical properties as shown in Table 2 and Figure 12. A nominal 0.051 mm (0.002 inch) room temperature interference between the ceramic stub shaft and mtallic sleeve was selected to permit assembly at 888.5K (1140°F). Analytical evaluation of the shrink-fit concept is in process to determine surface stress distribution.

TABLE 2. INCALOY 903 TENSILE PROPERTIES (TYPICAL).

Temp, K (°F)	α_{YP} 10^5 kPa (10^5 psi)	α_{ULT} 10^5 kPa (10^5 psi)	R.A. (%)
294 (70)	−11.03 (1.6)	13.10 (1.9)	40
922 (1200)	8.96 (1.3)	10.00 (1.45)	55

2.1.2.6 Thermal and Structural Analysis

Thermal grids were developed for an AGT power section structure and rotating group. Results were used to generate boundary conditions, and thermal and stress grids for the structure. These results were then used in the thermal and stress analyses.

Structure steady-state thermal and stress analyses were conducted at maximum power and idle power conditions, with and without thermal insulation.

Similarly, rotating group temperatures were determined for 1644K (2500°F) and 1422K (2100°F) turbine inlet temperatures; i.e., ceramic turbine and dual alloy metal turbine inlet temperatures, respectively.

2.1.2.7 Static Structure Thermal Analysis

Figure 13 illustrates a typical thermal grid network used in static structure analyses. Housings modeled included the intake plenum, compressor diffuser, outer die cast housing, turbine housing, turbine shroud and diffuser, turbine discharge housing, turbine back shroud, combustor baffle and transition housings, and foil bearing housing. Figure 13 includes fibrous high temperature insulation in the cavities between the combustor baffle and turbine back shroud, and between the turbine discharge housing and compressor diffuser ducts.

The models incorporated appropriate boundary conditions, as required, for the insulated and uninsulated analyses, including gas temperatures and temperature gradients, flow rate distributions, heat transfer coefficients, and free convection and radiation between housings without insulation for both maximum power and idle conditions. In addition, heat generated by the foil bearing for the two power conditions was shared equally in the model by the bearing housing and journal.

ORIGINAL PAGE IS
OF POOR QUALITY

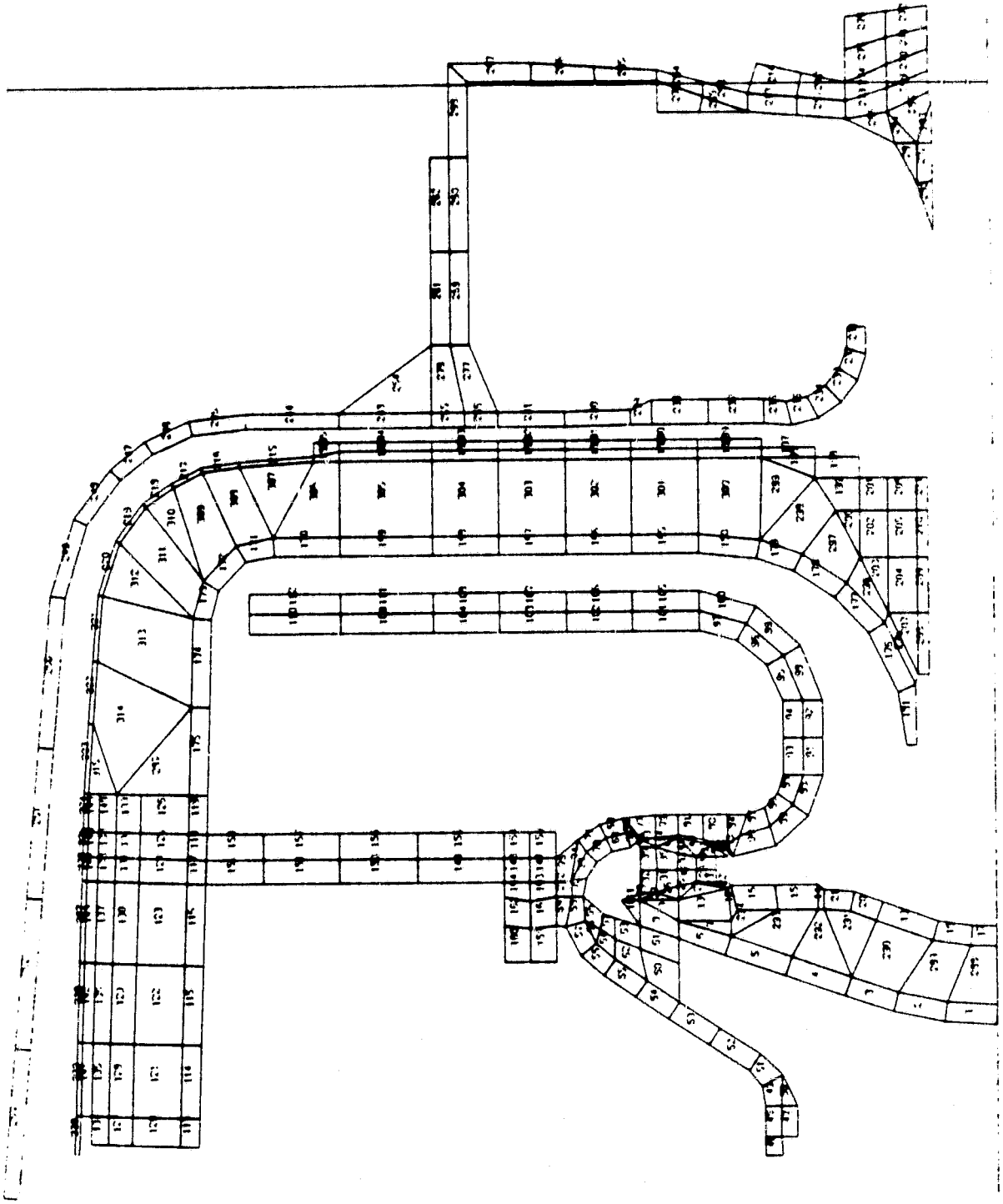

Figure 13. Thermal Grid of Static Structure with Insulation.

2.1.2.8 Steady State Temperatures

The analyses revealed that the uninsulated structure would not be satisfactory. The use of insulation is necessary to reduce thermal loads into the turbine rotor and foil bearing housing, and reduce thermal gradients across the turbine exhaust housing and LAS flow separator housing. For these reasons only the insulated configuration, Figures 14 and 15, is presented. These figures are thermal maps for the maximum power and idle power conditions, respectively.

Maximum temperatures throughout the structure for the two steady state operating conditions were found to be at acceptable levels for the materials used, except for the compressor inlet and diffuser housing. Based on these results the use of cast iron for compressor inlet and diffuser housings is currently being investigated.

Rotating group thermal maps for the 1644K (2500°F) turbine inlet temperature are given in Figures 16 through 19.

In addition, preliminary results have been obtained for interaction between the stationary and rotating parts of the foil bearing. These results are shown in Figure 20.

2.1.2.9 Ceramic Structures

Preliminary 2-dimensional stress and deflection analyses were completed for the selected RPD major ceramic structural components (see Figure 21). No major structural or thermal problems were revealed except for the turbine shroud (Figure 22) which had significant mechanical and thermal deflection. This deflection would cause variation in the turbine-to-shroud clearance and subsequent performance variation. Therefore, the housing was modified to the configuration shown in Figure 23.

Maximum power rotating group clearances have been calculated for the modified turbine shroud duct with an aluminum and cast iron compressor inlet housing and are given in Figures 24 and 25, respectively.

Evolution of ceramic components to the configuration shown in Figure 26, as compared to the reference configuration, has been the result of thermal and structural analyses, gas path aerodynamic improvements, ceramic material technology limitations, regenerator growth, and engine assembly considerations.

Further evolution of existing geometries is anticipated. In particular, this will involve the flow separator housing, combustor outer discharge housing, combustor baffle turbine nozzle, turbine back shroud, turbine outer and inner diffuser housings, and combustor. The same factors as discussed previously will govern these changes.

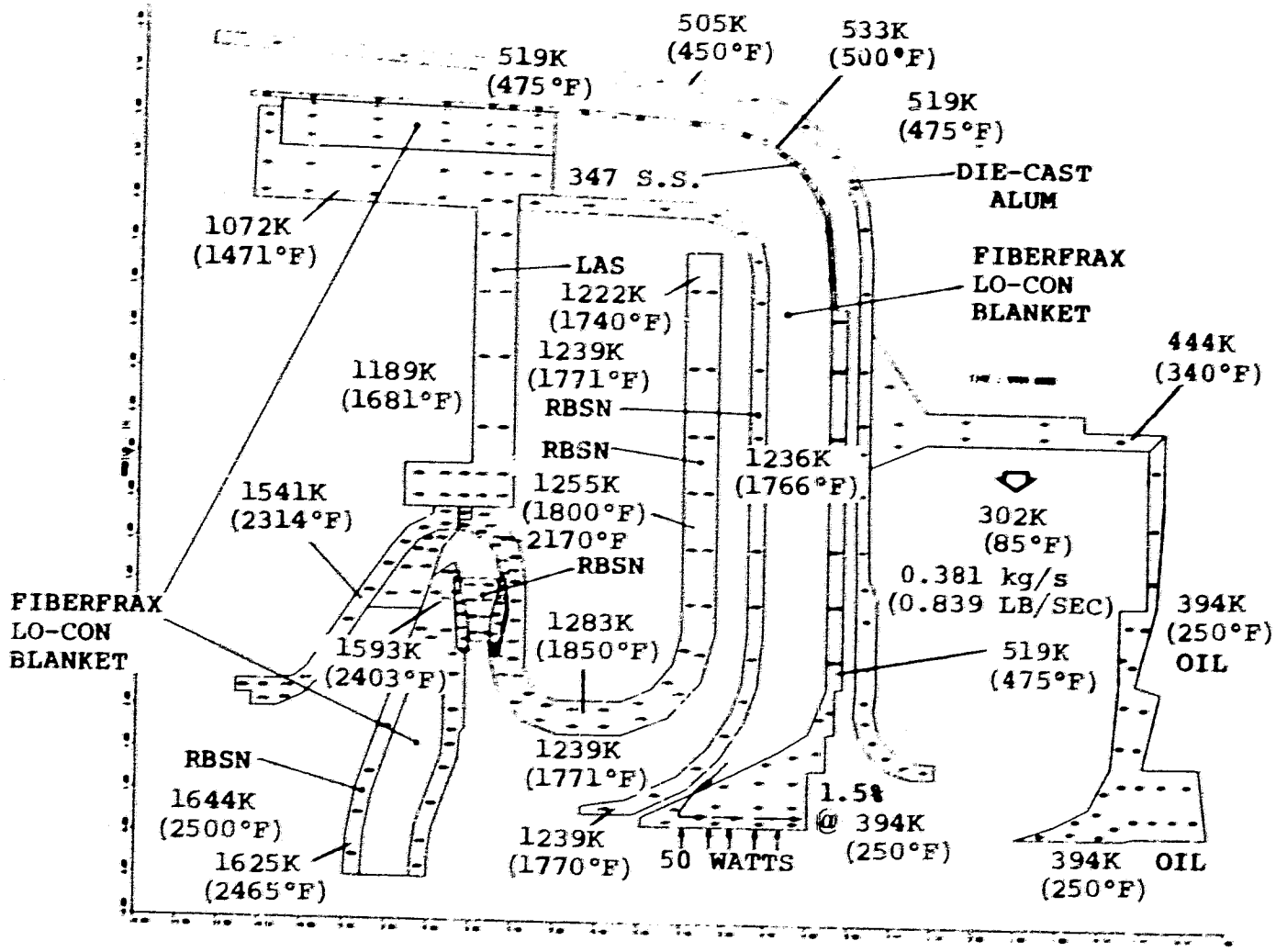

Figure 14. Temperature Distribution in Static Structure with Insulation at Maximum Power.

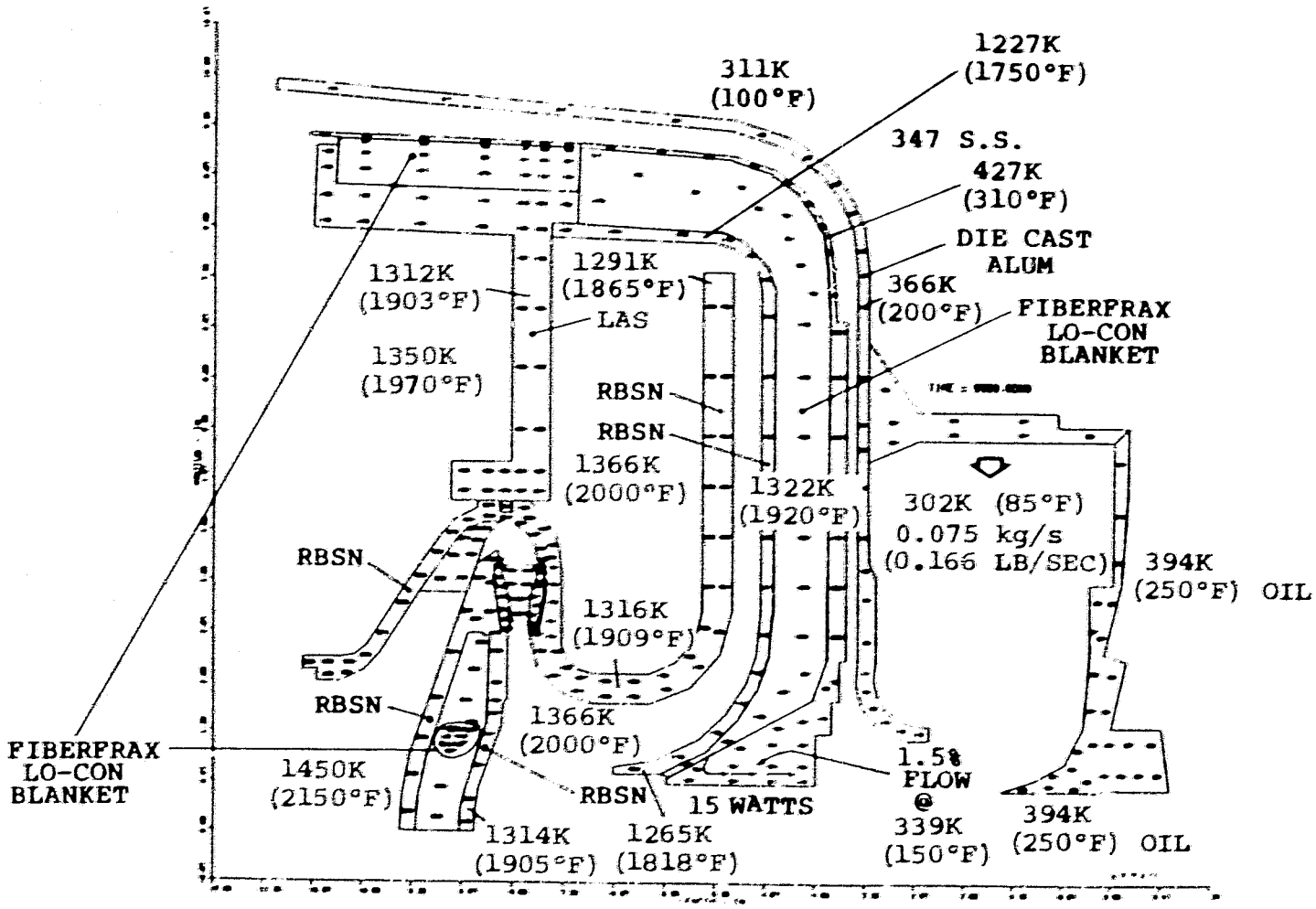

Figure 15. Temperature Distribution in Static Structures with Insulation at Idle Power.

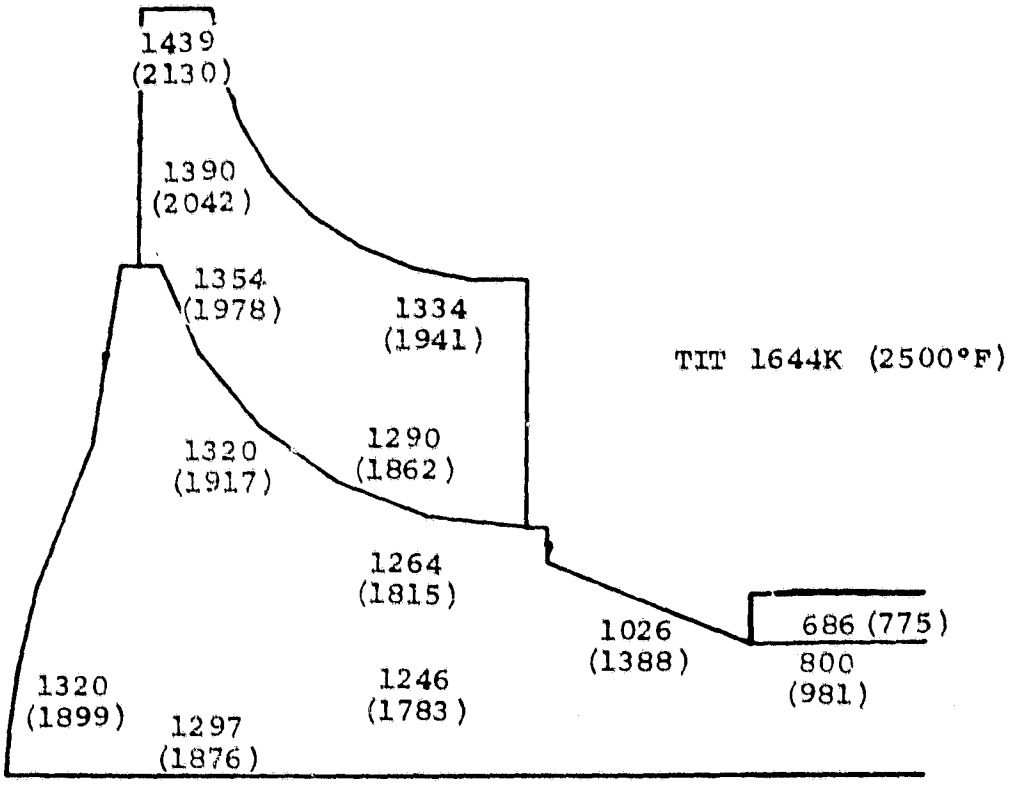

Figure 16. Thermal Map of Turbine Rotor.

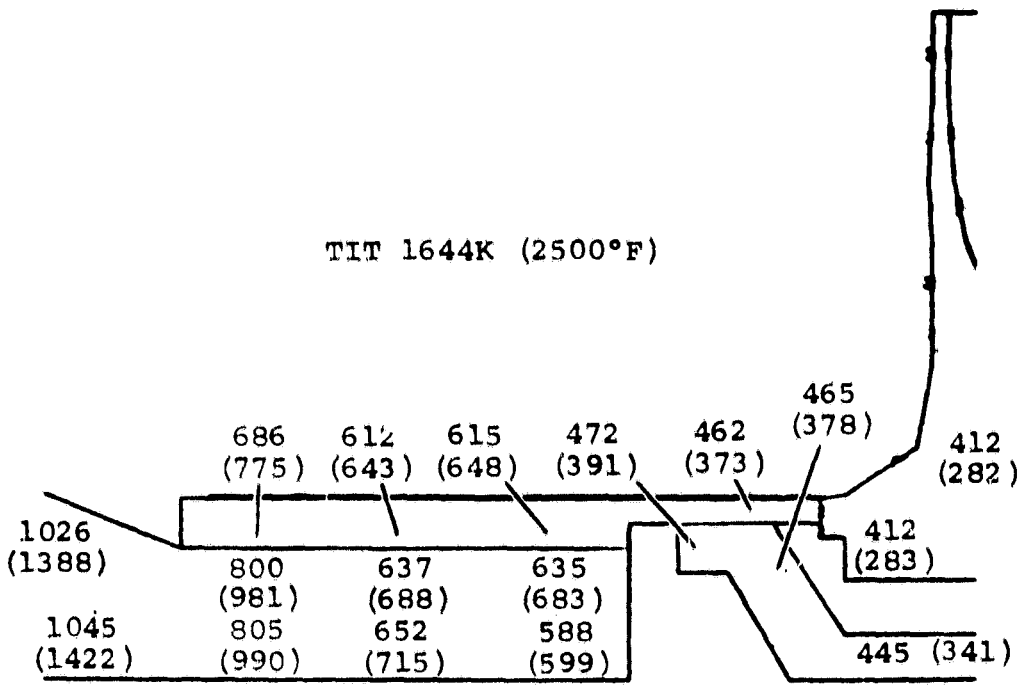

Figure 17. Thermal Map of Foil Bearing.

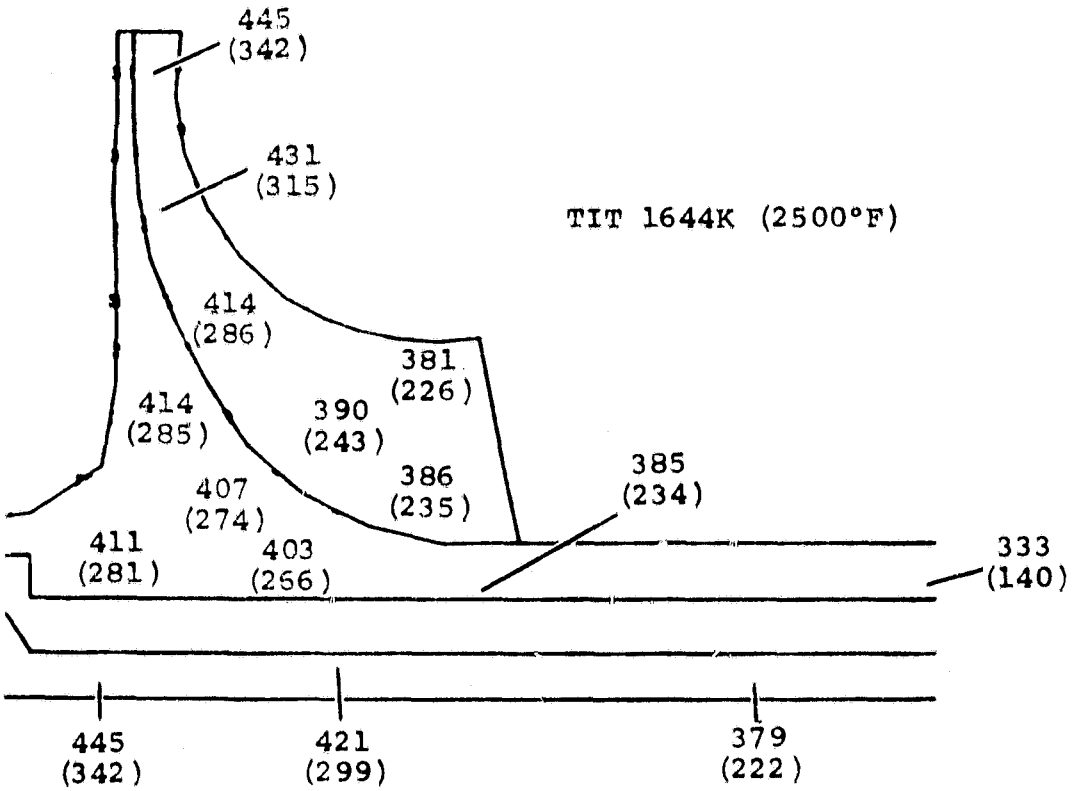

Figure 18. Thermal Map of Compressor Impeller.

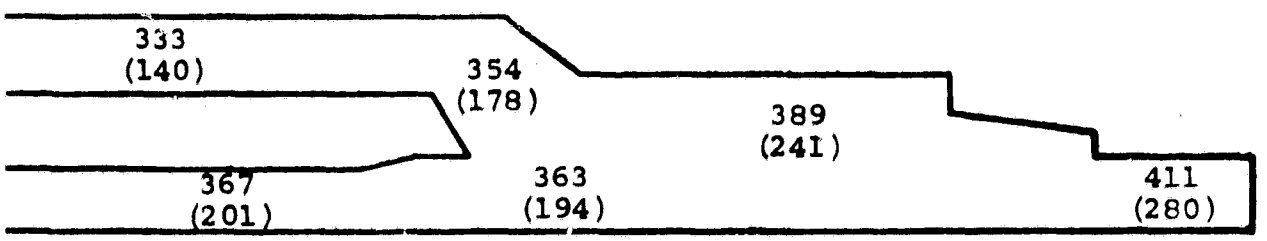

TIT=1644K (2500°F)

Figure 19. Preliminary Thermal Map of Shaft (Output End).

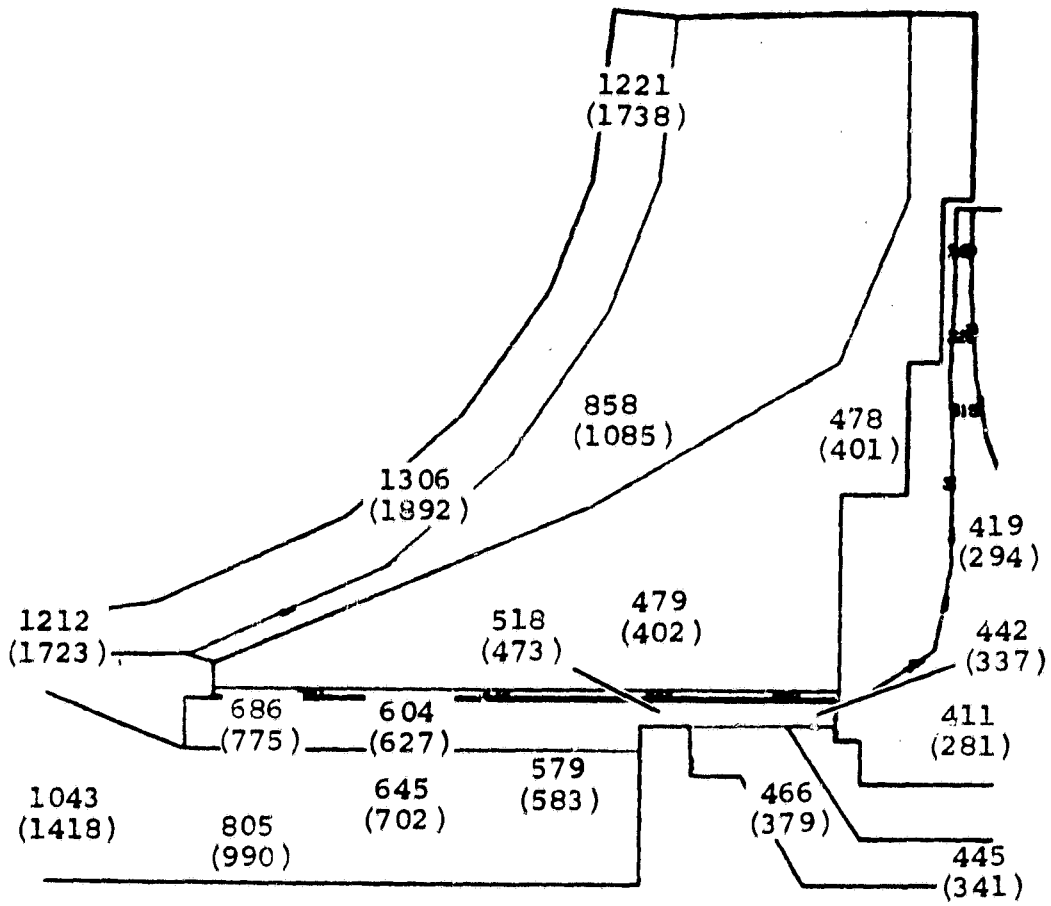

Figure 20. Foil Bearing — Junction Steady-State Temperatures At Maximum Power.

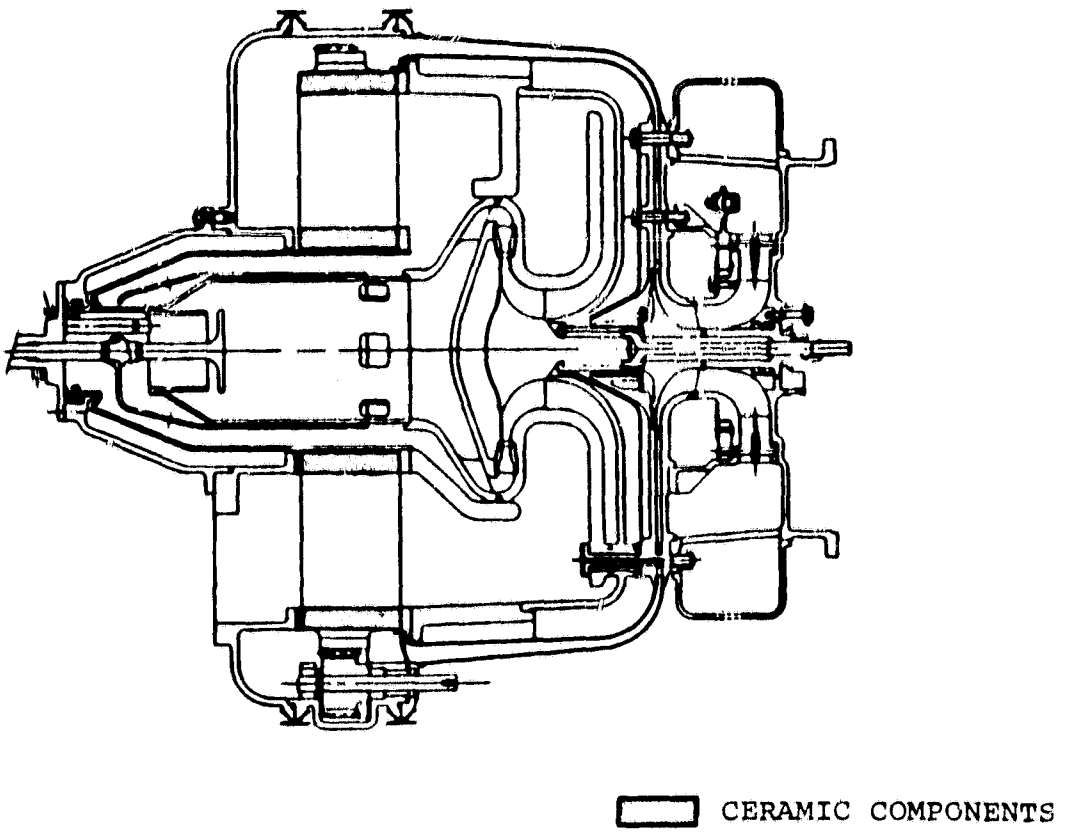

Figure 21. Preliminary AGT Engine.

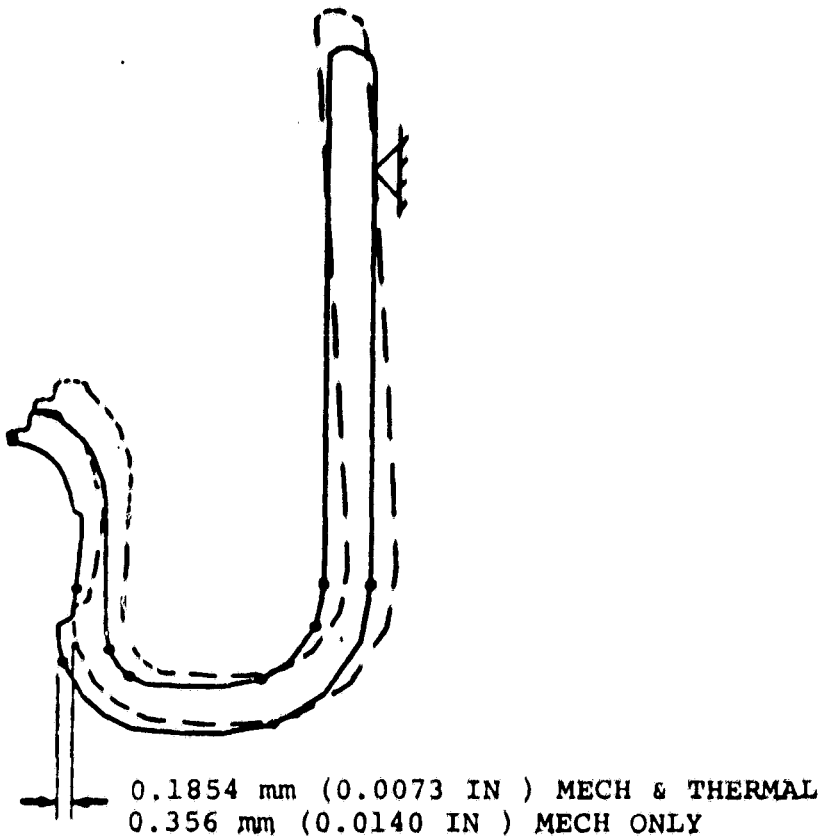

Figure 22. Initial Design Turbine Shroud Deflection.

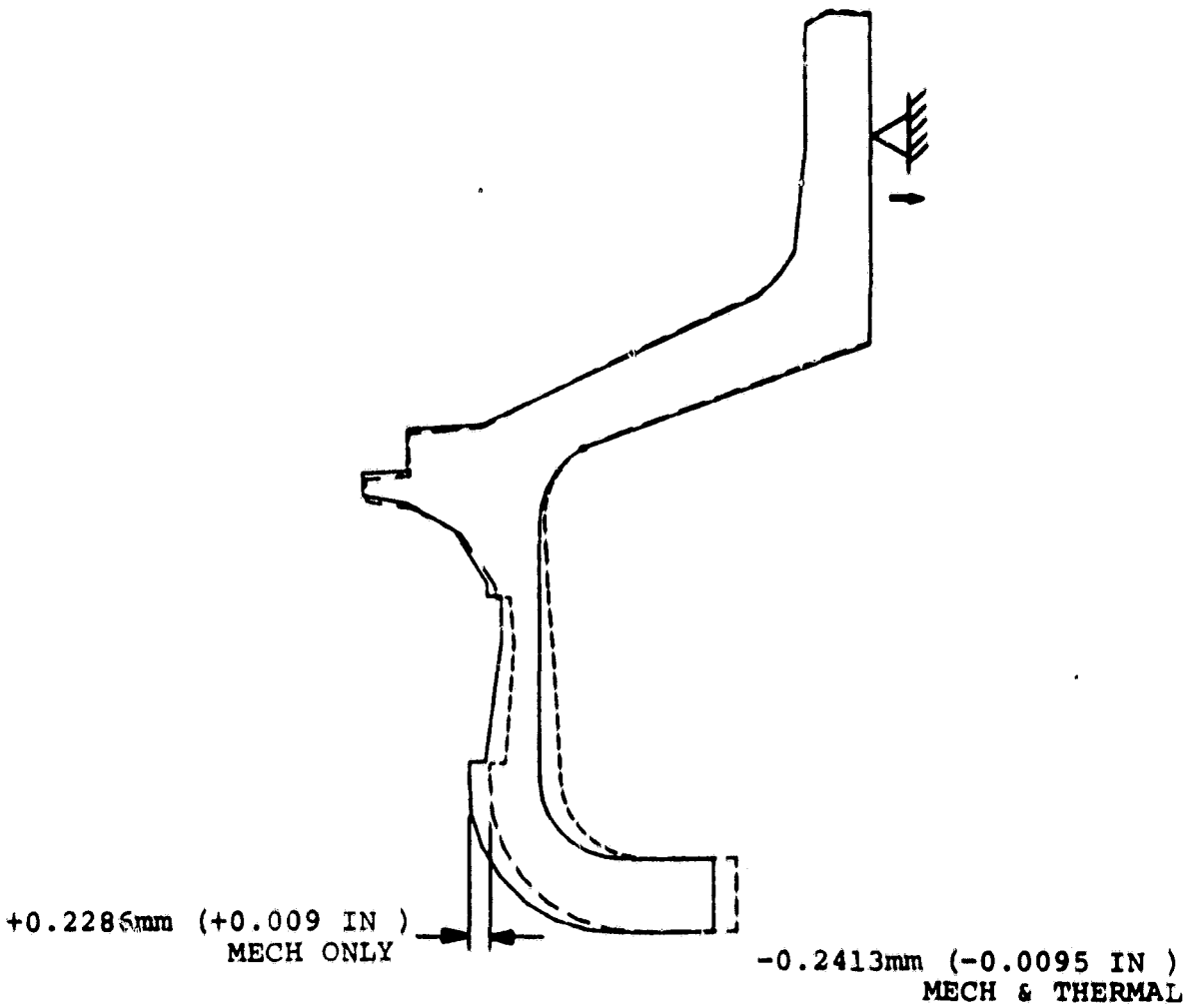

Figure 23. Modified Turbine Shroud.

2.1.3 Gearbox

During evaluation of RPD over the CFDC with the differential gearbox, the VSTC is required to operate briefly under a negative speed ratio during the first 6.4 to 9.7 km/h (4 to 6 mph) of vehicle speed. Specific VSTC characteristics under negative speed ratios could not be confirmed during the study. As a consequence, a second gearbox configuration with a variable speed gearbox not requiring negative speed ratios is being investigated. Preliminary analysis has indicated that either configuration meets the performance goals.

2.1.3.1 Differential VSTC Gearbox

The differential VSTC gearbox is shown in Figure 27. A schematic of the final recommended configuration is shown in Figure 28 and defines the gear sizes, tooth numbers, ratios, and range of speeds for the various components.

The following features reflect the current design:

- Carrier planet center distance was decreased to as small a dimension as possible to decrease planet bearing centrifugal loads and provide an increased ratio down to the FIOD input. The first mesh ratio was changed to 11.2727 from 11.00 to eliminate high common factors in this critical mesh. Planet clearance was maintained

- Diametral pitch of the first mesh was increased to 28.7 to allow sufficient wall thickness under the high speed pinion teeth and enough inside diameter to fit on the main rotor shaft with the 202 series ball bearing. The 28.7 diametral pitch was also selected to achieve the proper planet center distance with the compound planet and ring gear

- A tooth tip compressive stress problem with the 14-tooth planet at low vehicle speeds and high torque ratios was solved by a change to 16 teeth. This changed the 'R' ratio (fixed carrier compound ratio) from 47.8571 to 47.5114

  These small ratio changes were largely compensated for by adjustment of the reversing 'X' ratio on the torque converter input side. This is a fixed carrier planetary with the reduction ratio changed to 2.2143 from 2.2449. The sun gear was maintained large enough to clear the modulating clutch outside diameter

  Face width is critical only at the small 16-tooth planet gear where 14.5 mm (0.57 inch) maximum was used. This is approximately one pitch diameter. The high speed pinion face width is 6.35 mm (0.25 inch)

- High loading and the need for extreme light weight dictates carburized AISI 9310 material for the rotating carrier planet gears. In addition, the high speed pinion and small ring gear will be carburized steel. All other gears may be induction hardened or through hardened AISI 4340 or equivalent

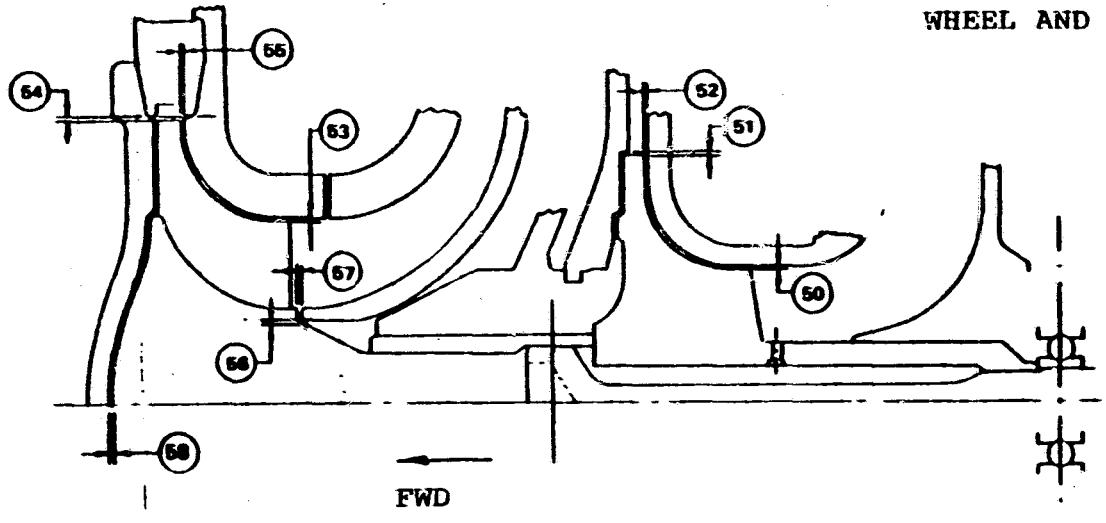

RELATIVE GAPS FOR AGT

RELATIVE THERMAL GROWTHS WITH Si_3N_4 TURBINE WHEEL AND A356 ALUMINUM INLET HOUSING

	MAX POWER POINT		
NO	IN		mm
50	0.0013	CLOSES	0.0330
51	0.0021	OPENS	0.0533
52	0.0111	CLOSES	0.2819
53	0.0023	CLOSES	0.0584
54	0.0034	CLOSES	0.0864
55	0.0094	CLOSES	0.2388
56	0.0009	CLOSES	0.0229
57	0.0055	CLOSES	0.1397
58	0.0089	OPENS	0.2261

Figure 24. Design Rotor Clearances.

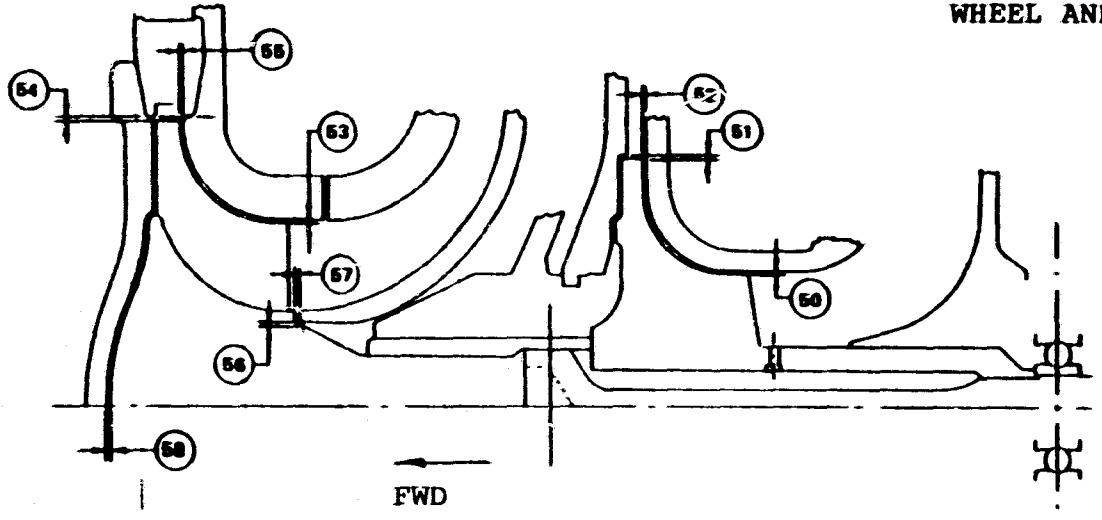

RELATIVE GAPS FOR AGT

RELATIVE THERMAL GROWTHS WITH Si_3N_4 TURBINE WHEEL AND CAST IRON INLET HOUSING

	MAX POWER POINT		
NO	IN		mm
50	0.0013	CLOSES	0.0330
51	0.0021	OPENS	0.0533
52	0.0080	CLOSES	0.2032
53	0.0023	CLOSES	0.0584
54	0.0034	CLOSES	0.0864
55	0.0063	CLOSES	0.1600
56	0.0009	CLOSES	0.0224
57	0.0055	CLOSES	0.1397
58	0.0120	OPENS	0.3048

Figure 25. Design Rotor Clearances.

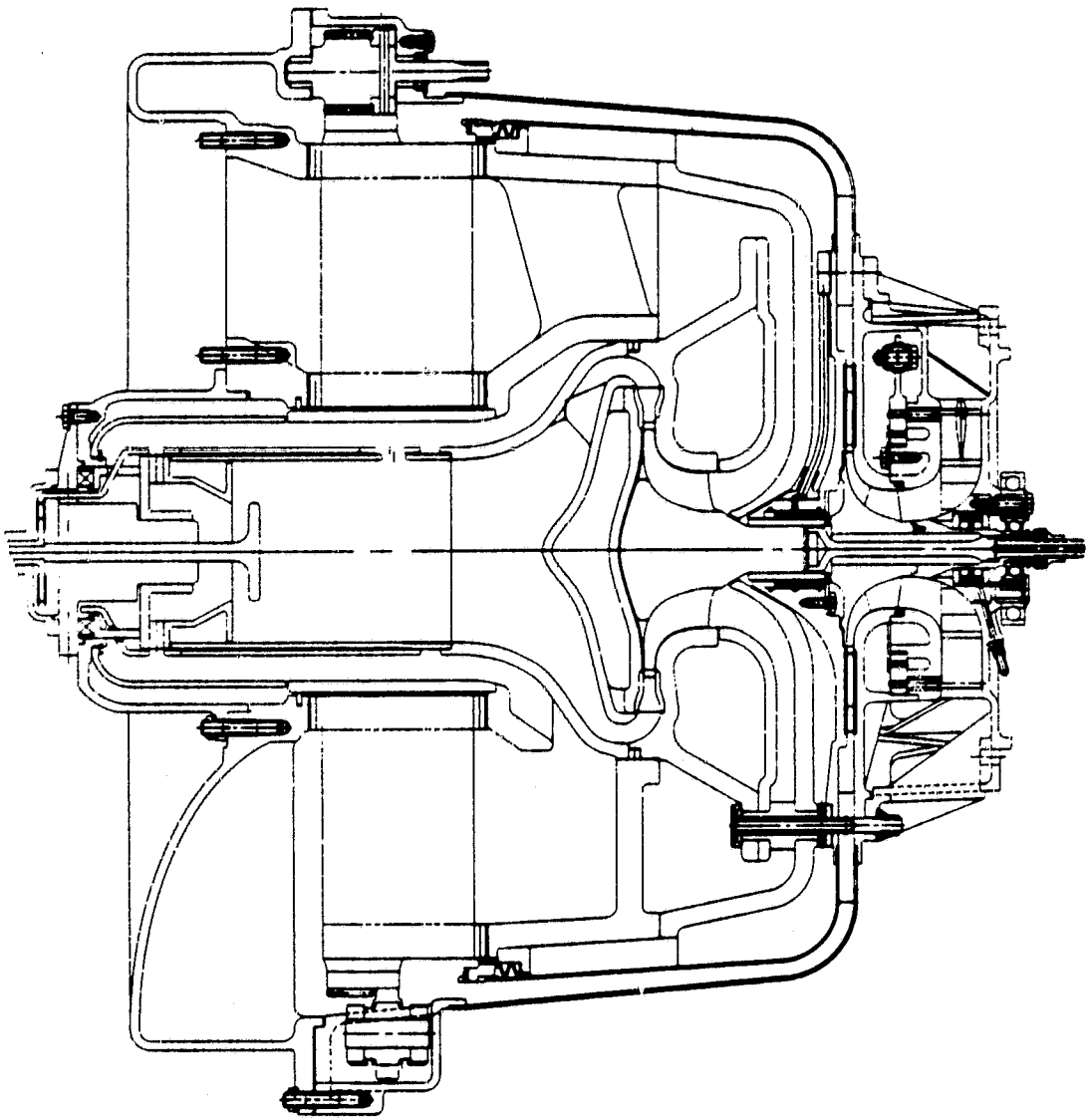

Figure 26. AGT Power Section.

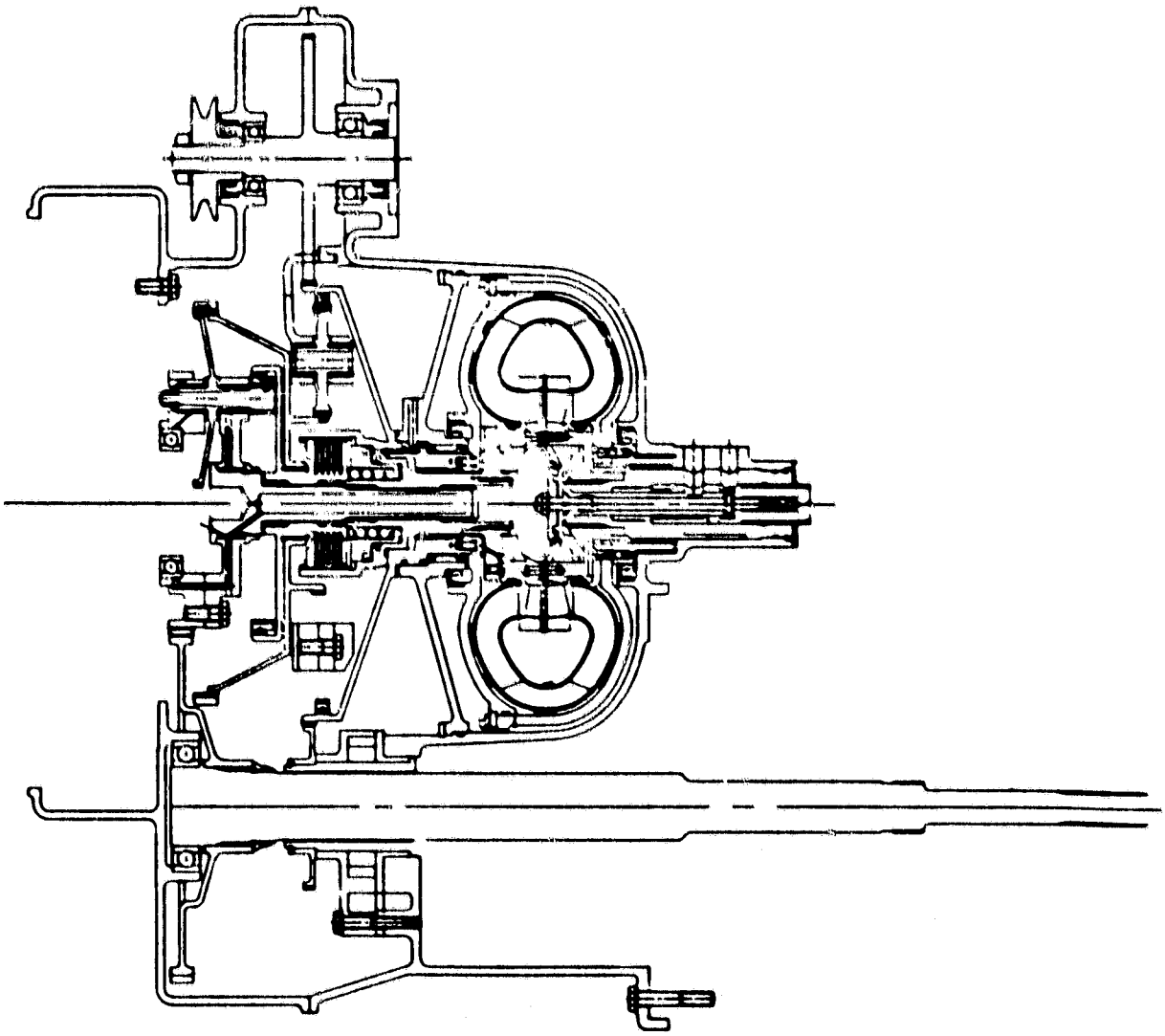

Figure 27. Differential VSTC Gearbox.

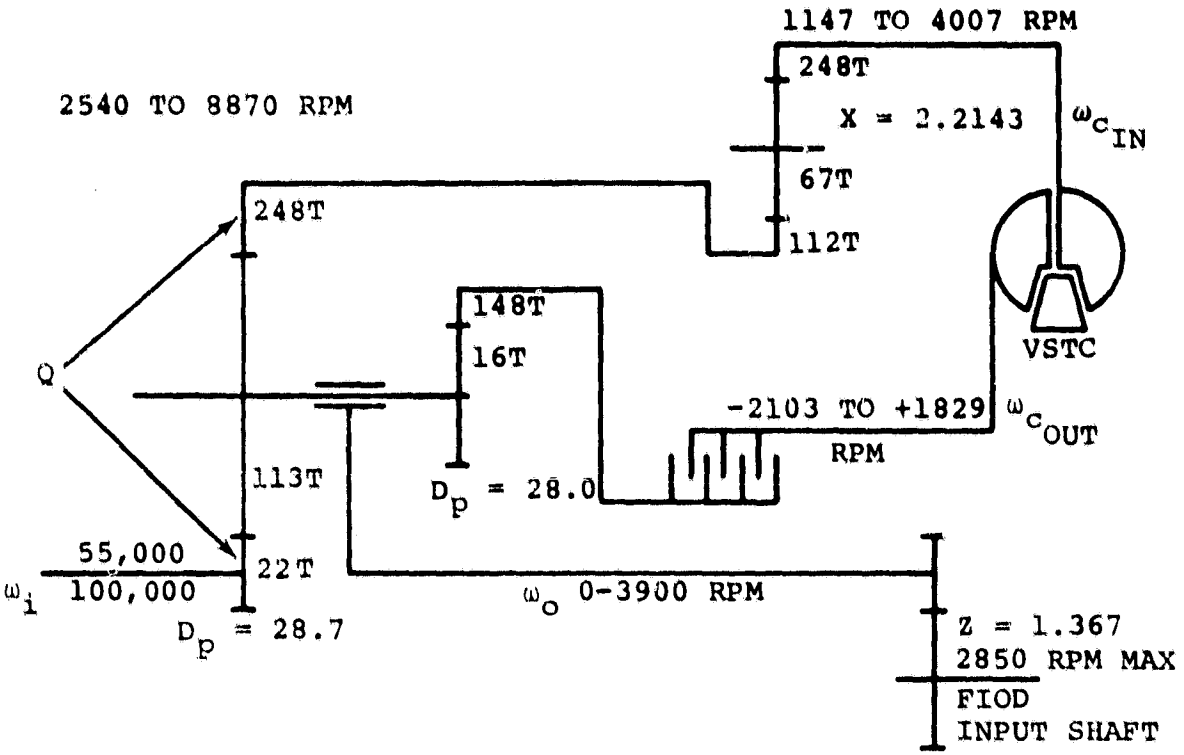

R = COMPOUND RATIO 113/22 X 148/16 = 47.5114
Q = RING GEAR/PINION 248/22 = 11.2727
X = REVERSING RATIO 248/112 = 2.2143
NEGATIVE SPEED RATIO (ω_o = 0) = -0.5253
SPEED RATIO (VSTC) SR = $\omega_{e_{in}} / \omega_{e_{out}}$

$$\frac{\omega_i}{\omega_o} = \frac{R\,(Q+1)\,SR + QX\,(R+1)}{R\,(SR) + QX}$$

D_p = DIMETRAL PITCH

Figure 28. Differential VSTC Gearbox.

- The 'Z' ratio (gearset between differential output and FIOD input) was designed as a 15 diametral pitch helical mesh with a helix angle of approximately 23 degrees. A gear face width of 13.2 mm (0.52 inch) assures an overlap ratio of exactly one, precluding axial load shift through the plane of action

- Critical bearings were analyzed for 100-hour test conditions at the most severe loadings. Needle bearings supporting the planets will provide sufficient life at the highest carrier speed of 3937 rpm. Hollowed shafts and holes in the planet gears will be utilized for weight reduction

- The 'Z' ratio gears, one on the carrier and one on the FIOD input shaft, are adequately supported on ball bearings that react to the helical gear thrust

2.1.3.2 Split Path VSTC Gearbox

The alternate split path VSTC gearbox is shown in Figure 29. A schematic of the configuration is shown in Figure 30. The split path design differs from the differential design primarily in the path the VSTC power is returned to the output shaft of the gearbox. In the split path design, a portion of the input power is delivered to the single compound planetary ring gear, through the 'X' ratio reversing gear set into the VSTC and to the output shaft via a clutch. The balance of the input power is transmitted directly into the planetary carrier and output shaft.

In the differential VSTC design, input power is also split into two paths. One power path is through one of two ring gears meshing with the compound planetary, through the VSTC, a clutch, and then back into the compound planetary via the second of the two ring gears. The balance of the input power is transmitted into the planetary carrier and output shaft as in the differential design.

The split path design incorporates a compound planetary gearset with a compound ratio of 14.52:1 as compared to a ratio of 47.5:1 for the differential gearbox. The lower numerical compound ratio results from use of larger compound planet gears with corresponding lower stresses. The first mesh of high-speed pinion and planet gears was made identical to the initial differential gearbox design to facilitate early performance comparisons of the two gearbox designs. Optimization of the split path design would ultimately result in equalizing the compound planetary ratios so that the first mesh would be approximately 4:1 instead of the 5:1 shown on the schematic. This change would reduce the carrier diameter and gear stresses.

2.1.4 Transmission

A modified FIOD automatic 4-speed transmission with the variable speed gearbox provides a close approximation of an infinitely variable transmission required for single-shaft gas turbine vehicle engines. Modifications to the FIOD would include:

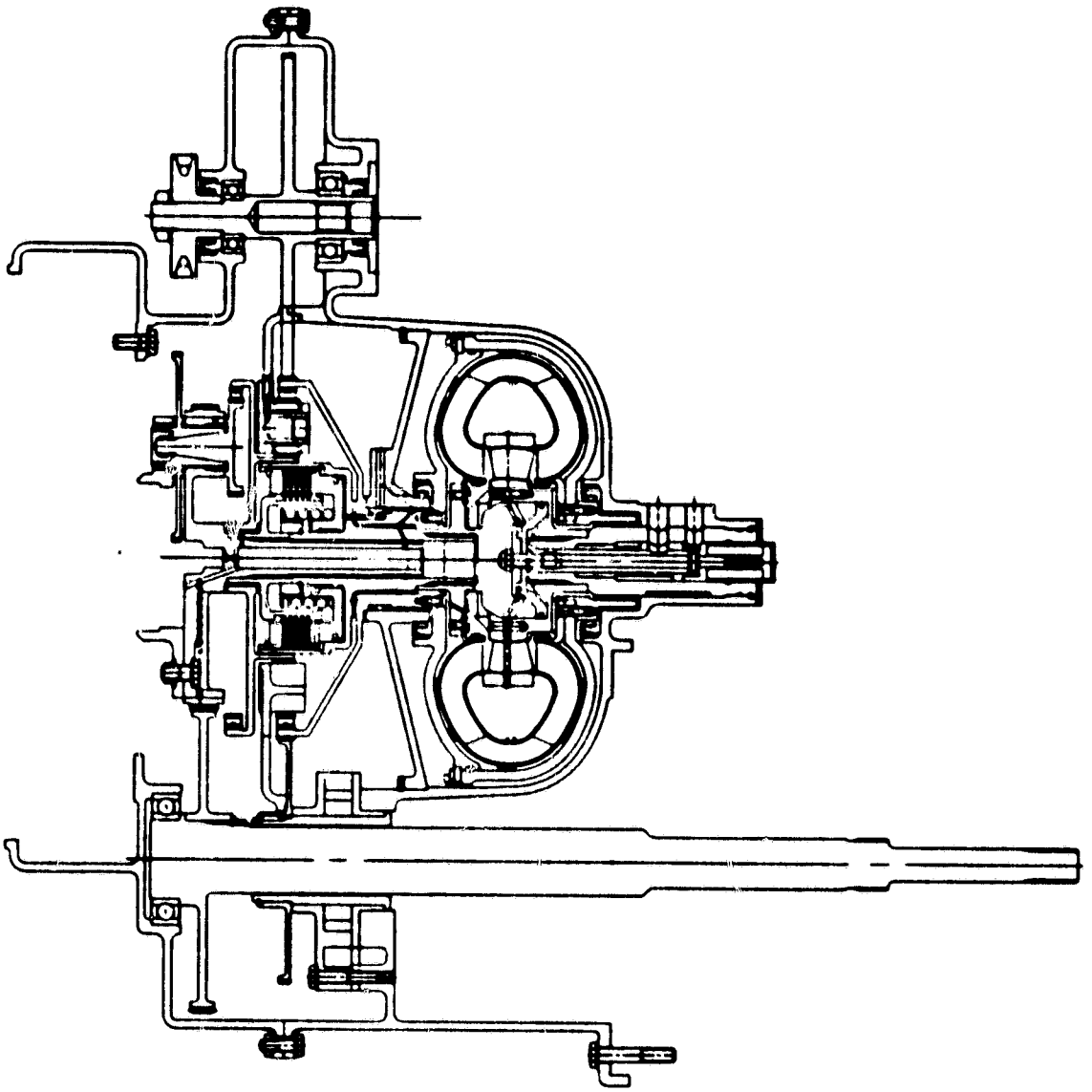

Figure 29. Split Path VSTC Gearbox.

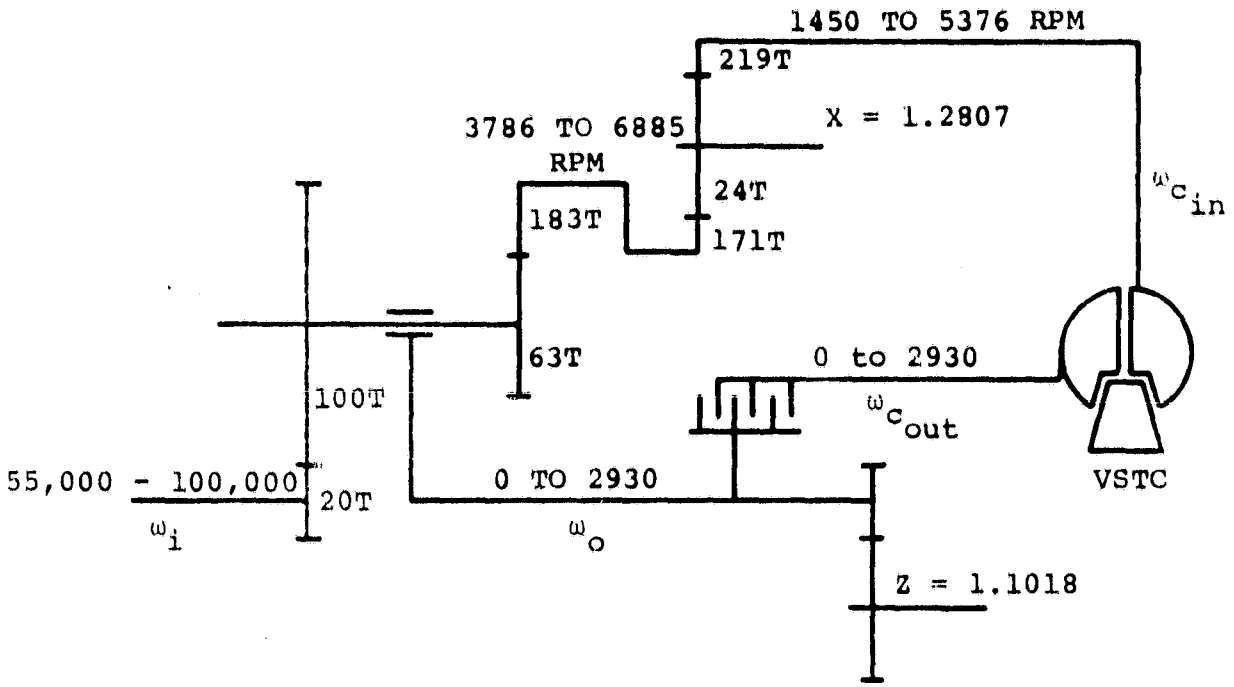

R = COMPOUND RATIO = 100/20 X 183/63 = 14.5238

SPEED RATIO (VSTC) SR = $\omega_{c_{out}} / \omega_{c_{in}}$

X = REVERSING RATIO = 219/171 = 1.2807

$$\frac{\omega_i}{\omega_o} = R\ (1 + X/S\ R\ ) + 1$$

Figure 30. Split Path VSTC Gearbox.

- Fixed stator torque converter removal
- Transmission bell housing removal and adaptation to gearbox case
- Transmission control and shift logic integration with AGT control microprocessor
- Gearbox and FIOD lubrication systems integration

The FIOD transmission is a fully developed production transmission currently used in 1980 Ford vehicles. No other modifications would be required.

2.1.5 Controls Analysis

2.1.5.1 Control System Analysis

The control system defined for the AGT is shown schematically by Figure 31. The system was programmed for dynamic computer studies of the powertrain vehicle operating system. Some temporary simplifications were made to expedite operation of the computer model along with changes to improve computer operation.

2.1.5.2 Controls Model

The logic incorporated into the model is essentially that described in the prior study, with the following exceptions:

- Engine characteristics are defined as algorithms rather than by partial derivatives to provide better accuracy from the design points and is more efficient with respect to computer time
- Variable combustor geometry is not included
- Only a simplified shift logic is presently incorporated in the program
- No active power split logic is included in the model. However, a passive power split exists in which VSTC vanes are controlled as a function of temperature (either TIT or regenerator, whichever is closer to the limit)
- A major deviation from the prior study incorporates a clutch adjacent to the torque converter turbine. This was determined to be necessary for the differential gear system operating at idle and at very low vehicle speeds due to the high torque converter drag on the engine. The computer logic is for the clutch to slip at engine speeds less than 54.5 percent and temperatures in excess of the set points (i.e., turbine inlet and regenerator temperature set points)

2.1.6 Cycle Analysis

The RPD engine cycle analysis has been completed for maximum power and a vehicle cruise condition of approximately 64.4 km/h (40 mph) and is shown in Figures 32 and

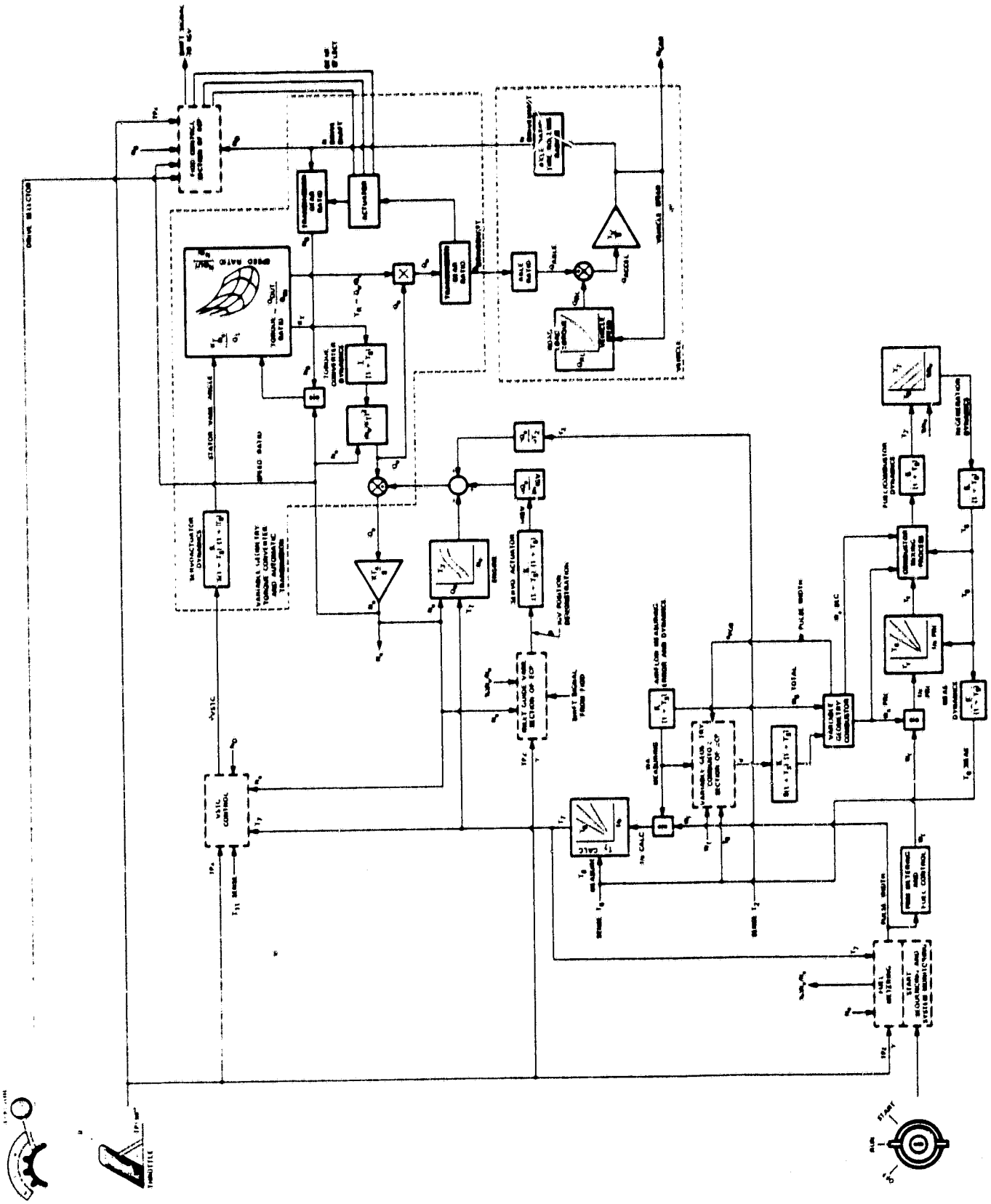

Figure 31. AGT System Control Schematic.

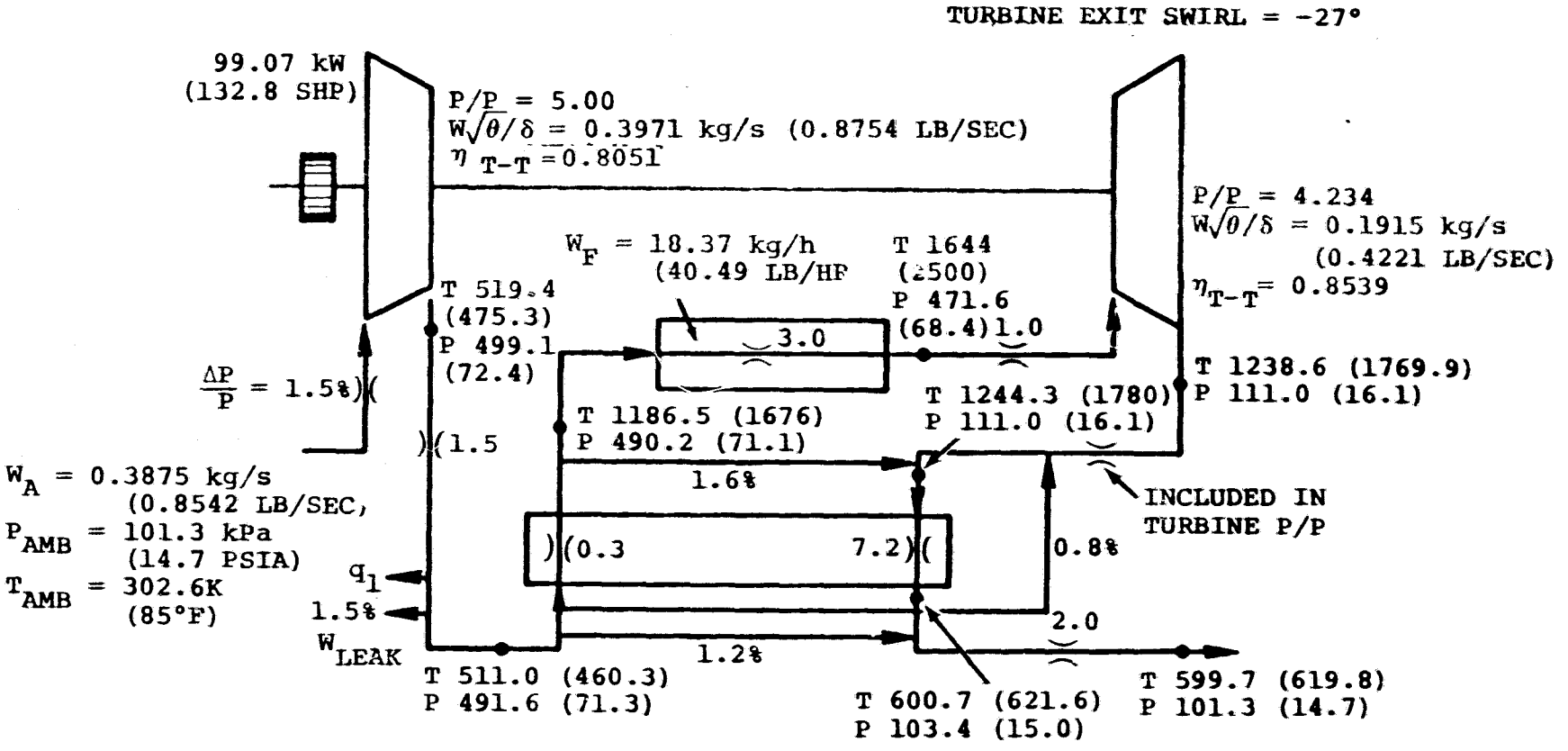

q_1 = SKIN HEAT REJECTION 3122.8 J/s (2.96 BTU/SEC)

T K(°F)
P KILOPASCALS (PSI)

Figure 32. Maximum Power Operating Condition — AGT Engine.

33, respectively. The cycle was established using a −27 degree turbine exit swirl design, which provides the best driveability measured by the 4 second distance.

The engine provides a nominal 96.94 kw (130 horsepower) into the gearbox under maximum power conditions obtained at 100,000 rpm turbine speed. Compressor mass flow is 0.39 kg/sec (0.85 lb/sec) with a 5:1 pressure ratio. The turbine operates at 1644K (2500°F) TIT with a regenerator inlet temperature of 1244K (1780°F).

The cruise condition cycle provides approximately 11.19 kw (15 hp) with a compressor mass flow of 0.13 kg/sec (0.28 lb/sec) and a pressure ratio of 1.72. Regenerator inlet temperature limits of 1366K (2000°F) cause the turbine to operate at 1516K (2270°F) under this cruise condition.

RPD engine specific fuel consumption (sfc) characteristics are shown in Figure 34. Engine power up to 13.42 kw (18 horsepower) can be obtained with a turbine idle speed of 55,000 rpm by modulating only the compressor inlet guide vanes (IGV). Power requirements above 13.42 kw (18 horsepower) require an increase in turbine speed and IGV modulation. A specific fuel consumption under 0.30 is obtained at power levels between 27.59 and 82.03 kw (37 and 110 horsepower). Approximately 7.46 kw (10 horsepower) can be obtained at a specific fuel consumption of 0.61 mg/J (0.36 lb/hr-shp).

2.1.7 Vehicle Performance

Vehicle performance was established for the AGT engine using both the differential VSTC and split-path VSTC gearboxes. Vehicle rear axle ratios were selected to provide the best performance for each type of gearbox. A comparison of the CFDC mileage, 4-second distance, and 0 to 96.6 km/h (0 to 60 mph) acceleration time for each gearbox design is given in Table 3. Performance was established for a 1434.7 kg (3163 pounds) gross vehicle weight.

TABLE 3. AGT PERFORMANCE COMPARISON 1435 kg (3163 LB) GVW

GEARBOX TYPE	REAR AXLE RATIO	VEHICLE DESIGN SPEED km/H (MPH)	CFDC RUEL ECON km/LITER (MPG)	4-SECOND DISTANCE METERS (FEET)	0-96.6 km/H (0-60 MPH) ACCELERATION TIME (SECONDS)
Differential VSTC	3.08	158.0 (98.2)	15.3 (36.0)	20.8 (68.1)	11.9
Split-Path VSTC	2.73	157.6 (97.9)	15.3 (36.0)	20.0 (68.8)	11.6

Fuel is gasoline with LHV of 43,838 kJ/kg (18,860 Btu/lb).

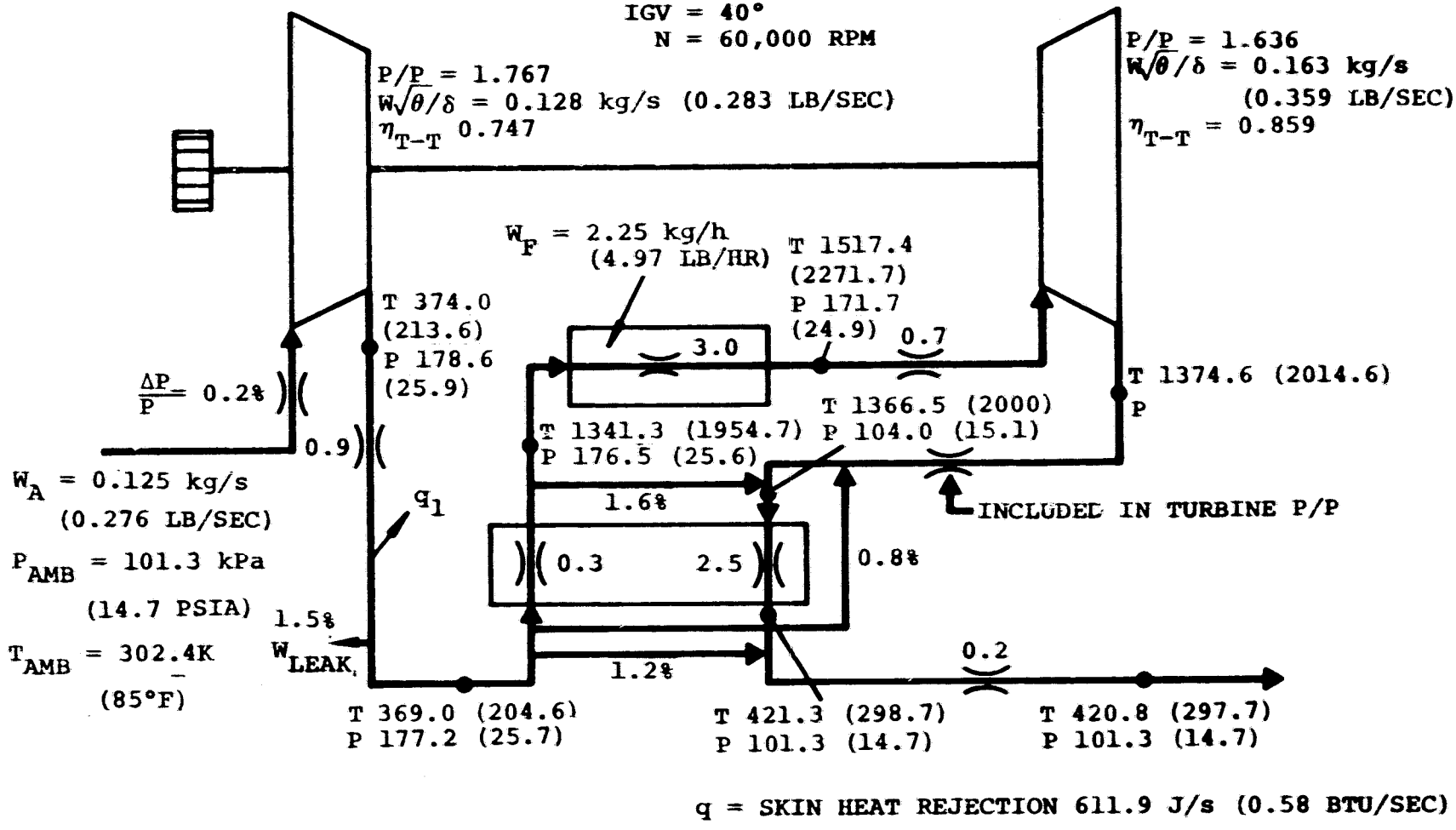

Figure 33. Cruise Condition (40 mph).

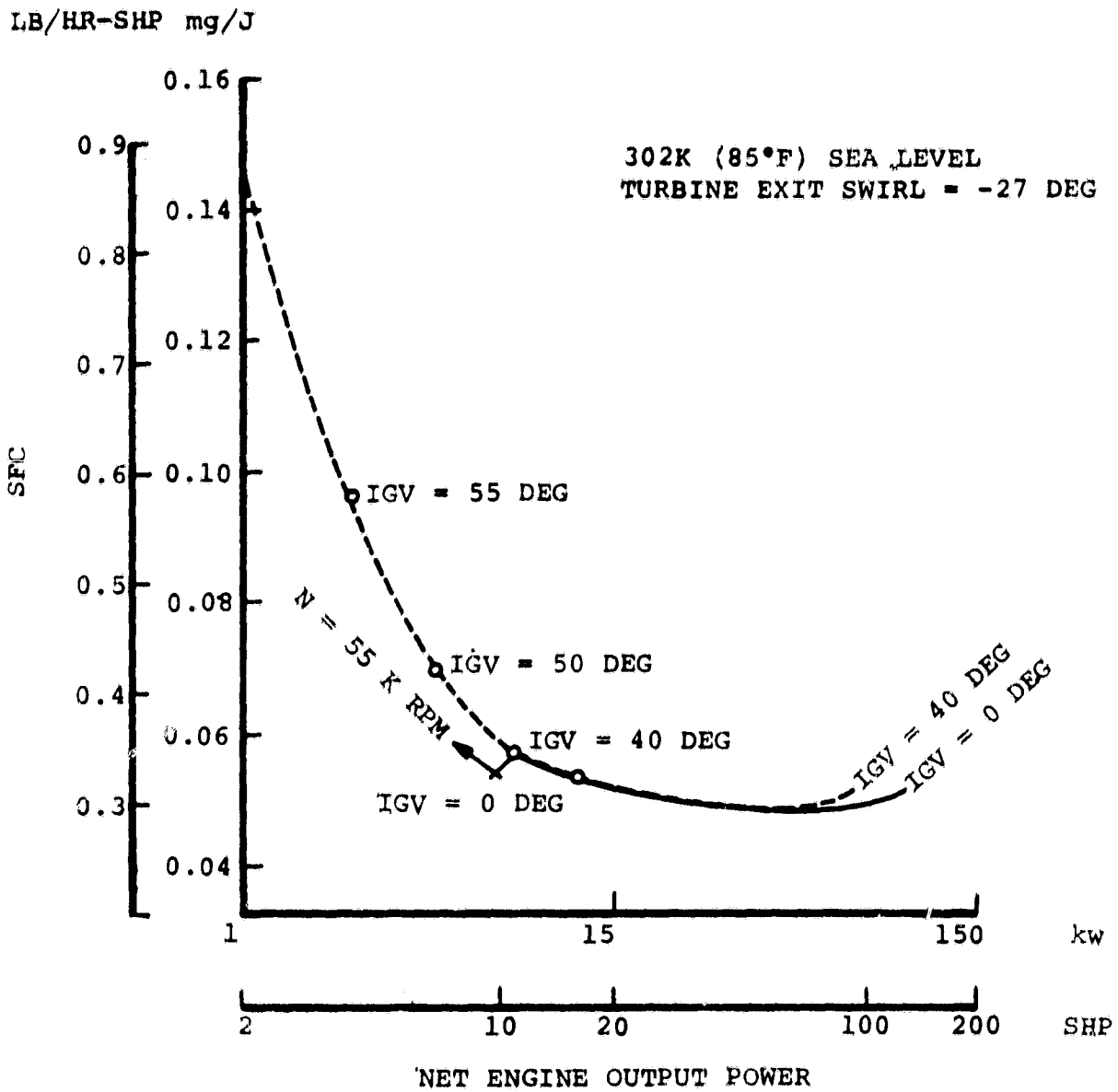

Figure 34. SFC Characteristics — RPD Engine.

2.1.8 Compressor Definition

The compressor selected for further evaluation on the AGT engine is an aluminum, single-stage, centrifugal-type with a backward curved impeller, a radial vaned diffuser with deswirl vanes, and variable inlet guide vanes (IGV). The radial IGVs are provided for flow and pressure ratio control and power amplification at low speed off-design operation. Meridonal flowpath and station designation is shown in Figure 35.

Aluminum has been chosen for the impeller for low cost and ease of manufacturing considerations. An additional advantage of aluminum is the inherent lightweight and low polar moment of inertia, which aids engine response time.

Figure 36 presents "state-of-the-art" and 1983 projections for peak stage total-to-total efficiency of machined and cast compressors operating at optimum specific speed. Figure 37 reflects AiResearch experience concerning efficiency at speeds other than optimum specific speed. "State-of-the-art" values are based on test results of several existing designs, including production units. The 1983 projection indicates that a 1.5 points efficiency improvement is expected to be achieved at a pressure ratio of 5:1.

It must be emphasized that performance levels in Figure 36 represent the maximum attainable with no major design restrictions. In the normal series of compromises encountered during development and the AGT "system design"; philosophy, peak compressor efficiency will most likely be sacrificed for the more important system goal; i.e., more efficient low-power operation of the powertrain. In addition, operation at optimum specific speed may be precluded by mechanical or impeller range considerations.

Cycle matching studies completed to date have produced a reference engine cycle for AGT engine system optimization. Aerodynamic and geometric features of the compressor corresponding to this reference engine are presented in Table 4.

This compressor has been selected with an objective of minimizing aerodynamic risk while providing performance that allows program goals to be achieved and/or exceeded. Important aerodynamic parameters, such as shroud relative diffusion ratio, inducer inlet relative Mach number, and radial diffuser inlet Mach number, have been set at levels shown to result in successful compressors.

2.1.8.1 Compressor System Optimization

The AGT compressor system design was initiated by performing a parametric study using the AiResearch centrifugal compressor preliminary design program to optimize certain compressor design parameters. The preliminary AGT compressor meridional flowpath is shown in Figure 35. The following quantities were varied in the parametric analysis:

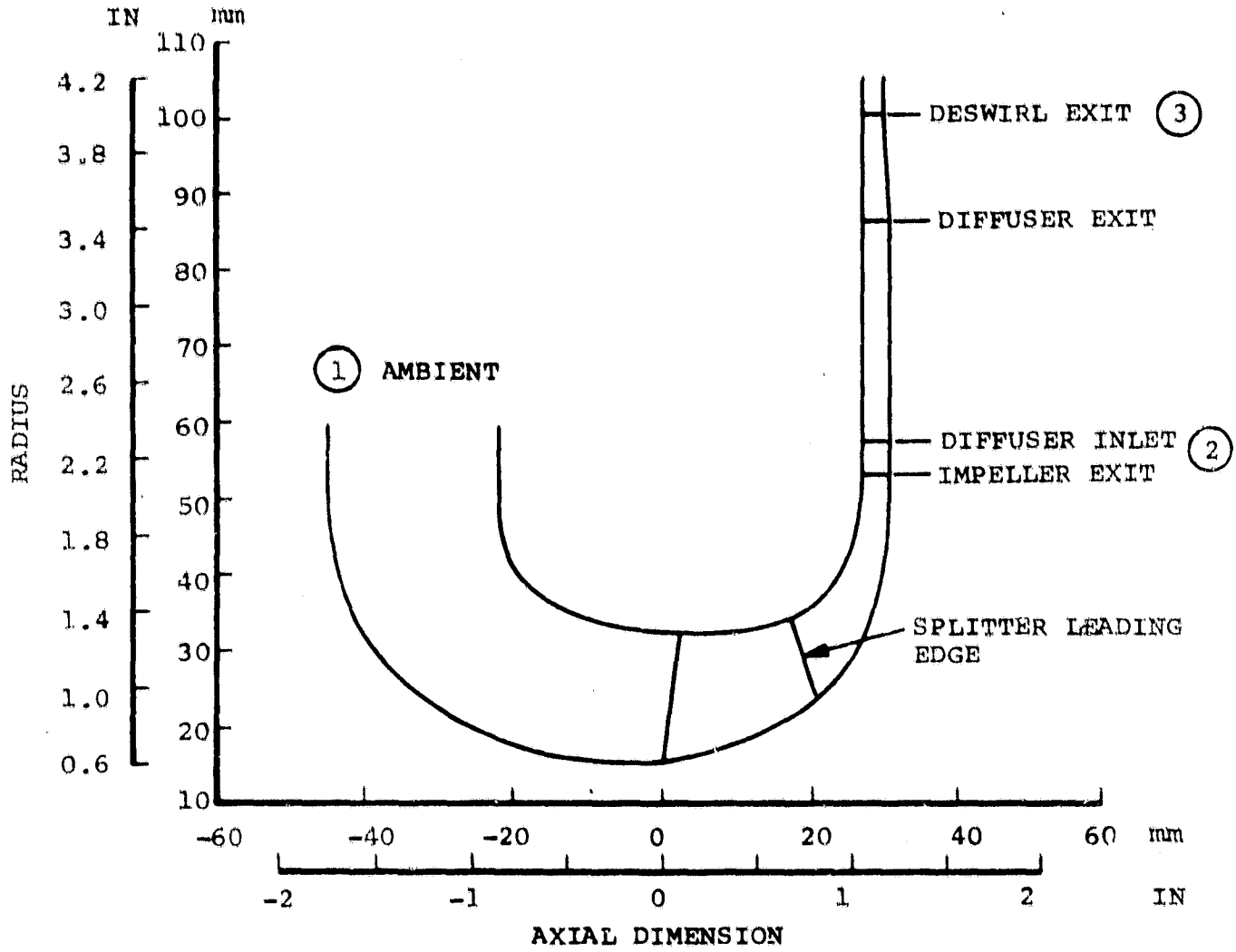

Figure 35. AGT Compressor Meridional Flowpath.

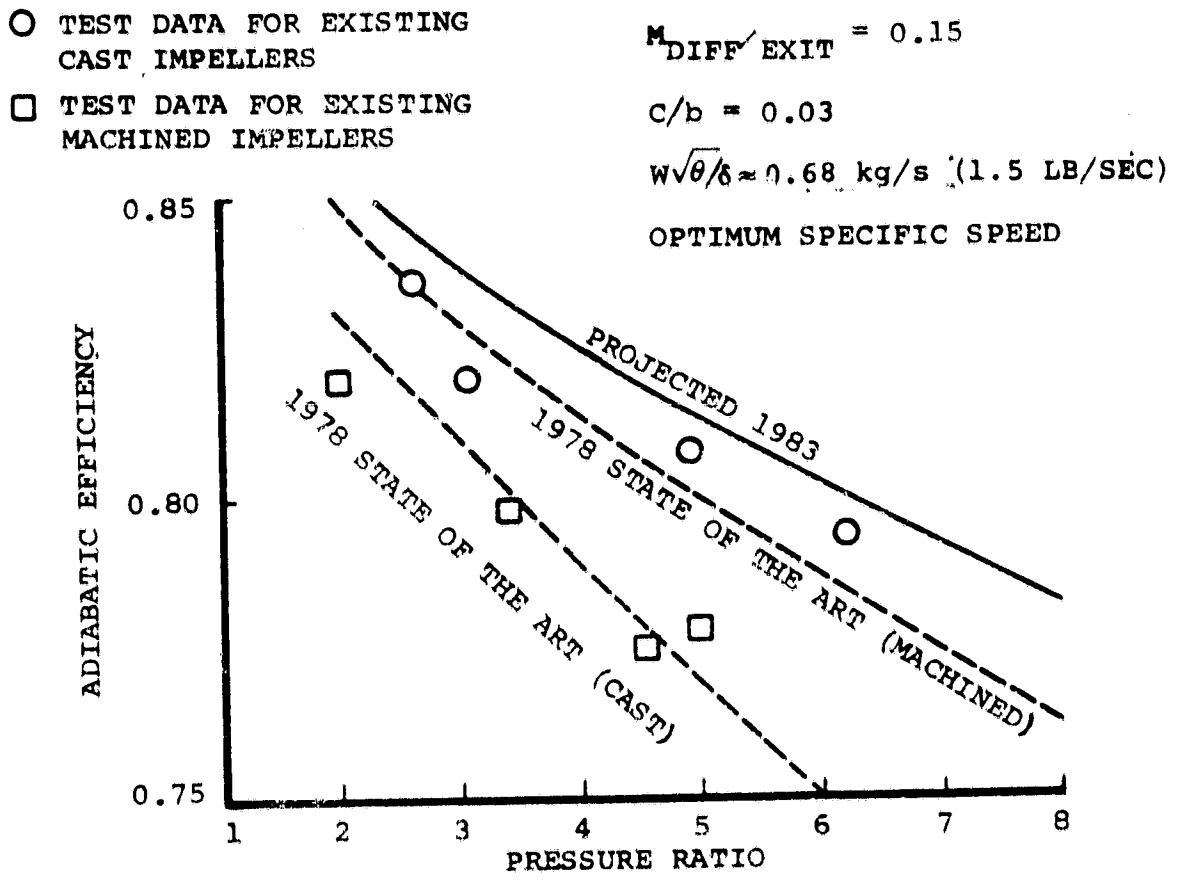

c/b = CLEARANCE/BLADE HEIGHT

Figure 36. Current and Projected Compressor Efficiencies.

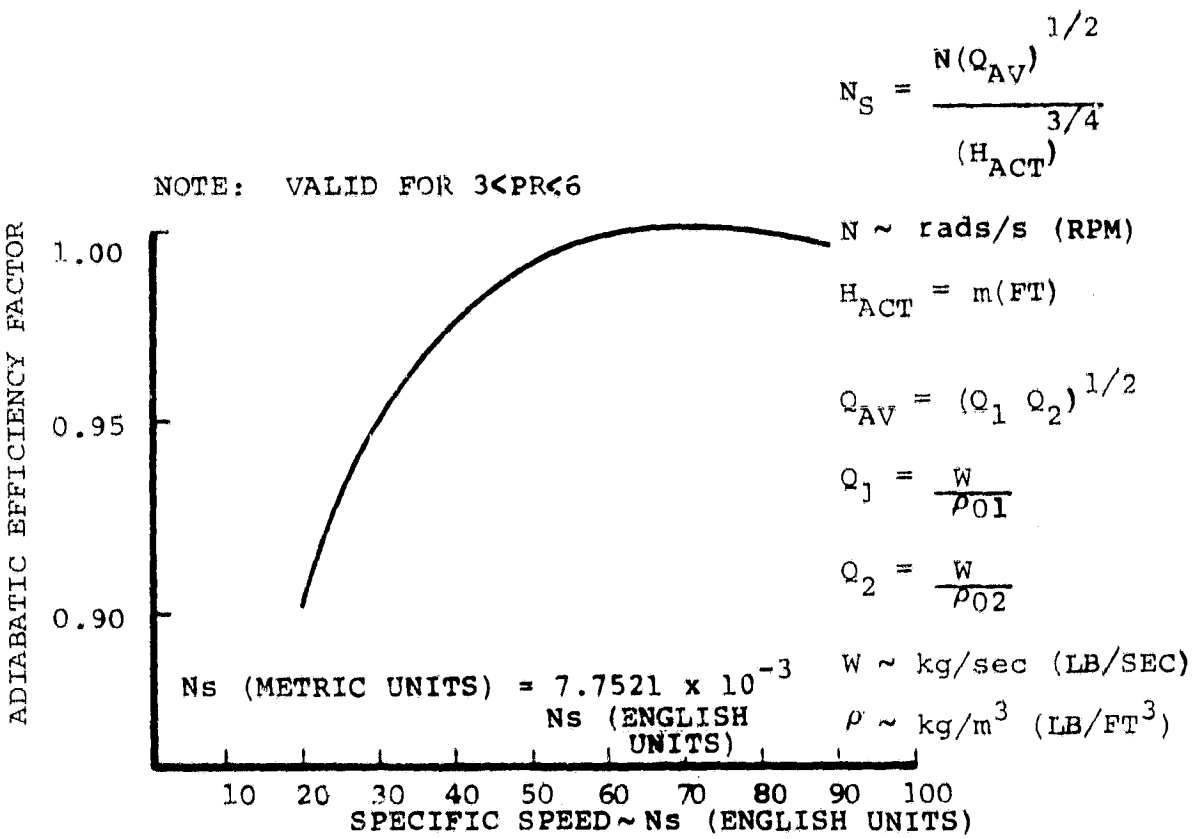

Figure 37. Adiabatic Efficiency Factor Versus Specified Speed.

TABLE 4

REFERENCE COMPRESSOR FEATURES

	Impeller	Stage
Physical Flow, kg/s (lb/sec)	0.388 (0.855)	
Total-Efficiency $\eta_{t\text{-}t}$	0.897	0.805
Pressure Ratio, P_{T2}/P_{T1}	5.633	P_{T3}/P_{T1} 5.0
Temperature Rise, $\Delta T/T$	0.703	
Specific Speed, N_S*	32.4 (58.6)	
Number of Blades	12 Full / 12 Splitters	
Slip Factor	0.949	
Compressor Inlet Temperature, T_1,K (°R)	302.6 (544.7)	
Compressor Inlet Pressure, P_1, Kilopascal (PSIA)	99.81 (14.476)	
Speed, N_{PHYS} (RPM)	100,000	
Tip Diameter, mm (in.)	108.229 (4.261)	
Inducer Hub Diameter, mm (in.)	30.5 (1.2)	
Inducer Tip Diameter, mm (in.)	65.735 (2.588)	
Inducer Tip Normal Thickness, mm (in.)	0.38 (0.015)	
Exit Blade Angle, Degrees	50	
Axial and Radial Clearances, mm (in.)	0.076 (0.003)	

*N_S is Defined as:

$$\frac{N\sqrt{Q_{AVG}}}{H_{ACT}}^{3/4}$$

WHERE: N = RPM

$Q_{AVG} = (Q_1Q_2)^{1/2}$, m^3/s (FT^3/SEC)

H_{ACT} = HEAD, m (FT)

- Impeller blade exit angle (backward curvature)
- Shroud exit/inlet relative velocity ratio
- Vaneless diffuser exit Mach number
- Radial diffuser exit Mach number
- Impeller blade count

The following quantities were held constant for the analysis:

- Inlet shroud/mean meridional velocity ratio (ν_{mrat}) of 1.25
- Hub radius 15.24 mm (0.600 inch)
- Deswirl vane exit angle (0 degrees)

An impeller with splitter blades was used for this study.

Analytical results, for a radial diffuser vane exit Mach number of 0.25, an impeller having 12 full blades and 12 splitters, and a diffuser inlet Mach number of 0.9, are shown in Figure 38. Shroud relative velocity ratio was varied from 0.5 to 0.6 with virtually no difference in performance. The strong effect is the rotor exit blade angle, which indicates continued efficiency improvement up to the highest angle (50 degrees) for which calculations were made.

Parameters for the optimization of the diffuser system, which has not yet been completed, are shown in Figures 39 and 40. An impeller relative velocity ratio of 0.6, radial diffuser vane exit Mach number of 0.25, and vaneless space radius ratio of 1.075 were held fixed. In all cases, the deswirl vane exit angle (Figure 35) was set to 0 degrees while the deswirl vane two theta (2θ) diffusion rate was varied from 6 to 12 degrees.

The analysis again shows peak efficiency to occur for the maximum impeller exit blade angle. A two theta (2θ) of 6 degrees gives the best stage efficiency. Further analysis is to be conducted using a revised deswirl vane exit loss model which accounts for turning of the flow.

Blade count study results are shown in Figure 41. The exit blade angle for this calculation was 50 degrees, diffuser exit Mach number was 0.2, and inlet Mach number was held at 0.85. The trend indicates increasing efficiency for decreasing blade count. Final selection of blade count is discussed in the following paragraphs.

2.1.8.2 Initial Impeller Blade Design

The following parameters were selected to begin initial impeller blade design:

- Exit blade angle, 40 degrees
- Shroud relative velocity ratio, 0.6
- 12 full blades, 12 splitters

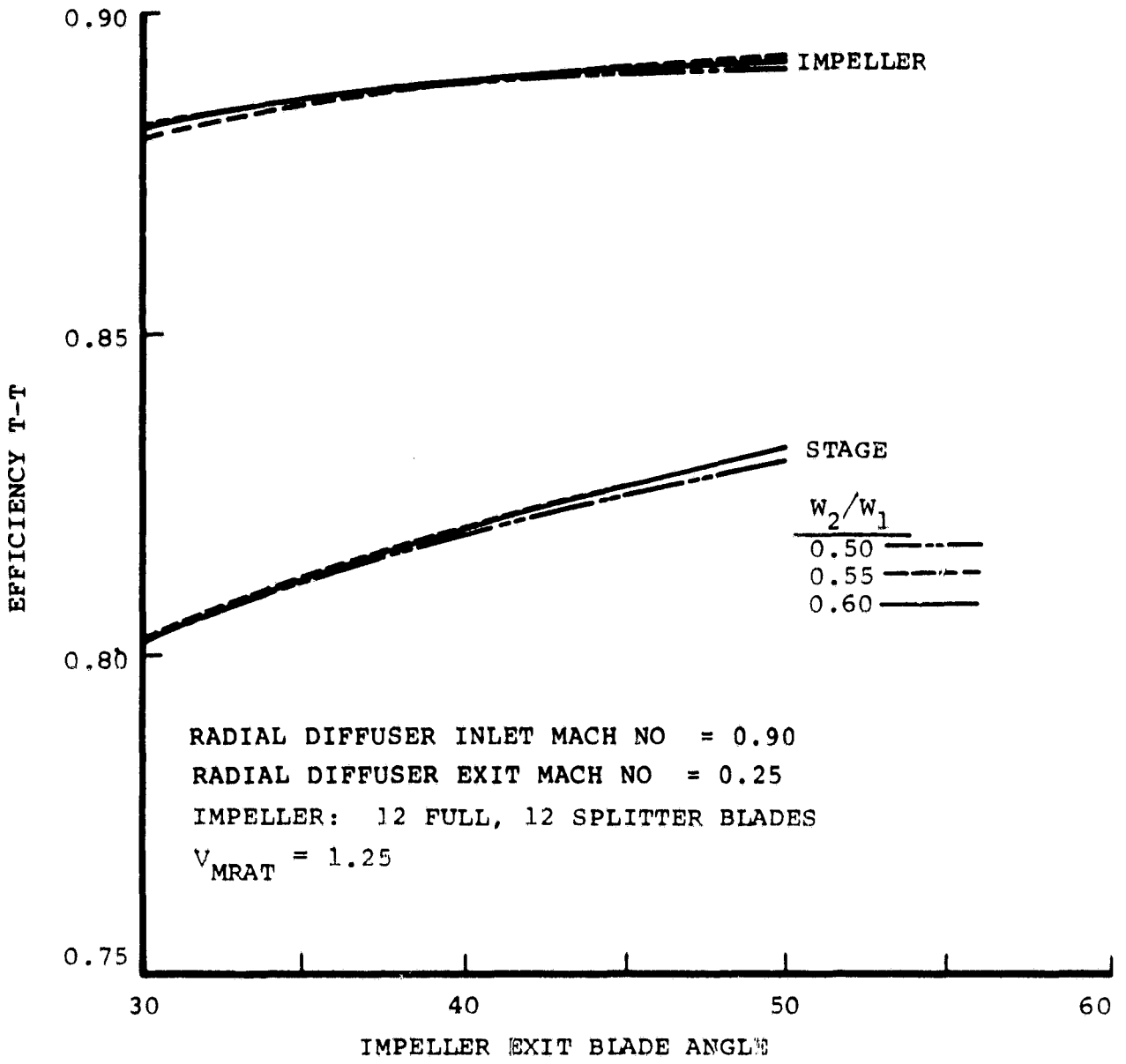

Figure 38. Efficiency Versus Impeller Exit Blade Angle.

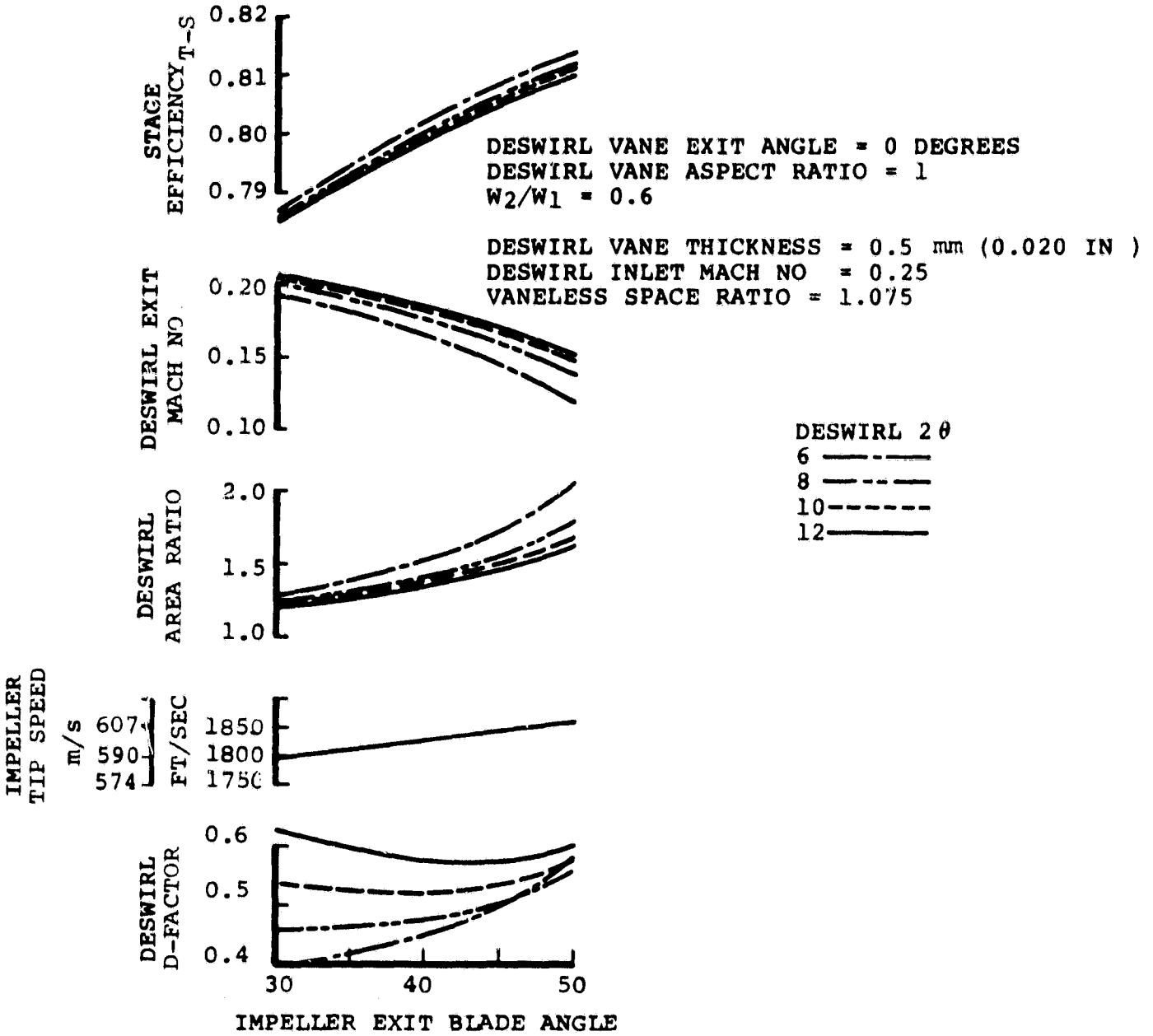

Figure 39. AGT Compressor Optimization.

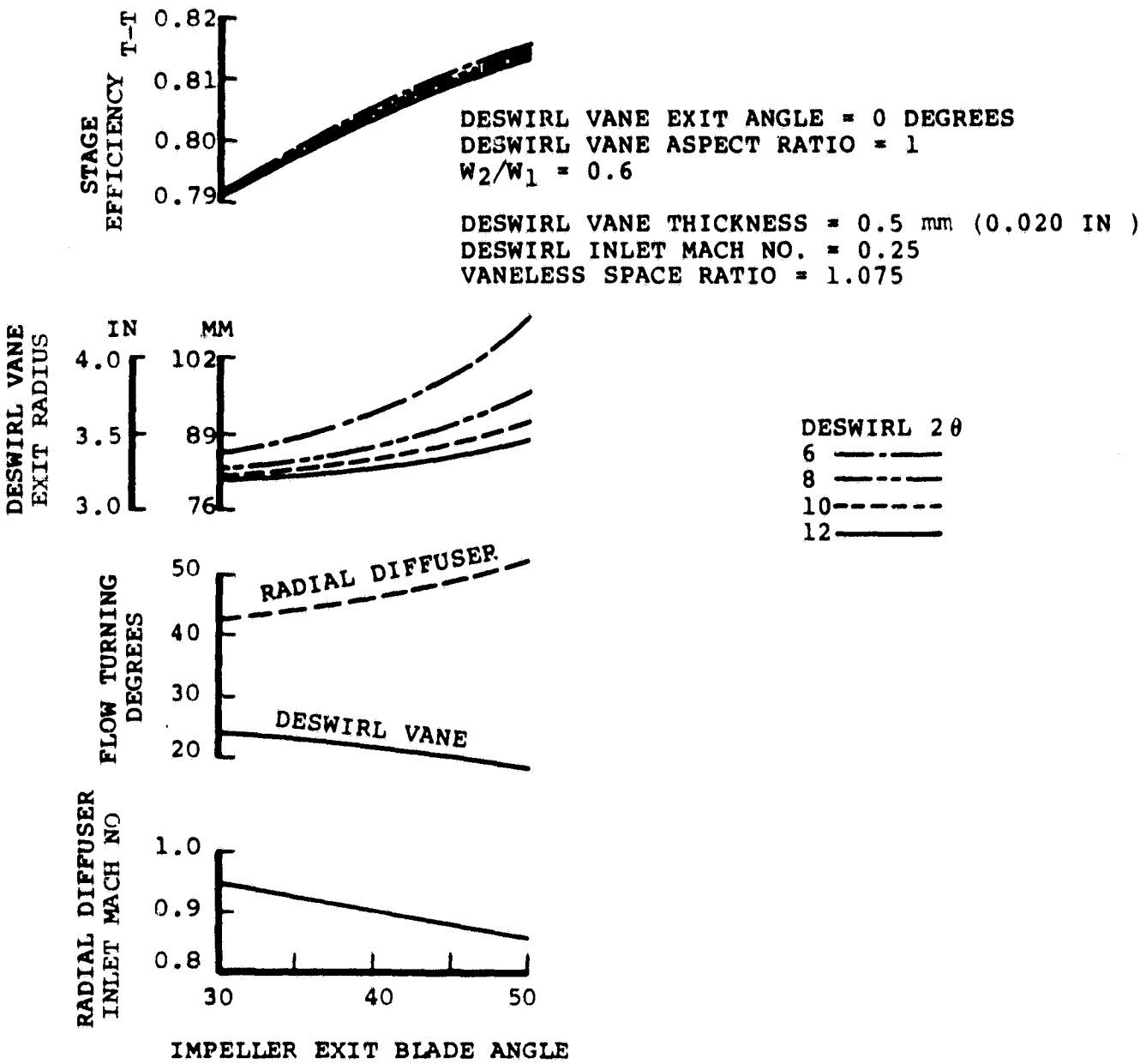

Figure 40. AGT Compressor Optimization.

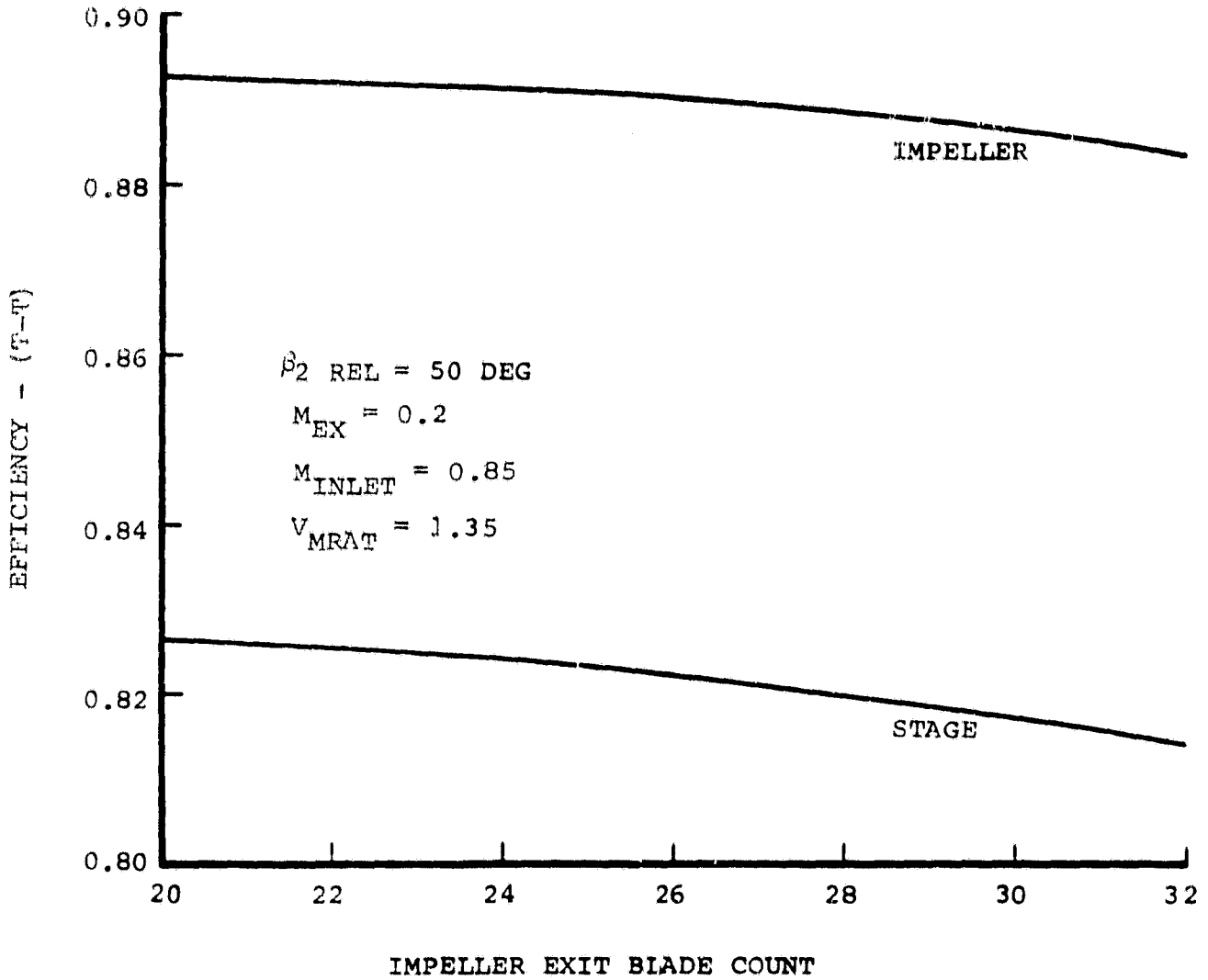

Figure 41. Efficiency Versus Impeller Exit Blade Count for AGT Compressor Design.

An exit blade angle of 40 degrees was the limit set by the assumed maximum allowable blade stress; aerodynamically, a higher angle would be desirable. Selection of a shroud relative velocity ratio of 0.6 was based on past experience which indicates better rotor discharge velocity profiles when less diffusion (higher relative velocity ratios) occurs in the impeller. Impeller exit blade count was set at 24 exit blades, since a lower number did not offer significant gains in stage efficiency. Final decision on blade count will be made based on blade surface Mach No. distribution.

Two inlet flowpaths were evaluated during this analysis as shown in Figure 42. The shortened inlet was required to improve engine rotor dynamics as discussed in Section 2.1.2.3. The effect on compressor inlet surface velocities is compared in Figure 43. The short inlet effectively eliminated shroud diffusion and reduced hub diffusion, which are detrimental to the surface boundary layer.

Initial blade geometry design indicated a high blade stress at the hub trailing edge. Therefore, blade root thickness was increased in this region from 0.635 to 1.016 mm (0.025 to 0.040 inch) and a new blade generated. Resulting blade stresses are shown in Figure 44.

Blade surface and meanline velocity distributions are shown in Figures 45, 46, and 47. Along the shroud streamline, efforts were made to reduce the diffusion rate near the leading edge and, thereby, limit overshoot in suction surface velocity. This helped to assure adequate impeller surge margin. On the hub streamline, pressure surface diffusion from the leading edge to the minimum value, which occurs just ahead of the splitter, was minimized. This is advantageous for impeller surge margin and efficiency considerations. These adjustments were made by changes in area control varing parameters such as blade shape, blade angle and flowpath geometry.

2.1.8.3 Compressor Test Rig

The compressor test rig layout is shown in Figure 48. Power is derived from a drive turbine system composed primarily of the AiResearch Model TV81 Turbocharger hot flowpath components. Actual power section compressor stage hardware (VIGVs, impeller, and diffuser) is utilized in the rig to permit detailed compressor design performance mapping. As shown in Figure 48, power section ducting has been incorporated to establish any effects of flow phenomena resulting from transitioning compressor discharge flow to the regenerator high pressure inlet. In addition, the inlet air filter and associated ducting (not shown) can be accommodated to verify aerodynamic design intent and again establish any detrimental flow effects resulting from the installation.

Compressor rig rotor dynamics have been analyzed and are presented in Figures 49 and 50. Using bearing stiffness values of approximately 4378 kN/m (25,000 lb./in.), the first three undamped critical speeds are 27,000, 49,000, and 180,000 rpm, respectively. The first and second critical speeds are predominantly rigid body modes, whereas the

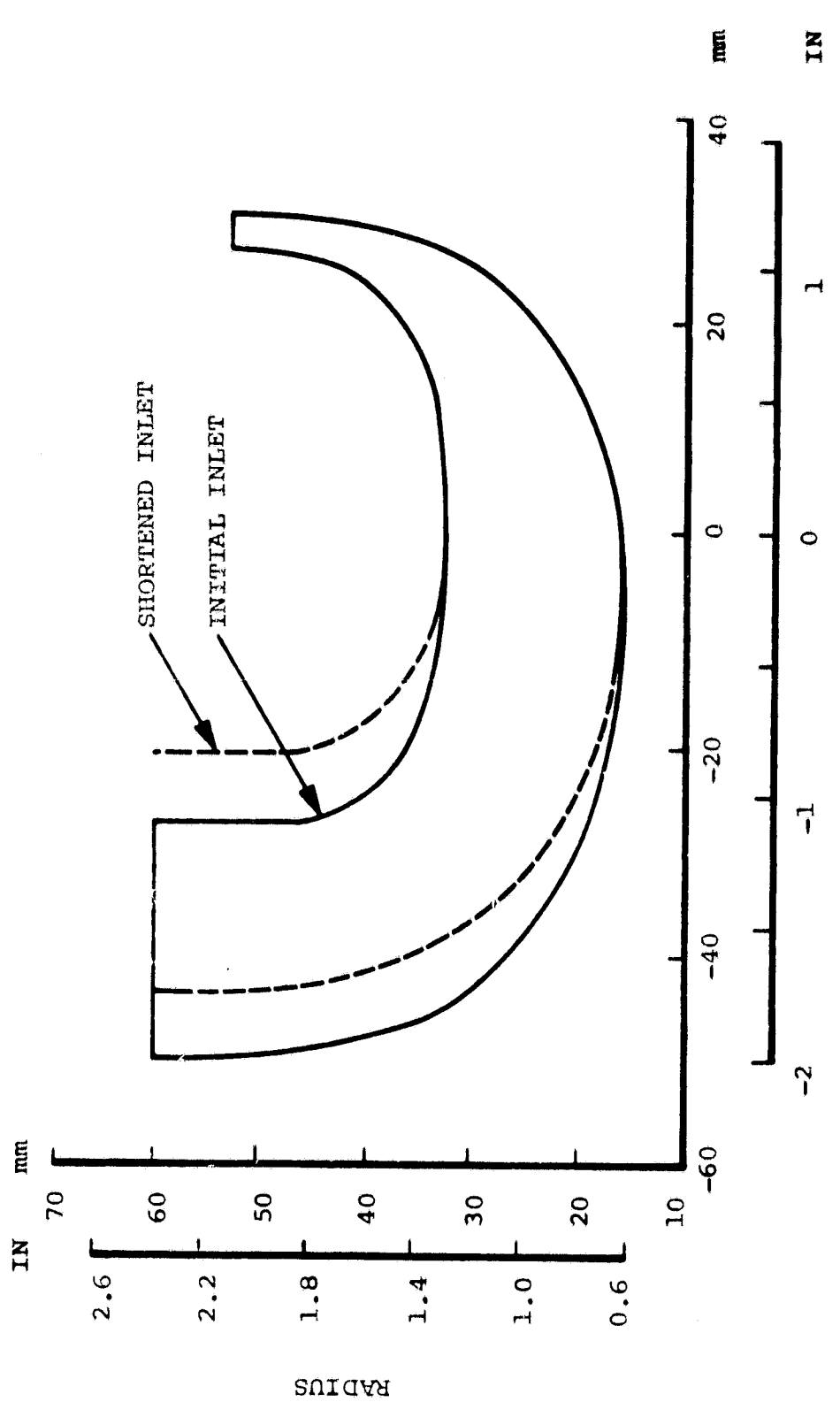

Figure 42. AGT Compressor.

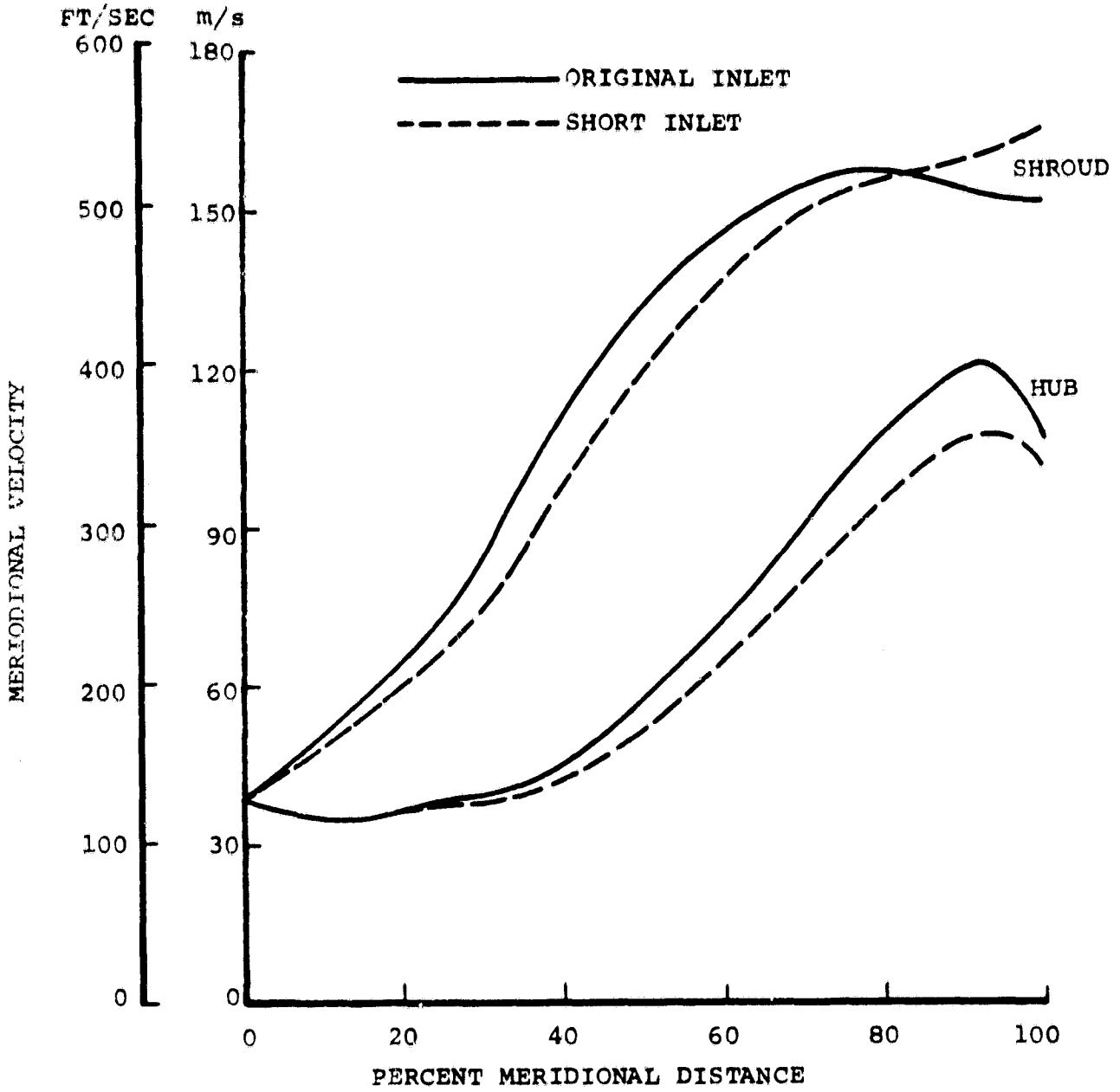

Figure 43. AGT Compressor Inlet Surface Velocity

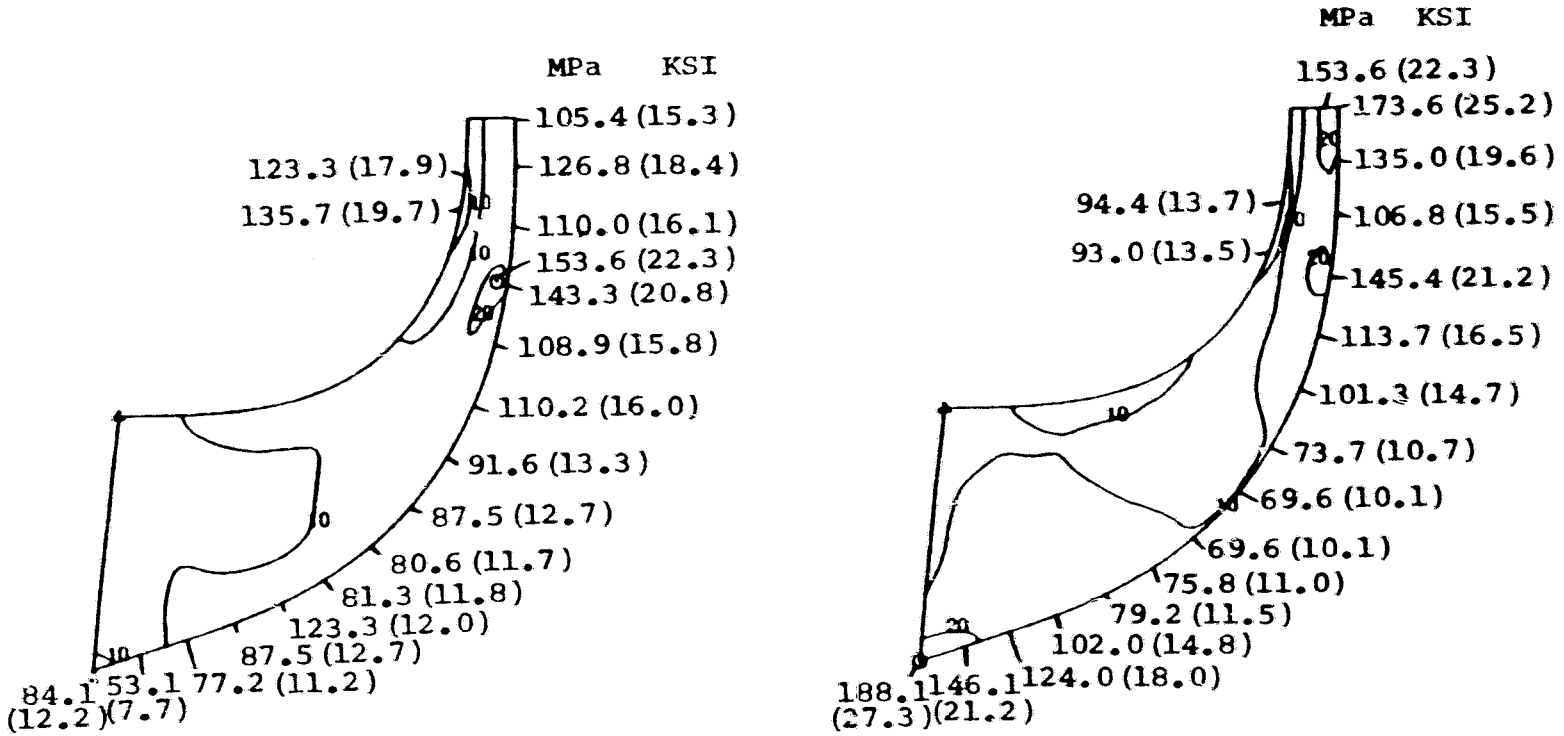

Figure 44. AGT Impeller Blade Stress (40° Exit Blade Angle) at 100,000 RPM.

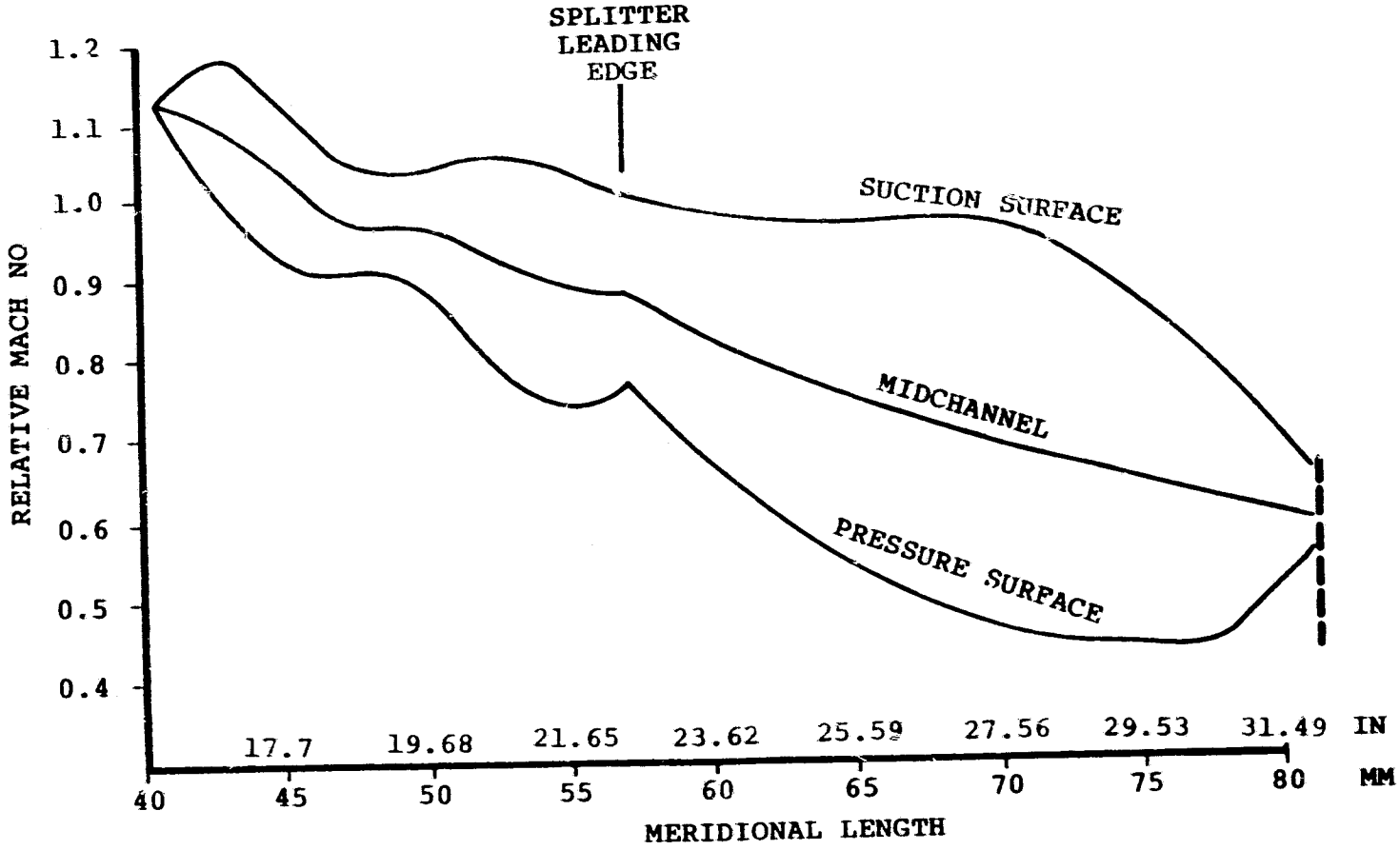

Figure 45. Shroud Streamline (40° Blade Exit Angle).

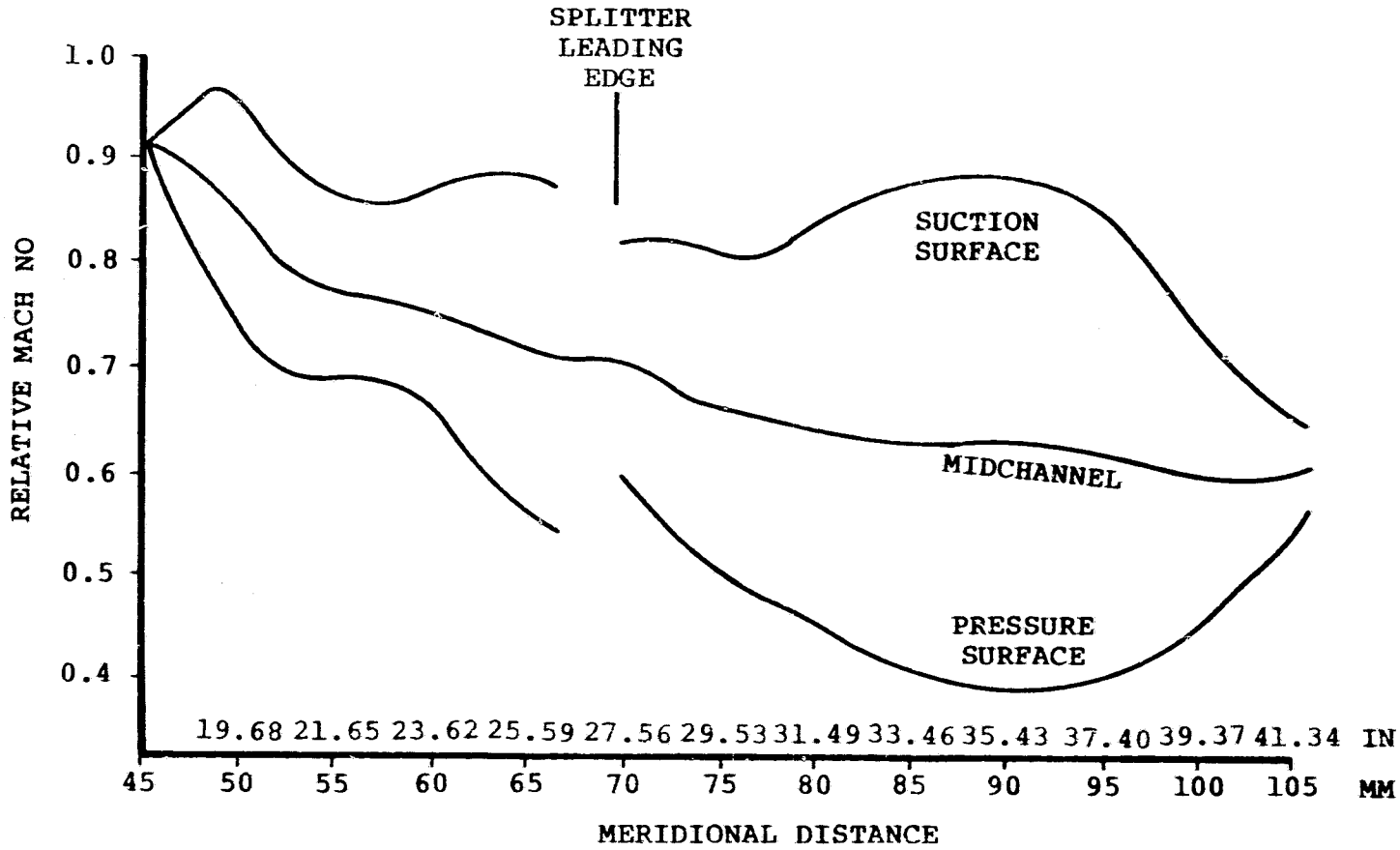

Figure 46. 50 Percent Flow Streamline (40° Blade Exit Angle).

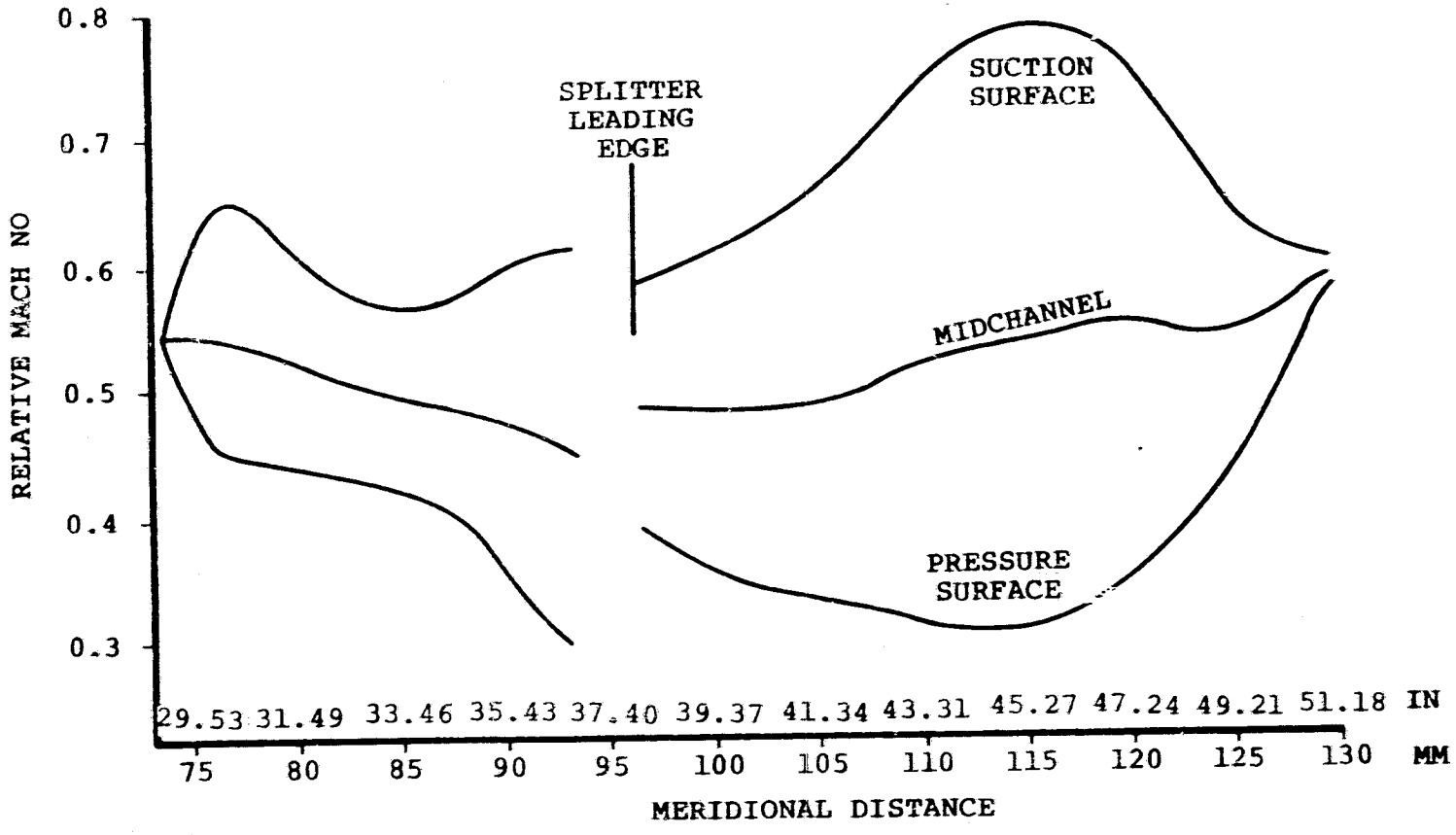

Figure 47. Hub Streamline (40° Blade Exit Angle).

third critical is a bending mode. Past experience with hydraulically mounted bearing systems has indicated that the first two criticals will be sufficiently damped and pose little problem during operation of the test rig. The third critical has sufficient margin above the operating envelope and is consistent with AiResearch Phoenix design technology.

The rig incorporates the capability for controlling and evaluating critical compressor running clearances based on capacitance probe measurements at selected stations along the impeller meridional flowpath. The clearance control mechanism is based on a design concept successfully used in the improved surge margin centrifugal compressor program for the U.S. Army Air Mobility R&D Laboratory. This mechanism features an ACME thread, used to axially adjust the position of the compressor rotor. This is accomplished by fixing the internal thread and turning the external thread, thus forcing the externally threaded members, which are connected to the impeller, to move axially. A cylindrical worm gear set is used to drive the external ACME thread. The splined drive shaft for the compressor is required to move axially relative to the external ACME thread due to axial positioning of the compressor, deflections, and thermal gradients. Friction in the splines creates high forces that resist this movement and induce high loads on the bearings, worm gear, and ACME thread. Therefore, a ball spline is incorporated to minimize this axial load from spline friction.

Clearance control capability will allow thermal stabilization of the test rig at test point conditions, followed by a reduction of running clearances, to the small desired values [0.076 mm (0.003 inch)]. This mode of operation will allow testing to proceed in a safe, rapid, and cost-effective sequence.

The compressor rig incorporates extensive instrumentation to allow performance evaluation of all stage components as well as overall parameters. This will include:

- Inlet total pressures and temperatures
- Shroud line static pressures
- Impeller exit static pressures
- Vaneless space static pressures
- Diffuser static pressures
- Stage exit total pressures and temperatures
- Inlet and exit flow measurement
- Provisions for stage exit surveys
- Clearance probe measurements

Instrumentation is of a size consistent with the small stage dimensions and of sufficient number and spacing to provide realistic average values for all parameters measured.

2.1.9 Regenerator Definition

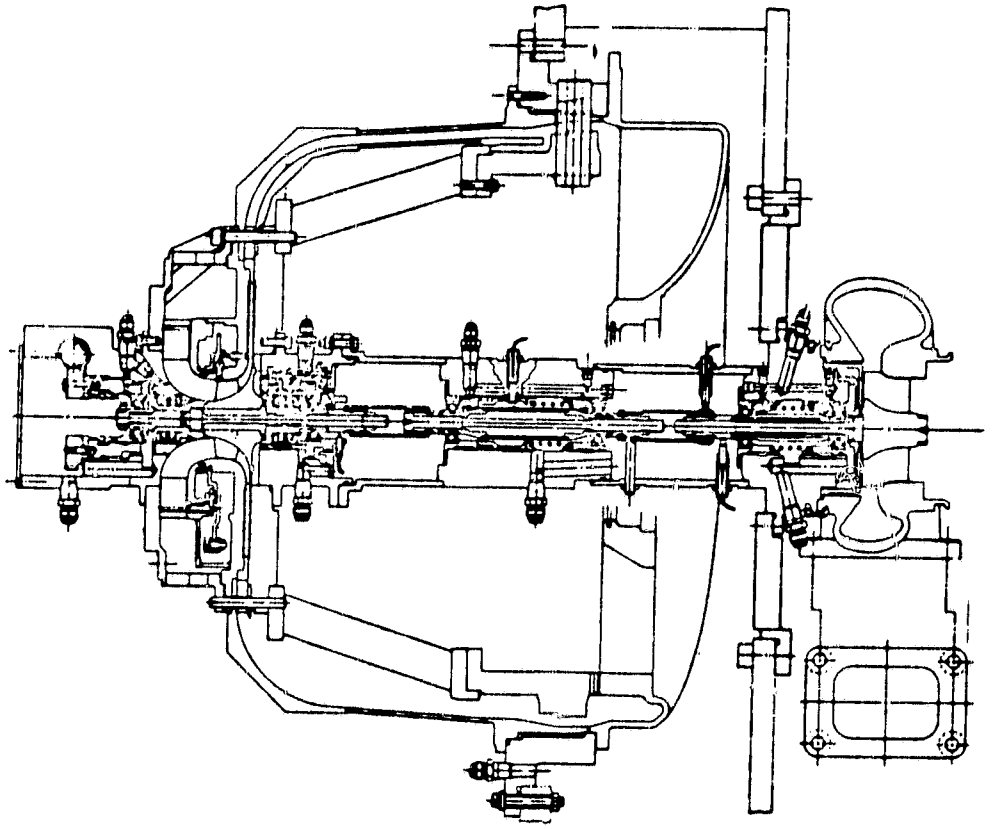

Figure 48. Compressor Test Rig Layout.

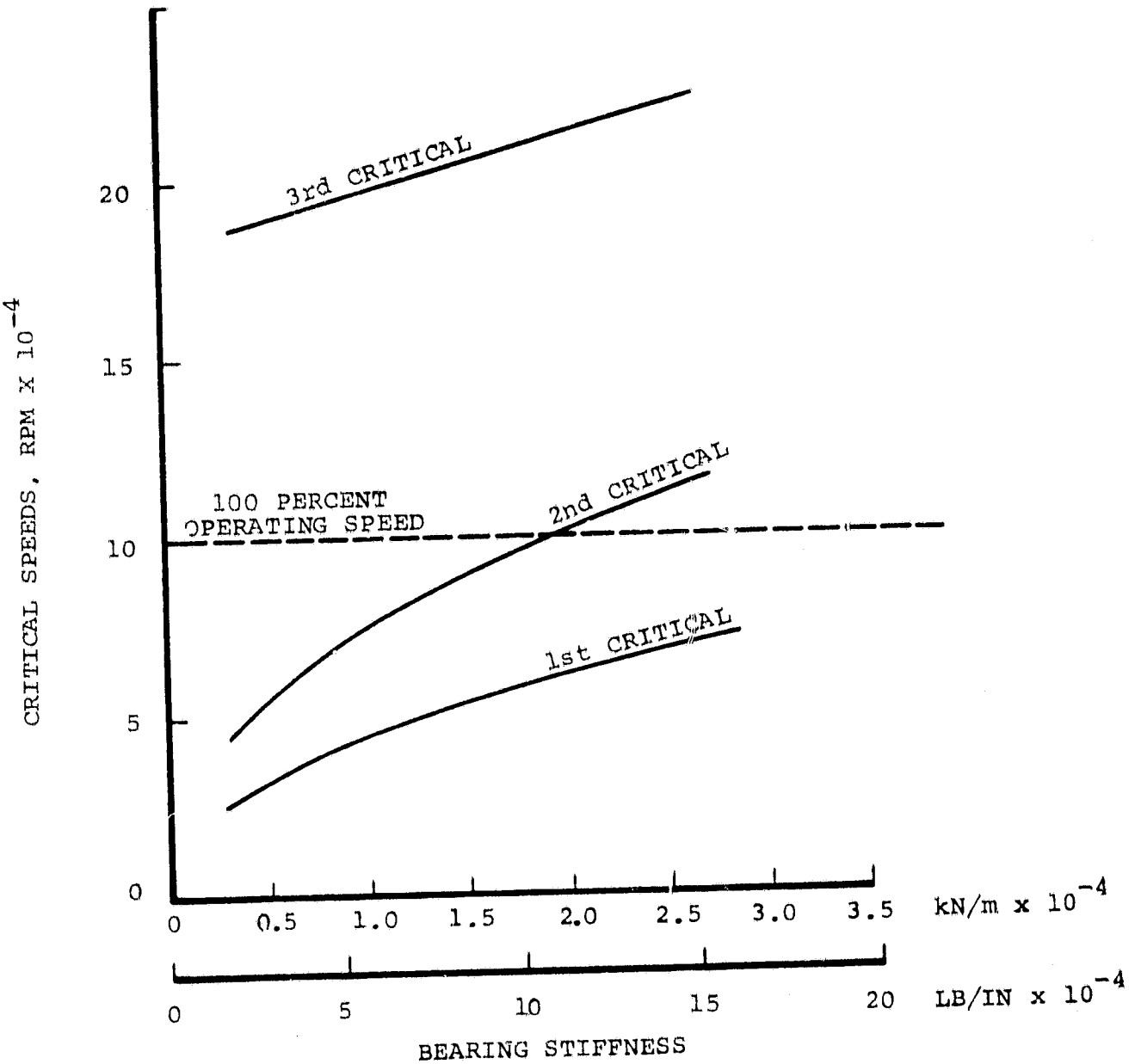

Figure 49. Compressor Rig Critical Speeds.

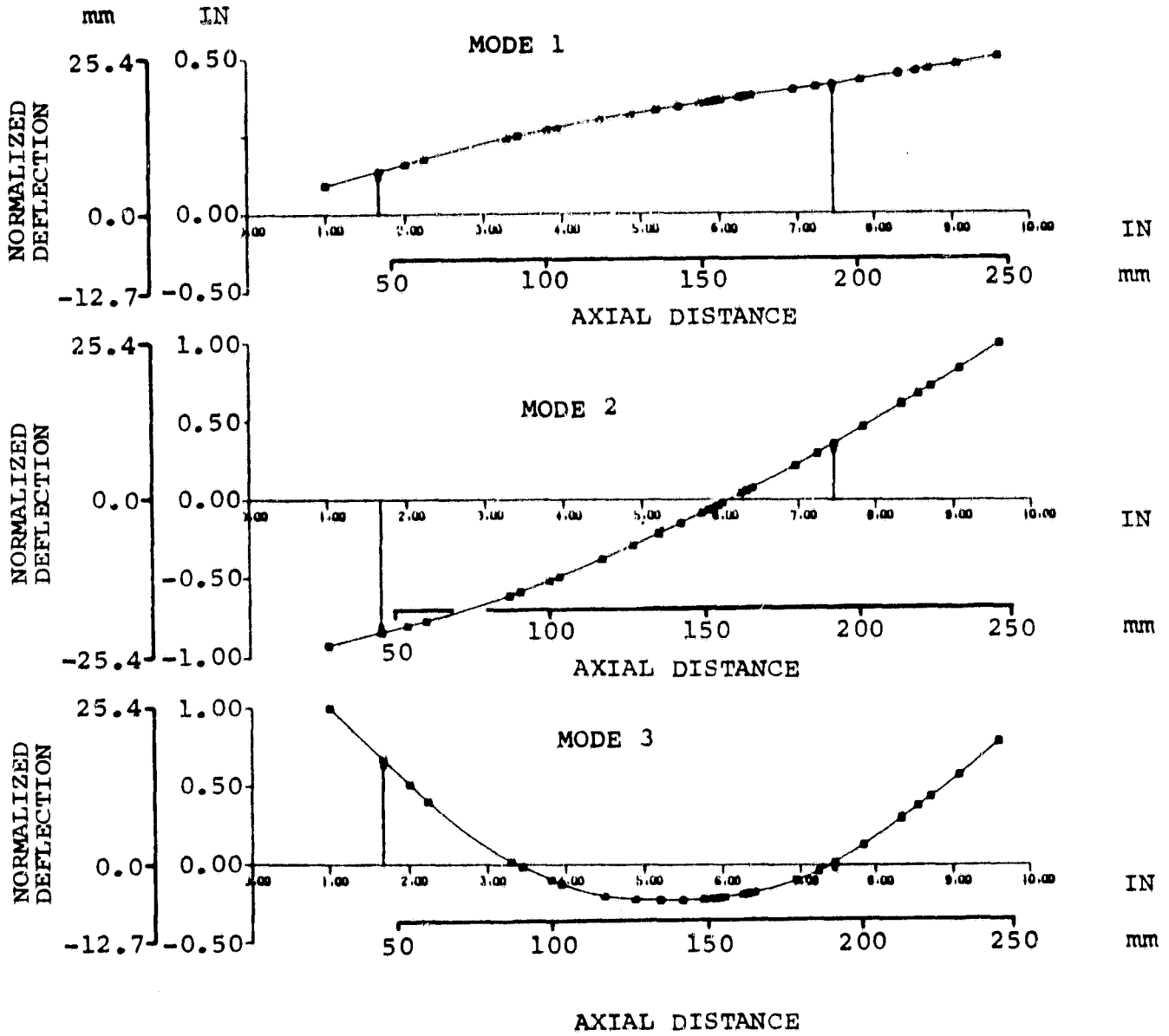

Figure 50. Compressor Rig Rotor Dynamics.

2.1.9.1 Regenerator Core and Seal Configuration

The initial regenerator size selected for the design study was 444.5 mm OD (17.5 in) x 139.7 mm ID (5.5 in) x 71.12 mm (2.8 in) thick. A performance objective was established yielding 92.9 percent effectiveness with 7.5 percent pressure drop at maximum power conditions.

This performance is based on an extruded isosceles triangular matrix configuration with a 4.572 mm (0.018 in) hydraulic diameter (DH) and 0.0889 mm (0.0035 in) material thickness that is expected to be developed by 1983. At the present time a sinusoidal triangular structure fabricated by Corning Glass with 0.061 mm (0.0024 in) material wall thickness represents the best state-of-the-art fin configuration for the AGT engine. For the selected core size an effectiveness of 90.2 percent with 6.25 percent pressure drop can be expected at full power conditions. Since the pressure drop for the state-of-the-art fin geometry is considerably less than the design objective, the regenerator thickness can be increased. By increasing the thickness from 71.12 mm (2.8 in) to 83.82 mm (3.3 in) the state-of-the-art matrix should increase regenerator effectiveness from 90.2 to 91.9 percent with a pressure drop of 7.3 percent which is still below the design objective of 7.5 percent. By increasing the hydraulic diameter requirement for the future extruded isosceles triangular structure from 0.457 mm (0.018 in) to 0.508 mm (0.020 in) for the thicker regenerator size, the original performance objective can be maintained. Based on these results the regenerator size recommended for continued study was 444.5 mm OD (17.5 in) x 139.7 mm ID (5.5 in) x 83.82 mm (3.3 in) thick.

During the study a regenerator performance analysis was conducted to evaluate the effect of flow area unbalance on regenerator effectiveness and pressure drop. This preliminary information was required in order to determine the initial regenerator inner and outer seal crossarm shape. Three inner seal design configurations were evaluated as illustrated in Figure 51. Configuration No. 1 is similar to the seal developed for the Ford Stirling engine. The equal flow area split (balanced heat exchanger) provides the best regenerator effectiveness and pressure drop combination throughout the engine operating range. Although configurations No. 2 and 3 offer certain advantages from the standpoint of seal fabrication and leakage, a significant increase in regenerator core diameter would be required to attain equivalent effectiveness and pressure drop with respect to configuration No. 1. For this reason, configuration No. 1 was selected for continued design evaluation.

Further system optimization studies regarding secondary cooling air for the combustor, indicated an increase of regenerator core inner diameter was required. The inner diameter was increased from 139.7 mm (5.5 in) to 160.48 mm (6.318 in). To maintain the same regenerator performance the outer diameter was increased to attain equivalent frontal area. As a result the regenerator recommended for the AGT RPD engine is 454.05 mm OD (17.876 in) x 160.48 mm ID (6.318 in) x 83.82 mm (3.3 in) thick.

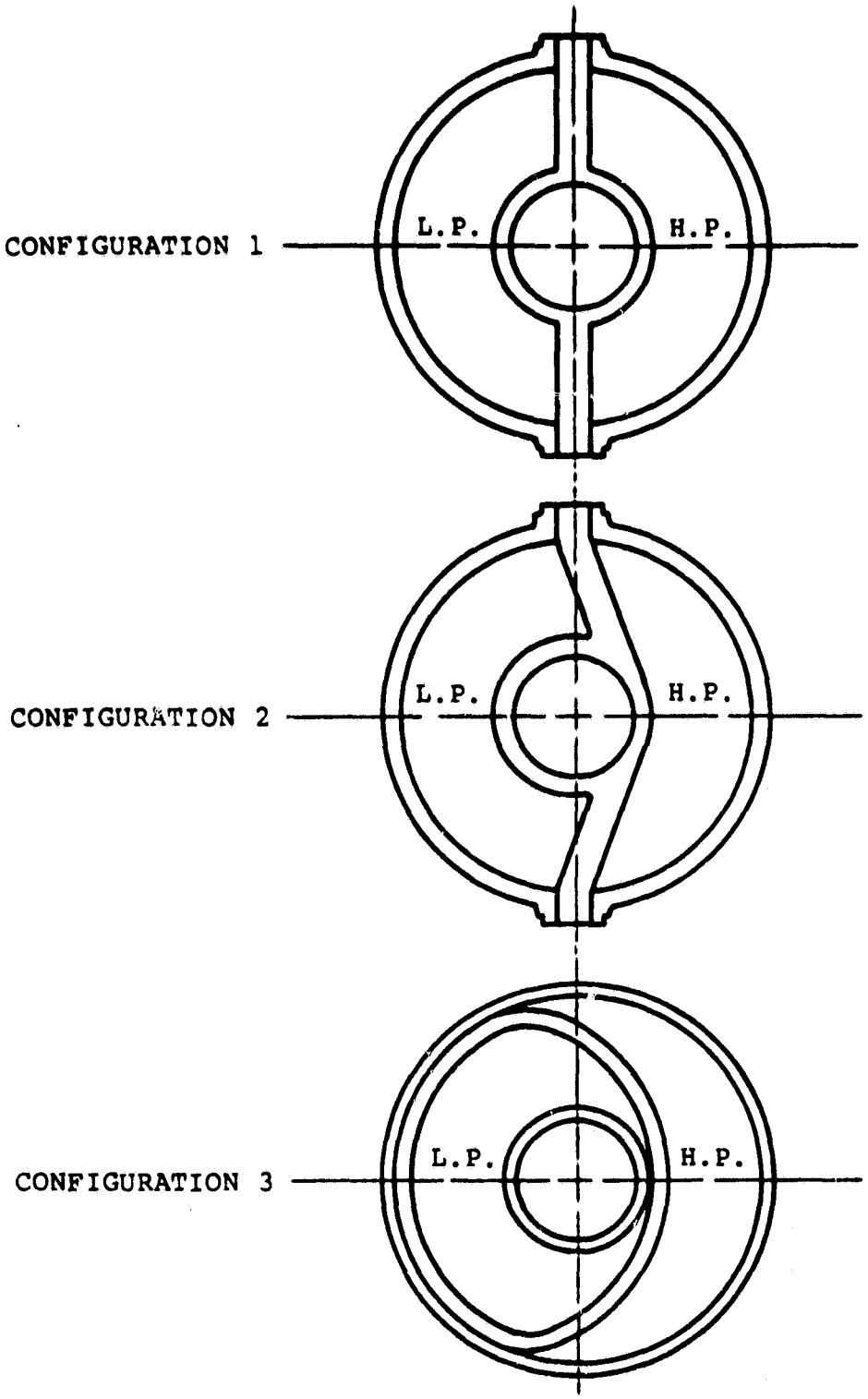

Figure 51. Regenerator Inner Seal Configurations.

As an alternative to the extruded isosceles triangular matrix with a hydraulic diameter of 0.508 mm (0.020 in), a design study was completed for optimization of an extruded rectangular matrix with a hydraulic diameter 0.584 mm (0.023 in) to 0.610 mm (0.024 in). Both designs should attain equivalent performance. This study also established the tooling requirements for the regenerator core suppliers. Meetings were held with representatives from Corning Glass Works and NGK Insulators to discuss the status of their matrix extrusion process. Both companies expressed confidence in developing this process to produce the thin-wall regenerator matrix structures, which are required for compact high performance heat exchangers.

A two-dimensional heat transfer analysis was initiated to define the temperature and thermal stress distribution for the regenerator assembly.

2.1.9.2 Regenerator Drive System

Based on prior Ford experience, Table 5 contains generalized gear geometry that has been established for the regenerator pinion and ring gear.

TABLE 5. REGENERATOR PINION AND RING GEAR DATA

	Pinion	Gear
Teeth	30	341
Center Dist, mm (in.)		261.8 (10.306)
Diameter Pitch	18	18
Pressure Angle, Degrees	22.5	22.5
Working Add, mm (in.)	1.35 (0.053)	0.91 (0.036)
Dedendum, mm (in.)	1.78 (0.070)	2.36 (0.093)
Tooth Thick, mm (in.)	2.35 (0.0924)	1.85 (0.0729)
Tip Thick, mm (in.)	1.12 (0.044)	1.09 (0.043)
Face Width, mm (in.)		25.4 (1.00)
Pitch Diameter, mm (in.)	42.3 (1.667)	481.2 (18.944)
Bonding Stress, KPA (psi)	68223 (9896)	61287 (8890)
PVT Factor, nm/sec/cm (lb ft/sec/in.)	564.2 (1638)	436.0 (1266)
PV Factor, nm/sec (lb ft/sec)	18540 (13673)	18920 (13953)
Peak Torque, nm (lb ft)	23.86 (17.6)	271.2 (200)
Peak Speed, (rpm)	284	25

The regenerator core torque requirement at full power engine conditions was estimated based on a previous analysis performed on the Ford 707 engine regenerator system. Since the seal configuration for the AGT engine has not been finalized, this approach represents an initial approximation. The 707 engine analysis was modified based on the AGT engine pressure and seal width and radius.

Utilizing a design core torque requirement of 200 lb-ft at full power condition the location of the fixed and spring roller was optimized with respect to the present pinion location and inner and outer seal crossarm orientations. The design criterion selected were as follows:

1. Fixed roller reaction load to be less than half of the 707 engine, which incorporates a yoke to accommodate the total load.

2. Minimum spring roller load to ensure ring gear engagement with the pinion.

3. Minimum force transmitted to the fixed roller due to increased spring roller loads.

By minimizing the fixed roller loads, the graphite bearing system that has been successful in the 707 engine can be incorporated.

Subsequent analysis was completed to determine the roller reaction loads resulting from a variation in torque requirements of 50 to 400 lb-ft. The results illustrated on Figure 52 assume sliding friction at the pinion roller location and rolling friction at the spring and fixed roller locations.

2.1.9.3 Regenerator Test Rigs

Preliminary layout design of the two regenerator cold flow rigs, shown in Figures 53 and 54, has been completed. The objective of these rigs is to obtain a flow match between the regenerator core high and low pressure sides through various header designs (Figures 55, 56, and 57). Complete velocity distribution mapping immediately down stream of the core will be accomplished through use of hot wire anemometers in which a uniform radial and circumferential velocity profile is desired.

To obtain the desired flow match, an iterative test approach will be utilized. Tangential and radial flow patterns resulting from various header designs will be used as input into a 3-dimensional nodal analysis to obtain immediate feedback on test configurations. Therefore, optimum design can be derived with effects on core and engine performance predicted throughout the engine operating range.

2.1.10 Combustor Definition

Definition of a single-can, variable-geometry, ceramic combustor was initiated. Prime combustor design was derived from Ford variable-geometry combustor technology and

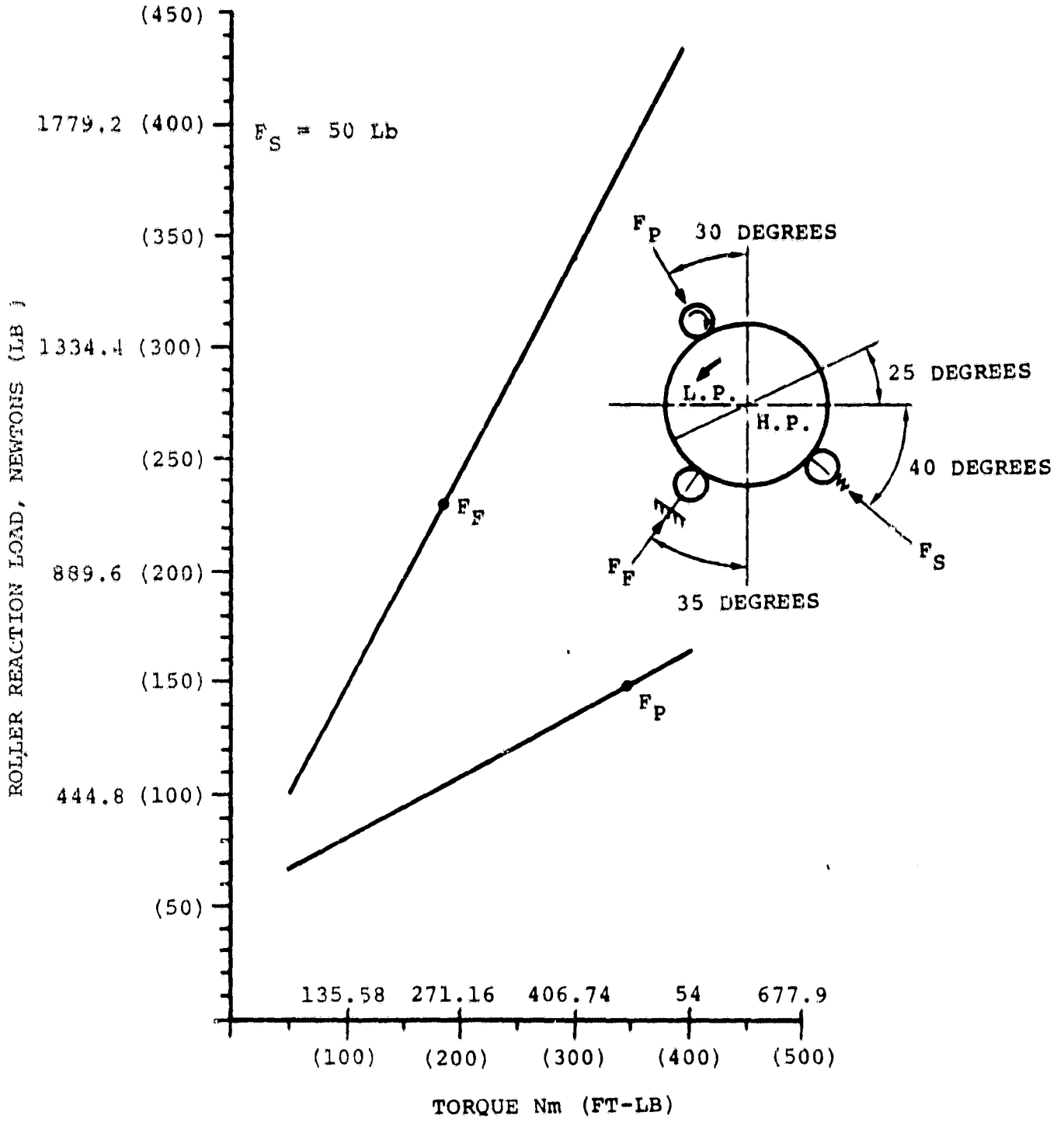

Figure 52. Drive Support Reaction Loads Vs. Core Torque

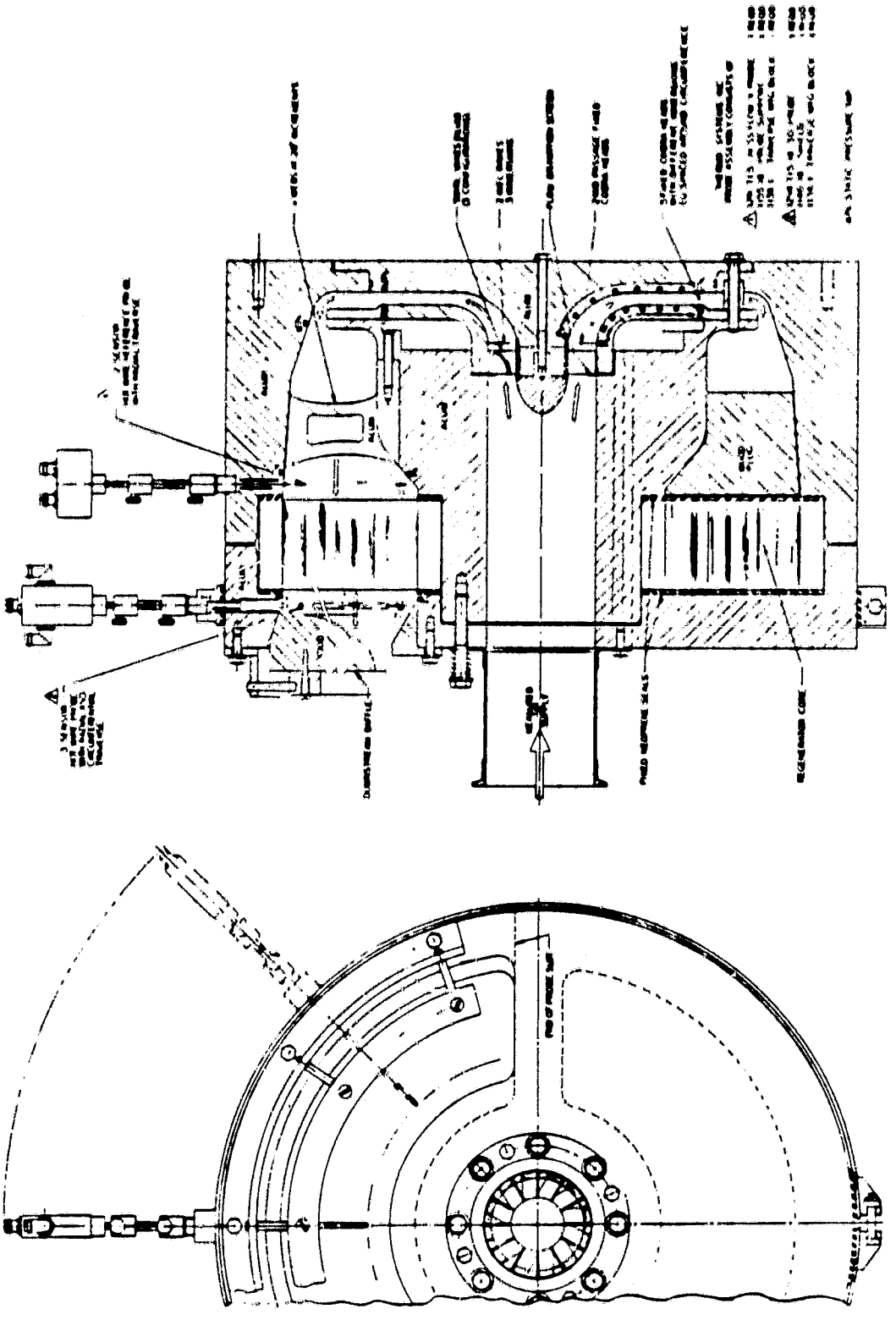

Figure 53. Engine Ducting Cold Regenerator Flow Rig (Gas Side).

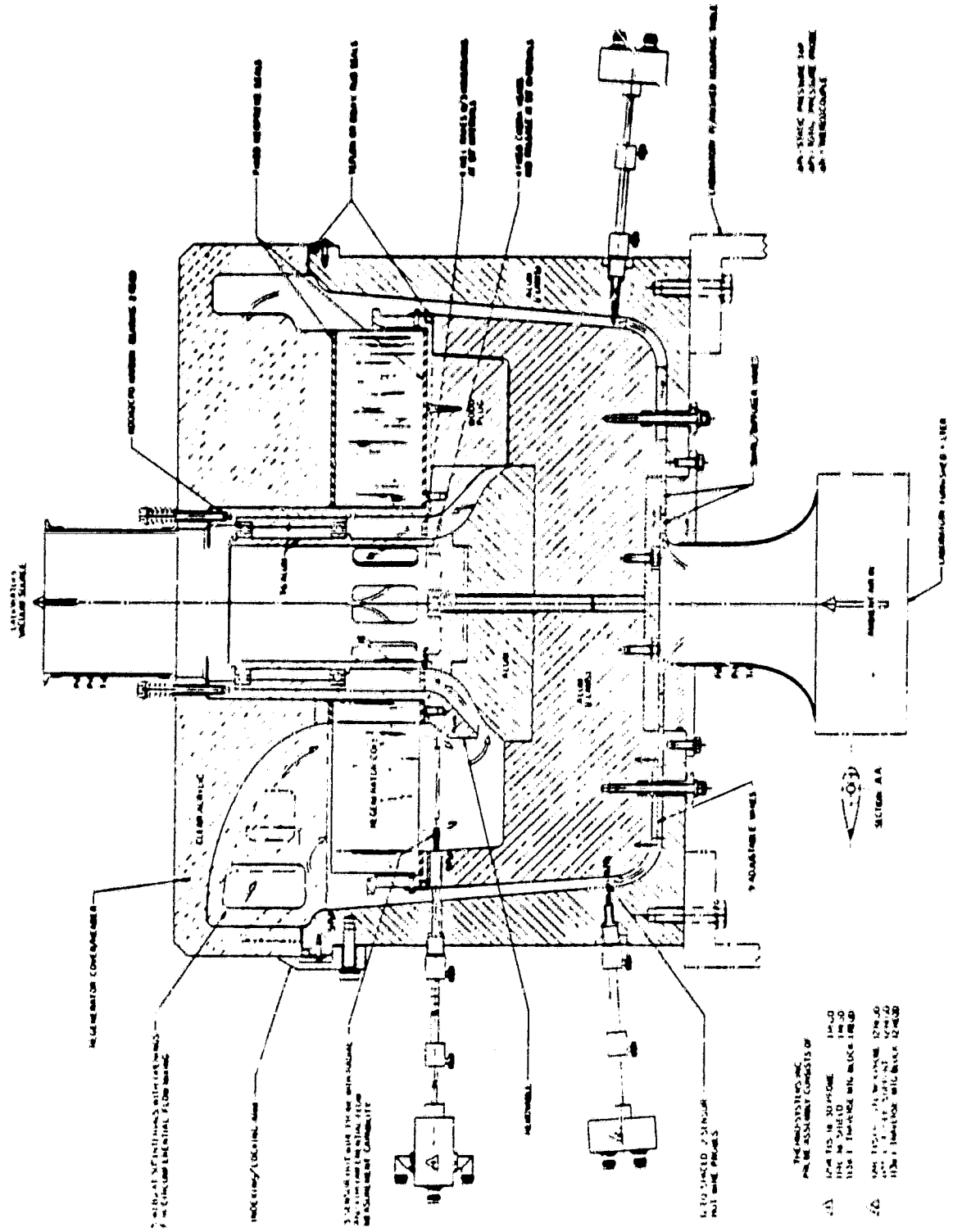

Figure 54. Engine Ducting Cold Regenerator Flow Rig (Air Side).

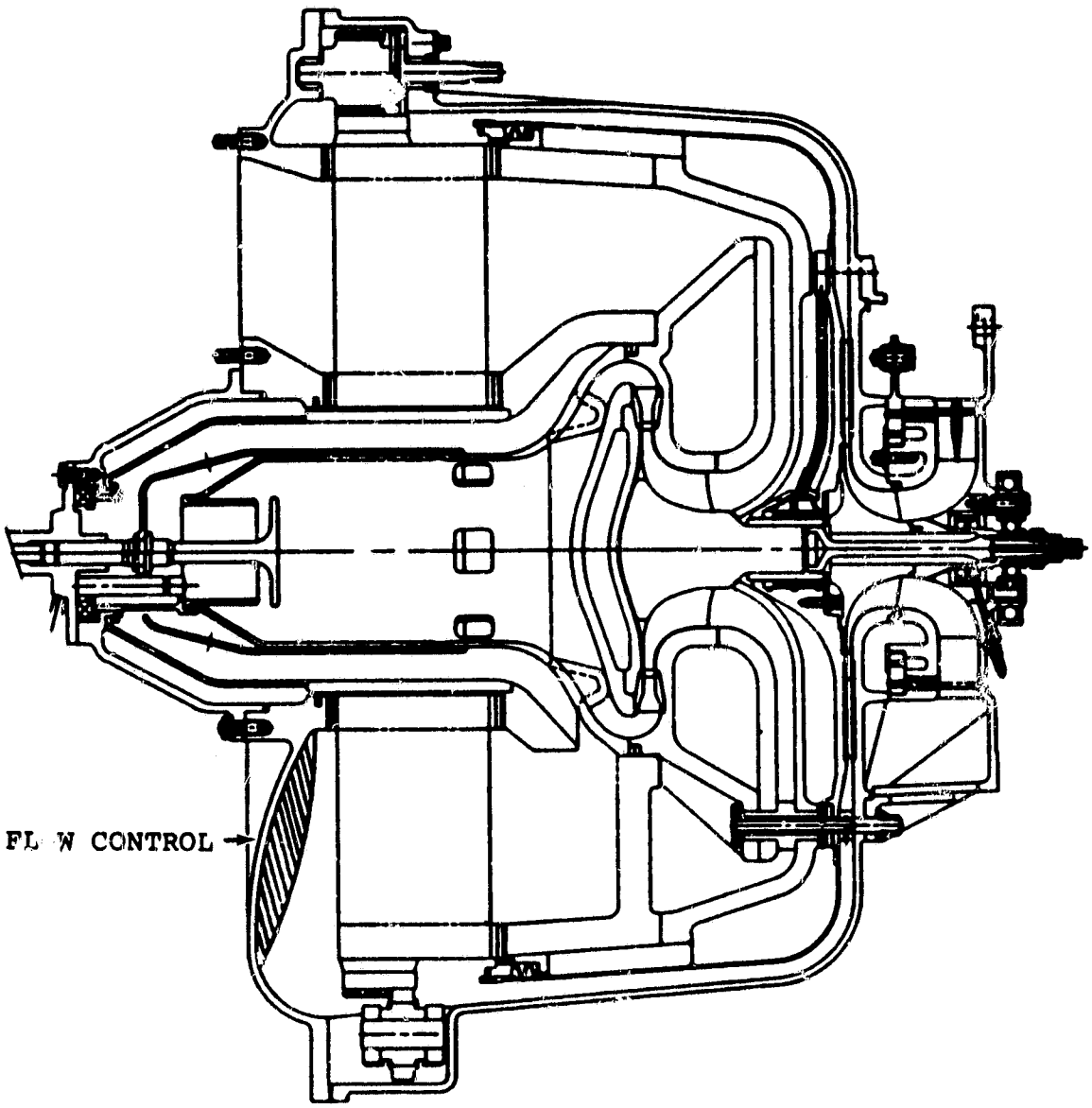

Figure 55. Air Side Alternate Header Design.

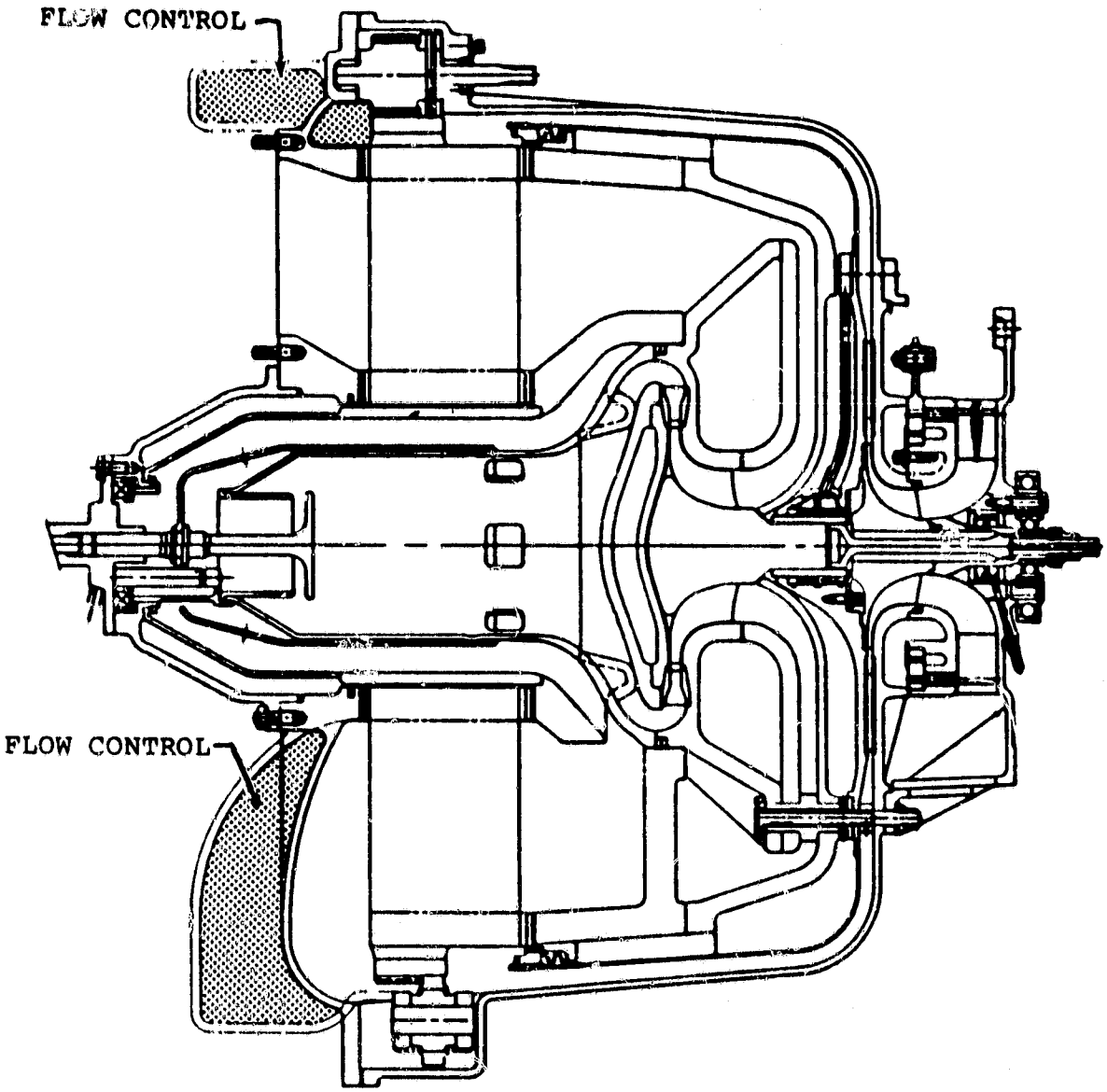

Figure 56. Air Side Alternate Header Design.

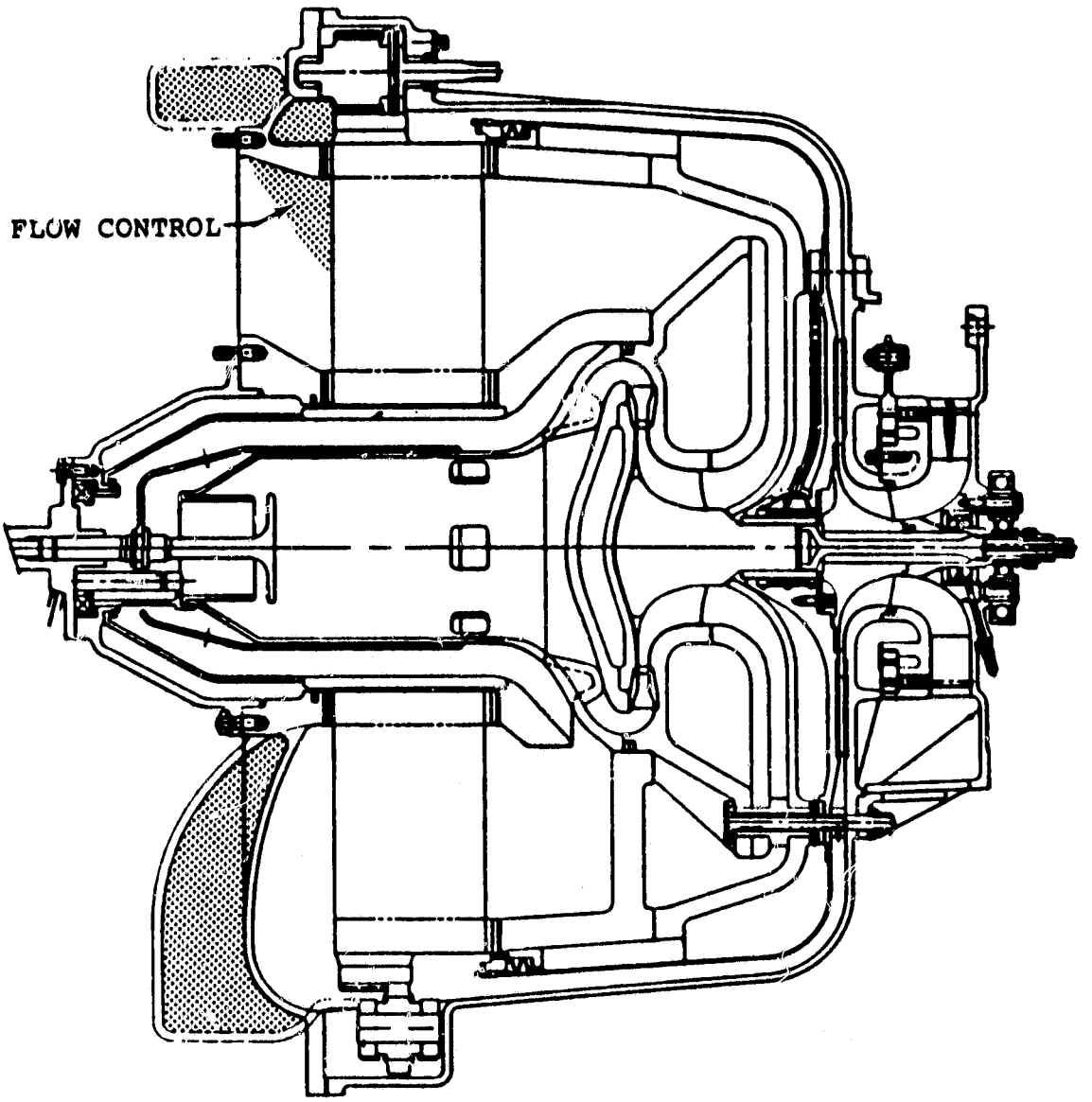

Figure 57. Air Side Alternate Header Design.

AiResearch empirical/analytical combustor design approaches. As a goal, the combustion system will be below the following emission levels for a fuel economy goal of 15.3 Km/L (36 mpg) using gasoline:

Oxides of nitrogen, NO_X	0.25 gm/km (0.40 gm/mile) or less than 5.7 gm/kg fuel
Total unburned hydrocarbons, HC	0.26 gm/km (0.41 gm/mile) or less than 5.8 gm/kg fuel
Carbon monoxide, CO	2.11 gm/km (3.4 gm/mile) or 44.8 gm/kg fuel
Total particulates	0.12 gm/km (0.2 gm/mile) or 2.6 gm/kg fuel

In addition to emission goals, the combustor will have the ability to use a variety of alternate fuels. The following combustor performance parameters have been established to assure that the selected combustor is compatible with the selected engine concept.

• Combustion efficiency	99 percent at all engine operating conditions including altitude cold start, acceleration and deceleration
• Combustor pressure drop	3 percent
• Combustor exit pattern factor	0.15 at the design condition

Based on Ford work with several different combustor rigs in 1973 and 1974, it was established that low emissions could be attained throughout the operating range of the Ford Model 820 turbine engine by using a premixing, prevaporizing combustion system with a properly designed variable-geometry actuation system. The Ford design is shown schematically in Figure 58. Combustor flow conditions for the IGT engine were sufficiently close to the Ford Model 820 turbine engine to afford scaling. Combustor scaling results are shown in Table 6.

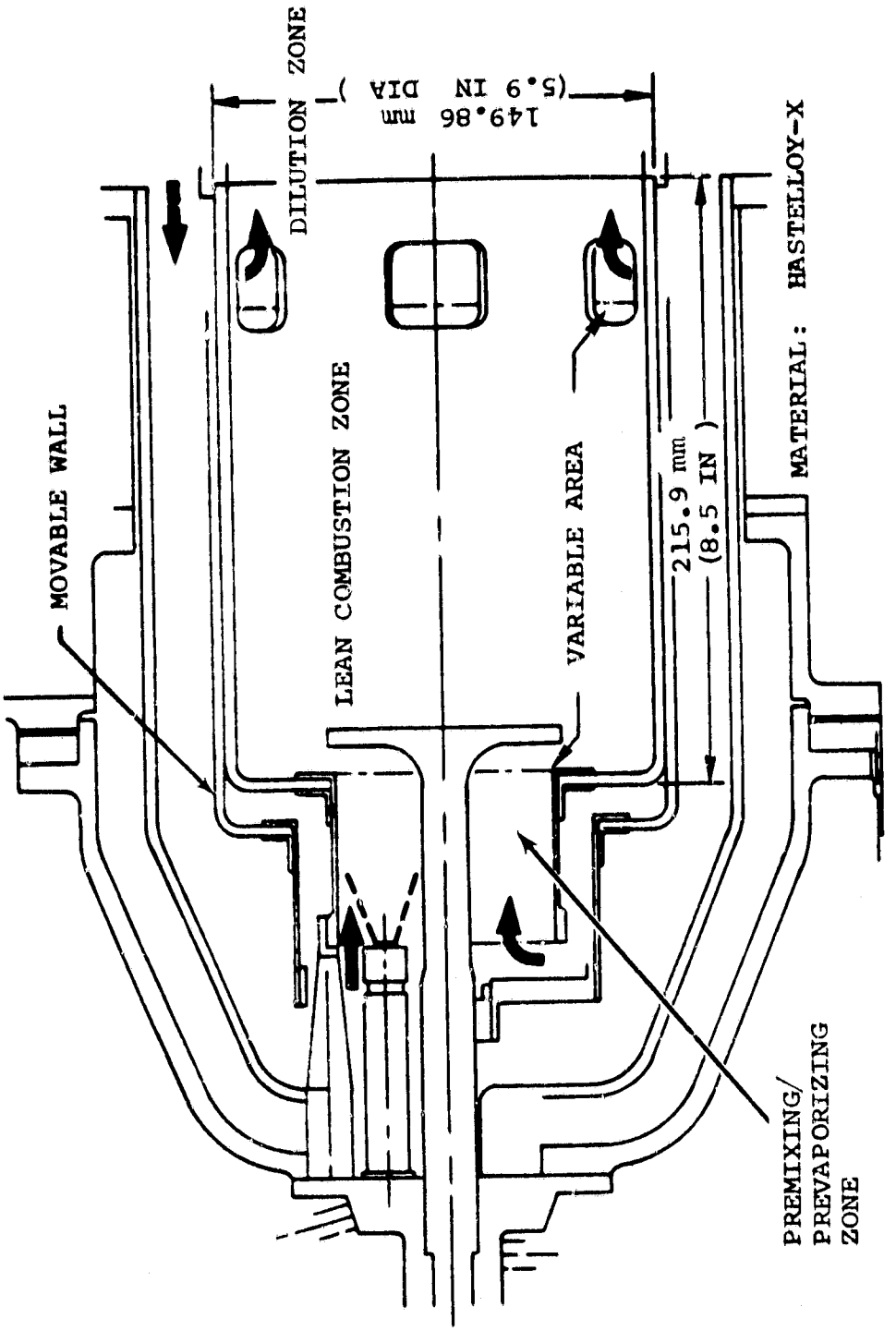

Figure 58. Schematic of Ford 820 PM/PV Variable-Geometry Combustor

TABLE 6

COMPARISON BETWEEN FORD VG COMBUSTOR AND PROPOSED AGT COMBUSTOR

	FORD COMBUSTOR	PROPOSED COMBUSTOR	COMMENTS
Combustor Diameter, mm (in.)	158.75 (6.25)	101.6 (4.0)	
Combustor Length mm (in.)	215.9 (8.50)	146.05 (5.75)	
Combustor L/D	1.36	1.44	PF
Loading Parameter at Idle, kg/s-m^3 (PPS/FT^3)	1.83 (0.114)	0.43 (0.027)	Idle Emissions
Design, kg/s-m^3 (PPS/FT^3)	0.63 (0.039)	0.40 (0.025)	Idle Emissions
Residence Time, MS	7.1	4.7	NO_X
Idle TIT, K (°R)	888.9 (1600)	1344.4 (2420)	Idle Emissions

In describing the combustor, it is convenient to separate its operation into three areas; prevaporized-premixer channel, variable-geometry feature, and fuel nozzle. The following discussion describes various phases of design methodology and presents the latest combustor configuration.

The purpose of the prevaporized-premixer channel is to vaporize liquid fuel prior to entering the burning zone. A problem encountered in the vaporizing zone is the potential of flashback or premature burning in the prevaporizing channel. Ford successfully eliminated this problem through selection of an appropriate reference velocity in the premixing zone. Thus, the AGT reference velocity of 31.21 m/sec (102.4 ft/sec) and prevaporizing diameter of 58.4 mm (2.3 inch) were scaled from the Ford configuration. The prevaporizer length was established by calculating the distance required for the fuel droplets to completely vaporize without impinging on a solid boundary. Two spray cone angles (45 and 70 degree) were studied in conjunction with two initial droplet sizes; Sauter Mean Diameters (SMD), of 50 and 25 microns. Results of this study indicated that a prevaporizing length of 58.4 mm (2.3 inch) provides adequate distance for the fuel droplets to vaporize at all operating conditions, including a margin allowing for the presence of excessively large diameter droplets. The importance of complete vaporization prior to wall impingement can be seen from information based on pre-ignition studies on internal combustion engines indicating that ignition will occur if fuel contacts surfaces with temperatures in excess of 1144K (1600°F).

The importance of the variable geometry mechanism for the AGT combustor is paramount. Changes in geometry should duplicate the area changes required, as well as the ability to respond quickly. Since the AGT primary zone fuel-air ratio will be lean for NO_X control, lack of a quick acting variable geometry system could either increase the fuel-air ratio, which would cause an increase in emissions, or decrease the fuel-air ratio causing blow out.

Prevaporizer and secondary orifice flow split is dictated by emissions considerations. The control of unburned hydrocarbons (HC) and carbon monoxide (CO) can be accomplished by assuring uniform and complete mixing of the fuel and air. This should be accomplished by proper injector-prevaporizing zone design. The formation of nitrogen oxides (NO_X) can be minimized by burning at very lean fuel air ratios. Work presented in NASA conference publication 2078, Figure 59, reported that if the maximum combustor temperature is kept below 1922K (3000°F) for a residence time not exceeding two milliseconds, the amount of NO_X produced is equal to 2.0 kg NO_X/1000 kg fuel assuring achievement of the program goals. To maintain a 1922K (3000°F) combustor temperature, the flow-split between the prevaporizer and secondary orifices would be as shown in Figure 60.

The combustor burner metering open area will not only be varied to obtain the desired flow-splits, but also to maintain a combustor pressure drop of three percent of combustor inlet pressure. Since inlet conditions to the combustor vary considerably, depending on the power setting, some compromises will be necessary. Combustor inlet conditions versus shaft horsepower are shown in Figures 61 through 65. Variations result from different compressor VIGV settings in correlation to different engine controlling limits dependent on speed. Thus variations in inlet conditions will necessitate that nominal design emissions goals be set sufficiently below program goals to ensure that emissions encountered at the more severe operating conditions will not exceed overall driving cycle goals.

Present baseline combustor configurations are shown in Figure 66. The fuel injector in subjected to combustor pressure drops under all conditions, and primary zone airflow is increased by metering flow through a swirler concentric about the fuel nozzle. Swirling primary air should increase the rate at which air and fuel mix thereby creating a more homogeneous mixture. The main burner for both combustor configurations is identical except for differences in the premixer-vaporizer section. One configuration employs an axial swirler vane surrounding the fuel nozzle, whereas the other design uses a radial inflow swirler surrounding the fuel nozzle. The radial inflow swirler configuration reduces the fuel nozzle length immersed in hot combustor inlet gases as well as simplifying variable geometry controlling devices.

The swirler metering section, center body plunger, and dilution zone metering are all linked together. As fuel flow increases, the plunger moves in, as does the swirler metering block, increasing air flow to the swirler. At the same time, the secondary area is closed off maintaining approximately the same total combustor open area. Methods for calculating both vaporizer and combustor size were accomplished. In the first step the

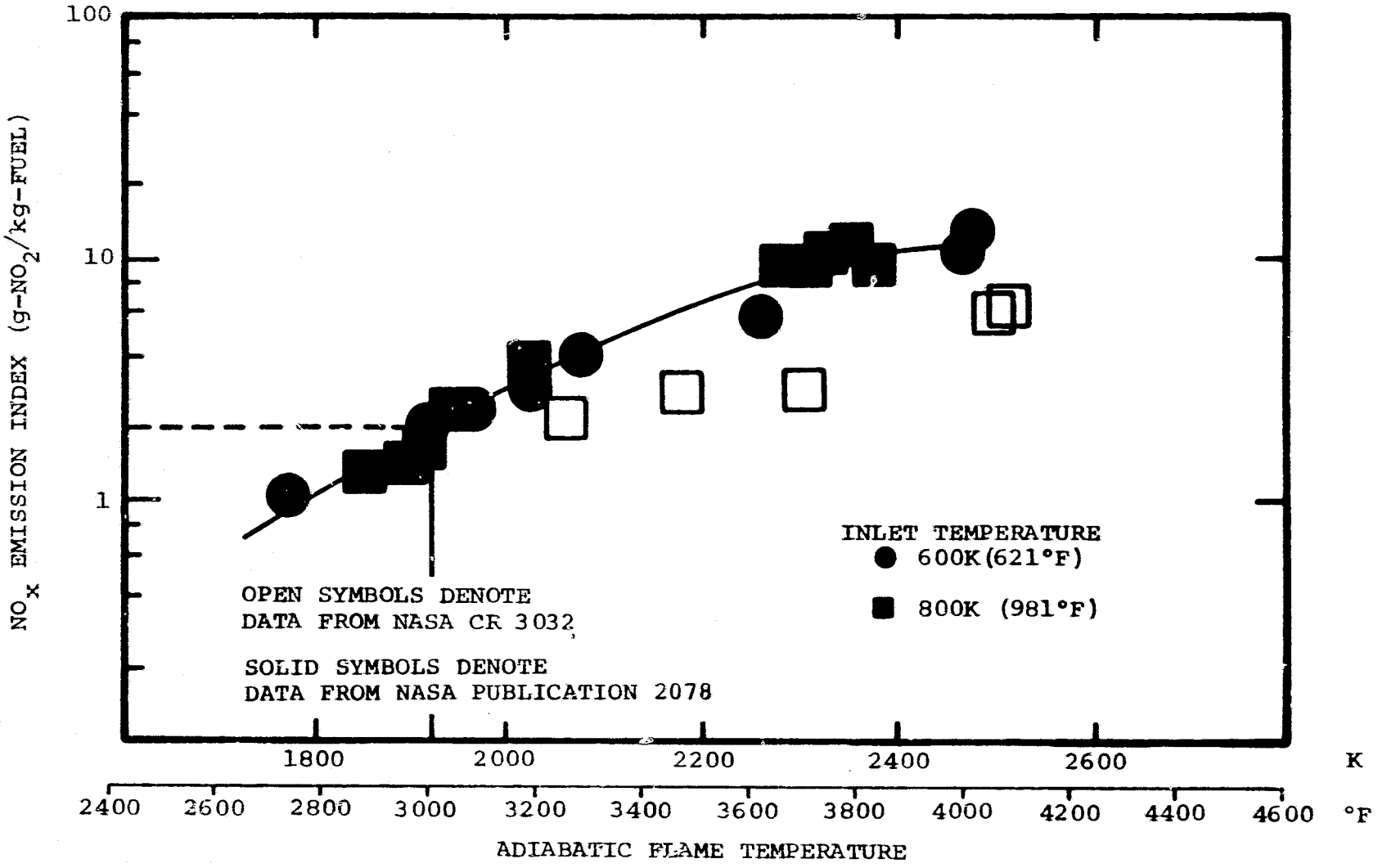

Figure 59. Correlation of NO_x Emission Index for 2 ms Residence Time with Adiabatic Flame Temperature.

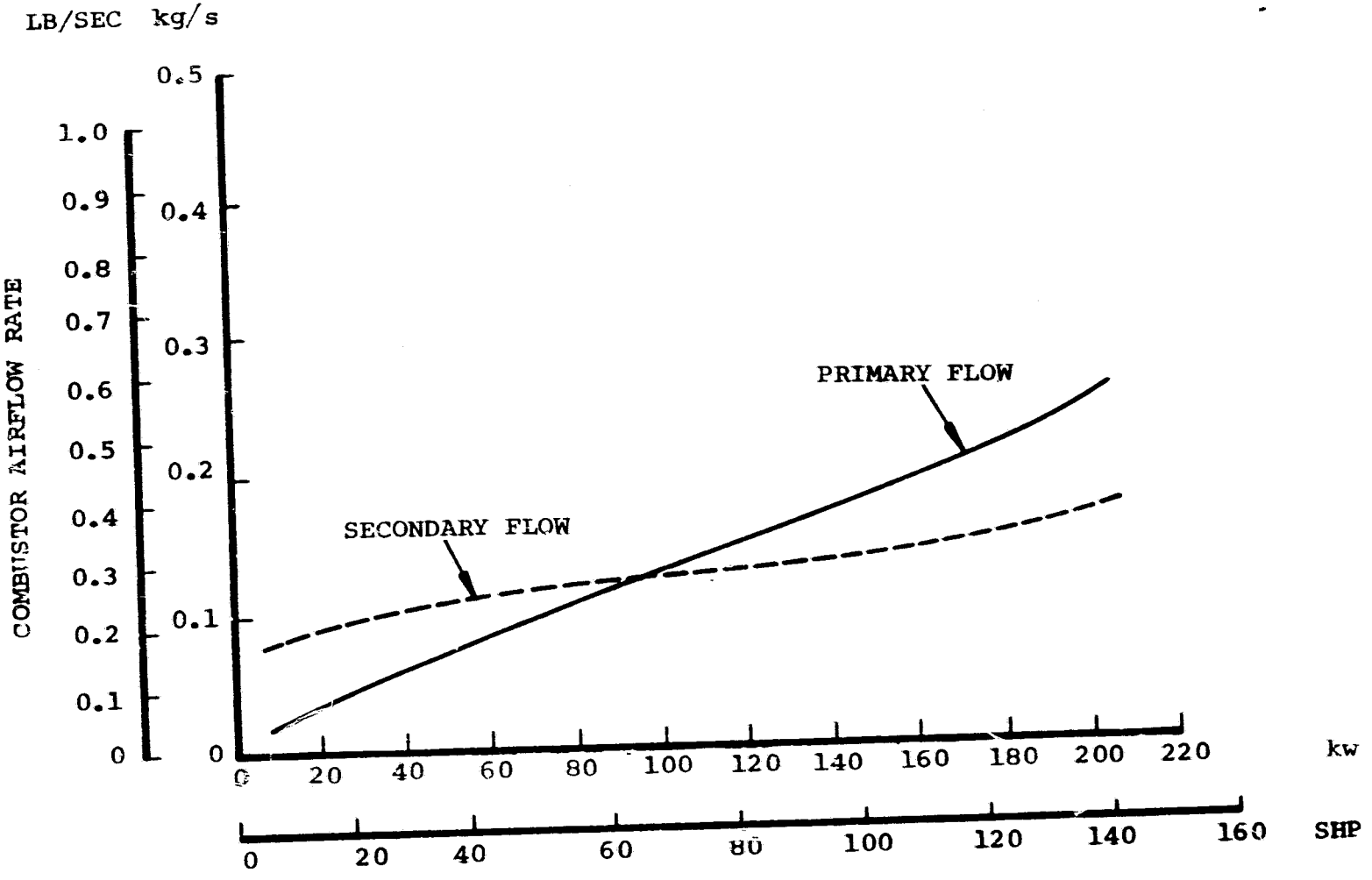

Figure 60. Flow Split Between the Vaporizer and Dilution Orifices to Maintain a Maximum Primary Zone Combustion Temperature of 1922K (3000°F) at Various Power Settings.

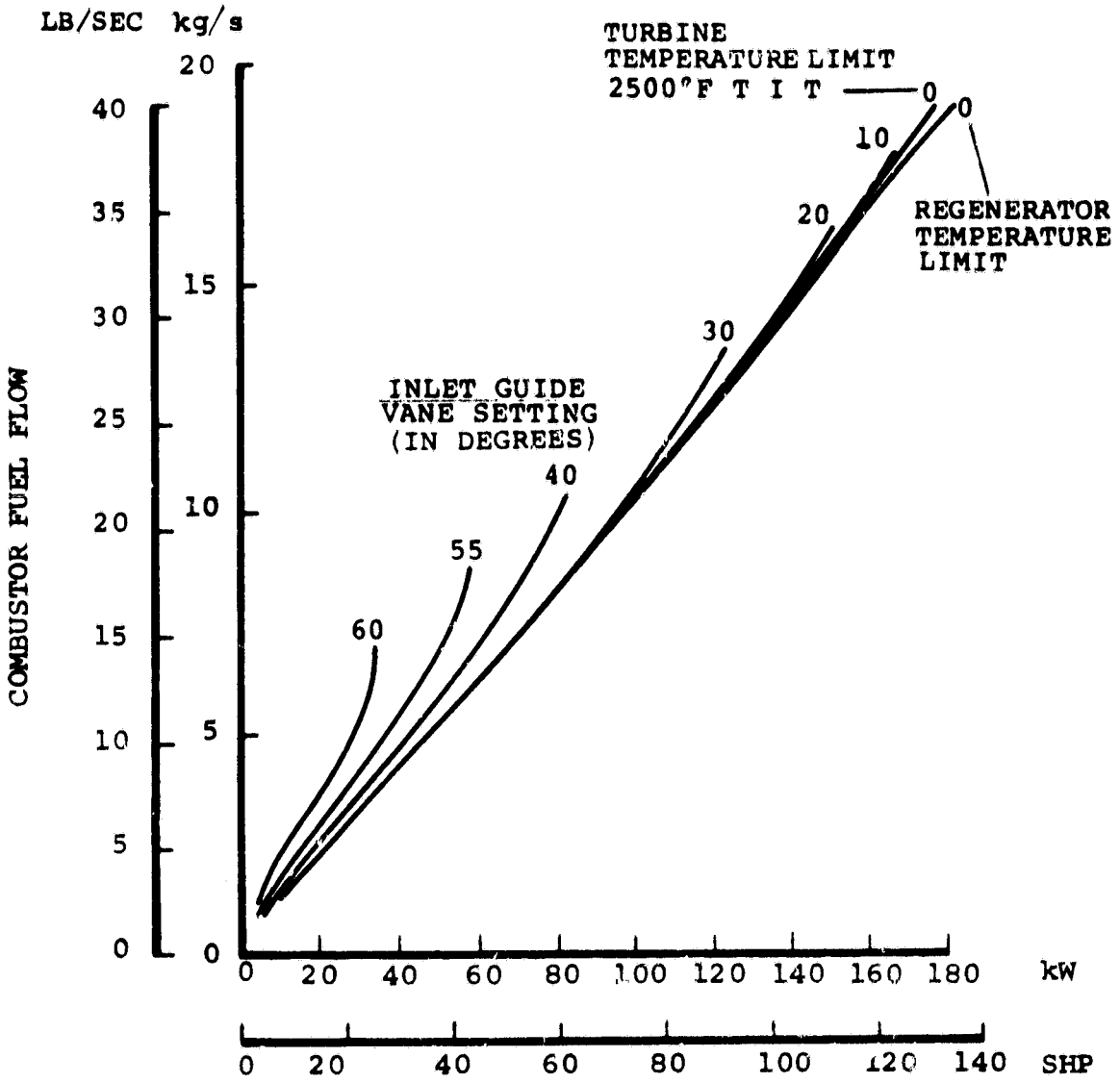

Figure 61. Effect of Engine Power on Combustor Fuel Flow.

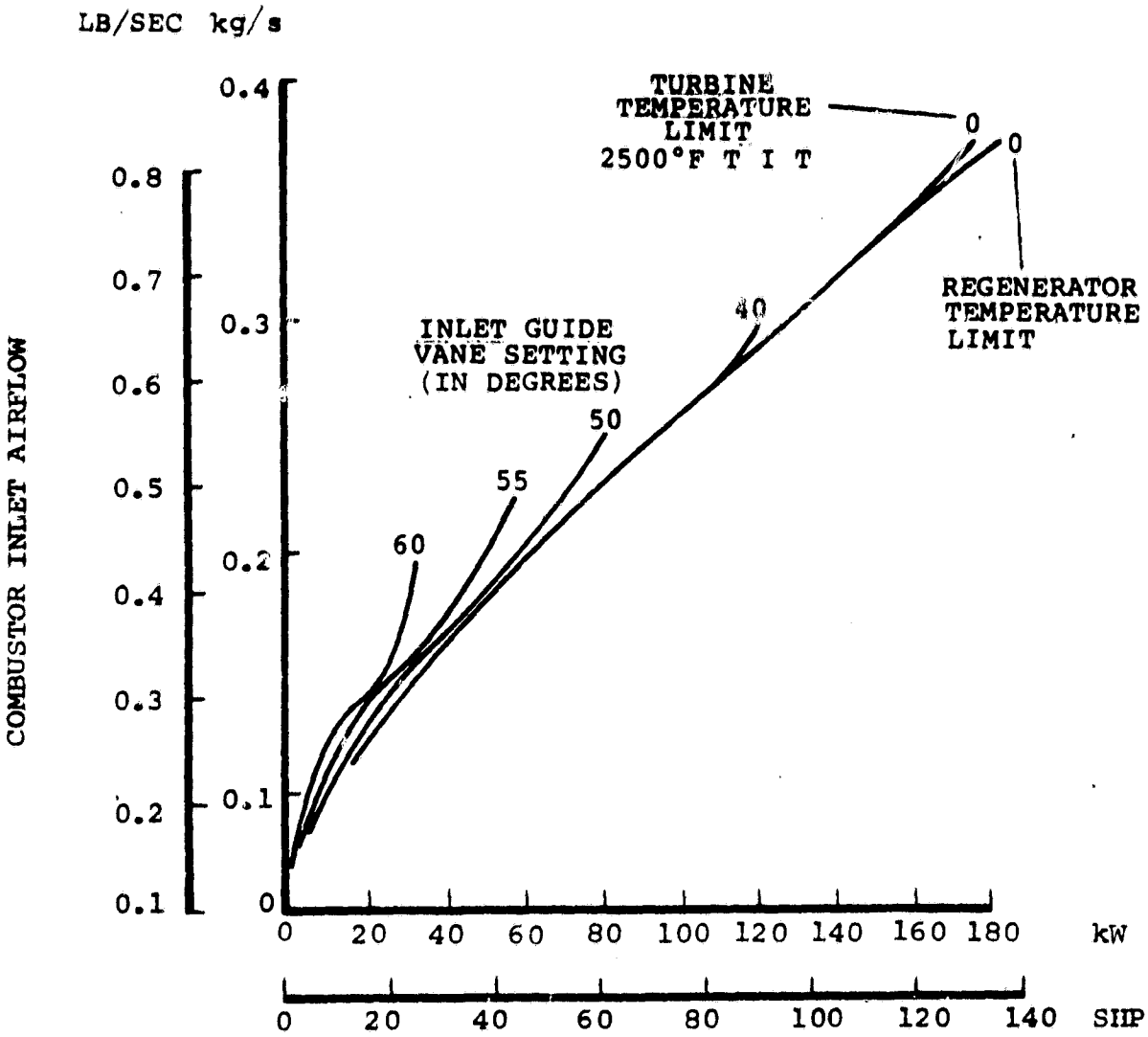

Figure 62. Effect of Engine Power on Combustor Airflow

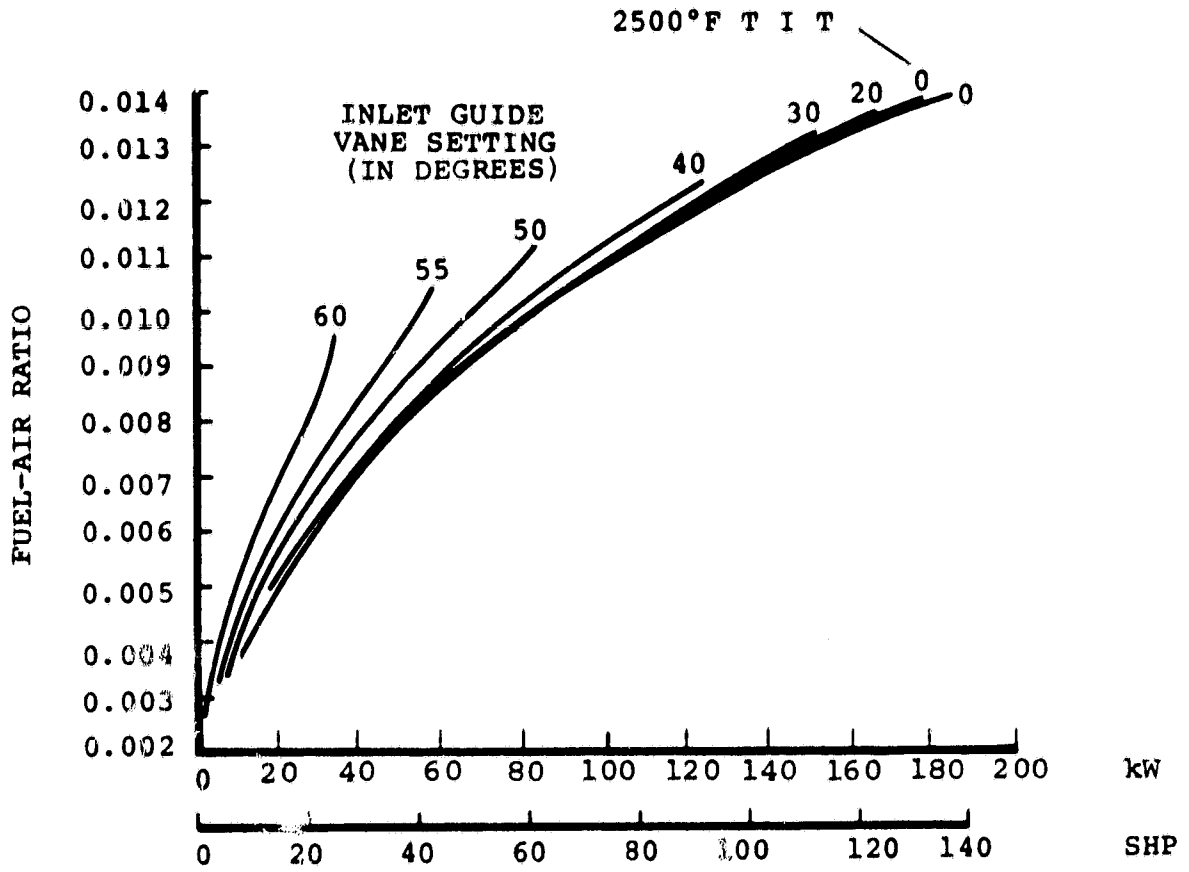

Figure 63. Effect of Engine Power on Combustor Fuel-Air Ratio

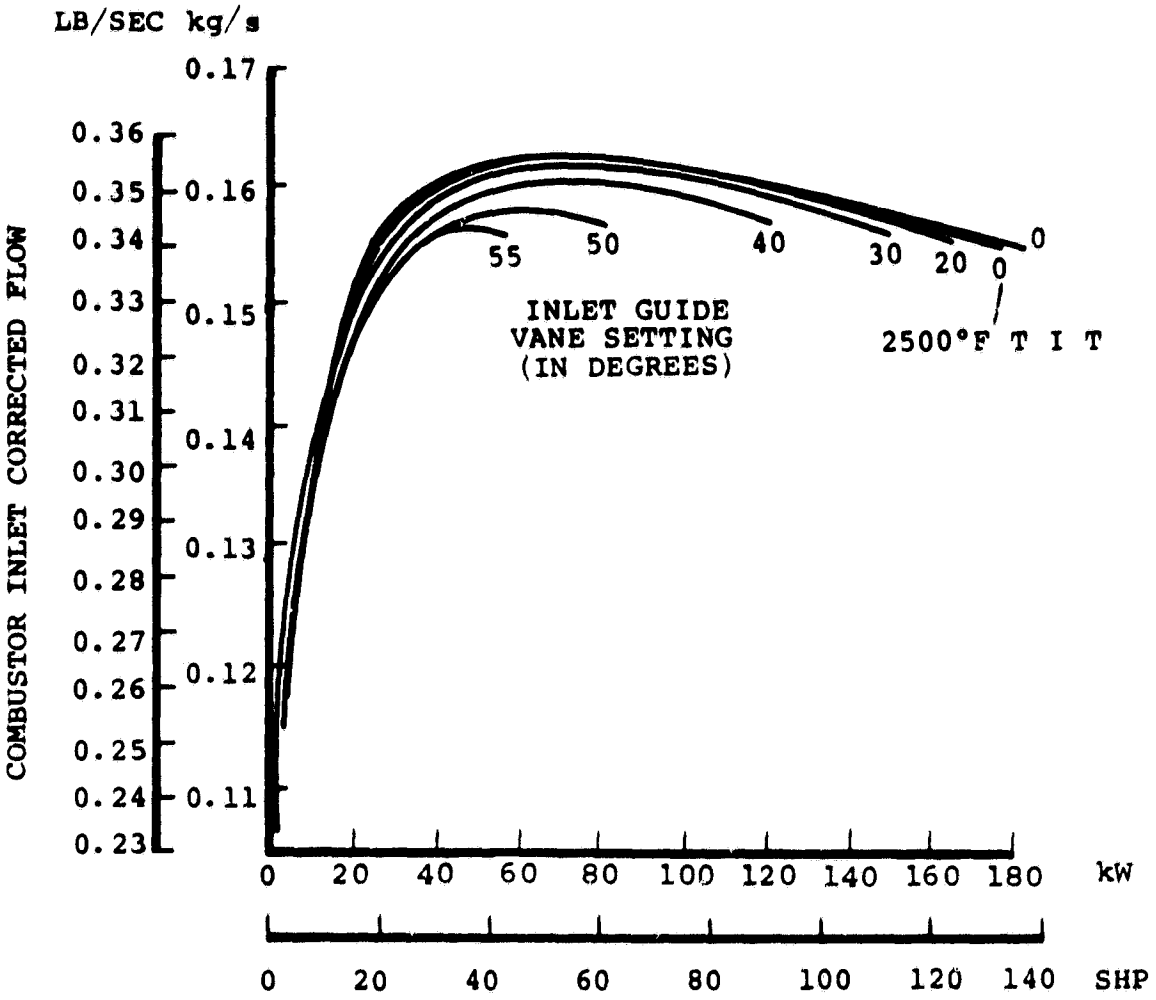

Figure 64. Effect of Engine Power on Combustor Corrected Airflow.

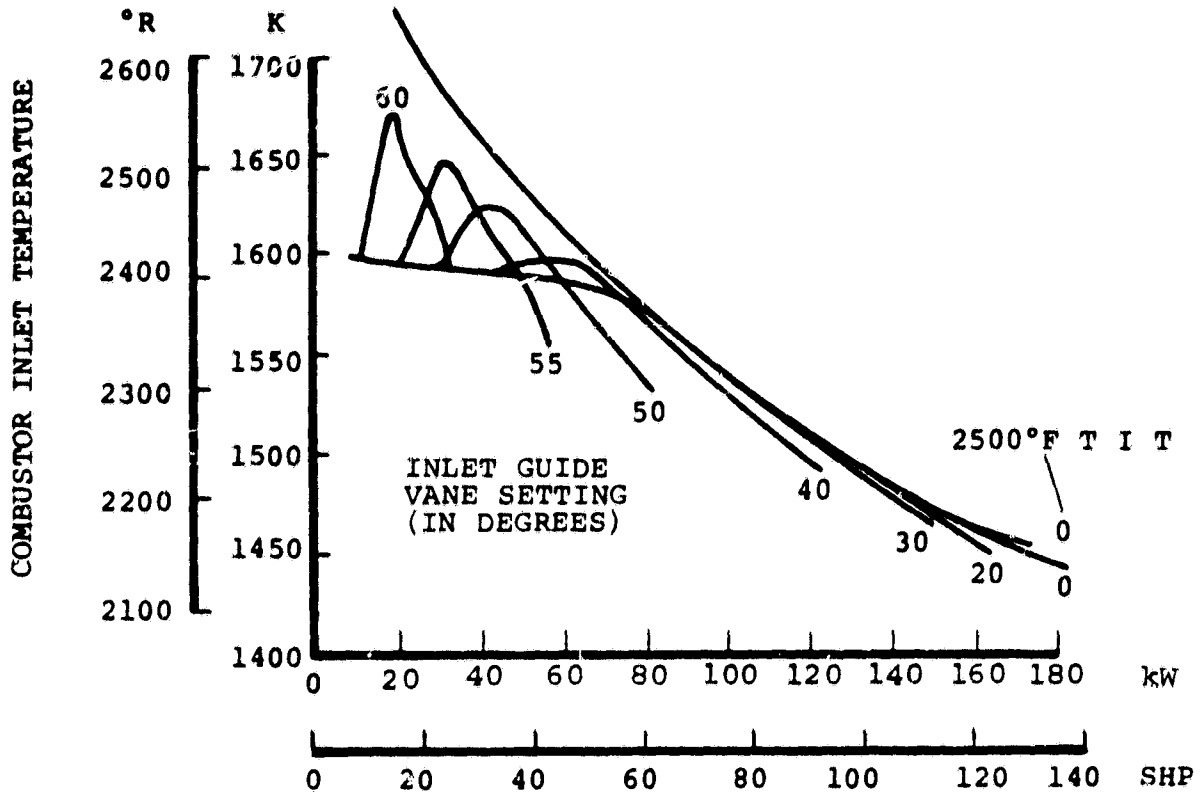

Figure 65. Effect of Engine Power on Combustor Inlet Temperature.

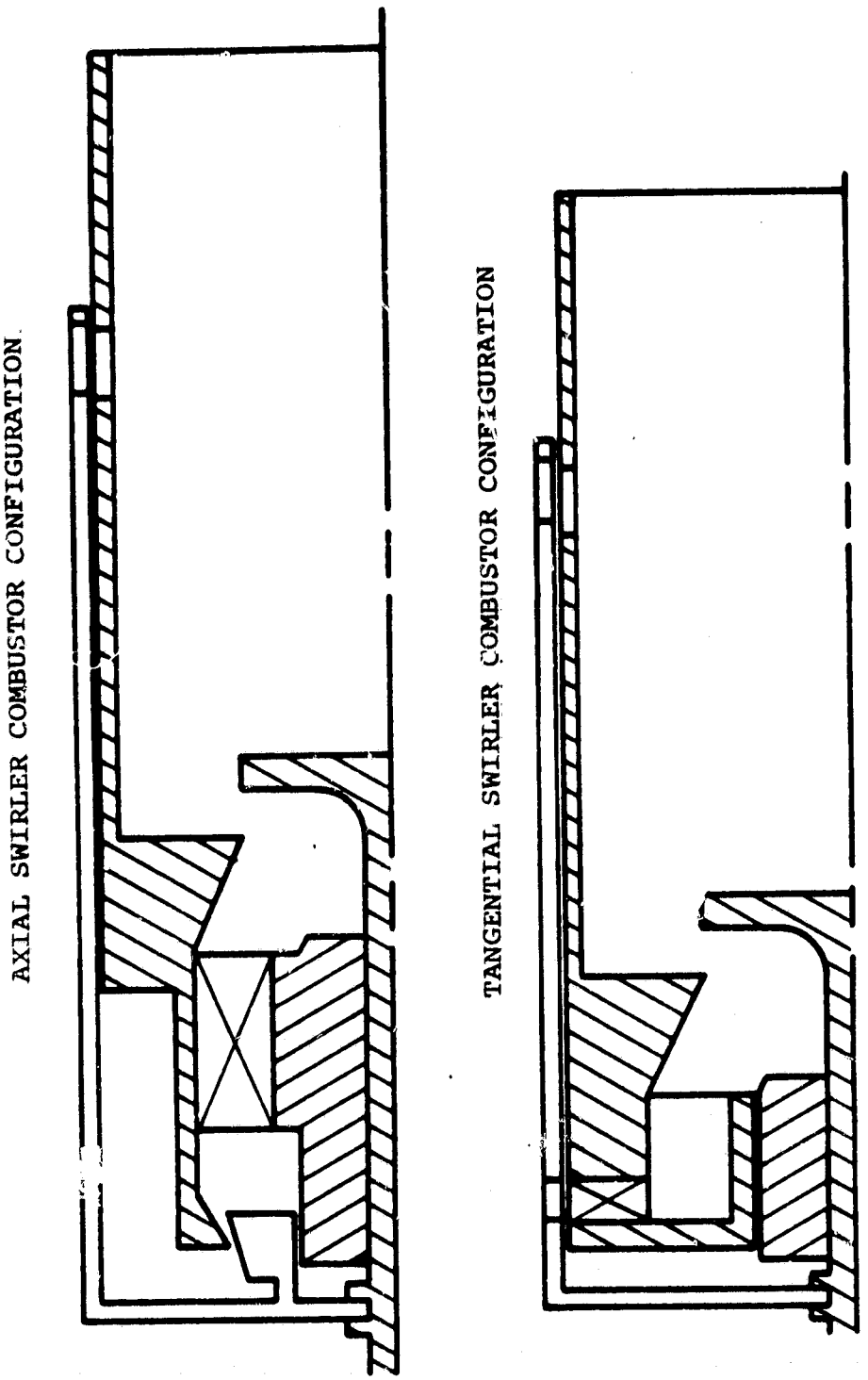

C-2

Figure 66. Combustor Configurations.

combustor effective open area for various metering locations was calculated for 88 different sets of combustor inlet conditions, based on predictions by the performance model. Points covered were from idle to maximum power, including acceleration points. Various areas were calculated to yield a primary zone temperature of 1922K (3000°F). Plots of various open areas as a function of fuel flow are shown in Figures 67, 68, and 69. As can be seen, area variation for a given fuel flow is significant necessitating fitting a curve through the area plots such that one distinct area existed for a given fuel flow as shown in Figure 70. With this area variation, the model was then used to predict the variation in primary zone temperature, shown in Figure 71. Points above 2177K (3460°F) coincided with short time period (approximately 2 seconds) engine acceleration points, which should have little effect on the overall cycle emissions.

AGT fuel nozzle development offers a unique challenge. The high combustor inlet temperature environment could cause fuel degradation and cracking within the nozzle resulting in plugging and reduced auto ignition effectiveness. Also, pre-ignition can occur if the fuel-air mixture contacts any surface exceeding 1144K (1600°F).

The preliminary fuel injection system design under investigation for the AGT combustor differs from the Ford system in that a single, centrally located fuel nozzle is used, whereas the Ford system employed three individual nozzles. Preliminary studies have shown that the single nozzle located concentric about the shaft will produce a more uniform circumferential fuel distribution. A conceptual design is shown in Figure 72. Cycle analysis is currently being conducted regarding effects of compressor bleed as a source for air assist.

Surrounding the airblast fuel injector is a swirler with turning vanes set at 30 degrees with respect to the combustor axis. The swirling airflow around the nozzle enhances mixing of the fuel and air creating a uniform fuel-air mixture, thereby minimizing local rich and lean regions. The tentative flow split within the nozzle is as follows:

Passage	Percent of Total Nozzle Airflow, Percent
Inner airblast	23.9
Outer airblast	37.0
Shroud	39.1

The ratio of inner to outer airblast airflow was selected based on a survey of flow splitters in various airblast nozzles currently being used at AiResearch Phoenix. Shroud air was selected to be approximately two-thirds of the inner and outer airblast air combined. This should produce a spray cone angle between 50-70 degrees as demonstrated on a previous combustor program.

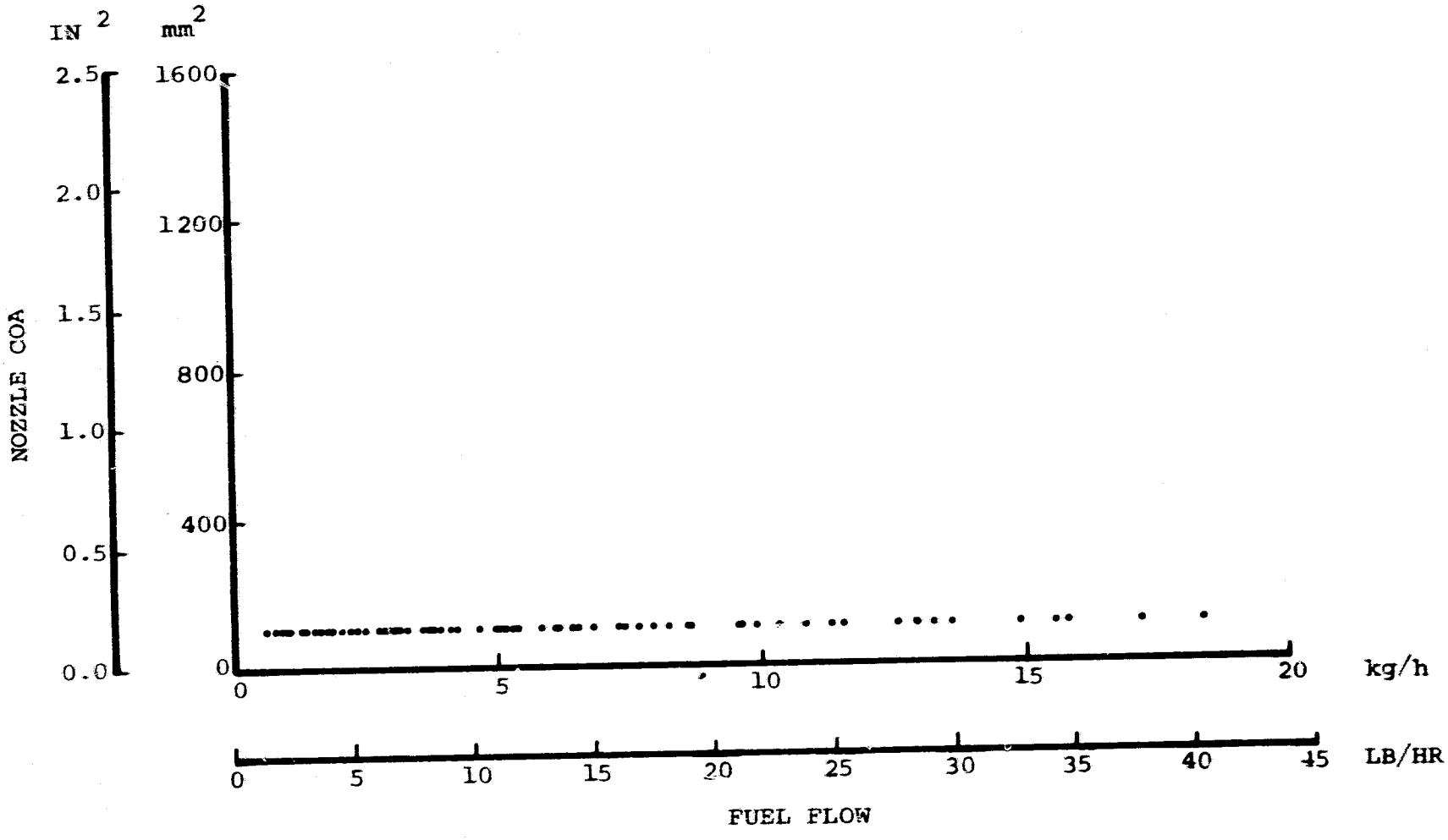

Figure 67. Nozzle Effective Area Versus Fuel Flow for a 1922K (3000°F) Primary Zone Temperature.

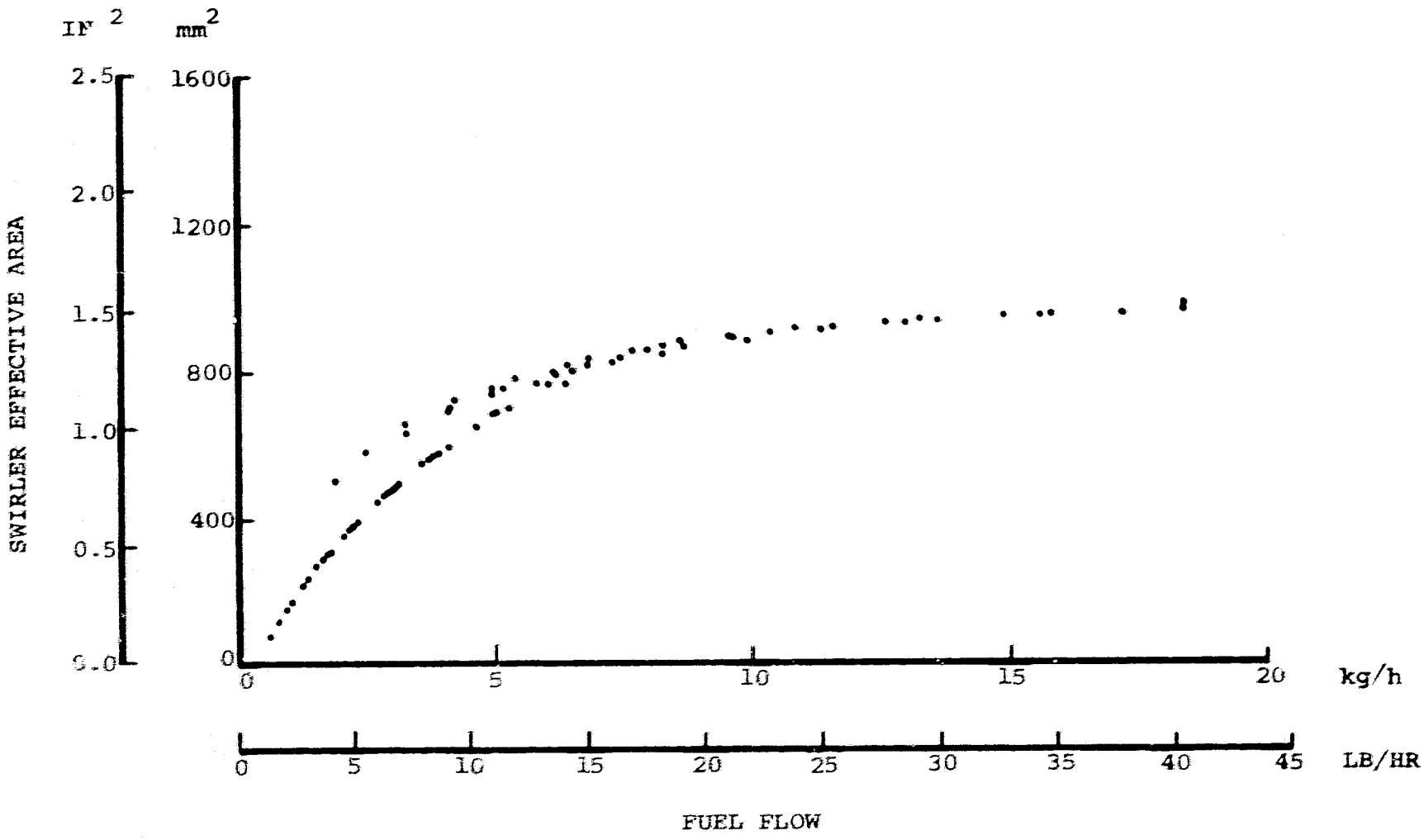

Figure 68. Swirler Effective Area Versus Fuel Flow for a 1922K (3000°F) Primary Zone Temperature.

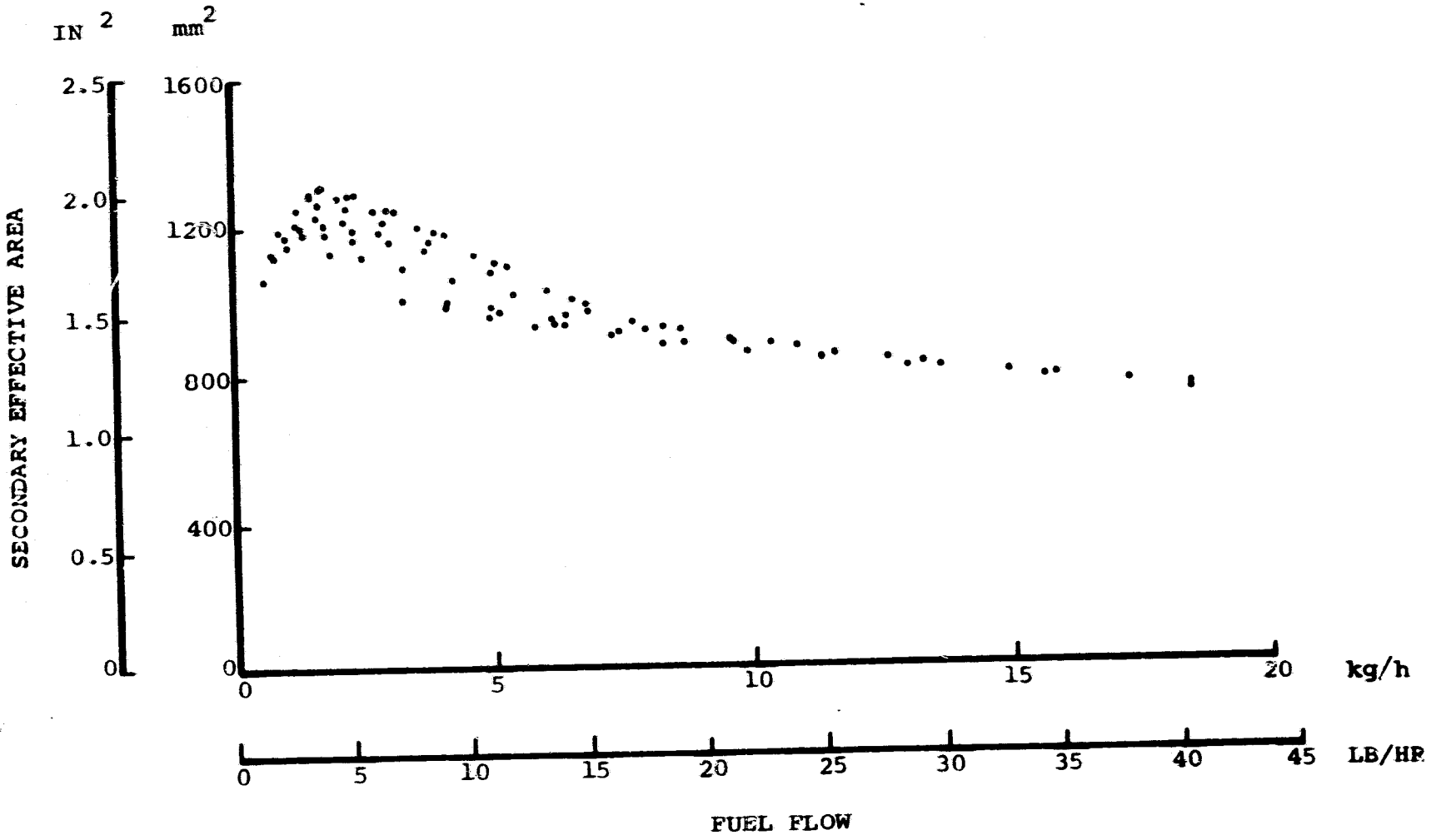

Figure 69. Secondary Effective Area Versus Fuel Flow for a 1922K (3000°F) Primary Zone Temperature.

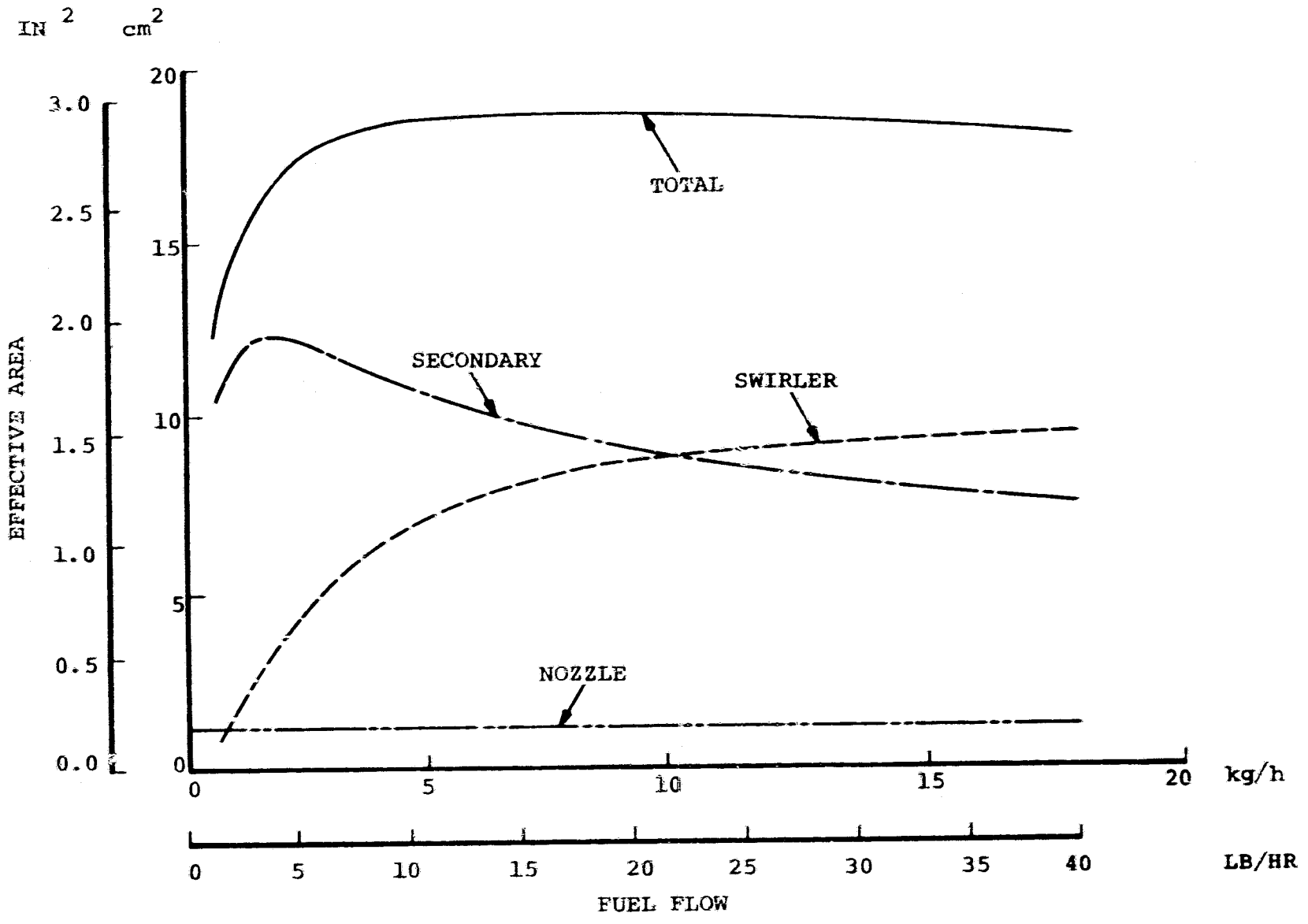

Figure 70. Combustor Open Effective Area for Various Locations as a Function of Fuel Flow.

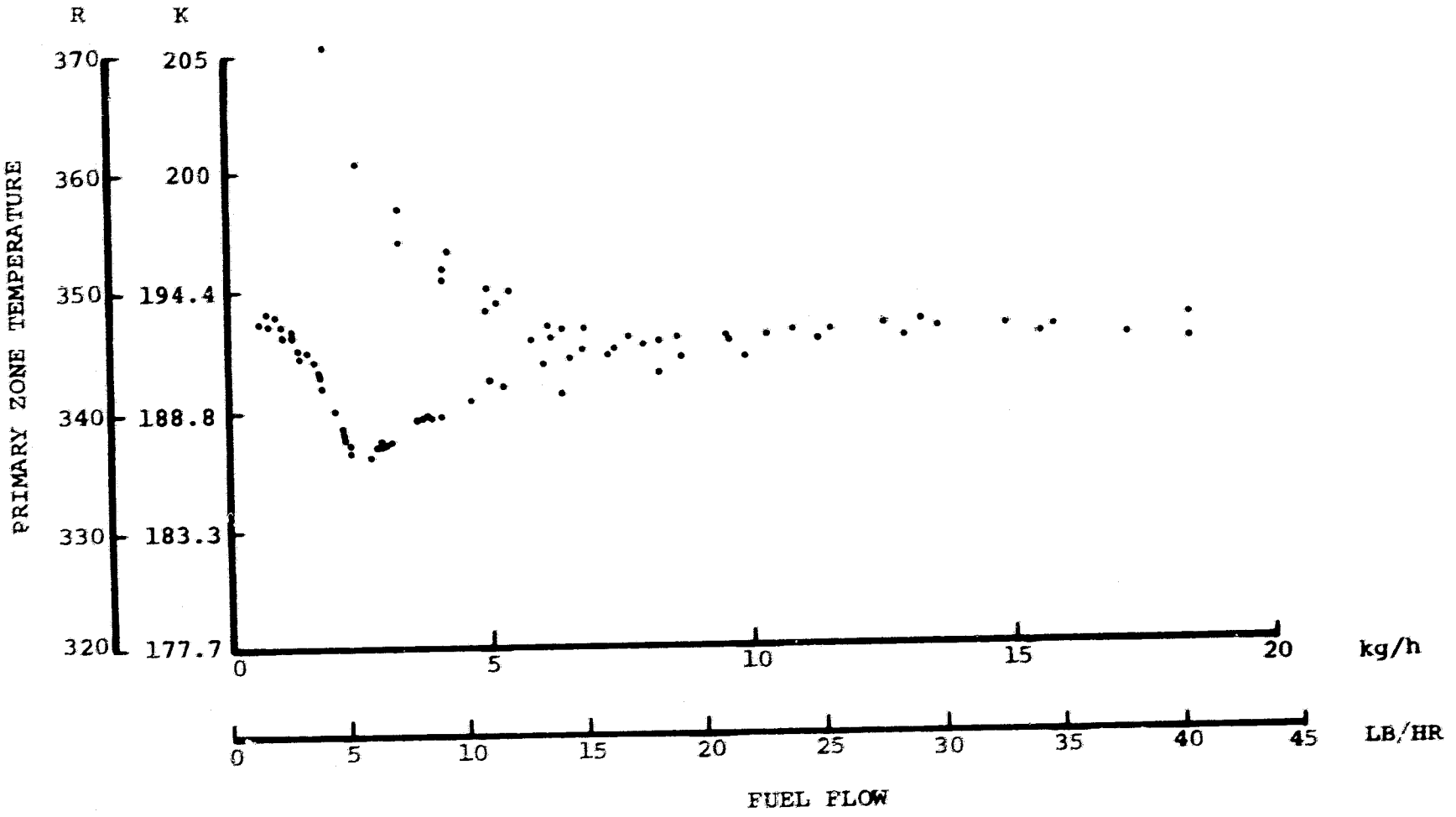

Figure 71. Variation of Primary Zone Temperature as a Function of Fuel Flow.

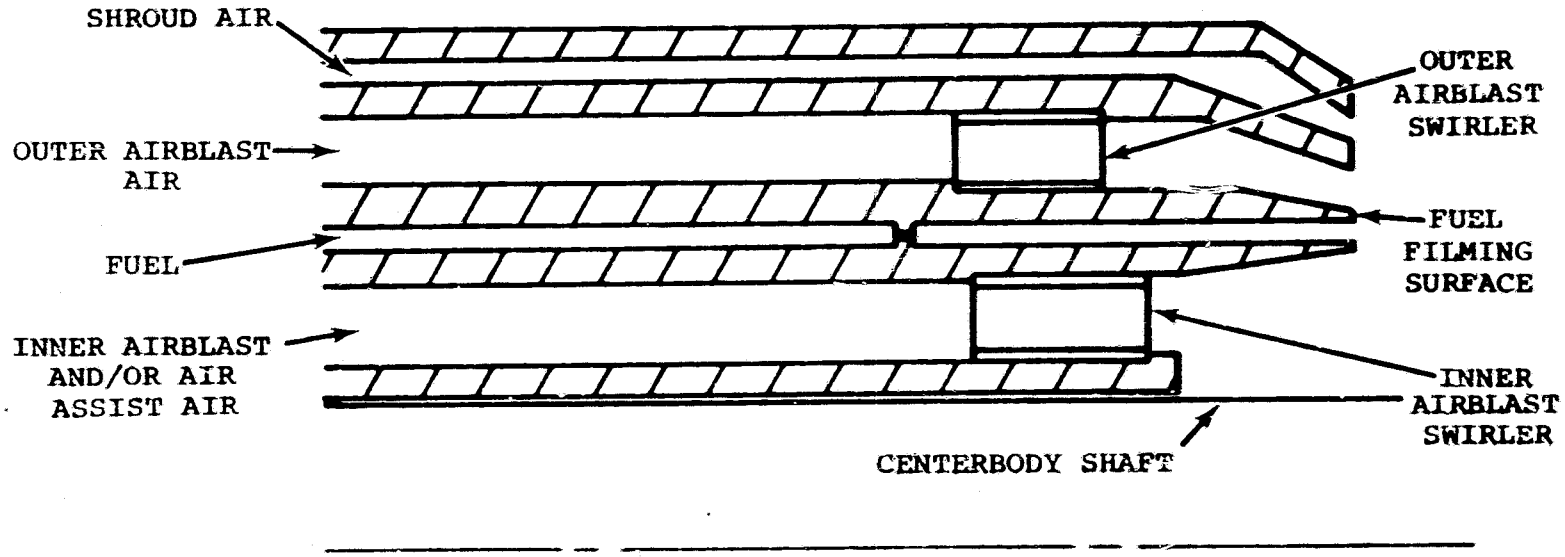

Figure 72. Fuel Nozzle Schematic.

To avoid preignition, it will be necessary to keep vaporizer residence time below the ignition delay time. As shown in Figure 73 ignition delay for octane is 0.7 milliseconds at 1366K (2000°F). Data taken at 1477K (2200°F) indicated a delay time of 0.2 milliseconds. Short vaporizer residence time impact on the fuel injector is such that the injector must supply a finely atomized spray on the order of 20 micron SMD to achieve vaporization of the majority of the fuel in the 0.7 millisecond range. The effect of initial droplet size on time to evaporate the fuel is shown in Figure 74. For a 0.7 millisecond residence time, maximum allowable fuel droplet size is 24 microns, which would necessitate an average droplet size of approximately 15 microns. At the present time, several novel fuel injection devices are being evaluated at NASA-LeRC that show promise in a vaporizer application. However, airblast injection is a more proven method of injecting fuel at a small droplet size over a wide range of fuel flows.

Due to design complexity associated with the fuel nozzle, the decision was made to contact nozzle vendors for design concepts. A nozzle envelope, similar to a previously mentioned AiResearch design, and nozzle inlet conditions at various engine conditions have been given to several fuel nozzle vendors. Specific nozzle requirements include good atomization at all operating conditions including starting, minimal fuel pressure drop across the nozzle, and the possibility of internal nozzle cooling including both air and fuel as the cooling media.

2.1.10.1 Combustor Test Rig

A test rig definition has been completed to facilitate testing of the variable geometry combustor. The test rig will be built in two configurations with relatively minor modifications required to convert from one configuration to the other.

Figure 75 shows a conceptual drawing of the first build. Thermocouple probes are not shown, but it is intended that these be located at a point near the burner discharge. The purpose of this build is to verify combustor operation and establish a temperature pattern at the burner discharge.

Figure 76 is a conceptual design for the second build. The duct section of the first build has been replaced by a nose cone. The purpose of this configuration is to simulate the engine flow path prior to the turbine and acquire temperatures and pressures at a point that will coincide with the turbine stator.

2.1.11 Turbine Definition

2.1.11.1 Preliminary Investigation

Need for high overall performance over the wide range of operating conditions for an automotive application requires that component performance be high at the idle and intermediate power operating conditions where the most fuel is consumed. However, to

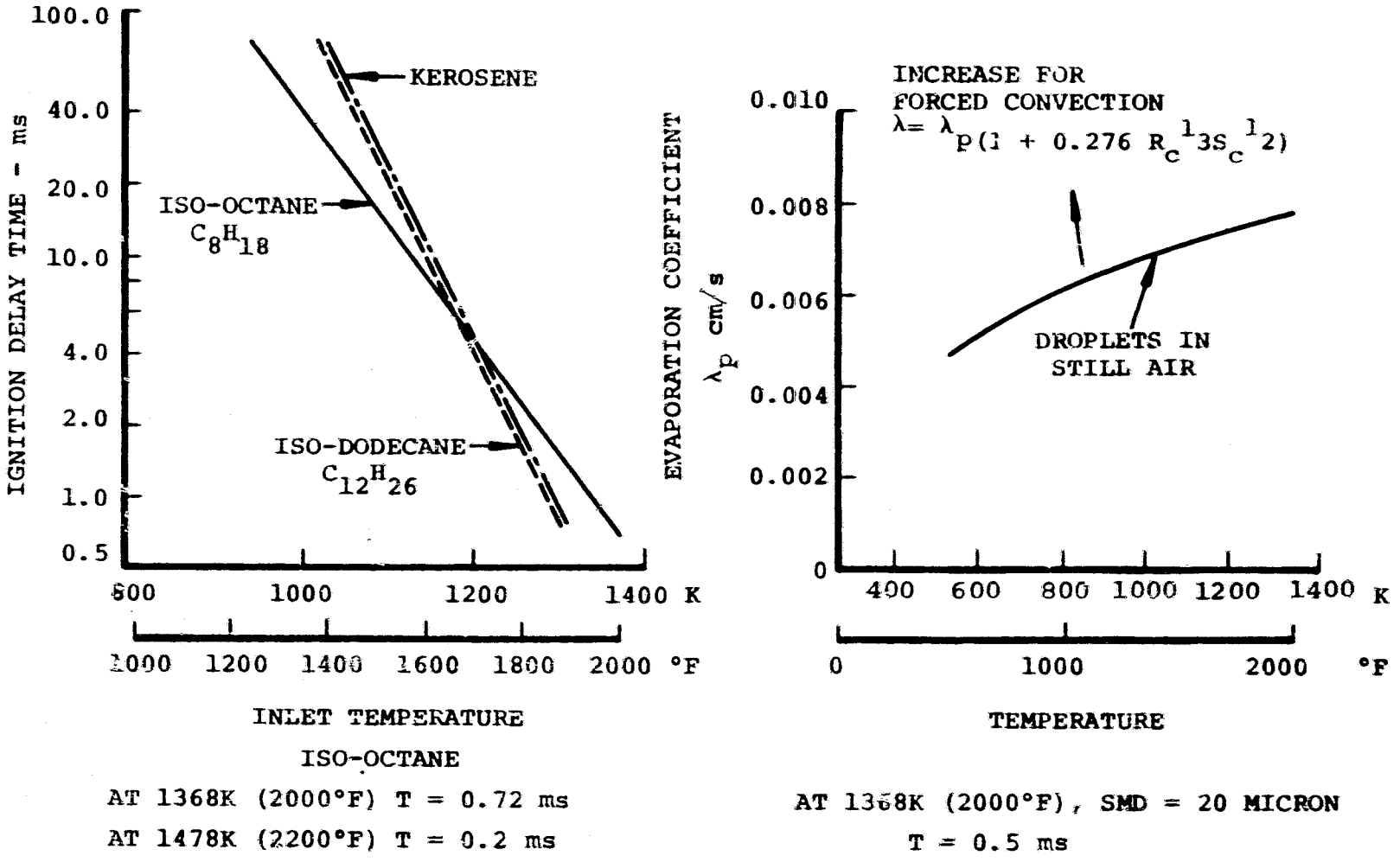

REFERENCE: ASME PAPER NO. 73-GT-11

Figure 73. Effect of Inlet Temperature on Ignition Delay and Evaporation Coefficient.

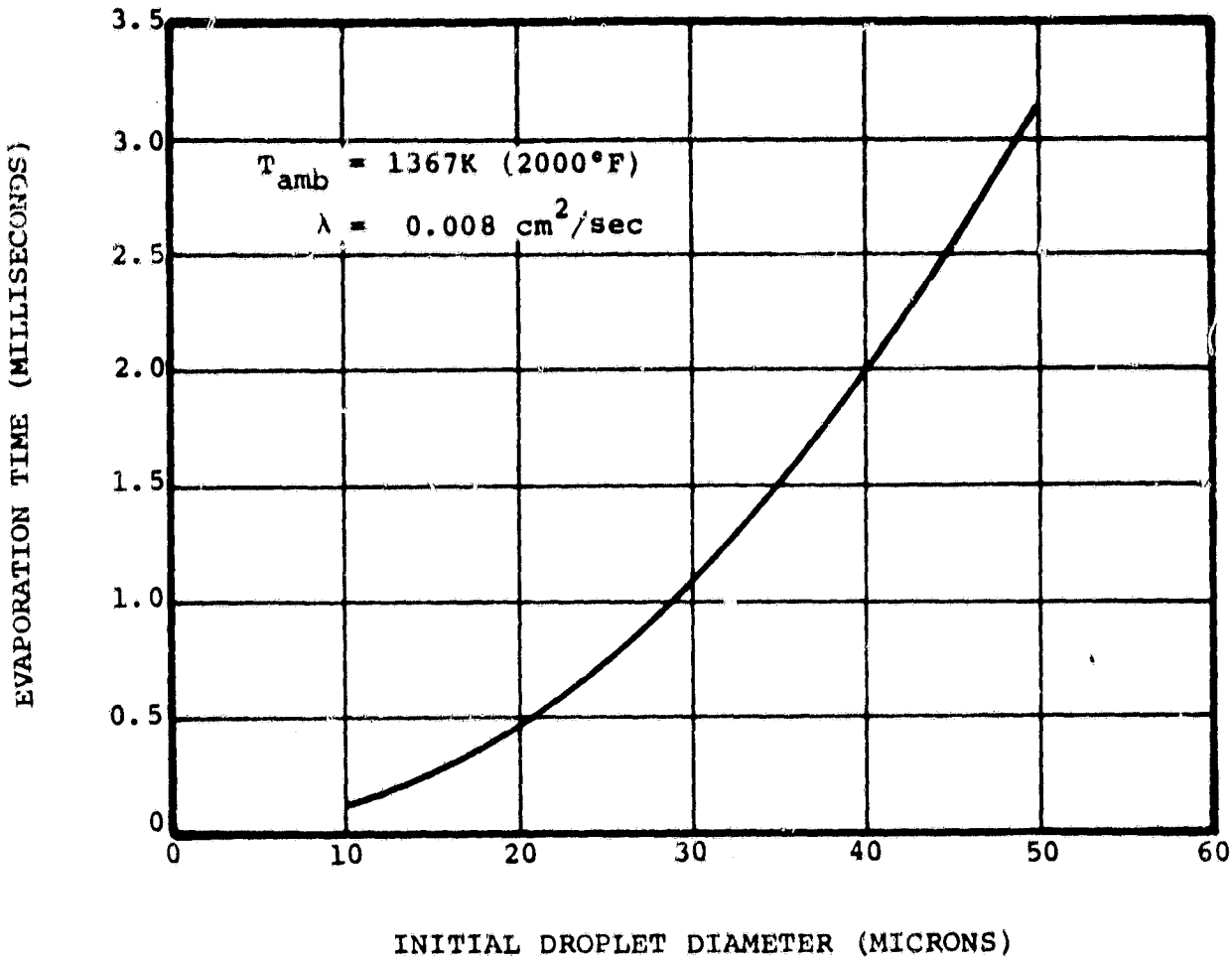

Figure 74. Effect of Initial Droplet Diameter on the Evaporation Time.

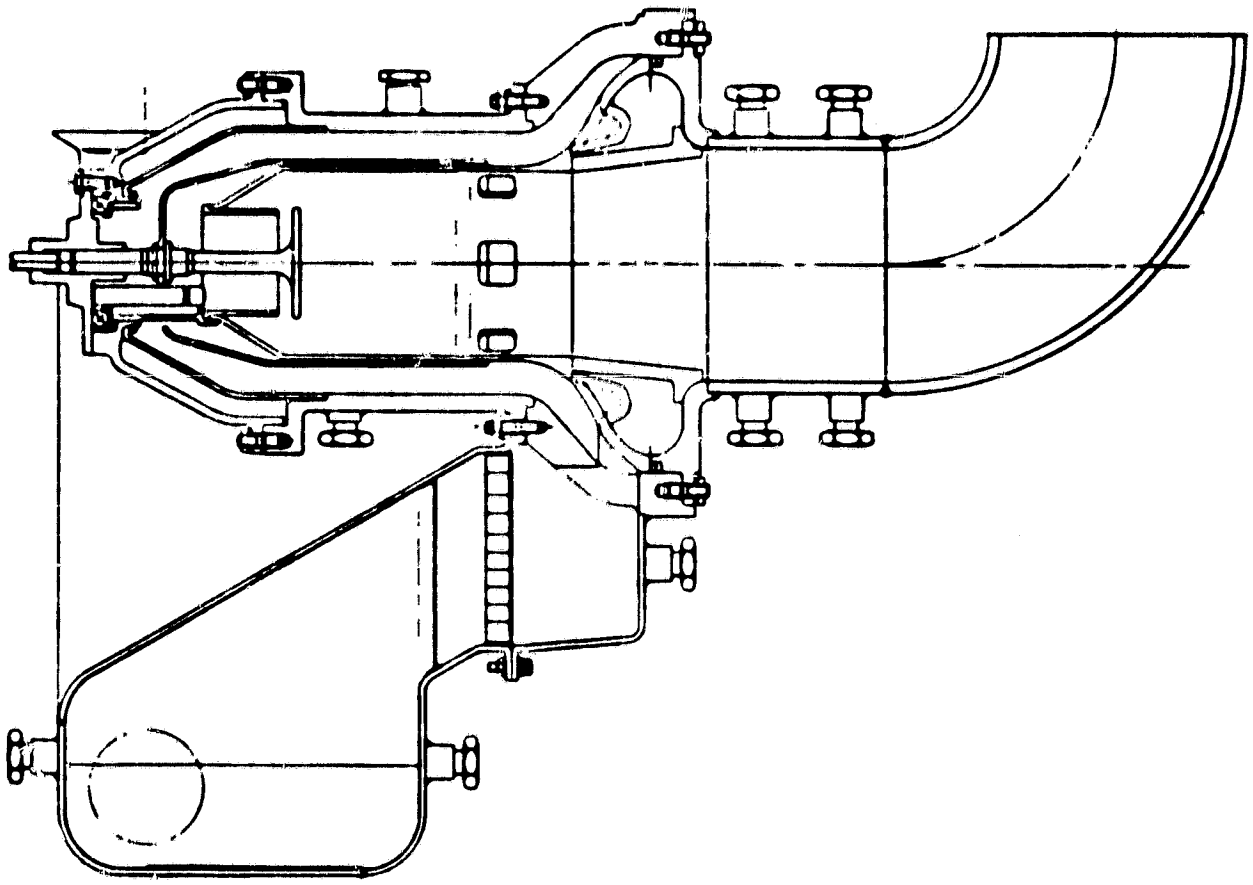

Figure 75. AGT Combustor Test Rig (Initial).

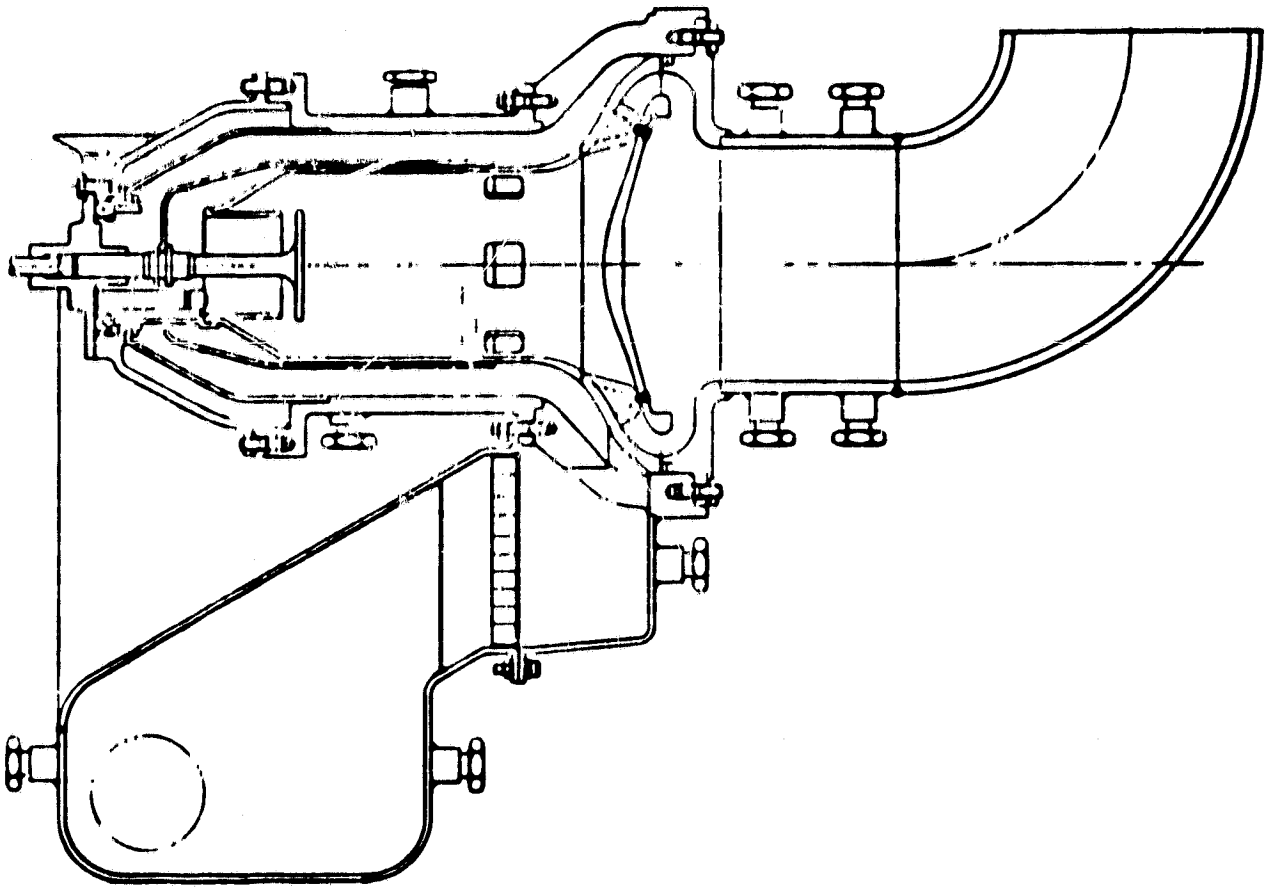

Figure 76. AGT Combustor Test Rig.

meet vehicle driveability characteristics, the turbine must be capable of producing maximum power at the cycle temperature limit and 100-percent shaft speed. This requirement leads to choosing a design point between the maximum power and minimum sfc operating conditions. This is in marked contrast to most gas turbine applications which require maximum efficiency at maximum power conditions and produce lesser efficiencies part-power performance.

To investigate the effect of turbine off-design operating conditions on engine performance, three design point vector diagrams were defined at the maximum power condition. The vector diagrams are identified by the degree of rotor absolute exit swirl (i.e. −9.8, −27 reference and 37 degrees). Efficiency and exit swirl characteristics from engine idle to maximum power are presented in Figure 77 based on the turbine off-design computer program. As engine speed is reduced for part power operation, the amount of turbine exit swirl increases (becomes more positive). The lowest swirl design has the highest efficiency at full speed, but the lowest efficiency at low speed. The highest negative swirl angle design has the lowest efficiency at maximum power and the highest efficiency at idle conditions. The reference design turbine is a good compromise, and has been the basis of all engine performance presented to date. However, higher efficiency at idle conditions, available from a high swirl (−37 degrees) turbine, is a potential advantage to driveability and fuel economy. The reference swirl turbine can be derived from the high swirl design by a simple cutback of the exducer blades.

Definition of the turbine stage has been concentrated in the following areas; stator inlet flowpath, stator design, rotor design, and rotor stress analysis. The paragraphs that follow discuss these efforts.

2.1.11.2 Stator Design

2.1.11.2.1 Stator Inlet Flowpath

The stator inlet duct definition consisted of examining alternate hub and shroud contours, axial lengths, and combustor exit transitioning. Table 7 summarizes geometries A through D examined to date and lists rating criteria used for the study (i.e., peak velocity which occurs on the stator hub inlet bend and the velocity gradient across the stator inlet plane). Configuration A was run with an increased axial length of 12.7mm (0.50 inch) to evaluate the impact of envelope constraints. The velocity distribution shown in Table 6 was not significantly improved, compared to the impact of adjusting the engine configuration. Therefore, an increase in axial length was not considered necessary to arrive at a satisfactory inlet duct velocity distribution.

Configurations B and C examined the tradeoff between peak velocity (maximum curvature) along the hub to the stator inlet velocity gradients. If the hub bend radii is decreased (Configuration B), the stator inlet contour can be maintained radial (90 degree inlet). This results in a higher velocity peak and diffusion, but a more uniform

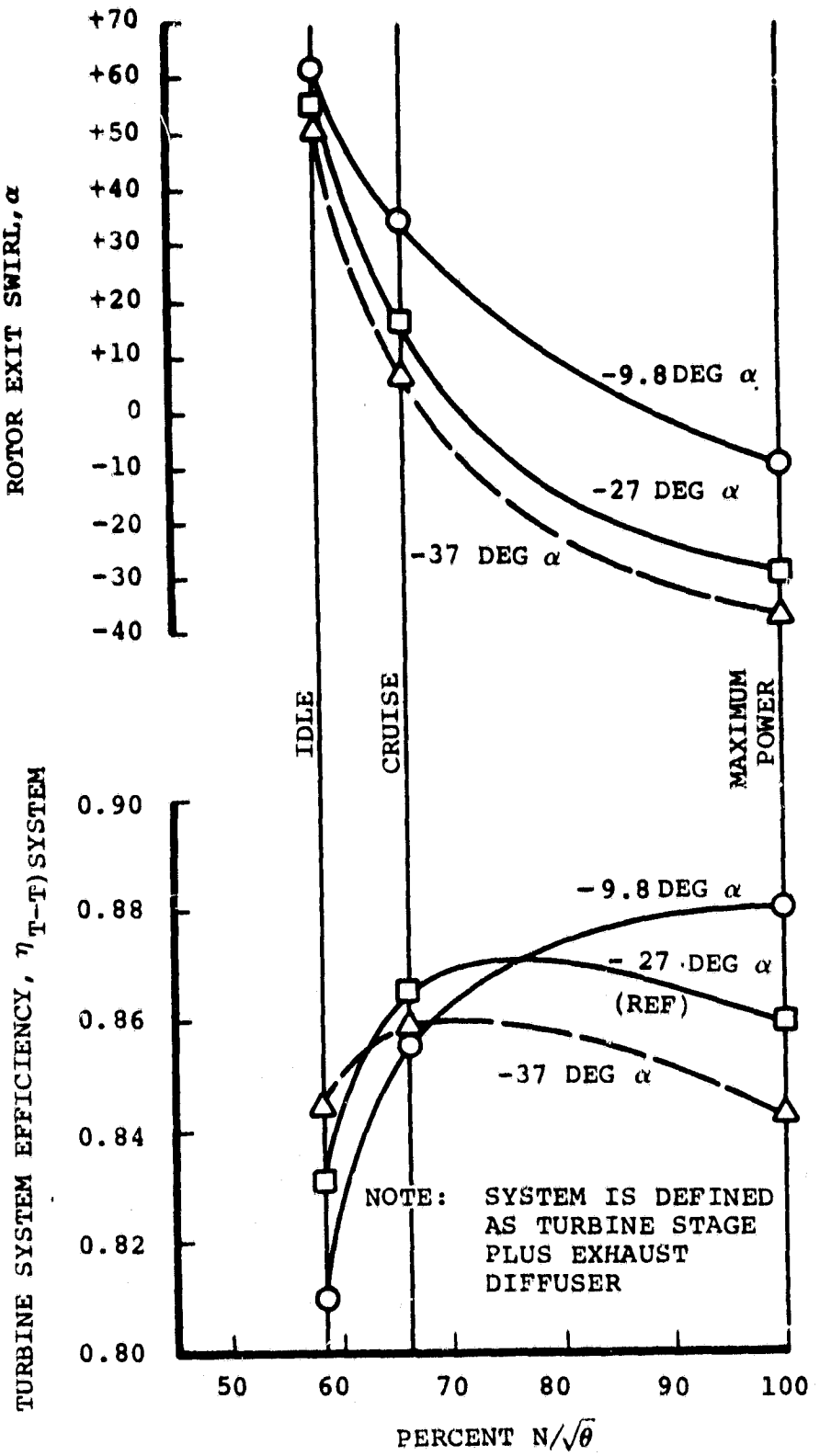

Figure 77. AGT Turbine Off-Design Optimization Study.

stator inlet cross passage velocity profile. Configuration B resulted in a peak velocity of 103.3 m/s (339 ft/sec), reducing the stator inlet velocity gradient to 38.4 m/s (126.0 ft/sec).

TABLE 7. STATOR INLET FLOWPATH CONFIGURATION STUDY

CONFIGURATION	DESCRIPTION	PEAK VELOCITY m/s (FT/SEC)	STATOR INLET VELOCITY GRADIENT m/s (FT/SEC)
A	Duct axial length (combustor exit to stator) increased by 12.7 mm (0.5 inch)	79.2 (260.0)	29.6 (97.0)
B	Original axial length, slope at stator inlet hub and shroud contour	90.8 (298.0)	46.9 (154.0)
C	Original axial length, 90 degree stator inlet hub and shroud contour	103.4 (339.1)	38.4 (126.0)
D	Original axial length, stator inlet configuration between B and C. Blend at combustor exit shroud region.	89.3 (293.0)	42.7 (140.0)

The other approach is to maximize the hub bend radius with a wall slope at the stator inlet (Configuration C). Table 6 shows that peak velocity is reduced to 90.8 m/s (298 ft/sec) and the stator inlet gradient increases to 46.9 m/s (154 ft/sec). Configuration D is a compromise between Configurations B and C and incorporates combustor exit-duct inlet blending in the shroud region. Figure 78 shows this configuration and also the location of six centerbody struts (NACA 16-021 profile) incorporated in the flow solution model. The velocity distribution with these features is presented in Figure 79. The next phase of the program will continue examining contour modifications and evaluating the hub and shroud boundary layer characteristics with two-dimensional methods. The goal is a non-separating design with minimum shroud diffusion and minimum stator inlet velocity gradient.

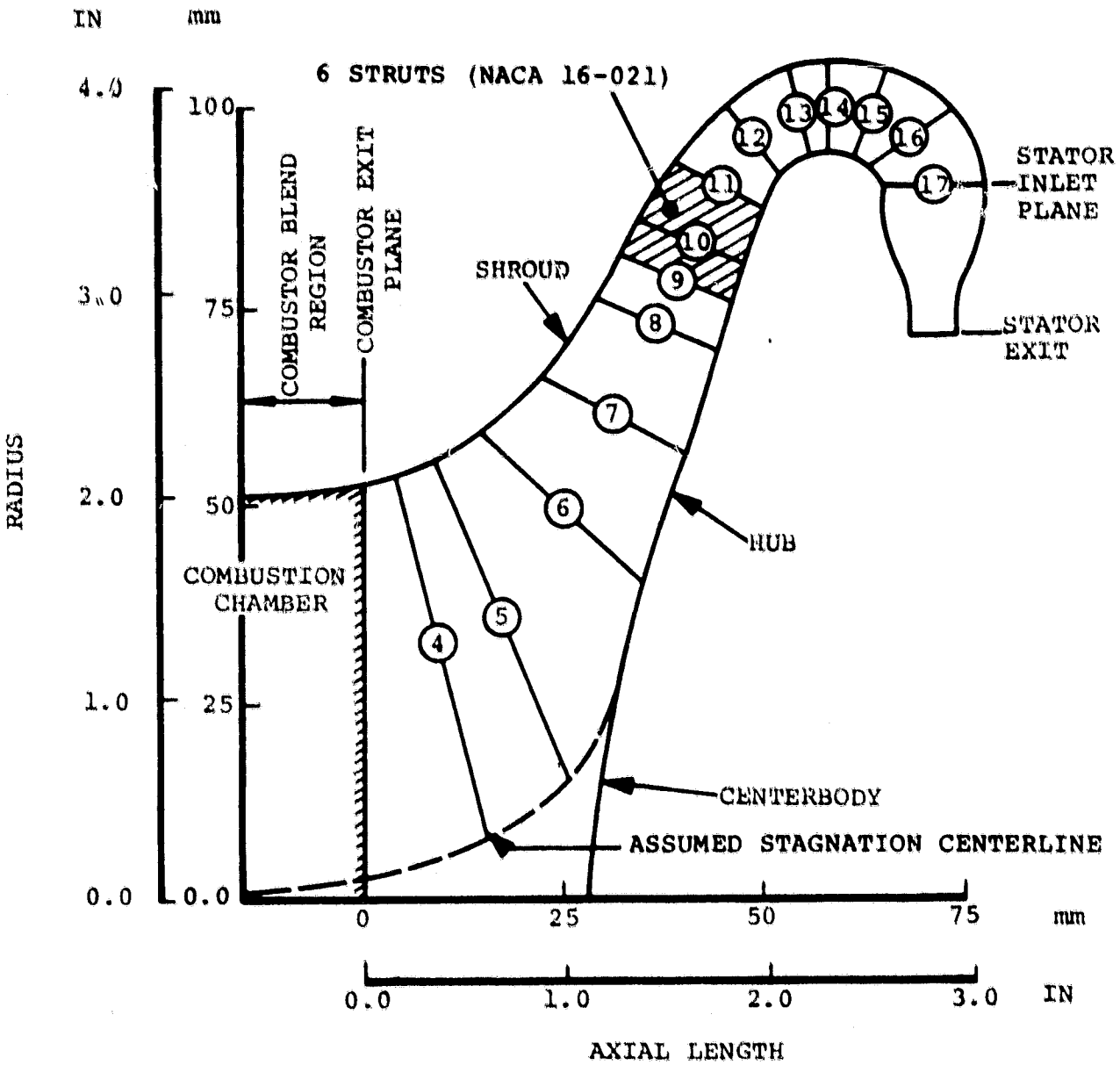

Figure 78. Turbine Inlet Duct, Configuration D.

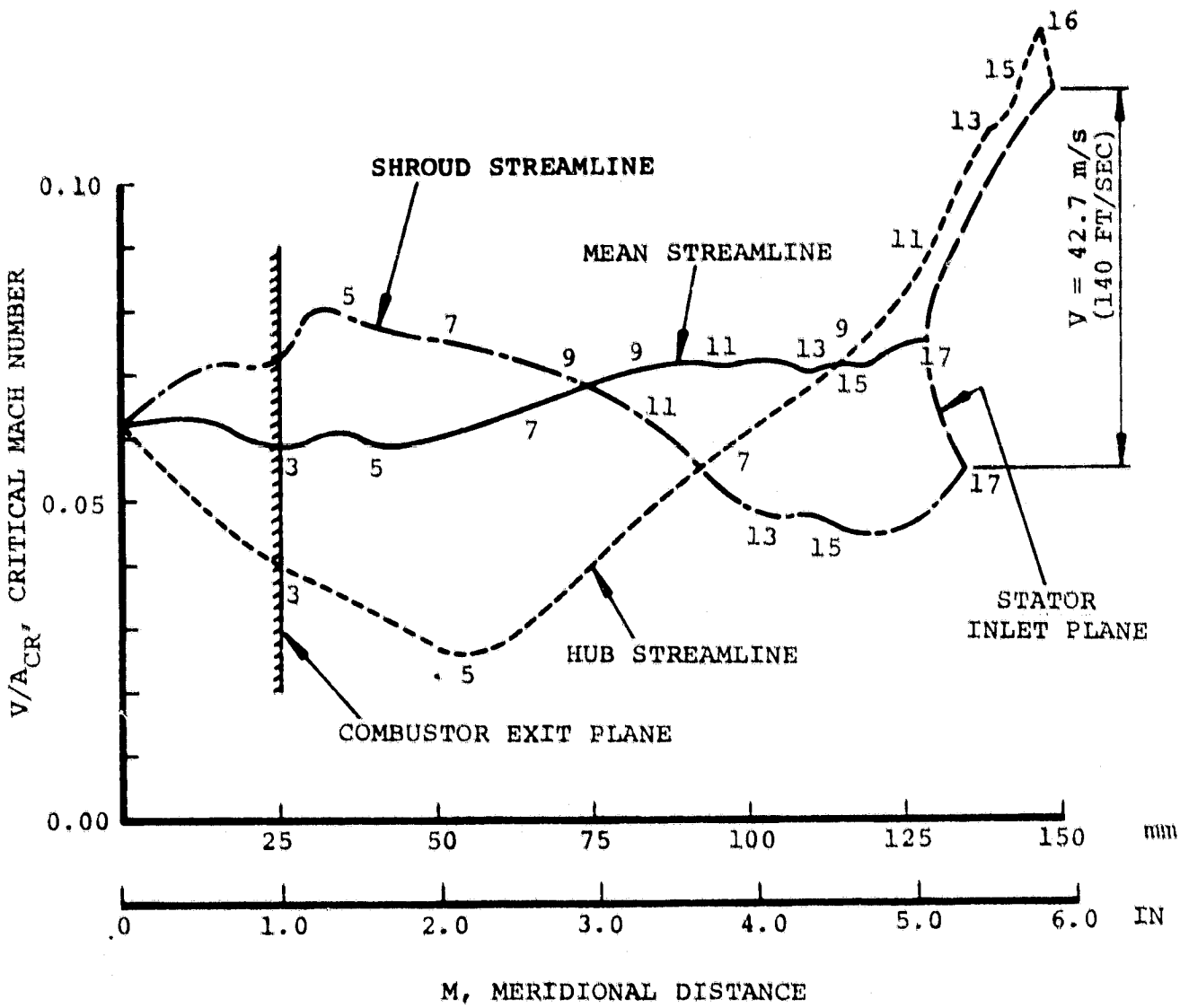

Figure 79. Turbine Inlet Duct Velocity Distribution For Configuration D.

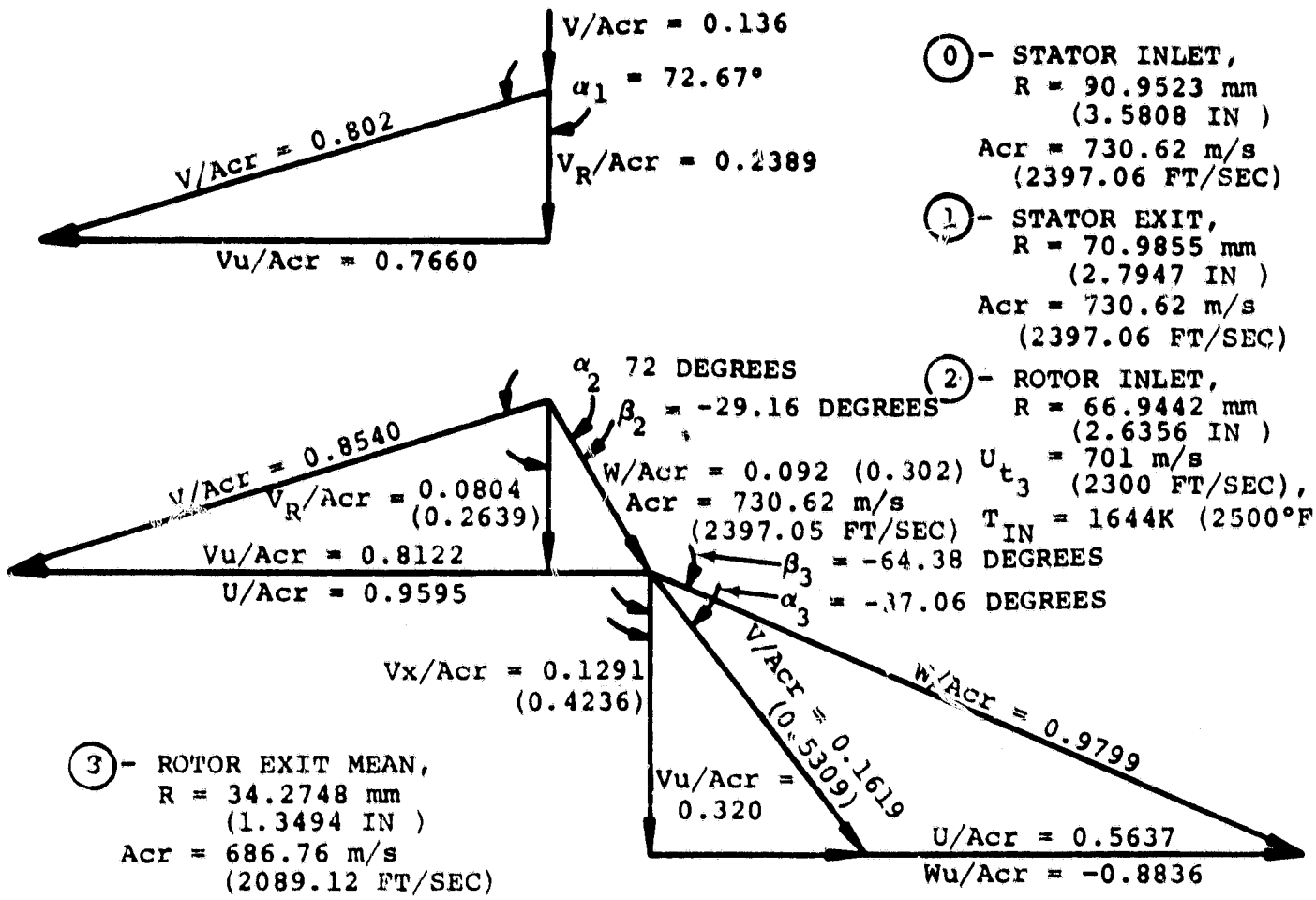

V = ABSOLUTE VELOCITY, m/s (FT/SEC)
Vu = ABSOLUTE TANGENTIAL VELOCITY, m/s (FT/SEC)
U = ROTOR WHEEL SPEED, m/s (FT/SEC)
W = RELATIVE VELOCITY, m/s (FT/SEC)
Wu = RELATIVE TANGENTIAL VELOCITY m/s (FT/SEC)
= ABSOLUTE FLOW ANGLE, DEGREES
= RELATIVE FLOW ANGLE, DEGREES

NOTE: THE STATOR INLET RADIUS AND VELOCITY ARE SHOWN WITH A PARALLEL END WALL AND 17 VANES

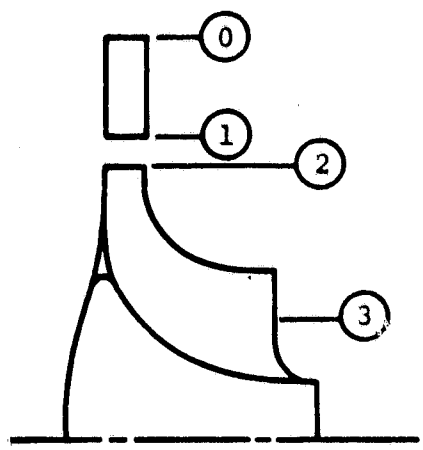

Figure 80. Turbine One-Dimensional Vector Diagram For High Swirl (−37.0 Degree) Design Point.

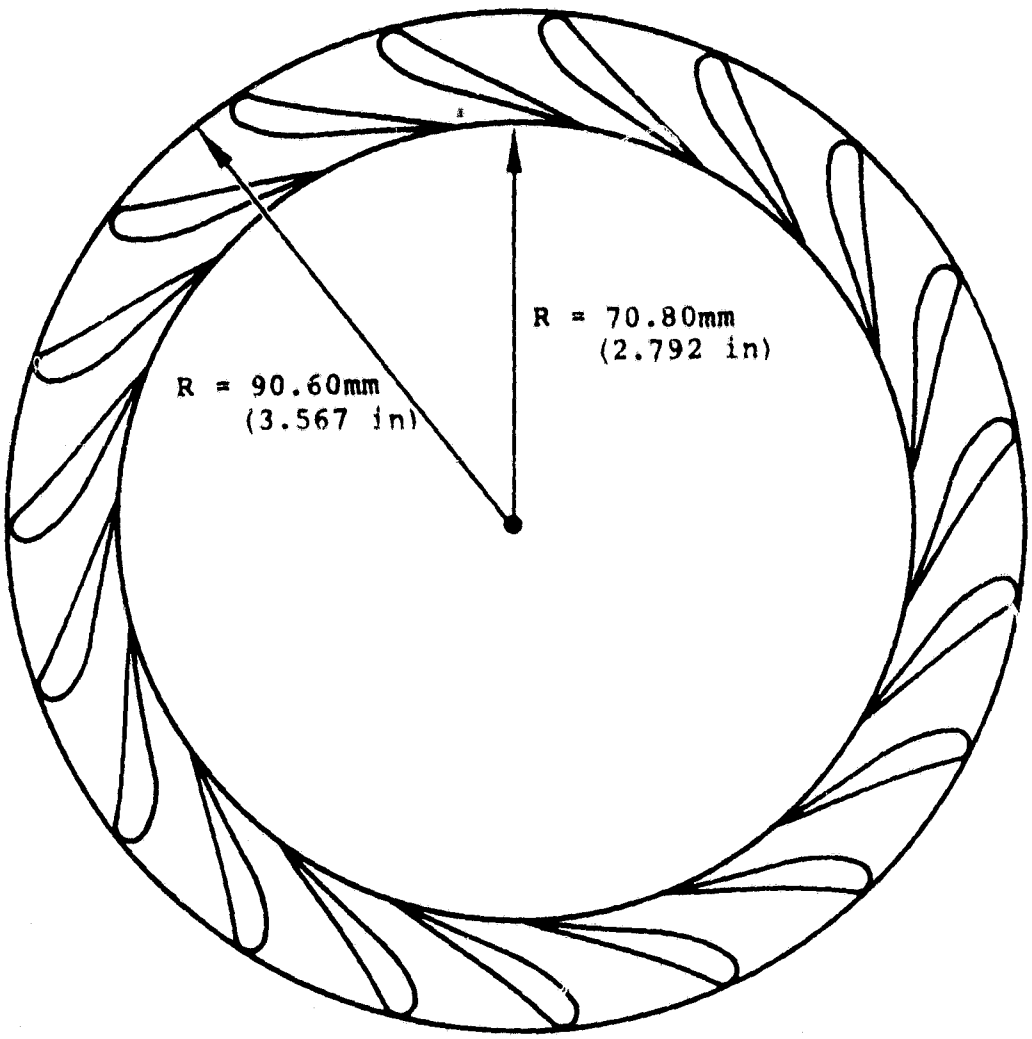

Figure 81. Preliminary Geometry For 19 Vane Ceramic Radial Turbine Stator.

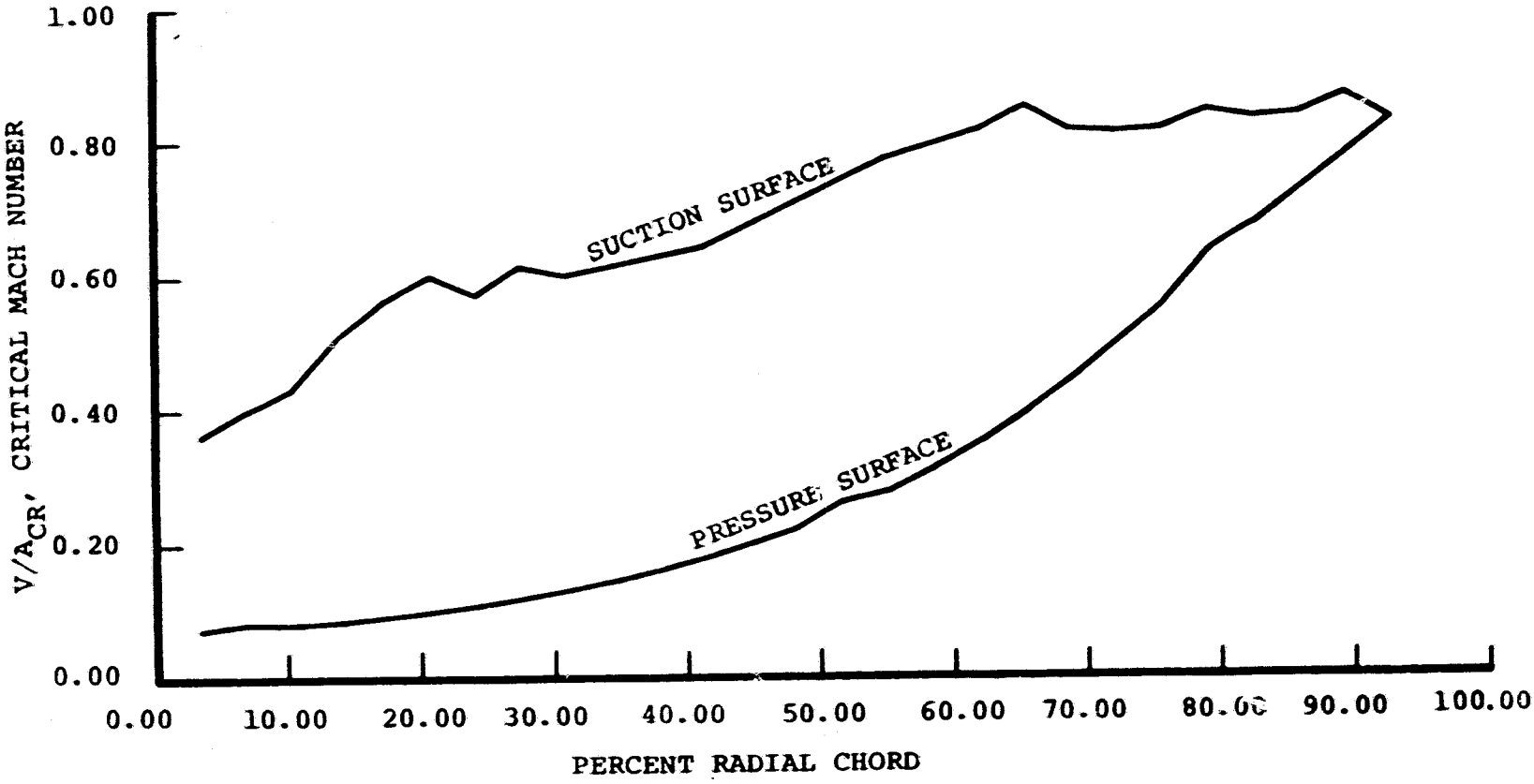

Figure 82. Ceramic Radial Turbine Stator Velocity Distribution For 19 Vanes and High Swirl (−37 Degrees) Vector Diagram.

2.1.11.2.2 Stator Aerodynamic Design

The stator and rotor detail design described in the following sections is based on the high exit swirl (−37.0 degrees) one-dimensional vector diagram presented in Figure 80. Although cycle analysis is continuing to investigate tradeoffs for a range of design point turbine exit swirl, designing the rotor at the high swirl configuration allows added flexibility of tailoring exit swirl by trailing edge cutback as the analysis continues.

Preliminary stator vane profiles have been investigated for a range of vane numbers from 17 to 23. The final vane number selected will be based on rotor blade vibration analysis results. Preliminary vibration analysis indicates a stator vane number between 19 and 21. A stator vane z-section ring for a 19 vane configuration is presented in Figure 81. The 2-dimensional vane surface velocity distribution for a parallel endwall is presented in Figure 82.

The objective of the vane profile design is to maximize stator inlet loading and minimize exit loading from the throat region to the trailing edge. This approach will minimize vane loading and, therefore, secondary flow losses when the contoured endwall is applied. The effect of stator endwall contouring is shown in Figure 83 for a 19-vane profile with reduced thickness. The symetrical endwall contour shown is similar to a previous design when a 50 percent reduction in stator loss was predicted. For the AGT, non-symetrical endwall configurations will also be examined to evaluate the effect on turbine inlet bend contour. The overall objective will be to optimize the turbine inlet-stator system.

In discussions with ceramic manufacturers, questions arose concerning stator trailing edge thicknesses and vane fillet radii. To investigate the effects of manufacturability on turbine performance, a trade-off study was conducted with varying fillet radii and trailing edge thickness. Figure 84 illustrates results of this analysis as a function of vane number and trailing edge normal thickness (based on axial turbine stator test results). As indicated, two configurations have been selected for further study. Configuration No. 1 is the AGT engine goal since no additional performance decrement is indicated. Configuration No. 2 is more favorable from a manufacturing standpoint and will, therefore, be designed and rig tested to verify the performance penalty associated with the increased trailing edge blockage.

Two other aspects of the profile design (maximum thickness and a straight line pressure surface) are also being investigated aerodynamically. From a thermal stress standpoint, a constant thickness profile would be ideal. Unfortunately, since the vane turning is over 70 degrees and the trailing edge thickness may be on the order of 0.508 mm (0.020 inch) and 0.762 mm (0.030 inch), maintaining a constant vane thickness is not aerodynamically feasible. However, a more uniform profile thickness can be achieved by reducing the vane maximum thickness as shown in Figure 85. It is also desirable to maintain a straight line pressure surface to facilitate ceramic tool removal. Therefore, once acceptable stator vane velocity distributions are obtained, the change in loading with a straight line pressure surface will be examined.

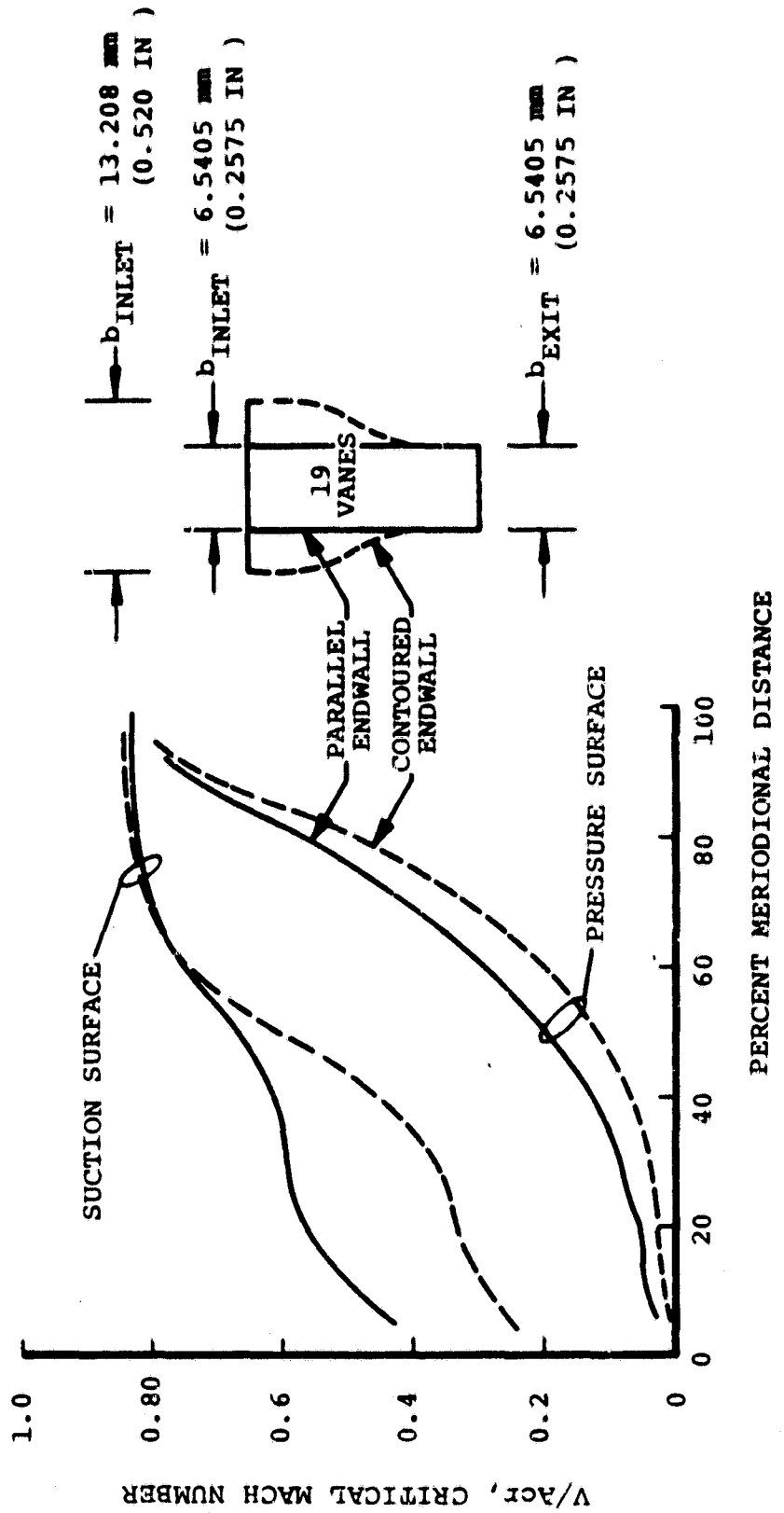

Figure 83. Ceramic Turbine Stator Velocity Distribution (19 Vanes).

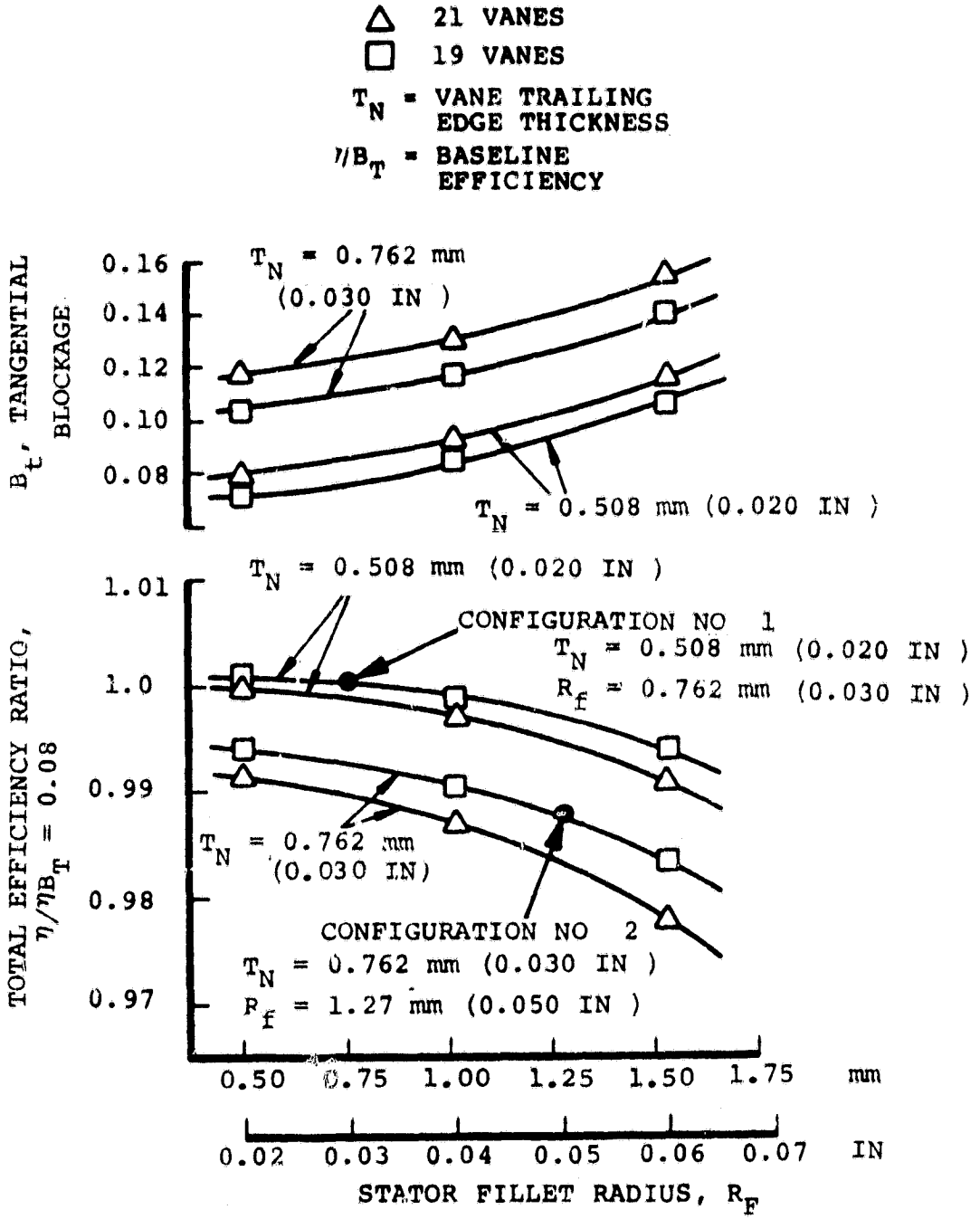

Figure 84. Effect of Stator Trailing Edge Thickness and Fillet Radius on Stator Exit Blockage and Turbine Performance.

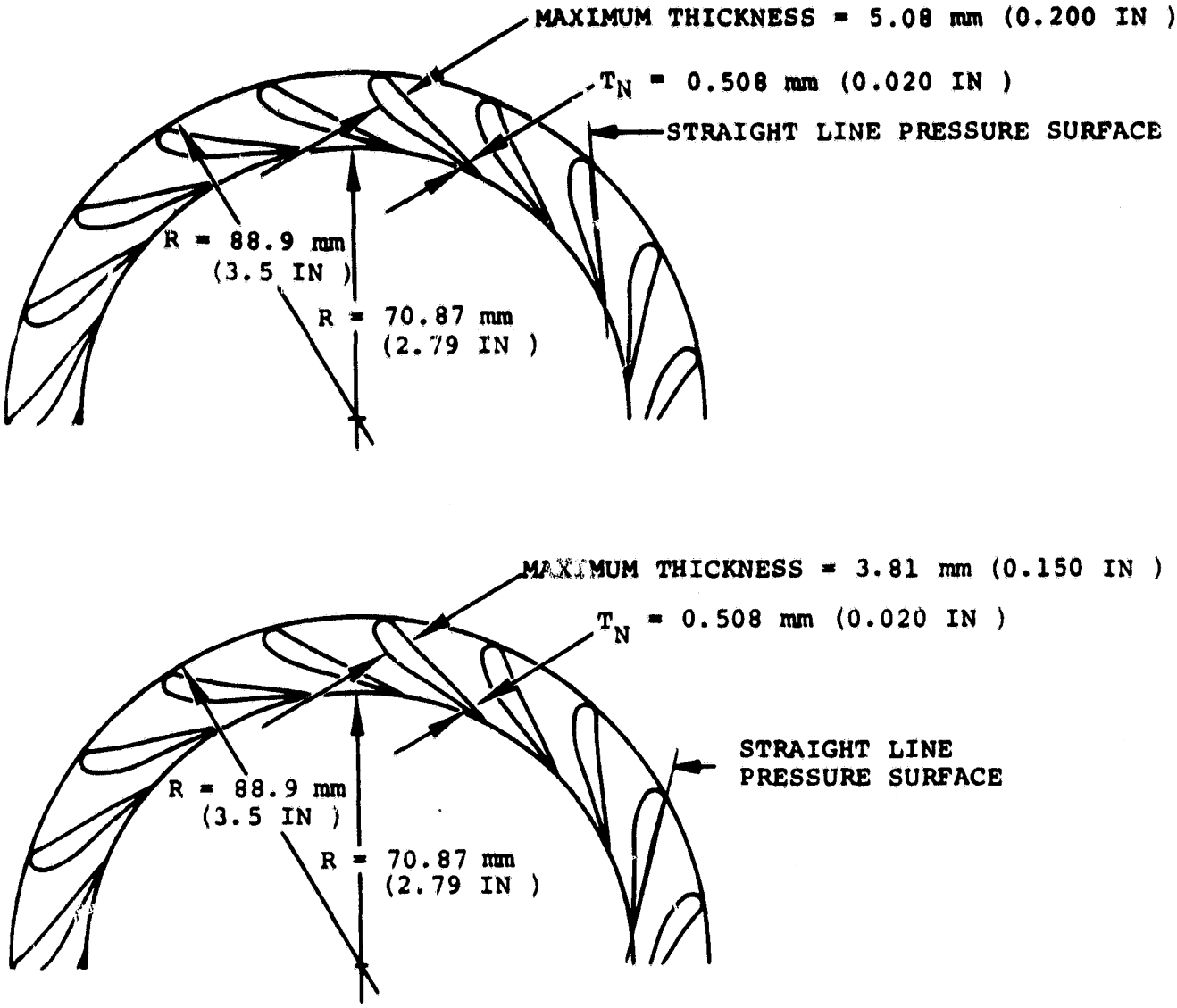

Figure 85. Turbine Stator Profile Designs (19 Vanes).

2.1.11.2.3 Stator Mechanical Design

A 3-dimensional finite element analysis of the reaction bonded silicon nitride (Si_3N_4) radial flowpath stator was done for the steady-state condition at 1644K (2500°F) TIT. A temperature plot for the 3-dimensional model is shown in Figure 86. The stator was analyzed for a segmented configuration and stress results are shown in Figure 87. Work is continuing on an integral configuration.

Maximum stator temperatures are largely governed by combustor discharge temperatures and are found to approach these values on the airfoil. Shroud temperatures contacting the combustor baffle are warmer than those contacting cooler turbine shroud components. The thermal model assumes that a gap was present over a substantial portion at the stator shroud/turbine shroud interface to minimize differences in stator shroud temperatures.

2.1.11.3 Turbine Rotor Design

2.1.11.3.1 Ceramic Rotor Aerodynamic Design

As stated previously, three levels of rotor exit swirl have been evaluated. In addition to the level of swirl at the rotor exit, two different blade number designs have been evaluated; 12 blades and 14 blades. Figure 88 illustrates the effects of blade number versus rotor hub blockage and efficiency. In addition, rotor hub principal stress is depicted as a function of blade number. Since little efficiency decrement is associated with either 12 or 14 blades, blade selection will be dependent on rotor stress and blade vibration analysis.

Turbine meridional flow path is presented in Figure 89. As indicated, the interim metallic rotor configuration is achieved by reducing the rotor tip speed from 701 m/s (2300 fps) to 640 m/s (2100 fps) by decreasing tip diameter. The exducer will also be cutback for the metallic design, if the -37.0 degrees exit swirl vector diagram is selected, to provide a further reduction in rotor inlet relative temperature. Rotor blade velocity distributions for the hub, mean and shroud streamlines are presented in Figures 90, 91, and 92 for the ceramic rotor based on the following conditions:

- Maximum power
- 14 blades
- 39.37 mm (1.55 in.) rotor axial length
- -37.0 degrees exit swirl vector diagram
- 100,000 rpm
- 701 m/s (2300 fps) tip speed

If 12 blades are selected, rotor inducer loadings would be more severe.

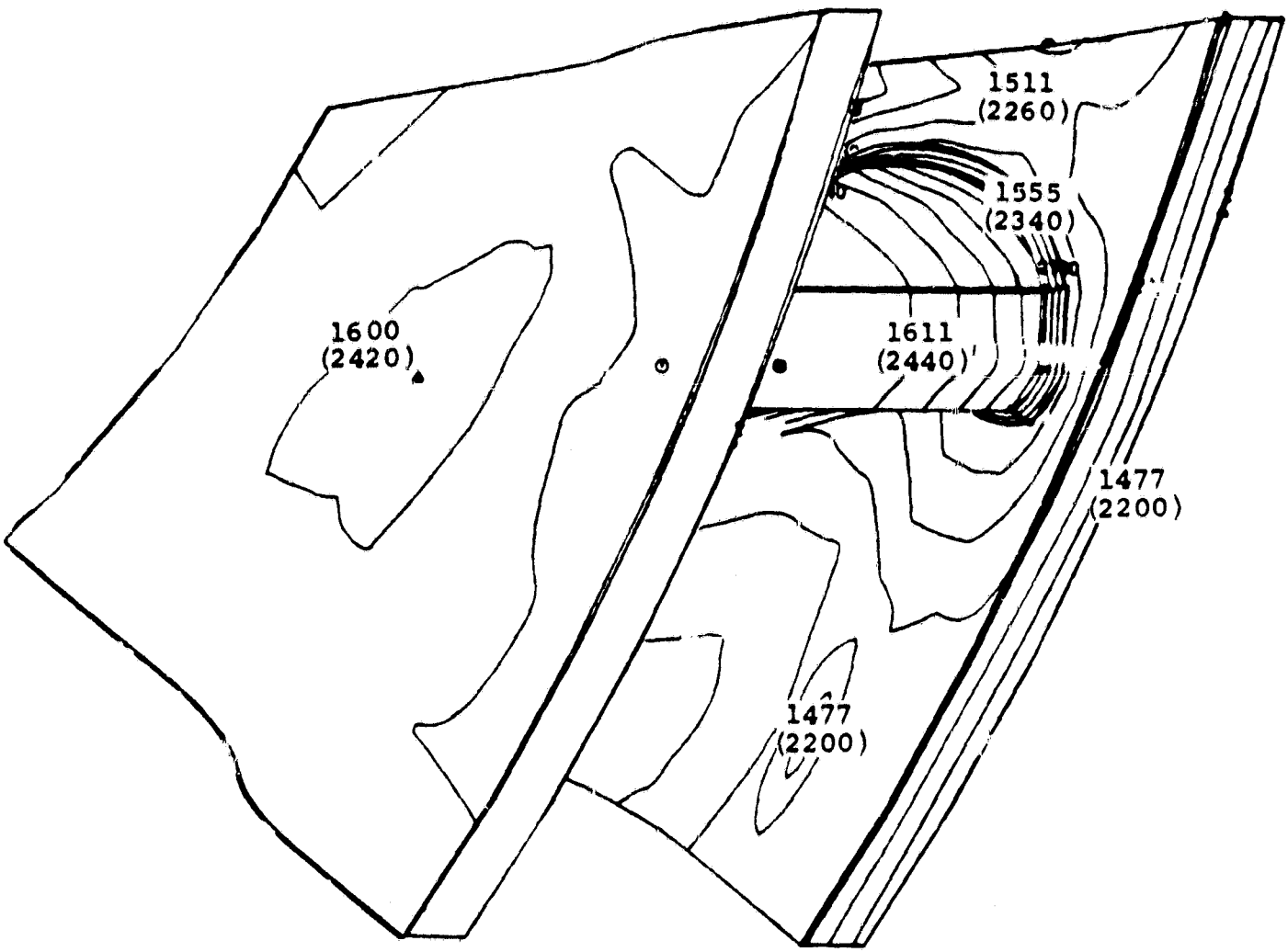

Figure 86. AGT Stator Sectional Temperature Display.

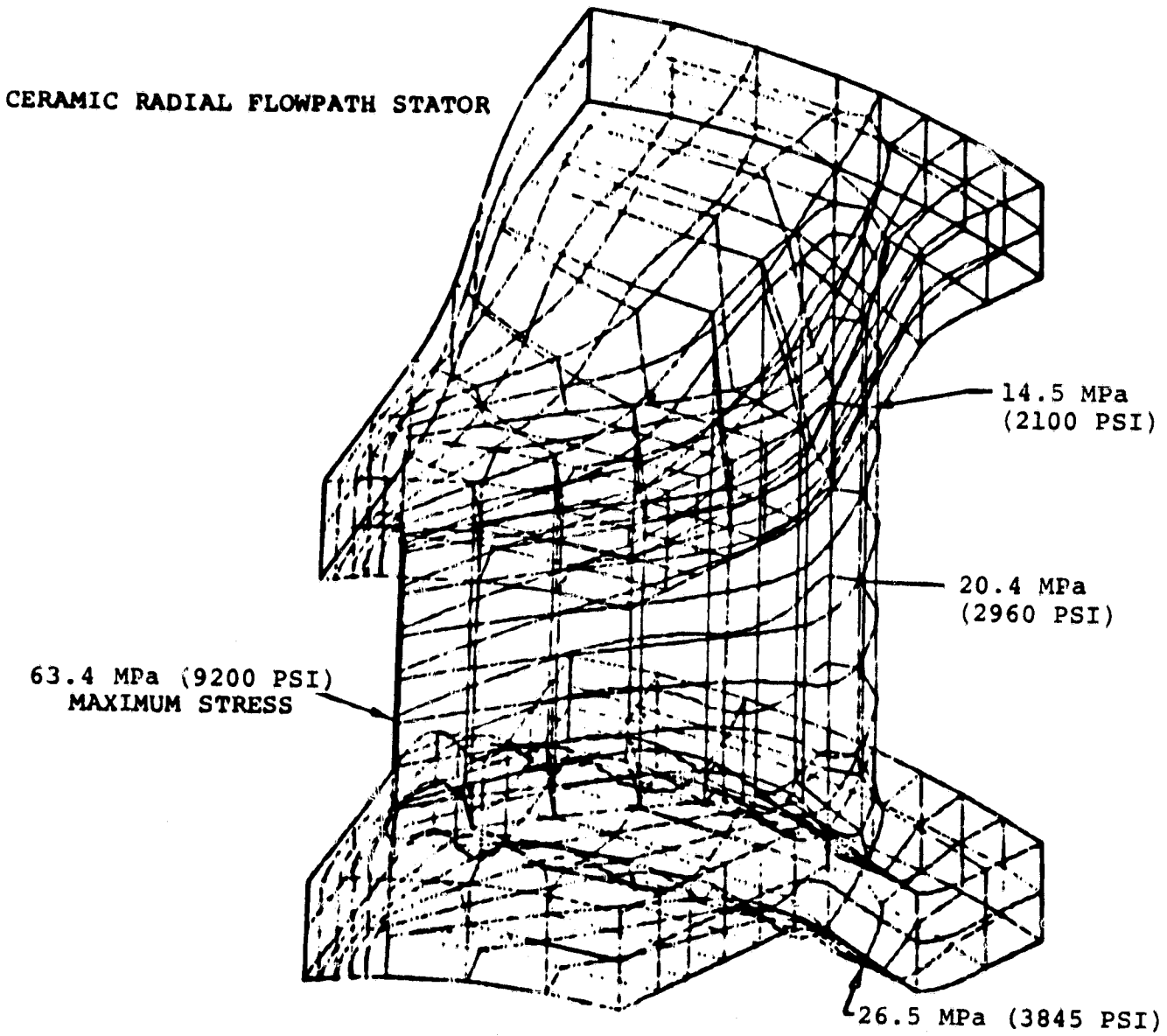

Figure 87. Segmented Stator Non-Integral Band Stress Analysis.

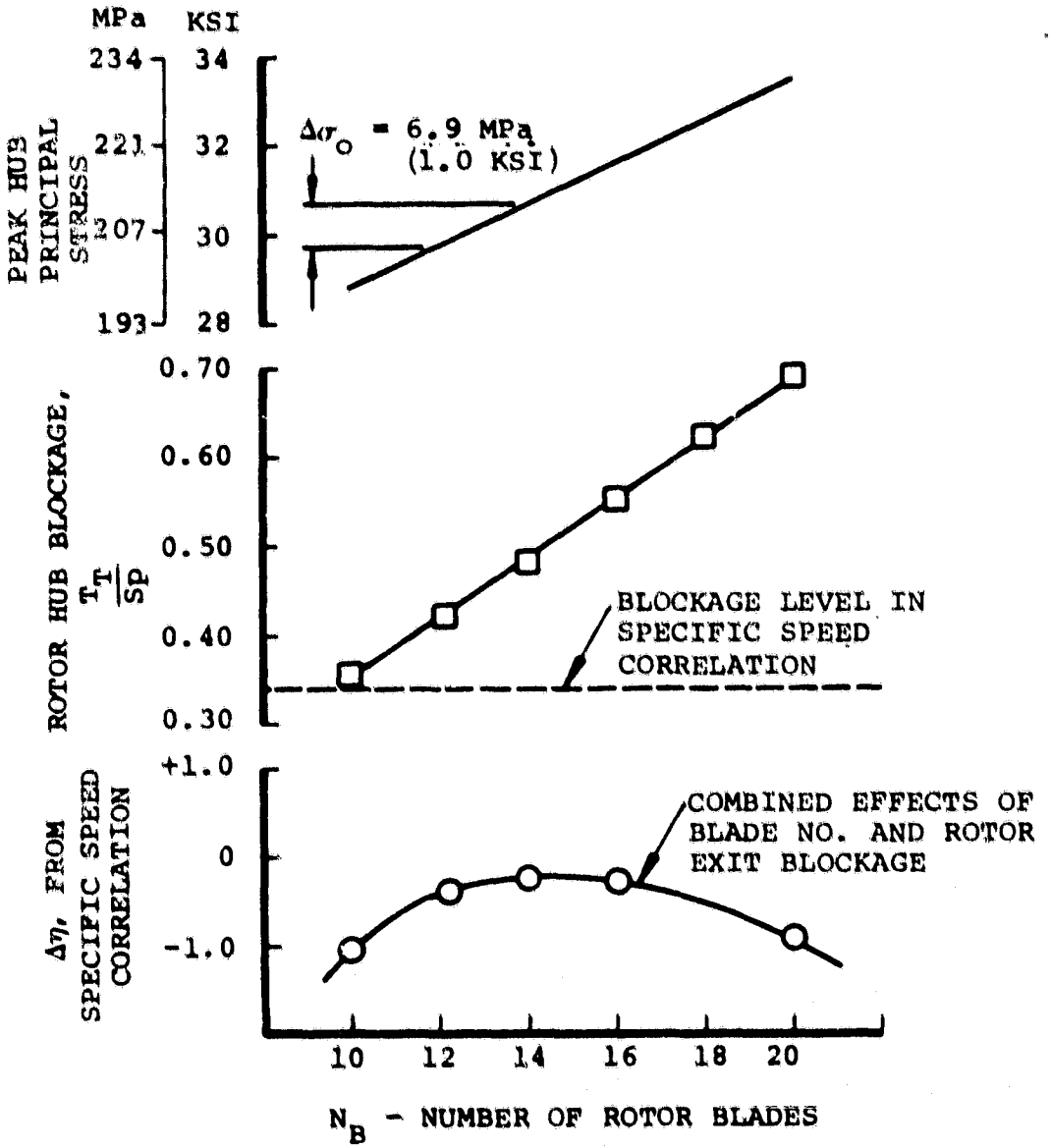

Figure 88. Effects of Blade Number and Exit Blockage on Turbine Performance and Rotor Disk Stress.

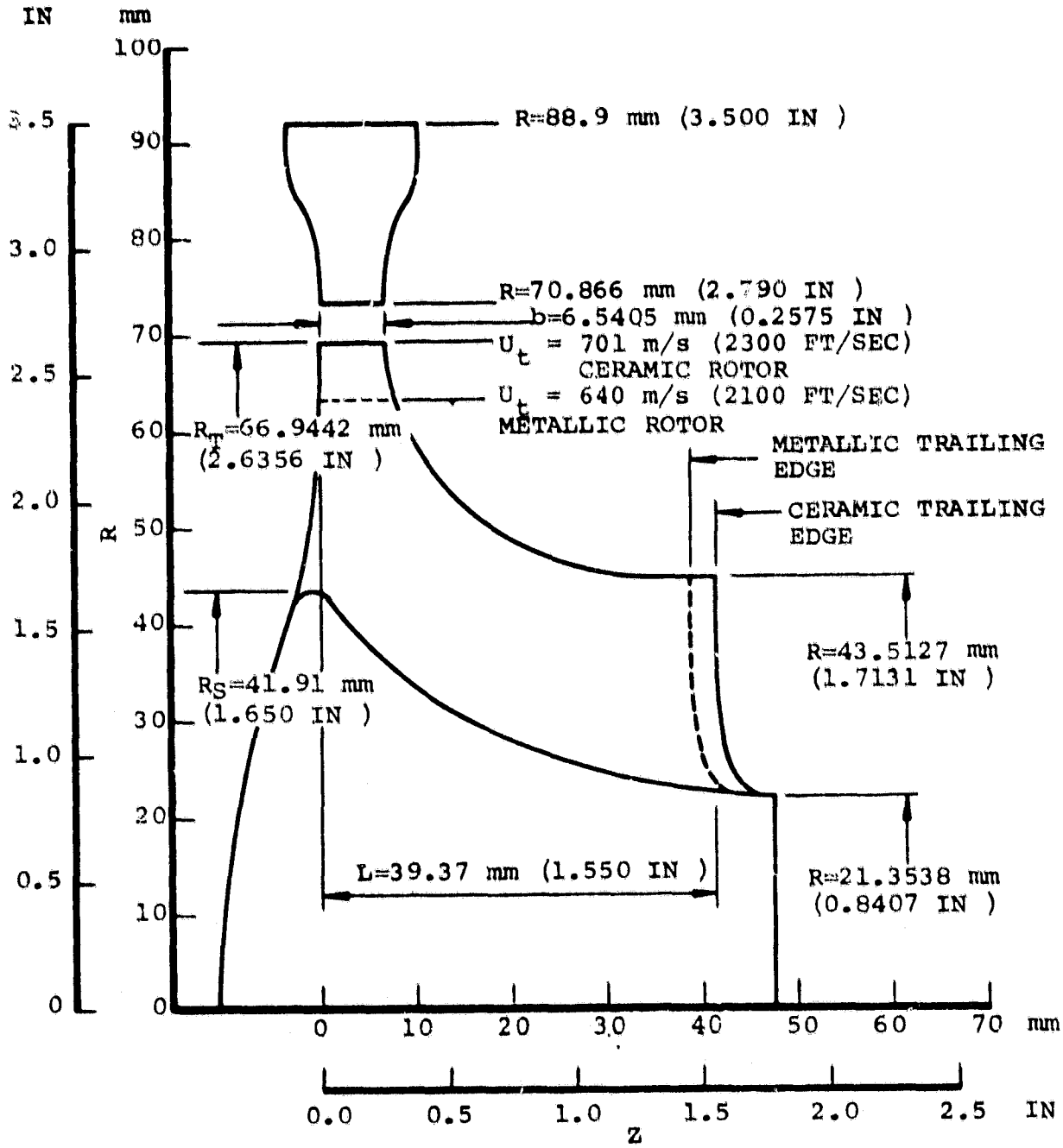

Figure 89. Turbine Meridional Flow Path.

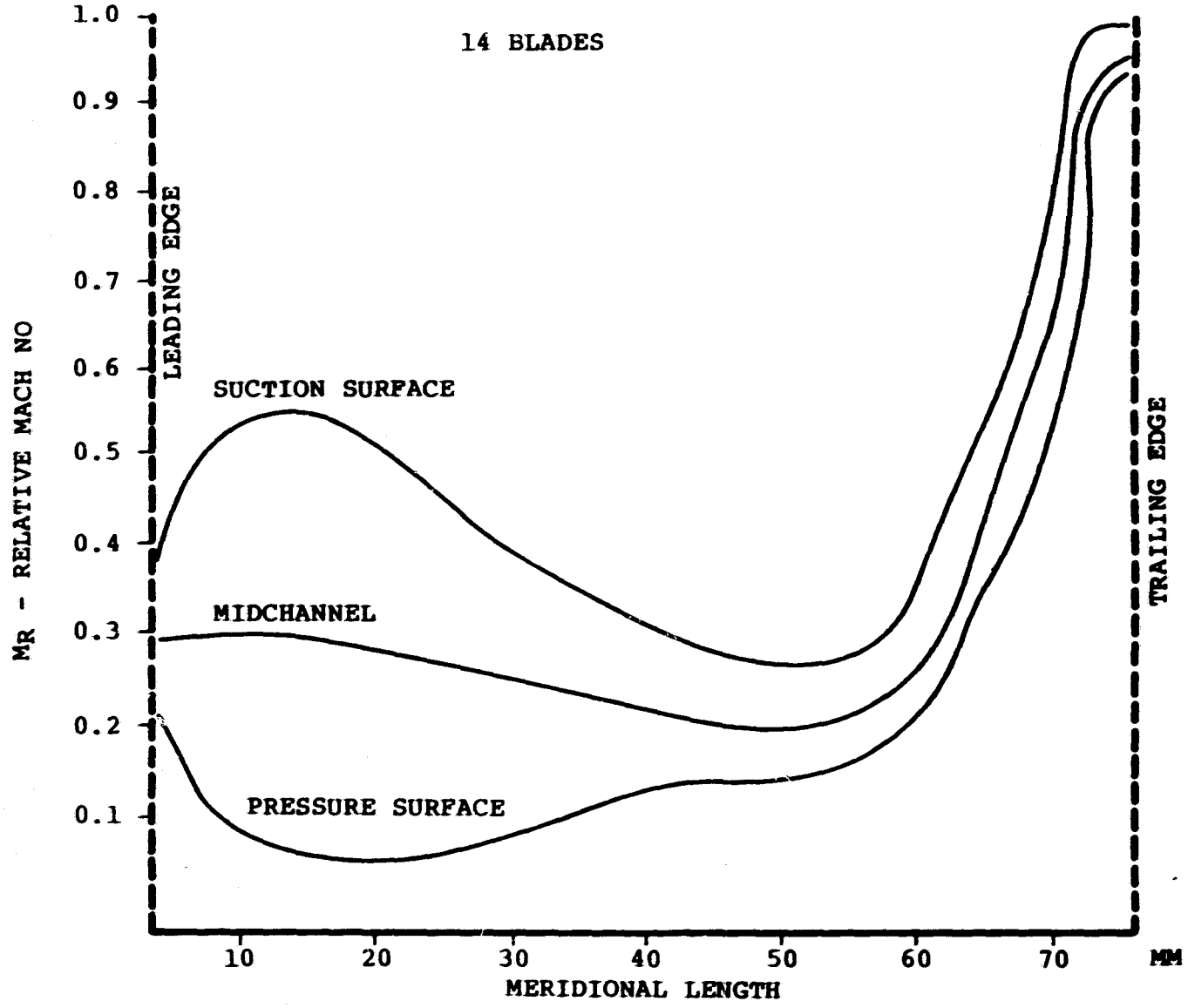

Figure 90. Ceramic Rotor Hub Streamline Velocity Distribution.

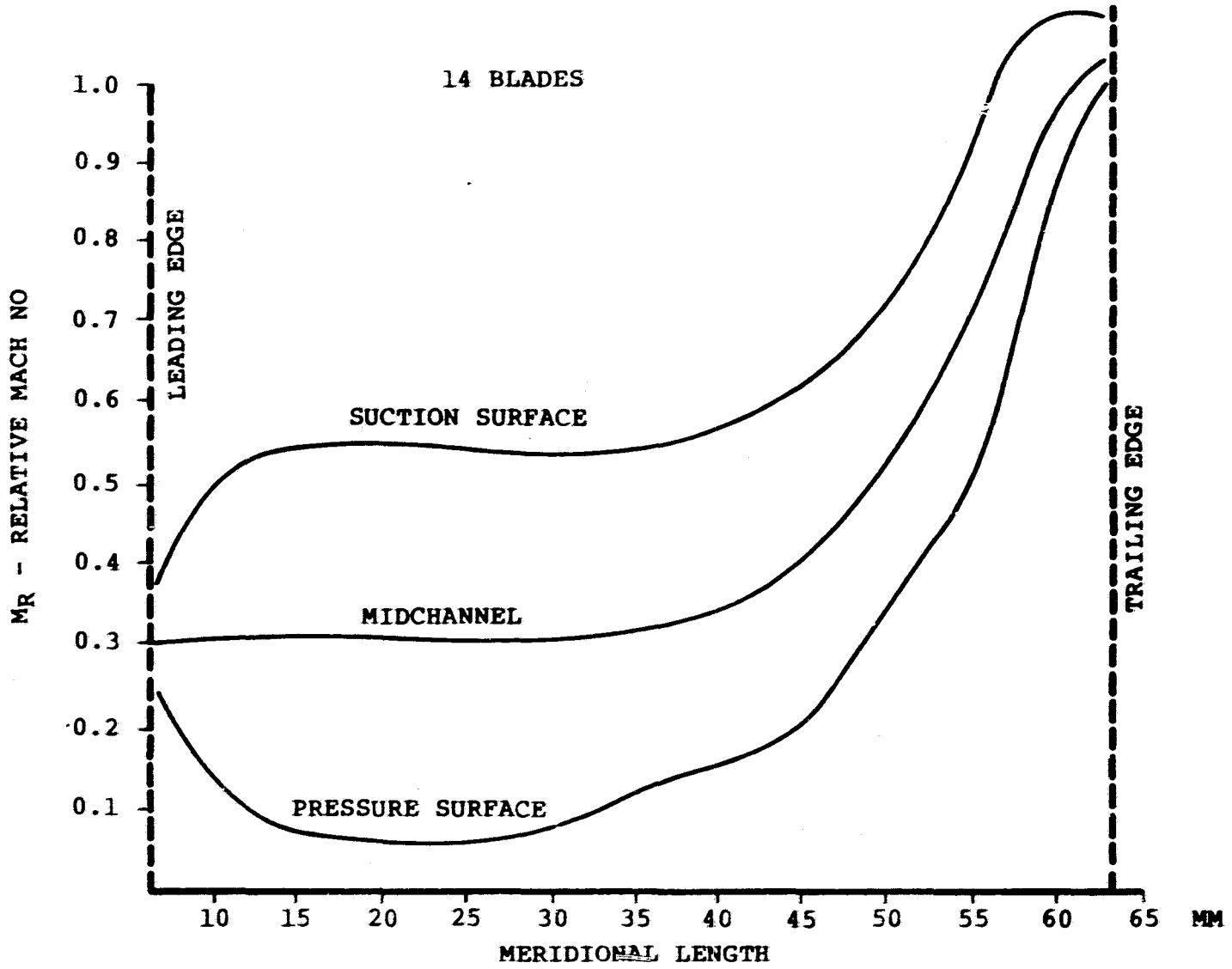

Figure 91. Ceramic Rotor Mean Streamline Velocity Distribution.

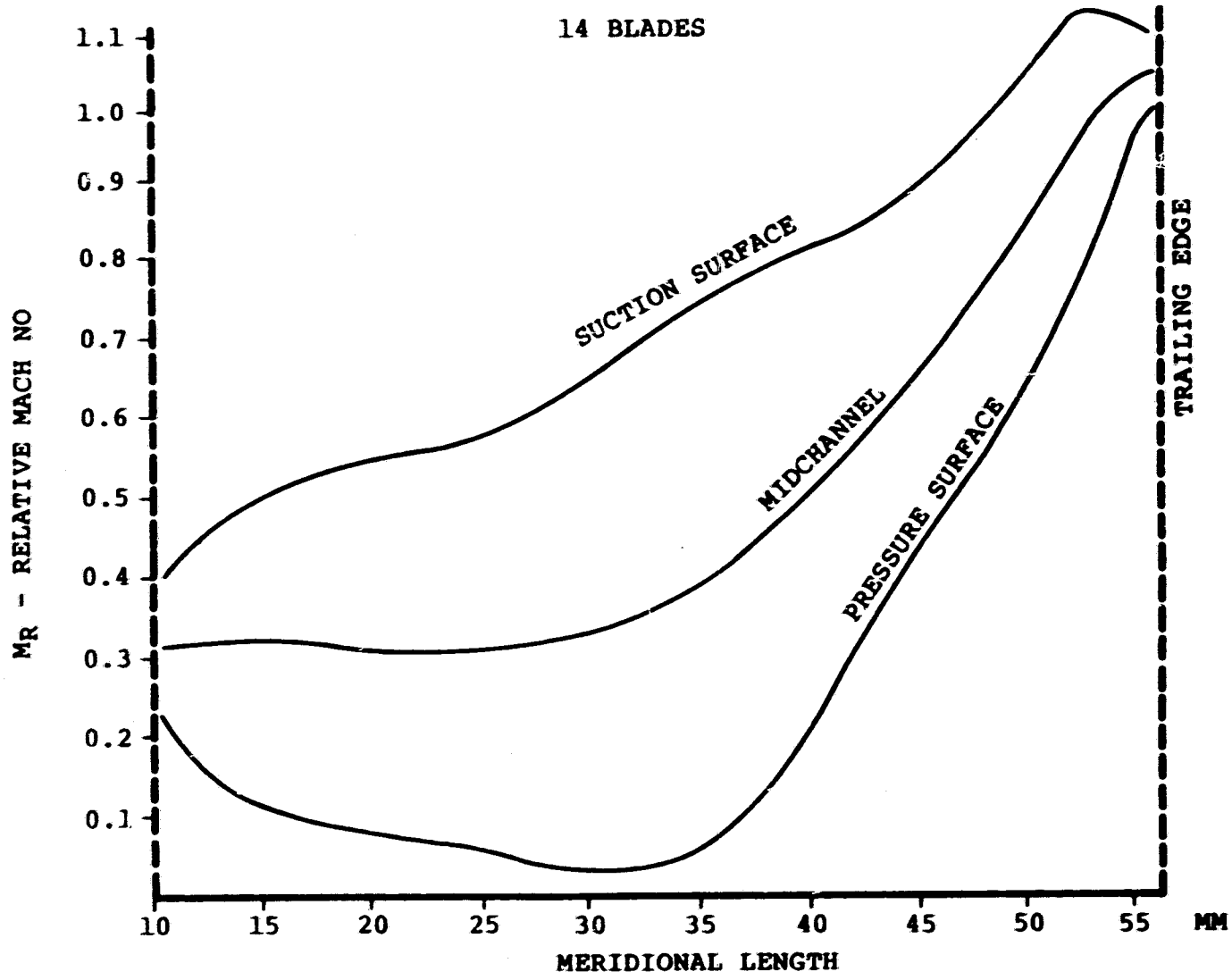

Figure 92. Ceramic Rotor Shroud Blade Surface Velocity Distribution.

2.1.11.3.2 Ceramic Rotor Mechanical Design

The 2-dimensional preliminary turbine rotor stress analyses have been completed. These studies were iterative in nature and were used to evaluate centrifugal stress effects of various aerodynamic and mechanical design parameters. Table 8 summarizes ceramic turbine rotor properties and operating conditions utilizing both sintered silicon nitride and sintered silicon carbide material. Figure 93 illustrates stress isopleths for these two candidate rotor materials. For the 2-dimensional analysis, blade stresses were purposely kept low to compensate for geometric stress concentrations which occur in the transition region between blade and disk.

TABLE 8. CERAMIC TURBINE WHEEL PROPERTIES

	SINTERED SILICON NITRIDE	SINTERED SILICON CARBIDE
Number of Blades	12	12
Density, g/cm^3 (lb/in^3)	3.27 (0.118)	3.16 (0.114)
Modulus, mPa (lb/in^2)	310 x 10^3 (45 x 10^6)	407 x 10^3 (59 x 10^6)
Poisson's Ratio	0.22	0.14
Weight, kg (lb)	0.62 (1.36)	0.60 (1.32)
I_p Nm-s^2 (lb-in-sec^2)	0.00037 (0.0033)	0.00037 (0.0033)
Operating Conditions at Maximum Power (100,000 RPM)		
Inlet Temperature, K (°F)	1644 (2500)	1644 (2500)
Tip Speed m/s (ft/sec)	701 (2300)	701 (2300)
Average Tangential Stress, mPa (ksi)	151 (21.9)	145 (21.1)

After completion of the 2-dimensional preliminary stress studies, three dimensional stress studies were initiated to better understand stress in the blade/disk transition region. Figures 94 and 95 illustrate the 3-dimensional finite element model. By utilizing

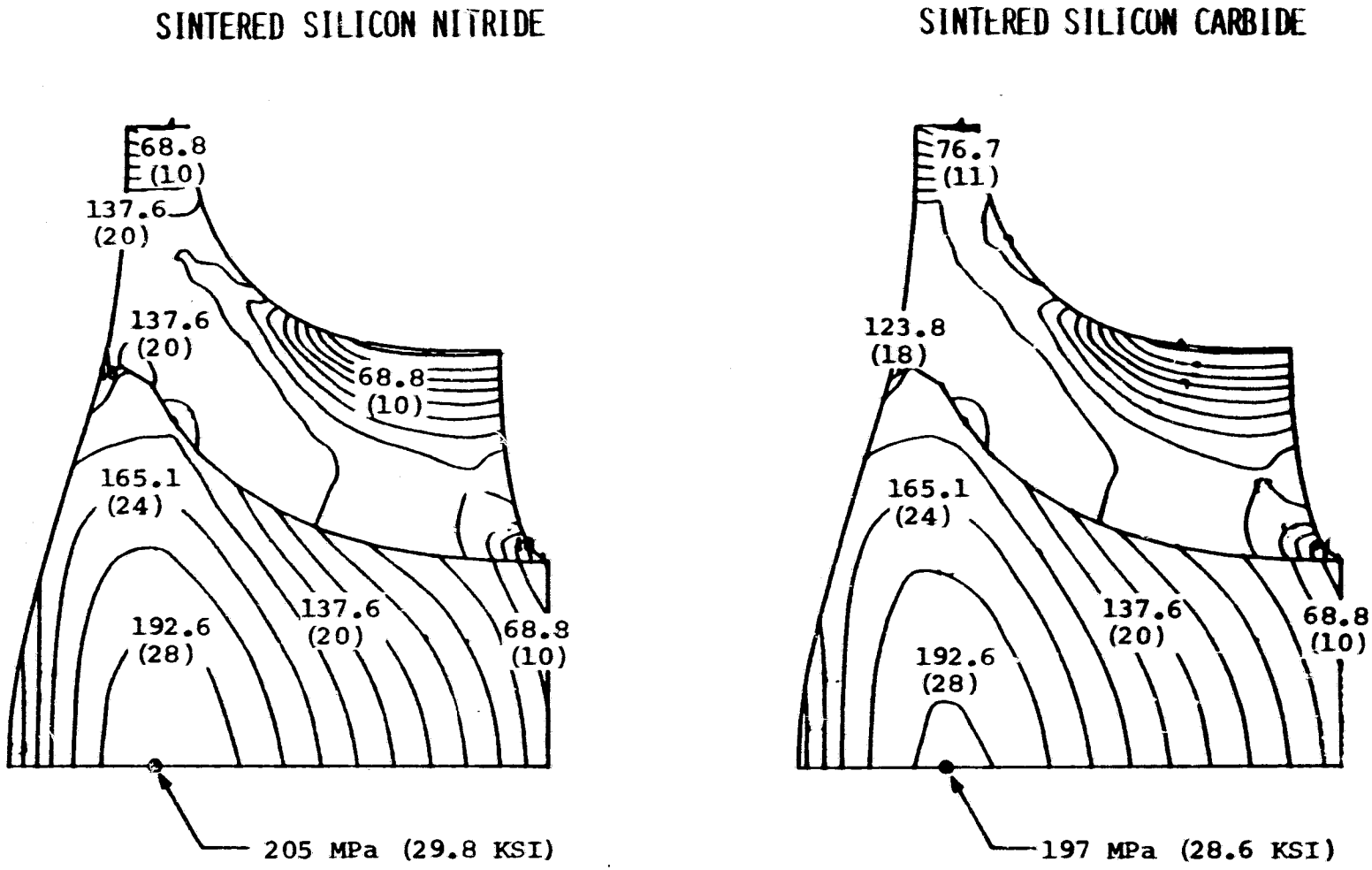

Figure 93. AGT Ceramic Turbine Wheel 2-D Maximum Steady-State Centrifugal Principal Stresses, MPa (KSI), 12 Blades at 100,000 RPM.

symmetry, it is necessary to model only one blade and a corresponding segment of the disk. Figure 96 illustrates good agreement between computed stresses for the 2- and 3-dimensional finite element models. The 3-dimensional stresses in this figure are computed at the center of the blade. Consequently, these do not include any stress concentrations in the blade/disk transition region. Zoom modeling techniques are being utilized to evaluate peak stresses in this blade root region.

Blade natural frequencies have been calculated for the ceramic turbine rotor. The Campbell diagram illustrated in Figure 97 is based on centrifugal effects using silicon nitride material. The Campbell diagram indicates no expected interference within the operating range with any low frequency excitations or with the stator passing frequency if either 19 or 21 stator vanes are used. Figures 98 and 99 show mode shapes for the first four blade natural frequencies.

2.1.11.3.3 Metallic Rotor Design

Metallic turbine rotor definition was accomplished by first matching the ceramic nominal swirl (-27 degrees rotor exit swirl) at 1422K (2100°F) over the entire engine duty cycle. This established the turbine off-design speed and pressure ratio characteristics for a design tip speed of 701 m/sec (2300 ft/sec) utilizing ceramic. Since metallic rotor life is highly dependent on rotor relative temperature, rotor inlet relative temperature distribution, as a function of engine speed, was calculated from off-design turbine vector diagrams as shown in Figure 100. Since metallic rotor turbine inlet temperature (TIT) was maintained at 1422K (2100°F) from maximum power to idle, the turbine inlet relative temperature increases as the rotor rotational speed is reduced below 80,000 rpm. Mechanical analyses indicated that under these conditions, a reduction in tip speed from 701 m/s (2300 ft/sec) to 640 m/s (2100 ft/sec) is required to maintain an acceptable life for the interim metallic rotor. This reduction in tip speed will be accomplished by reducing the rotor inlet tip diameter, thereby maintaining maximum engine speed of 100,000 rpm. Aerodynamically the effect of reducing rotor tip speed increases inducer incidence. Figure 101 shows a decrease in predicted overall turbine efficiency of approximately 1 point due to tip speed limitations.

Table 9 presents mechanical properties of the dual alloy metallic rotor. Figure 102 illustrates the resulting metallic rotor stress field at maximum operating conditions.

2.1.11.3.4 Cold Turbine Test Rig

The cold turbine test rig, shown in Figure 103, is an overhung design supported by two angular contact ball bearings. Power section ducting and flow geometry have been replicated.

Rotor dynamics analysis has been accomplished, results of which are depicted in Figures 104 and 105. The cold turbine testing operating envelope is shown on Figure

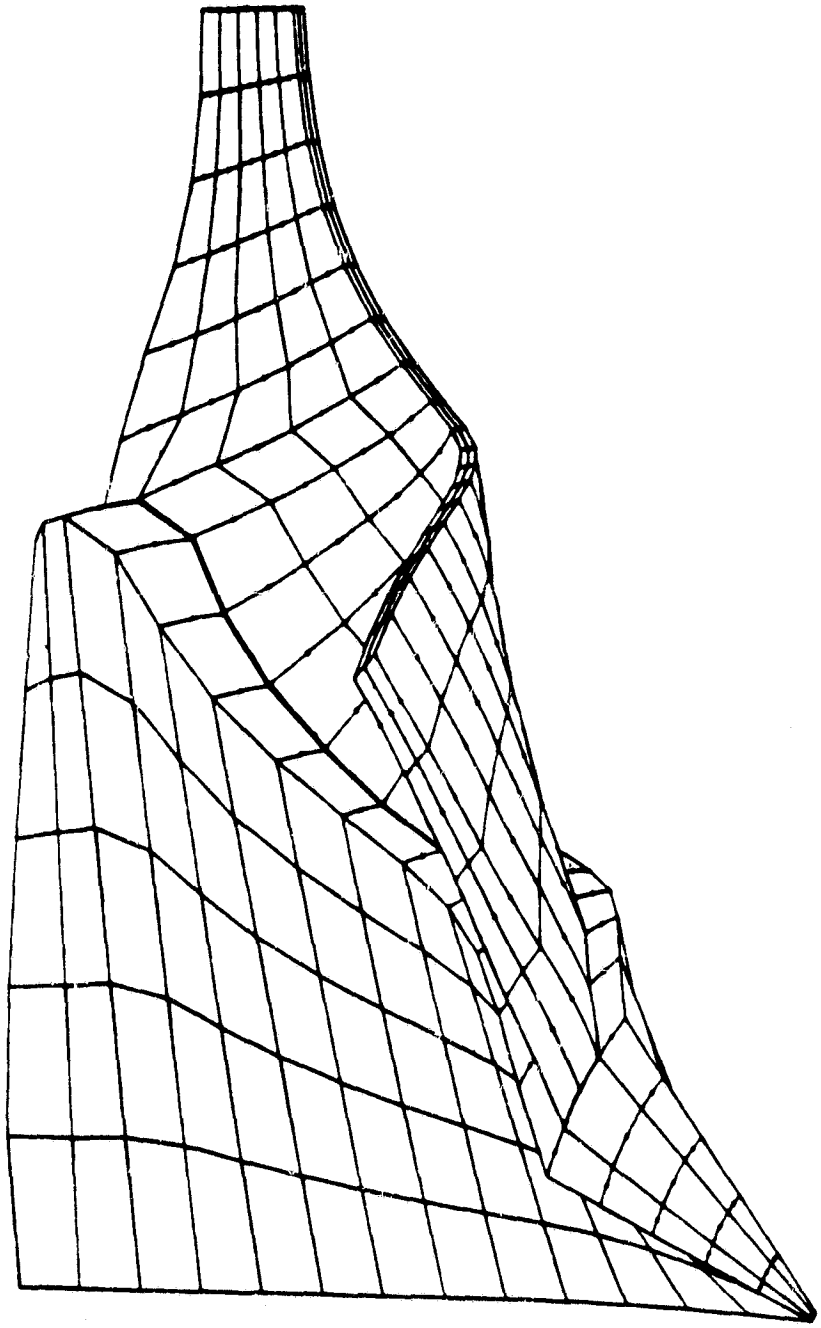

Figure 94. AGT Ceramic Blade and Disk Segment.

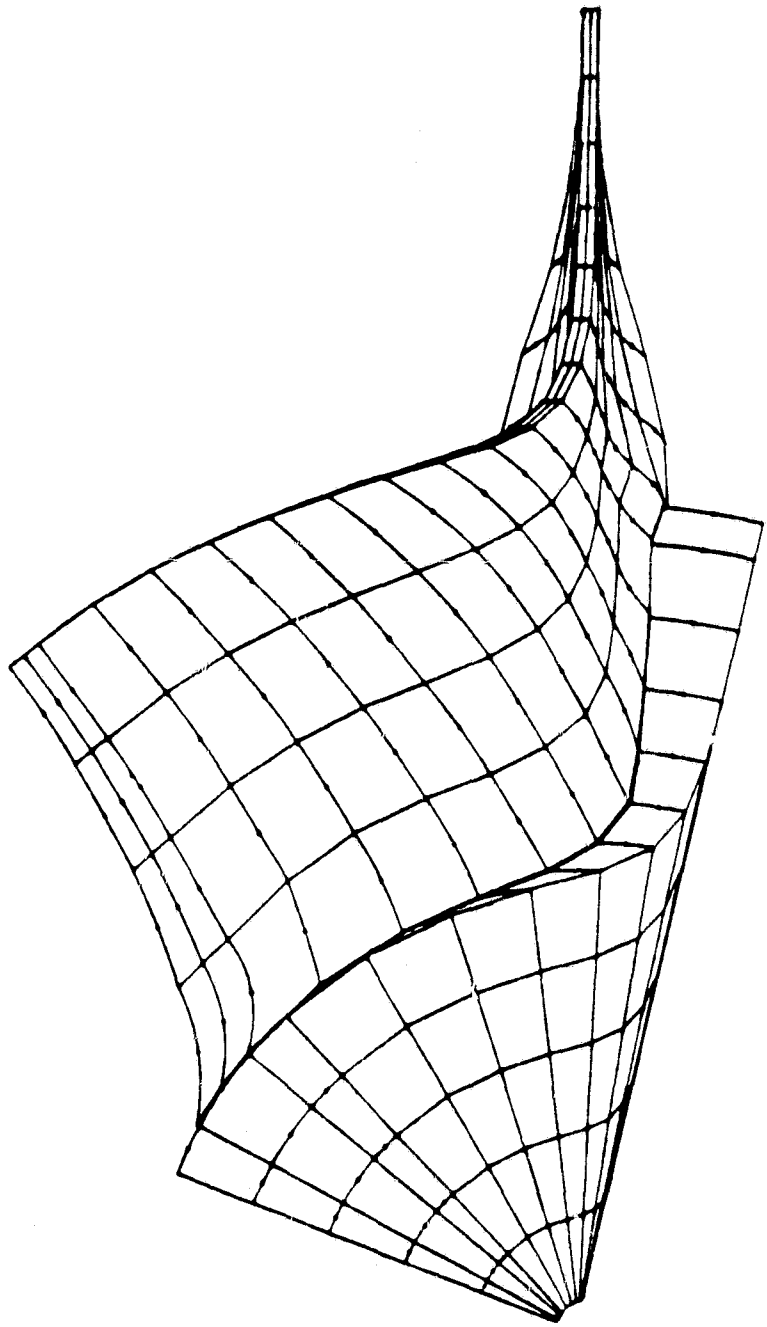

Figure 95. AGT Ceramic Blade and Disk Segment.

SINTERED SILICON NITRIDE PROPERTIES

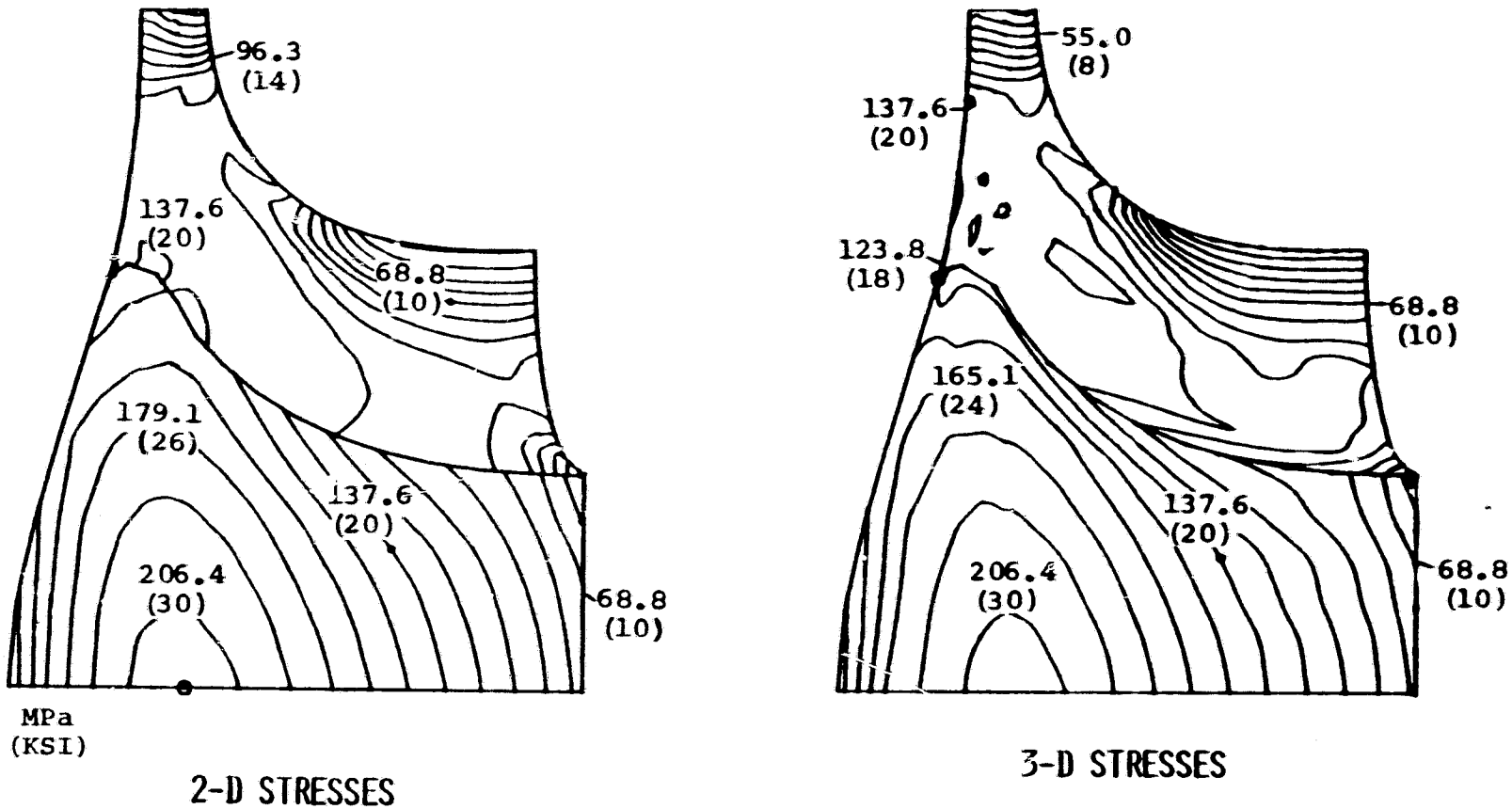

Figure 96. Comparison of 2-D and 3-D Maximum Centrifugal Principal Stresses, 14 Blades, 100,000 RPM.

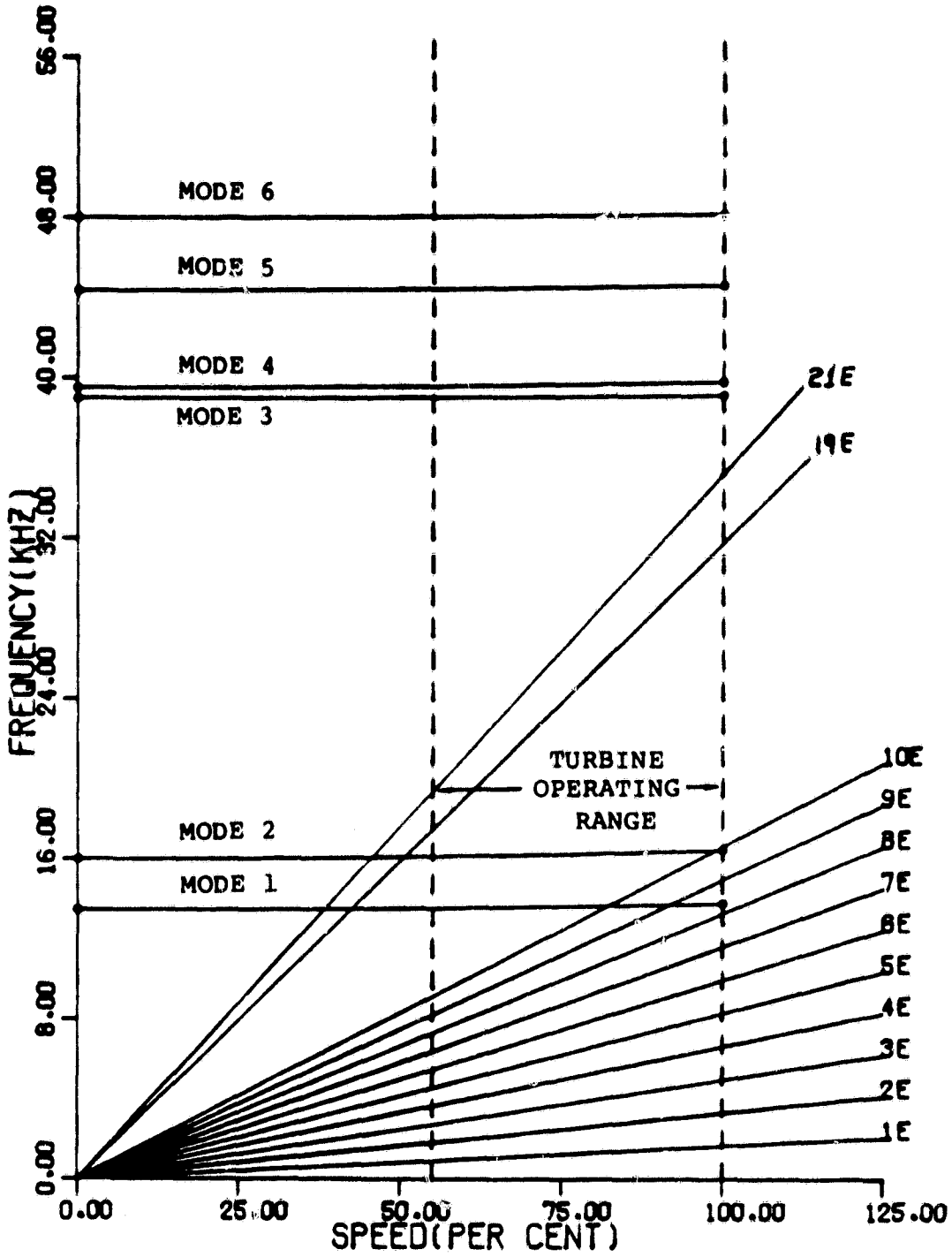

Figure 97. AGT Ceramic Blade Campbell Diagram.

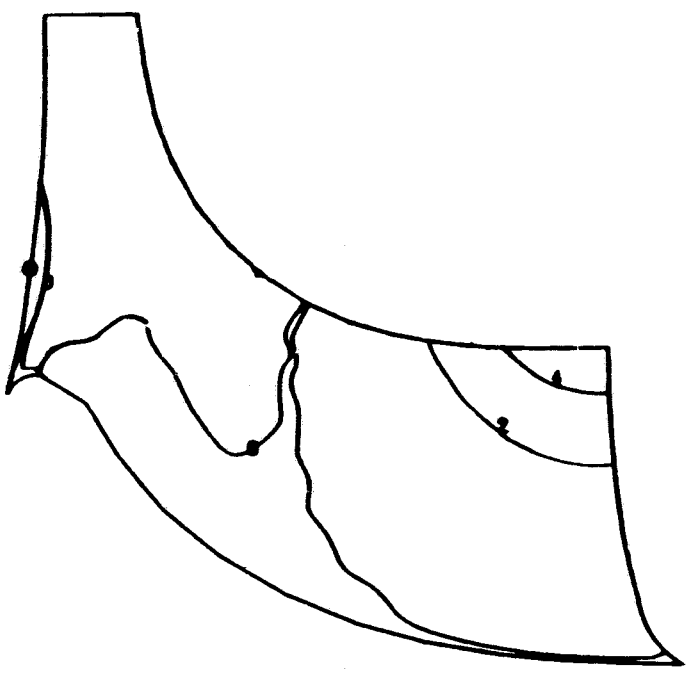

MODE 1 FREQ(HZ)= 13837

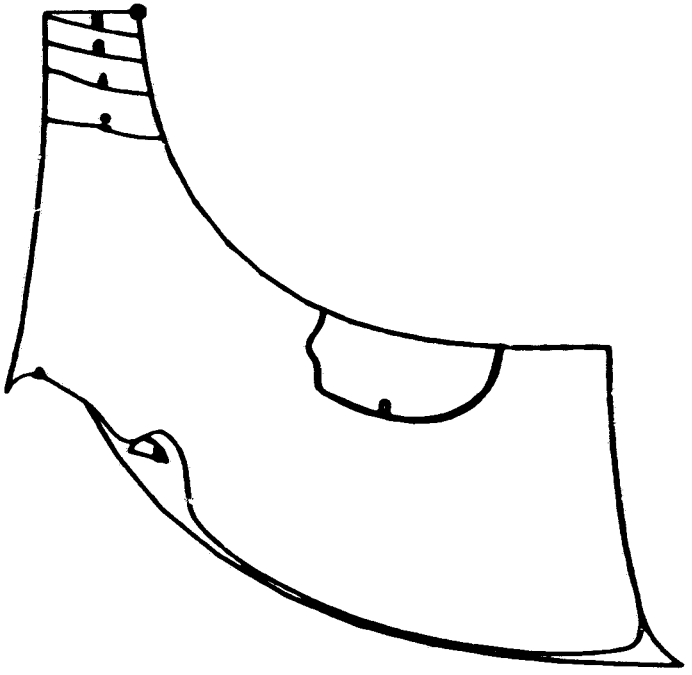

MODE 2 FREQ(HZ)= 16527

Figure 98. AGT Ceramic Blade Mode Shapes.

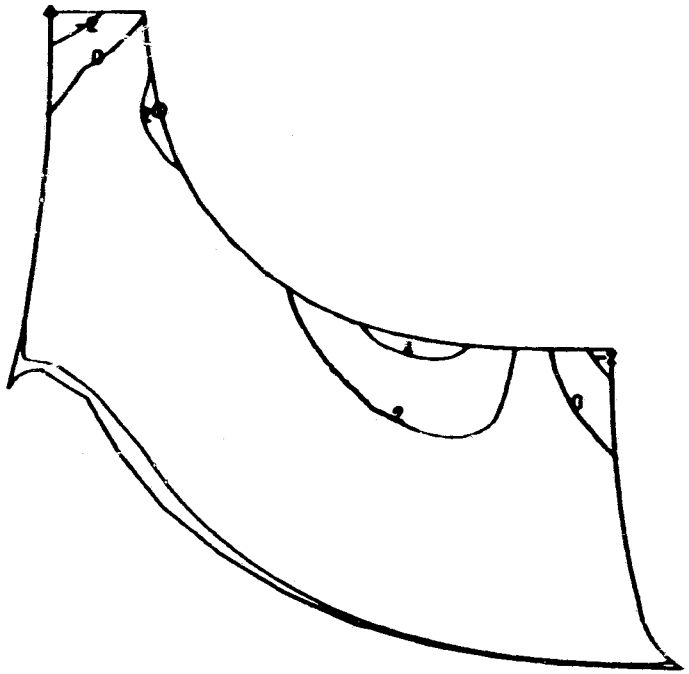

MODE 3 FREQ(HZ)=38199

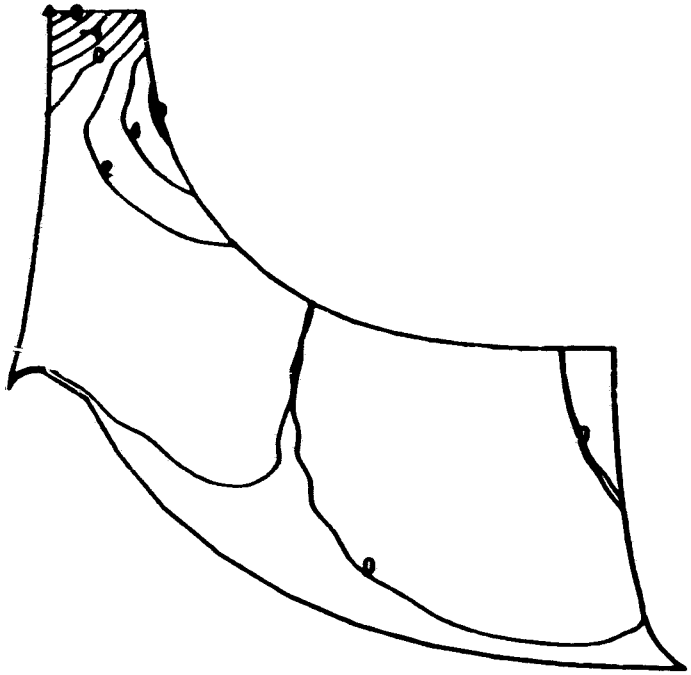

MODE 4 FREQ(HZ)=39879

Figure 99. AGT Ceramic Blade Mode Shapes.

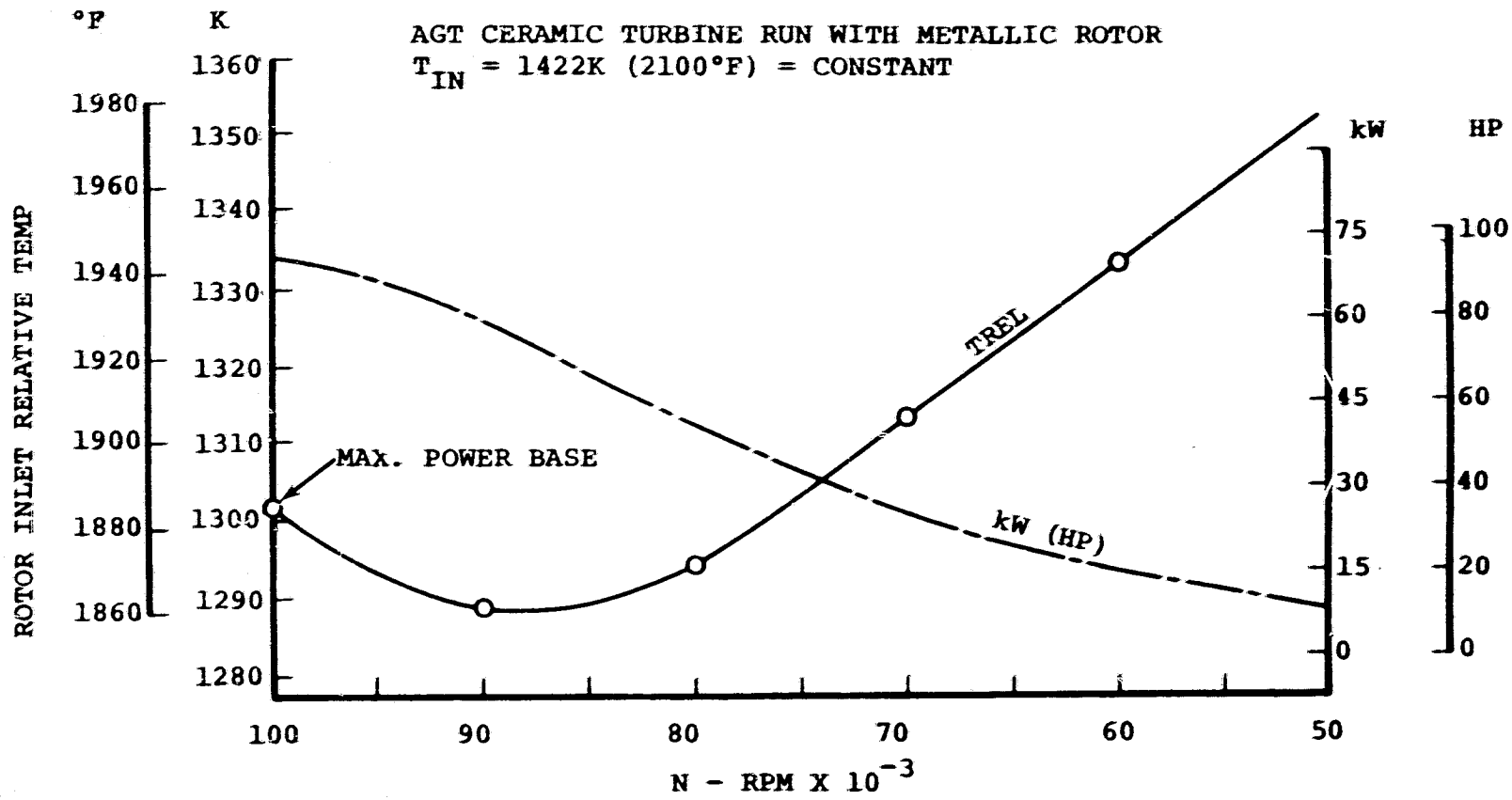

Figure 100. Metallic Rotor Relative Inlet Temperature and Power Output as a Function of Engine RPM.

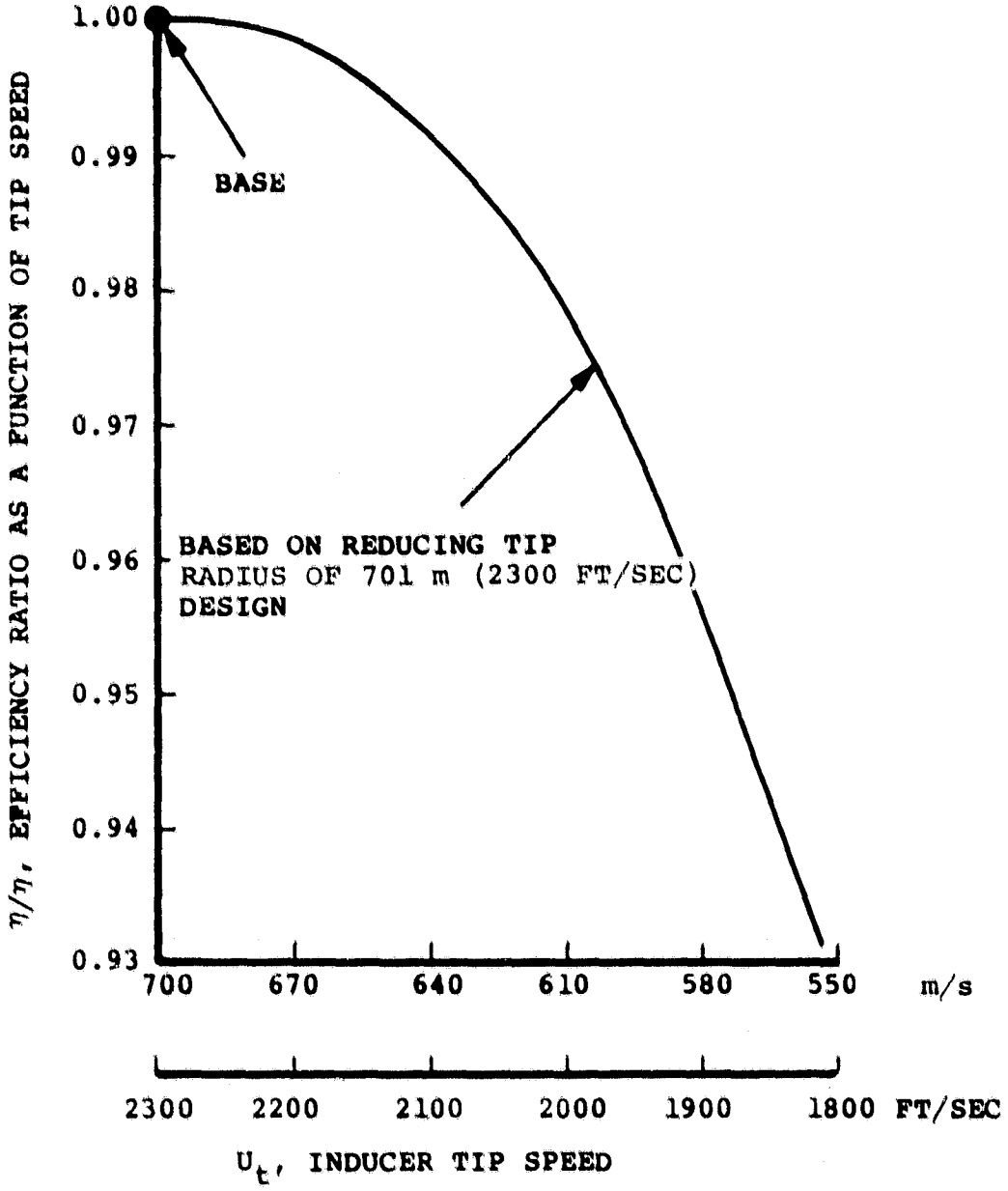

Figure 101. AGT, Metallic Turbine, Effects of Tip Speed on Efficiency [T_{in} = 1422K (2100°F)] at 100,000 RPM.

104. Using bearing stiffnesses of 4378 N/m (25,000 lb/in), the first and second undamped critical speeds are calculated at 10,000 rpm and 18,900 rpm, respectively. These modes, shown in Figure 105, are predominantly rigid body modes. The third critical is a rotor bending mode and is calculated at 80,000 rpm, providing 56 percent margin about the operating envelope. Since the bearings are hydraulically mounted, AiResearch Phoenix experience shows that characteristics of the mounts successfully damp the first and second modes. Therefore, turbine operation is considered safe throughout the operating range.

TABLE 9. METAL TURBINE WHEEL PROPERTIES

Number of Blades	12
Material	Mar-M-247 (DS)/Astroloy
Weight, kg (lb)	1.45 (3.20)
Ip (lb-in-sec^2)	(0.0089)
Operating Conditions at Maximum Power (100,000 RPM)	
Inlet Temperature K (°F)	1422 (2100°F)
Tip Speed m/s (ft/sec)	640 (2100)
Average Tangential Stress (ksi)	(69.7)
Burst Margin	1.34

Rotor operating clearance will be determined using clearance probes of suitable size at the inducer, exducer, and backface planes. Variations in clearance are accommodated through shim stacks and can be changed on the test stand.

Flowpath instrumentation will be located at the following stations:

- Stator inlet total pressure and temperature probes
- Stator static pressure sensor at the inlet, throat, exit, and selected pressure and suction surface locations
- Rotor inlet static pressure sensors
- Rotor shroud static pressure sensors
- Rotor exit total pressure and temperature probes
- Exhaust diffuser instrumentation
- Regenerator low pressure inlet instrumentation

Instrumentation will be sized consistent with small stage dimensions and be of sufficient number and spacing to provide realistic average values for all parameters measured.

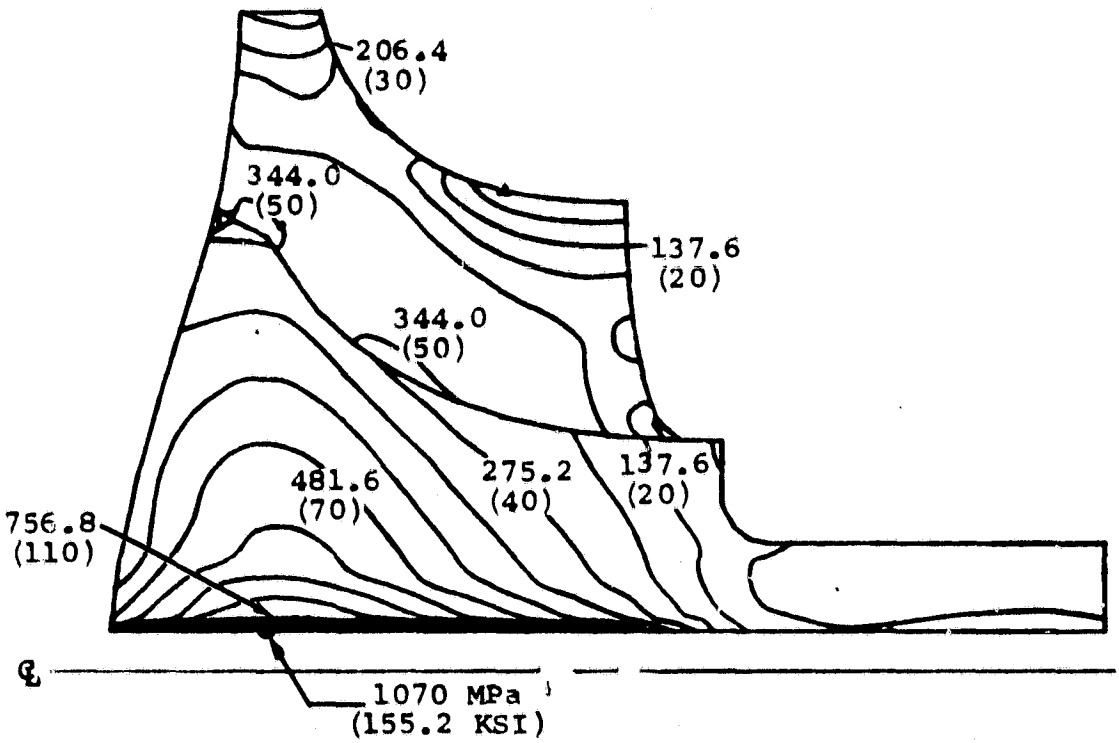

Figure 102. AGT Metal Wheel 2-D Centrifugal Equivalent Stresses — KSI, 12 Blades, 100,000 RPM.

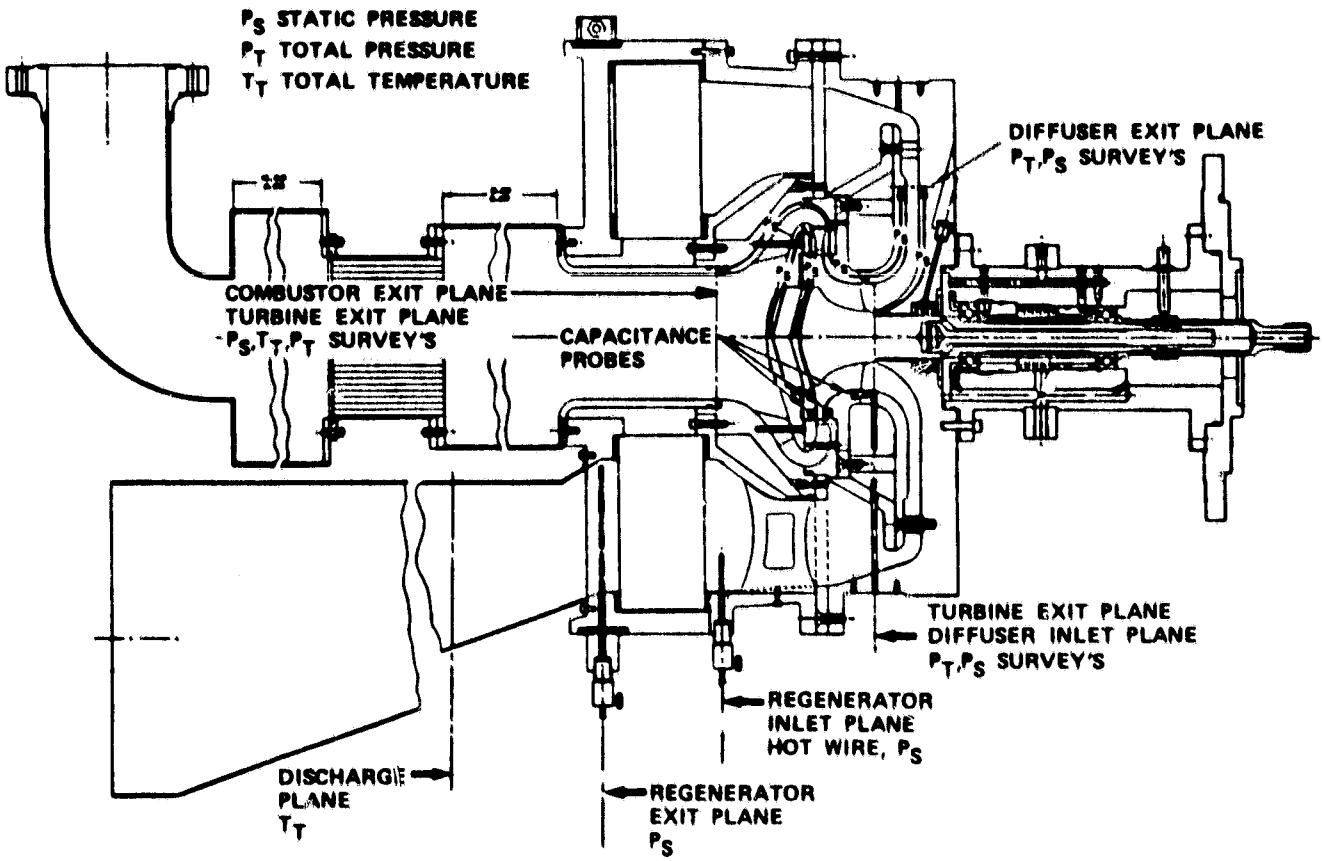

Figure 103. Cold Turbine Test Rig Layout.

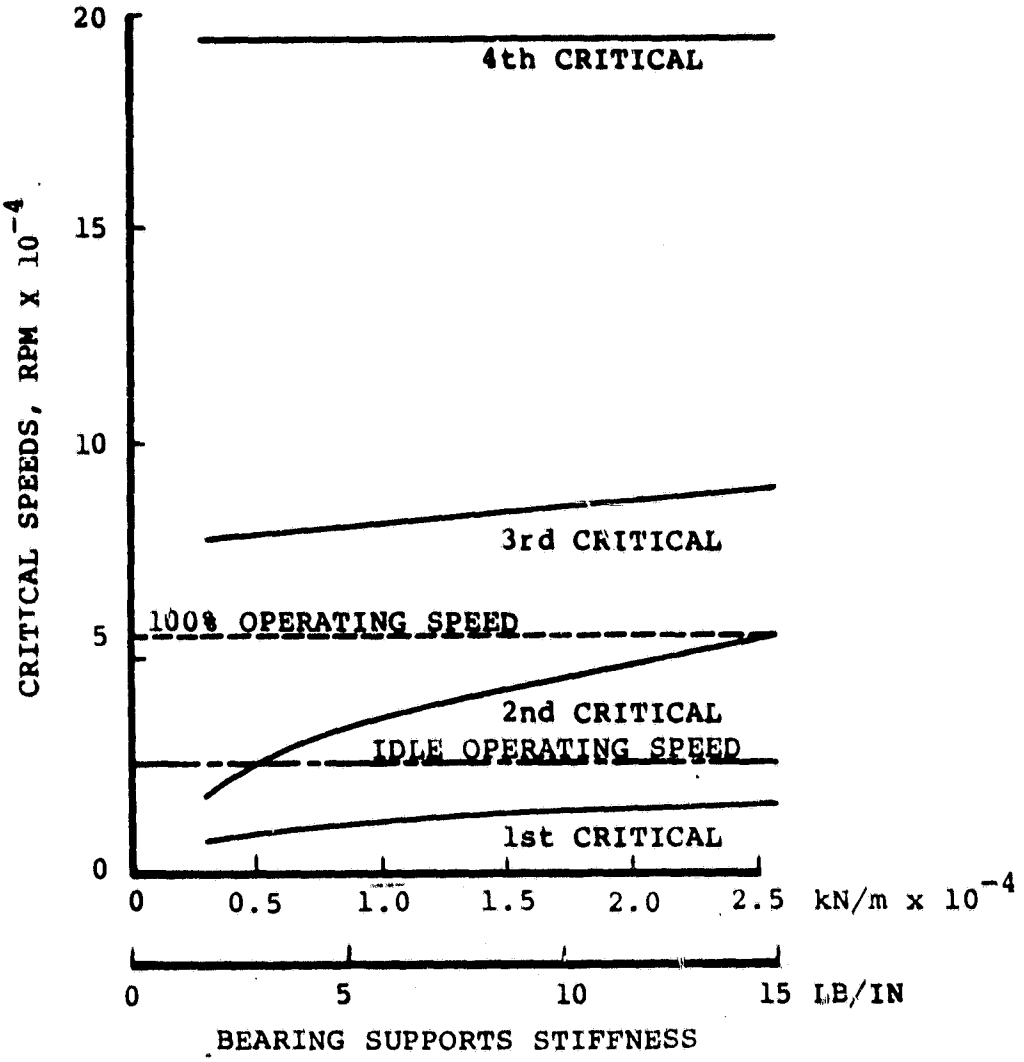

Figure 104. Turbine Test Rig Critical Speeds.

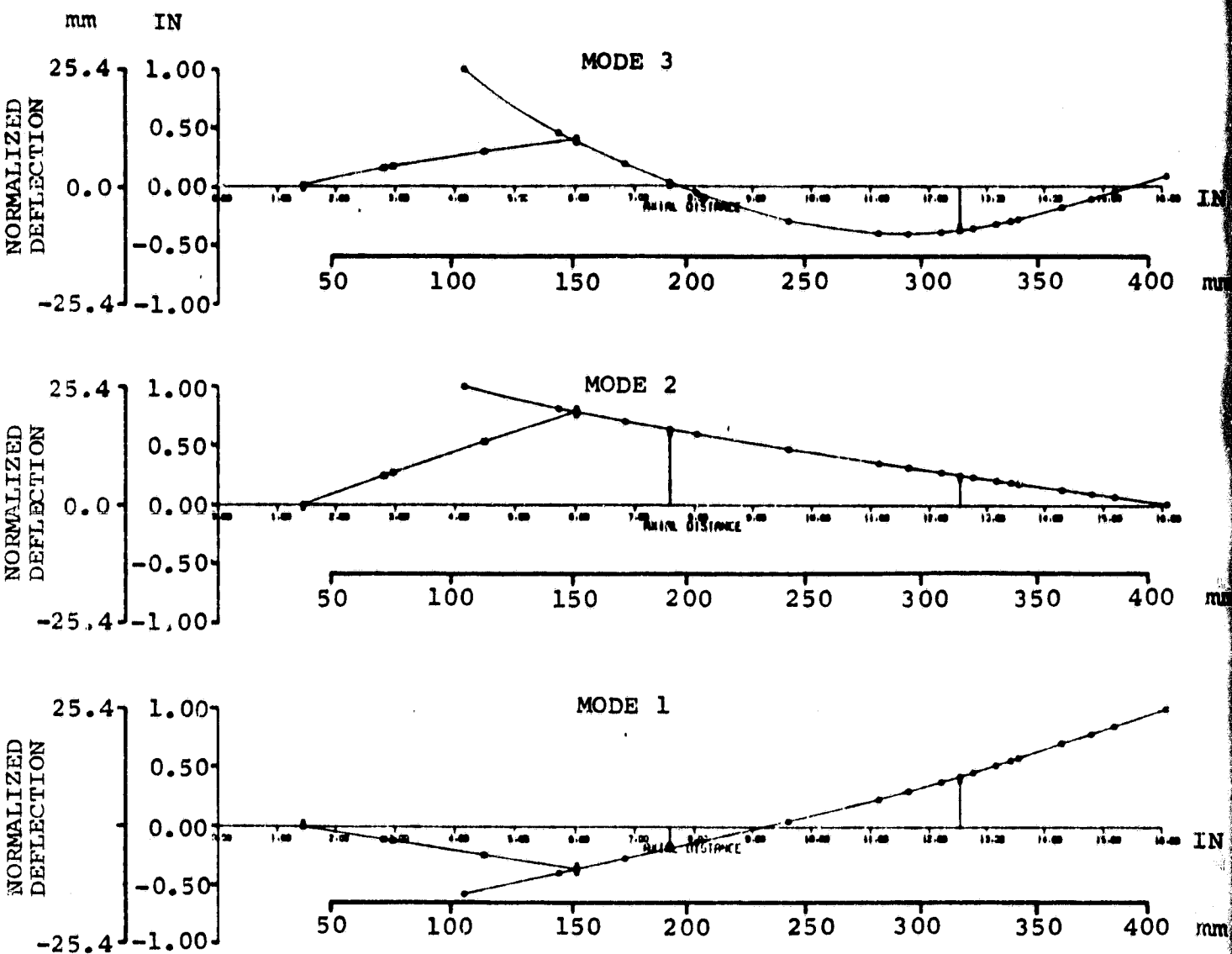

Figure 105. Turbine Rig Rotor Dynamics.

2.1.12 Ceramic Rotor Process Definition

2.1.12.1 Materials Selection

The ceramic radial rotor is the longest-lead, highest-risk ceramic component. Design studies indicate that hot-pressed silicon nitride (Si_3N_4) and silicon carbide (SiC) have adequate properties for the AGT turbine rotor, although they are difficult and expensive to fabricate in the required configuration. Emphasis must be on developing acceptable properties in ceramic materials that can be fabricated by net shape processes. Reaction-bonded Si_3N_4 has net shape capability, but does not have adequate strength and is not projected to have adequate strength by 1983, thereby eliminating it from further consideration. Sintered Si_3N_4 and SiC, reaction sintered SiC (RSSiC), and HIP Si_3N_4 have the potential for meeting project requirements within the development timetable.

Considering current levels of development, projected properties, net shape capability, and cost, the following materials and potential sources have been identified:

Sintered SiC	Carborundum
Sintered Si_3N_4	Ford
Sintered Si_3N_4	AiResearch Casting Company (ACC)
HIP Si_3N_4	AiResearch/Battelle
Reaction Sintered SiC	Pure Carbon/British Nuclear Fuels, Ltd. (BNFL)

The following paragraphs describe candidate materials, fabrication approaches, and sources for ceramic rotor process definition in more detail.

2.1.12.2 Sintered SiC

Sintered SiC from Carborundum appears to be a near-term material for process evaluation. Currently available SiC is variable with average flexural strength ranging from 310-448 mPa (45-65 ksi) with Weibull m ranging from 5-10 depending upon the batch. This is not adequate for a reliable radial rotor. Average strength of about 621 mPa (90 ksi) with a Weibull m of 15-20 is required. However, Carborundum has just completed a major new facility and can now conduct processing under dramatically improved conditions. Specimens fabricated under these type conditions have had an average strength approaching 621 mPa (90 ksi) with an m of 12. It is expected that, with continued development, comparable or better strengths will be routine.

Much development will be required to achieve high strength in an actual rotor. Carborundum has attempted to fabricate an integral radial rotor by injection-molding under the DOE/NASA/Chrysler program. To date they have not been successful due to the inability to remove the injection-molding plasticiser from the thick hub section. Currently, Carborundum is trying to solve this problem by evaluating alternate plasticisers and

removal procedures. Also being explored is the approach of injection molding a blade ring and bonding it to a hub prepared by a process not requiring a plasticiser. Excellent bonding has been achieved on a specimen and it appears this approach is feasible for a radial rotor.

2.1.12.3 Sintered Si_3N_4

A survey of technical literature for the past few years would suggest that sintered Si_3N_4 component technology has developed more slowly than SiC and is considered further from producing a reliable radial rotor. However, unpublished radial rotor fabrication studies at AiResearch Casting Company (ACC) and Ford Motor Company have demonstrated that sintered Si_3N_4 is just as viable as sintered SiC.

During the past two years, ACC has fabricated over 100 radial rotors of RBSN using existing tooling of a turbocharger design. About 50 of these were slip cast to net shape, requiring only minor shaft and balance machining. Recently, the same tooling and casting procedures have been successfully used to fabricate sintered Si_3N_4 rotors using GTE Sylvania SN502 powder.

ACC work to date has demonstrated manufacturing feasibility and has defined some of the tasks that would be required to develop a reliable rotor. Major tasks will be to optimize the material composition to achieve required properties (strength, stress rupture life, and oxidation-resistance in particular) and to eliminate processing flaws resulting from casting and sintering procedures.

Ford has also made significant progress in sintered Si_3N_4 technology that has not been published. Using their own high purity Si_3N_4 powder with suitable sintering aids added, Ford has injection-molded the 820 engine integral stator configuration and successfully sintered it to 99 percent of theoretical density. More recently, Ford has fabricated a radial rotor by slip casting and sintered it to 95 percent of theoretical density. Best strength values achieved to date for test specimens are a characteristic strength of 614 mPa (89 ksi) with an m value of 8 at room temperature, and 434 mPa (63 ksi) with an m of 11 at 1473K (2192°F). Although considerable development work remains, both strength and manufacturing feasibility have been demonstrated.

2.1.12.4 HIP Si_3N_4

AiResearch has conducted an in-house program on Hot Isostatic Pressing (HIP) of Si_3N_4 for the past 1½ years to evaluate HIP sources, explore Si_3N_4-Y_2O_3 compositions, and develop net-shape preform capability. From this study it appears that HIP is a viable approach for a high strength, low cost radial rotor.

Hot isostatic pressing of Si_3N_4 is in the early stages of development in the United States. Battelle has demonstrated full densification of Si_3N_4-MgO and Si_3N_4-Y_2O_3

compositions using Tantalum encapsulation. Glass encapsulation is required for low cost and complex shapes. Battelle is currently developing glass encapsulation technology under a DARPA/AFML program.

The most extensive HIP of Si_3N_4 work has been conducted in Sweden at ASEA involving glass encapsulation to successfully fabricate individual airfoils and an integral axial rotor. Currently ASEA technology is not available.

Discussions with Battelle Columbus Laboratories have resulted in the preliminary definition of a HIP program directed toward radial rotor fabrication. Three approaches have been identified as follows:

- Densification of powder preforms containing appropriate sintering aids
- Densification of reaction bonded Si_3N_4 shapes containing a suitable sintering aid
- Final densification of sintered Si_3N_4 or SiC

The initial task of this program would be to optimize compositions in the Si_3N_4-Y_2O_3, Si_3N_4-Y_2O_3-SiO_2 , and Si_3N_4-AL_2O_3 systems in terms of densification and properties. As a first step simple test bar shapes would be HIPped. At a later date, the shape would change to a simulated rotor having a mass comparable to the fully bladed rotor and finally, the actual rotor shape would be pressed. Parallel to this approach, reaction bonded Si_3N_4 containing Y_2O_3 would be HIPped, as would sintered rotors from ACC, Ford, and Carborundum. The best approach would be determined by spin testing.

Although initial HIPping of simple test bar shapes could utilize Tantalum for encapsulation, a fully bladed rotor will require that a suitable glass encapsulation technique be available. For this reason achievement of a suitable encapsulation glass has been identified as a critical development area.

2.1.12.5 Reaction Sintered SiC

Reaction sintered SiC (RSSiC) is also a potential rotor material, although not as much preliminary work has been conducted as on sintered SiC and Si_3N_4. Some potential advantages of RSSiC over sintered materials are:

- No shrinkage during densification
- Years of prototype and production experience
- Higher thermal shock resistance and fracture toughness
- Greater ease in incorporating fiber reinforcement
- Greater ease in fabricating a solid-hub design

REFEL SiC from Pure Carbon/British Nuclear Fuels, Ltd (BNFL) is currently the best RSSiC commercially available. Strength of pressed or injection molded REFEL is typically over 516.7 mPa (75 ksi). Development has recently begun at BNFL on a slip cast version of REFEL. Average strength has been over 551.1 mPa (80 ksi) with individual values over 689 mPa (100 ksi). Average strength over 620 mPa (90 ksi) should be achievable with further development.